



Kent Academic Repository

Birchall, Lee Terence (2019) *Synthesis of monomers for Ring-Opening Metathesis Polymerisation (ROMP): Optimisation and attachment of fluorophores.* Master of Science by Research (MScRes) thesis, University of Kent.,

Downloaded from

<https://kar.kent.ac.uk/83328/> The University of Kent's Academic Repository KAR

The version of record is available from

This document version

UNSPECIFIED

DOI for this version

Licence for this version

CC BY (Attribution)

Additional information

Versions of research works

Versions of Record

If this version is the version of record, it is the same as the published version available on the publisher's web site. Cite as the published version.

Author Accepted Manuscripts

If this document is identified as the Author Accepted Manuscript it is the version after peer review but before type setting, copy editing or publisher branding. Cite as Surname, Initial. (Year) 'Title of article'. To be published in *Title of Journal*, Volume and issue numbers [peer-reviewed accepted version]. Available at: DOI or URL (Accessed: date).

Enquiries

If you have questions about this document contact ResearchSupport@kent.ac.uk. Please include the URL of the record in KAR. If you believe that your, or a third party's rights have been compromised through this document please see our [Take Down policy](https://www.kent.ac.uk/guides/kar-the-kent-academic-repository#policies) (available from <https://www.kent.ac.uk/guides/kar-the-kent-academic-repository#policies>).

**Synthesis of monomers for Ring-Opening
Metathesis Polymerisation (ROMP): Optimisation
and attachment of fluorophores.**

Submitted by Lee Terence Birchall

To the University of Kent as a thesis for the

Degree of Master of Science

September 2019

Acknowledgments:

Firstly, I would like to thank my supervisor Dr. Stefano Biagini for his support, assistance and guidance throughout my masters degree. I really appreciate you introducing me into your area of research which I have thoroughly enjoyed. I would like to thank Dr. Chris Serpell for his support and help, especially with the DNA intercalation studies. I would like to thank Dr. Helena Shepherd for her assistance in obtaining crystal structures for my compounds. I would like to thank Dr. Ewan Clark for his assistance with NMR, especially his help running the T_1 measurements. I would like to thank Dr. Andrew Morrell for his assistance with GC-MS measurements.

I would also like to thank my many lab colleagues for their support and help in the lab and their suggestions when things did not go well. I would especially like to thank Sara Shehata for her constant support and help with polymerisation. I would also like to thank Saeed Akkad for his guidance on experiments, calculations and assistance with the use of unfamiliar equipment and software.

Finally, I would like to thank my family for their love and support, which has helped me through difficult times and allowed me to better myself. I would like to thank my fiancée Lauren for her love, support and encouragement throughout my time in university.

Abstract:

Optimised bulk (neat heating) and small scale (microwave) methods have been developed for the isomerisation of carbic anhydride (15 – 20 %), an important starting point in the synthesis of Ring-Opening Metathesis Polymerisation (ROMP) monomers. Several linker monomers have been synthesised, including *exo* himoyl glycine which had its crystal structure solved. The fluorophore rhodamine B has been attached to two different linkers by both ester and amide formation and for both the *endo* and *exo* isomers. Crystal structures for the novel *endo* and *exo* amide RhB compounds have been obtained. ROMP of *exo* himoyl glycine and *exo* amide RhB has been achieved using Grubbs 3rd generation catalyst. Intercalation of the *exo* amide RhB homopolymer into DNA was attempted and analysed by DLS and Fluorescence measurements.

Contents

Acknowledgments:	1
Abstract:	2
Table of Figures:	7
Table of Schemes:.....	17
Introduction.....	19
ROMP catalysts	20
Monomer Design.....	24
Polymerisable unit	24
Linkers.....	28
Adding functionality.....	29
Organic-Radical based Contrast Agents (ORCAs) for MRI	29
Fluorescence imaging.....	31
Multi-modal imaging	33
Theranostics	33
DNA Intercalation.....	34
Aims and Objectives:	35
Aims:.....	35
Objectives:.....	35
Results and Discussion:.....	37
Optimising the thermal isomerization of carbic anhydride:	37
Analysis procedure and examples	38
¹ H NMR analysis.....	39

GC-MS analysis	44
T ₁ analysis and GC-MS comparison.....	47
Assigning the ¹³ C NMR:	49
Infrared Spectroscopy:	51
Melting points:.....	52
Neat heating method:.....	53
Endo/Exo solubility:	54
Small scale microwave method:	58
Romp monomers – adding linkers	65
The importance of linkers	65
Amino acid linkers.....	65
Amino alcohol linkers	70
Endo amino alcohol product (N-(hydroxypentanyl)-cis-5-norbornene-endo-2,3-dicarboximide)	72
Exo amino alcohol product (N-(hydroxypentanyl)-cis-5-norbornene-exo-2,3-dicarboximide)	77
N-Diamine linkers	80
Functional unit addition	93
<i>Endo</i> ester RhB.....	94
<i>Exo</i> ester RhB	102
<i>Endo</i> amide RhB.....	108
<i>Exo</i> amide RhB	114
Crystallisation of <i>Exo</i> amide RhB	117
Fluorescence Resonance Energy Transfer (FRET).....	119
5,6-Carboxyfluorescein	119
Ring-Opening Metathesis Polymerisation (ROMP)	124

¹ H NMR of ROMP polymers – what is expected?	124
ROMP kinetic study.....	128
<i>Exo</i> himoyl glycine polymer	130
<i>Exo</i> amide RhB polymer	135
DNA intercalation	140
Water results:	141
TBE 1x buffer results:	143
TAMg 1x buffer results:.....	145
Conclusion:	148
Experimental:.....	150
General information:.....	150
Materials	151
Thermal isomerization of carbic anhydride:	151
Neat Heating method:	151
Recrystallisation of LTB-47-001:	152
Recrystallisation of LTB-47-002:	152
Recrystallisation of LTB-47-003:	152
Recrystallisation of LTB-47-004:	153
Microwave method:.....	154
Recrystallisation:.....	154
Synthesis of ROMP monomers – adding linkers:	155
<i>Exo</i> -himoyl glycine:	155
Recrystallisation of LTB-38-001:	155
Recovery from LTB-38-F01:	156

N-(hydroxypentanyl)- <i>cis</i> -5-norbornene- <i>endo</i> -2,3-dicarboximide:	156
N-(hydroxypentanyl)- <i>cis</i> -5-norbornene- <i>exo</i> -2,3-dicarboximide:.....	158
<i>Endo</i> -N-(2-Aminoethyl)-5-norbornene-2,3-dicarboximide:.....	159
<i>Exo</i> -N-(2-Aminoethyl)-5-norbornene-2,3-dicarboximide:	160
Synthesis of ROMP monomers – Adding functionality:	161
<i>Endo</i> -ester-RhB:	161
<i>Exo</i> -ester-RhB:	162
Columns:	163
<i>Endo</i> -amide-RhB:	164
Work-up:.....	164
Crystallisation:	164
<i>Exo</i> -amide-RhB:.....	166
Work-up:.....	166
Polymerisation:	167
Poly <i>exo</i> himoyl glycine:.....	167
Poly <i>exo</i> amide RhB:.....	168
DNA Intercalation:.....	169
References:	170

Table of Figures:

Figure 1 Common catalysts for Ring-Opening Metathesis Polymerisation (ROMP).	21
Figure 2 Chemical structures for Grubbs 1 st and 2 nd generation catalysts.....	21
Figure 3 Grubbs 3rd generation catalyst which is green when good (left vial) and brown when oxidised (right vial).	23
Figure 4 The three distinguishable sections of a typical monomer for ROMP - The Polymerisable unit, Linker and Functional unit.	24
Figure 5 Carbic anhydride (left) and its oxygen-containing analogue (right).	25
Figure 6 Representation of the steric clashes which result in poor reactivity for endo isomers.	26
Figure 7 Representation of the pi orbitals in furan which result in its aromaticity.	27
Figure 8 General structure of the spirocycloheyl nitroxide moiety.....	30
Figure 9 General structure of the statistical copolymers synthesised by Feng et al. ³⁹ for organelle specific imaging.	32
Figure 10 Annotated 1H NMR of endo carbic anhydride as bought from Acros Organics.	39
Figure 11 Annotated COSY NMR of endo carbic anhydride as bought from Acros Organics.	39
Figure 12 Representation of the 'Roofing effect' seen in 1H NMR spectra as a result of second order effects.	40
Figure 13 Annotated 1H NMR spectrum of exo carbic anhydride.	42
Figure 14 Annotated COSY NMR spectrum for exo carbic anhydride.	43
Figure 15 Crystal structure of the exo isomer of carbic anhydride.	44

Figure 16 GC trace of purified exo carbic anhydride.....	44
Figure 17 Mass spectrum of purified exo carbic anhydride.	45
Figure 18 GC trace of a crude sample containing both exo and endo carbic anhydride.	45
Figure 19 ¹ H NMR spectrum of a crude sample containing both exo and endo carbic anhydride.	46
Figure 20 Mass spectrum of the crude sample containing both exo and endo carbic anhydride.	46
Figure 21 Annotated ¹ H NMR of a crude sample containing both exo and endo carbic anhydride for T ₁ analysis.	48
Figure 22 Annotated ¹³ C NMR spectrum of exo carbic anhydride.	49
Figure 23 Annotated HSQC NMR spectrum for exo carbic anhydride.	50
Figure 24 Infrared spectrum for exo carbic anhydride.	51
Figure 25 GC trace of the crude product obtained using the optimised procedure from the patent.	58
Figure 26 GC traces used to analyse the effect of stirring after heating on the endo/exo composition in solution. Top left: Before stirring, exo = 58 %. Top right: After stirring (100 °C, 30 min), exo = 61 %. Bottom right: Repeat measurement before stirring, 62 %. Bottom right: Repeat measurement after stirring (100 °C, 30 min), exo = 60 %.	60
Figure 27 Suspected by-product of the isomerisation of endo to exo carbic anhydride which was detected by GC-MS.	61
Figure 28 Expected configuration of the endo adducts formed from the Diels-Alder reaction between cyclopentadiene and carbic anhydride.	61
Figure 29 Change in exo isomer composition in the reaction mixture as a function of reaction time.	62
Figure 30 GC trace of the first measurement at reaction time = 20 minutes (LTB-16-110). Impurity peaks are annotated.....	63

Figure 31 General structure of amino acids. Example R-groups are shown for the amino acids known as alanine and tryptophan.....	65
Figure 32 Annotated ¹ H NMR spectrum for exo-himoyl glycine.....	66
Figure 33 COSY NMR spectrum for exo-himoyl glycine.	67
Figure 34 Structure of exo-himoyl glycine as determined by single crystal XRD.	68
Figure 35 GC trace for exo-himoyl glycine.	68
Figure 36 Mass spectrum for exo-himoyl glycine.	69
Figure 37 GC trace for the product formed from the reaction between exo carbic anhydride and 5-amino-1-pentanol.....	71
Figure 38 Mass spectrum for the product formed from the reaction between exo carbic anhydride and 5-amino-1-pentanol (N-(hydroxypentanyl)-cis-5-norbornene-exo-2,3-dicarboximide).	72
Figure 39 Annotated ¹ H NMR spectrum of the product formed from the reaction between endo carbic anhydride and 5-amino-1-pentanol (N-(hydroxypentanyl)-cis-5-norbornene-endo-2,3-dicarboximide).	72
Figure 40 COSY NMR spectrum of the product formed from the reaction between endo carbic anhydride and 5-amino-1-pentanol (N-(hydroxypentanyl)-cis-5-norbornene-endo-2,3-dicarboximide).....	73
Figure 41 GC trace (1) for the product formed from the reaction between endo carbic anhydride and 5-amino-1-pentanol (N-(hydroxypentanyl)-cis-5-norbornene-endo-2,3-dicarboximide).....	74
Figure 42 GC trace (2) for the product formed from the reaction between endo carbic anhydride and 5-amino-1-pentanol (N-(hydroxypentanyl)-cis-5-norbornene-endo-2,3-dicarboximide).....	75
Figure 43 Mass spectrum for the product formed from the reaction between endo carbic anhydride and 5-amino-1-pentanol (N-(hydroxypentanyl)-cis-5-norbornene-endo-2,3-dicarboximide).....	75

Figure 44 Mass spectrum of the expected residual starting material in the sample.	76
Figure 45 Mass spectrum of an impurity detected in the GC trace in Figure 41 at RT = 3.332.	76
Figure 46 Structure of the suspected impurity detected on the GC trace in Figure 41 and corresponds to the mass spectrum in Figure 45.	77
Figure 47 Annotated ¹ H NMR spectrum of the product formed from the reaction between exo carbic anhydride and 5-amino-1-pentanol (N-(hydroxypentanyl)-cis-5-norbornene-exo-2,3-dicarboximide). .	77
Figure 48 COSY NMR spectrum of the product formed from the reaction between exo carbic anhydride and 5-amino-1-pentanol (N-(hydroxypentanyl)-cis-5-norbornene-exo-2,3-dicarboximide).	78
Figure 49 GC trace of the product formed from the reaction between exo carbic anhydride and 5-amino-1-pentanol (N-(hydroxypentanyl)-cis-5-norbornene-exo-2,3-dicarboximide).	79
Figure 50 Mass spectrum of the product formed from the reaction between exo carbic anhydride and 5-amino-1-pentanol (N-(hydroxypentanyl)-cis-5-norbornene-exo-2,3-dicarboximide).	80
Figure 51 Possible products from the reaction between carbic anhydride and ethylenediamine.	81
Figure 52 ¹ H NMR spectrum of the crude product from the reaction between endo carbic anhydride and ethylenediamine (endo-N-(2-aminoethyl)-5-norbornene-2,3-dicarboximide) after initial work-up with ethyl acetate.	82
Figure 53 ¹ H NMR spectrum of the crude product from the reaction between endo carbic anhydride and ethylenediamine (endo-N-(2-aminoethyl)-5-norbornene-2,3-dicarboximide) after extraction with toluene and water. Suspected to mostly contain the undesired bis product.	83
Figure 54 ¹ H NMR spectrum of the purified product from the reaction between endo carbic anhydride and ethylenediamine (endo-N-(2-aminoethyl)-5-norbornene-2,3-dicarboximide) after extraction from water with DCM.	85

Figure 55 Annotated ¹ H NMR spectrum of the purified product from the reaction between endo carbic anhydride and ethylenediamine (endo-N-(2-aminoethyl)-5-norbornene-2,3-dicarboximide) with expanded regions included.....	86
Figure 56 COSY NMR spectrum of the purified product from the reaction between endo carbic anhydride and ethylenediamine (endo-N-(2-aminoethyl)-5-norbornene-2,3-dicarboximide).	86
Figure 57 GC trace of the purified product from the reaction between endo carbic anhydride and ethylenediamine (endo-N-(2-aminoethyl)-5-norbornene-2,3-dicarboximide).	87
Figure 58 Mass spectrum of the crude product from the reaction between endo carbic anhydride and ethylenediamine (endo-N-(2-aminoethyl)-5-norbornene-2,3-dicarboximide).	88
Figure 59 Annotated ¹ H NMR spectrum of the purified product from the reaction between exo carbic anhydride and ethylenediamine (exo-N-(2-aminoethyl)-5-norbornene-2,3-dicarboximide) with expanded regions included.....	89
Figure 60 COSY NMR spectrum of the purified product from the reaction between exo carbic anhydride and ethylenediamine (exo-N-(2-aminoethyl)-5-norbornene-2,3-dicarboximide).....	90
Figure 61 GC trace of the purified product from the reaction between exo carbic anhydride and ethylenediamine (exo-N-(2-aminoethyl)-5-norbornene-2,3-dicarboximide).....	90
Figure 62 Mass spectrum of the purified product from the reaction between exo carbic anhydride and ethylenediamine (exo-N-(2-aminoethyl)-5-norbornene-2,3-dicarboximide).....	91
Figure 63 Chemical structures of 7-hydroxycoumarin and fluorescein.	93
Figure 64 Image depicting the column used to purify the endo ester RhB monomer which shows some of the fluorescent fractions obtained.	95
Figure 65 ¹ H NMR spectrum of the white needle-like crystals collected in the initial column fractions during the purification of the endo ester RhB monomer. Expected to be the by-product dicyclohexylurea (DCU) based off comparison to literature examples.	96

Figure 66 Representation of the chemical structure of the product endo ester RhB with the carbon atoms numbered for easy assignment of NMR spectra.	97
Figure 67 Partially annotated ¹ H NMR spectrum for the product between N-(hydroxypentanyl)-cis-5-norbornene-endo-2,3-dicarboximide and rhodamine B (endo ester RhB).	97
Figure 68 Annotated expanded regions from the ¹ H NMR spectrum for the product between N-(hydroxypentanyl)-cis-5-norbornene-endo-2,3-dicarboximide and rhodamine B (endo ester RhB).	98
Figure 69 COSY NMR spectrum for the product between N-(hydroxypentanyl)-cis-5-norbornene-endo-2,3-dicarboximide and rhodamine B (endo ester RhB).	98
Figure 70 ¹ H NMR spectrum for the product between N-(hydroxypentanyl)-cis-5-norbornene-endo-2,3-dicarboximide and rhodamine B (endo ester RhB). This sample was obtained from a single column fraction and is therefore cleaner than the spectrum in Figure 67.	101
Figure 71 Representation of the chemical structure of the product exo ester RhB with the carbon atoms numbered for easy assignment of NMR spectra.	102
Figure 72 Partially annotated ¹ H NMR spectrum for the product between N-(hydroxypentanyl)-cis-5-norbornene-exo-2,3-dicarboximide and rhodamine B (exo ester RhB).	103
Figure 73 Annotated expanded regions from the ¹ H NMR spectrum for the product between N-(hydroxypentanyl)-cis-5-norbornene-exo-2,3-dicarboximide and rhodamine B (exo ester RhB).	103
Figure 74 COSY NMR spectrum for the product between N-(hydroxypentanyl)-cis-5-norbornene-exo-2,3-dicarboximide and rhodamine B (exo ester RhB).	104
Figure 75 ¹ H NMR spectrum for the product between N-(hydroxypentanyl)-cis-5-norbornene-exo-2,3-dicarboximide and rhodamine B (exo ester RhB). This is the final combined product after multiple columns where fractions containing only one spot were combined.	105
Figure 76 Expanded regions from the ¹ H NMR spectrum for the product between N-(hydroxypentanyl)-cis-5-norbornene-exo-2,3-dicarboximide and rhodamine B (exo ester RhB). This is the final combined	

product after multiple columns where fractions containing only one spot were combined. Comparing to Figure 73 shows that this product contains impurities.	106
Figure 77 ¹ H NMR spectrum of Rhodamine B as bought from Sigma Aldrich.	107
Figure 78 Representation of the product endo amide RhB where the carbon atoms are labelled for easy assignment of NMR spectra.....	109
Figure 79 Partially annotated ¹ H NMR spectrum for the product from the reaction between endo-N-(2-aminoethyl)-5-norbornene-2,3-dicarboximide and Rhodamine B (endo amide RhB).....	109
Figure 80 Annotated expanded regions from the ¹ H NMR spectrum for the product from the reaction between endo-N-(2-aminoethyl)-5-norbornene-2,3-dicarboximide and Rhodamine B (endo ester RhB).	110
Figure 81 COSY NMR spectrum for the product from the reaction between endo-N-(2-aminoethyl)-5-norbornene-2,3-dicarboximide and Rhodamine B (endo ester RhB).....	110
Figure 82 Crystal structure of endo amide RhB where one of the Et groups in one of the NEt ₂ groups can be in one of two positions approximately 50% of the time.	113
Figure 83 Representation of the product exo amide RhB where the carbon atoms are labelled for easy assignment of NMR spectra.....	114
Figure 84 Partially annotated ¹ H NMR spectrum for the product from the reaction between exo-N-(2-aminoethyl)-5-norbornene-2,3-dicarboximide and Rhodamine B (exo amide RhB).	115
Figure 85 Annotated expanded regions from the ¹ H NMR spectrum for the product from the reaction between exo-N-(2-aminoethyl)-5-norbornene-2,3-dicarboximide and Rhodamine B (exo ester RhB).	115
Figure 86 COSY NMR spectrum for the product from the reaction between endo-N-(2-aminoethyl)-5-norbornene-2,3-dicarboximide and Rhodamine B (endo ester RhB).....	116
Figure 87 Crystal structure of exo amide RhB in the ring-closed lactam form.	118

Figure 88 1H NMR spectrum of crude product from the steglich esterification between N-(hydroxypentanyl)-cis-5-norbornene-endo-2,3-dicarboximide and 5,6-carboxyfluorescein (endo ester 5,6-FAM).	121
Figure 89 TLC analysis of the crude product endo ester 5,6-FAM.	121
Figure 90 1H NMR spectrum of a sample obtained from column fractions containing a single spot after running a column on the crude product from the steglich esterification between N-(hydroxypentanyl)-cis-5-norbornene-endo-2,3-dicarboximide and 5,6-carboxyfluorescein (endo ester 5,6-FAM).	122
Figure 91 Representation of a ROMP polymer showing the difference between the cis and trans 1H environments.	126
Figure 92 Diagram explaining the origin of peak broadening in the 1H NMR spectra of polymers.	127
Figure 93 1H NMR spectra taken at different time intervals during the ROMP of the exo himoyl glycine monomer (LTB-38 – See Figure 32 for 1H NMR of monomer) using CDCl ₃ as the solvent.	128
Figure 94 1H NMR spectra taken at different time intervals during the ROMP of exo himoyl glycine (LTB-38 – See Figure 32 for 1H NMR of monomer) using DCM as the solvent where the NMR tube contained a DMSO-d ₆ capillary.	129
Figure 95 Annotated 1H NMR spectrum of the polymer of exo himoyl glycine after work-up. Monomer and residual solvent peaks are present.	131
Figure 96 Annotated expanded region of the 1H NMR spectra of the polymer of exo himoyl glycine. Integration values are included for use in end-group analysis.	132
Figure 97 Annotated and assigned 1H NMR spectrum of the polymer of exo himoyl glycine.	133
Figure 98 1H NMR spectrum of the polymer of exo amide RhB. Some monomer is still present in the spectrum.	135
Figure 99 1H NMR spectra taken at 10-minute time intervals during the polymerisation of exo amide RhB using the new catalyst instead of the old degraded one.	136

Figure 100 Chemical structure of the repeatable unit in the polymer of exo amide RhB where the carbon atoms are labelled for the easy assignment of NMR spectra.	137
Figure 101 Partially annotated ¹ H NMR spectrum for the polymer of exo amide RhB after work-up. Residual solvent peaks are present and labelled.	137
Figure 102 Expanded and annotated regions of the ¹ H NMR spectrum for the polymer of exo amide RhB after work-up where the proton environments are tentatively assigned.	138
Figure 103 Graph showing the size distribution of particles by intensity in different solutions containing a mixture of the exo amide RhB polymer and DNA strands in water. Refer to Table 3 to determine which DNA strands were present, if any, in the samples.	141
Figure 104 Graph showing the raw correlation data for DLS measurements in different solutions containing a mixture of the exo amide RhB polymer and DNA strands in water. Refer to Table 3 to determine which DNA strands were present, if any, in the samples.	142
Figure 105 Graph showing the emission spectra recorded using fluorescence spectroscopy for different solutions containing a mixture of the exo amide RhB polymer and DNA strands in water. Refer to Table 3 to determine which DNA strands were present, if any, in the samples.	143
Figure 106 Graph showing the size distribution of particles by intensity in different solutions containing a mixture of the exo amide RhB polymer and DNA strands in TBE 1x buffer. Refer to Table 3 to determine which DNA strands were present, if any, in the samples.	143
Figure 107 Graph showing the raw correlation data for DLS measurements in different solutions containing a mixture of the exo amide RhB polymer and DNA strands in TBE 1x buffer. Refer to Table 3 to determine which DNA strands were present, if any, in the samples.	144
Figure 108 Graph showing the emission spectra recorded using fluorescence spectroscopy for different solutions containing a mixture of the exo amide RhB polymer and DNA strands in TBE 1x buffer. Refer to Table 3 to determine which DNA strands were present, if any, in the samples.	144

Figure 109 Graph showing the size distribution of particles by intensity in different solutions containing a mixture of the exo amide RhB polymer and DNA strands in TAMg 1x buffer. Refer to Table 3 to determine which DNA strands were present, if any, in the samples. 145

Figure 110 Graph showing the raw correlation data for DLS measurements in different solutions containing a mixture of the exo amide RhB polymer and DNA strands in TAMg 1x buffer. Refer to Table 3 to determine which DNA strands were present, if any, in the samples. 146

Figure 111 Graph showing the emission spectra recorded using fluorescence spectroscopy for different solutions containing a mixture of the exo amide RhB polymer and DNA strands in TAMg 1x buffer. Refer to Table 3 to determine which DNA strands were present, if any, in the samples. 146

Figure 112 ¹H NMR spectra of exo carbic anhydride after successive crystallisations. 154

Table of Schemes:

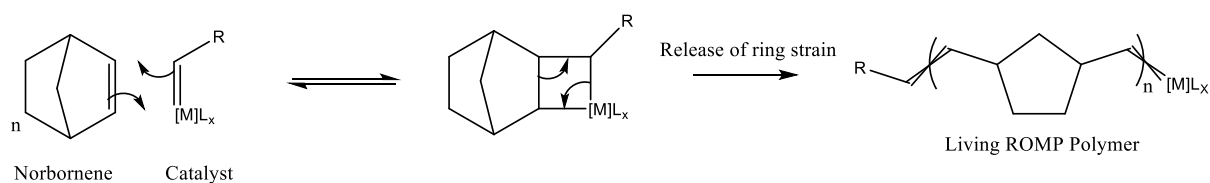
Scheme 1 Mechanism for Ring-Opening Metathesis Polymerisation (ROMP). ⁷	19
Scheme 2 Mechanism for the termination of Ring-Opening Metathesis Polymerisation (ROMP) and common terminating reactions.	20
Scheme 3 Frontier molecular orbital interactions leading to the kinetic (left) and thermodynamic (right) products for the Diels-Alder reaction between cyclopentadiene and maleic anhydride.	25
Scheme 4 The reported reactivity of exo carbic anhydride with ethylenediamine where only the bis product was found to form.....	29
Scheme 5 Reaction scheme for the synthesis of a metal ion binding homopolymer as synthesised by Yao et al. ³⁸ , which starts from exo carbic anhydride.....	31
Scheme 6 General reaction scheme for the synthesis of complex monomers containing imaging moieties to be used for ROMP.	36
Scheme 7 Reaction scheme for the isomerisation of endo carbic anhydride to exo carbic anhydride. The cyclopentadiene and maleic anhydride exist temporarily, as the Diels-Alder reaction occurs very readily under the reaction conditions.	37
Scheme 8 Mechanism for the reaction between carbic anhydride and aminoalcohols.	70
Scheme 9 Possible fragmentation pattern of the product from the reaction between carbic anhydride and ethylenediamine (endo/exo-N-(2-aminoethyl)-5-norbornene-2,3-dicarboximide) based off fragments detected in the mass spectra.....	92
Scheme 10 Reaction scheme for the steglich esterification between N-(hydroxypentanyl)-cis-5-norbornene-endo/exo-2,3-dicarboximide and rhodamine B, using DCC as the carbodiimide, DMAP as the base and DCM as the solvent.	95

Scheme 11 Representation of the open amide and closed lactam structures possible for endo/exo amide	
RhB. The curly arrows represent the transfer of electrons through the aromatic system.	112
Scheme 12 Representation of the ring closed lactone and ring-opened carboxylic acid forms of 5,6-	
Carboxyfluorescein.....	120
Scheme 13 a) Mechanism for Ring-Opening Metathesis Polymerisation (ROMP) b) Reaction scheme for	
ROMP that is annotated to show how different 1H environments are affected in an NMR spectrum	
when a monomer is polymerised.	125

Introduction

Ring-Opening Metathesis Polymerisation (ROMP) is a versatile technique that can create almost monodisperse¹, end-group functionalised² polymers that are designed for purpose through well-defined monomers³⁻⁵. These are ring-strained cycloalkene monomers such as norbornene and its derivatives. The release of ring-strain is a key driving force in the reaction that occurs with the help of a catalyst. Furthermore, norbornene and oxanorbornene monomers are very easy to modify⁶ and can be tailored to specific applications, making ROMP the versatile technique that it is.

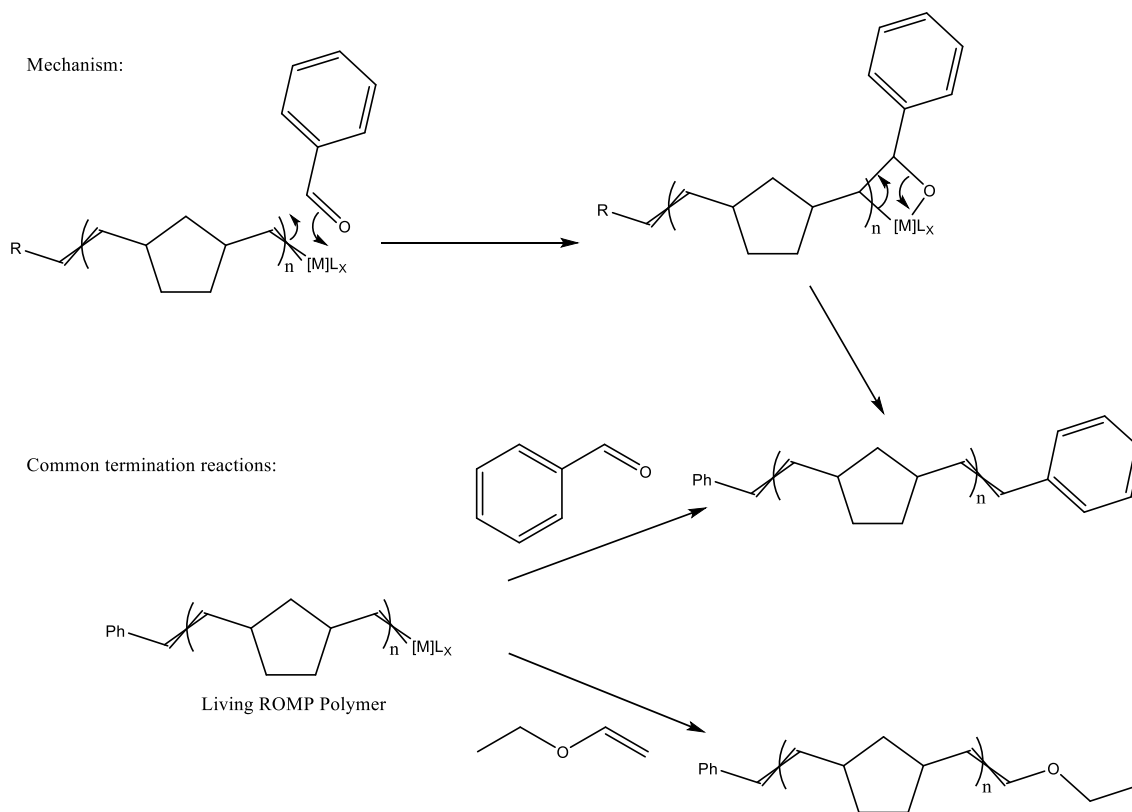
As stated above, ROMP relies on the release of ring-strain to drive the reaction forward. Typically, a norbornene based moiety is used in the monomer to provide the required ring strain and once polymerised, acts as the polymer backbone (Scheme 1).



Scheme 1 Mechanism for Ring-Opening Metathesis Polymerisation (ROMP).⁷

ROMP is a type of 'living' polymerisation. This means that whilst the reaction is occurring in a controlled environment, it will not finish until the reaction is quenched by a terminating agent. Therefore, interesting and complex block copolymers⁸ can be synthesised with relative ease by performing a homo-polymerisation until all monomer is used and then introducing a different monomer which will polymerise until all monomer is used. This is very powerful as polymers can be synthesised to provide dual and multi-modal functionalities⁹. Thus, the design of interesting and functional monomers is an extremely important aspect of ROMP. The polymers can be further functionalised by the choice of end group, providing even greater functional versatility^{2,10}.

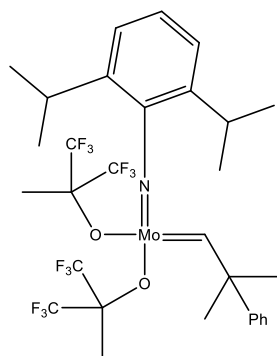
The mechanism for the termination is shown in Scheme 2 below, along with examples of some common terminating agents:



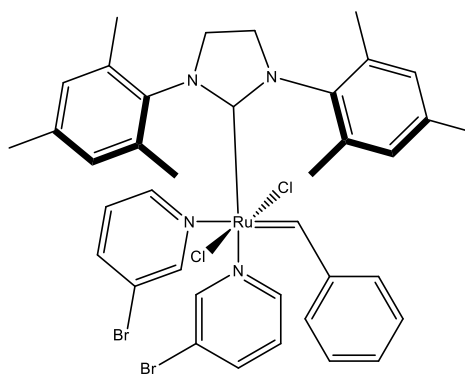
Scheme 2 Mechanism for the termination of Ring-Opening Metathesis Polymerisation (ROMP) and common terminating reactions.

ROMP catalysts

ROMP employs the use of organometallic catalysts such as the 'Schrock catalyst'¹¹ and 'Grubbs catalyst'¹ which are shown in Figure 1. In the past the 'Schrock catalyst'¹¹ was used extensively as the main catalyst for ROMP³. It is still a viable option today for use with certain monomers that are bulky or electron deficient. However, molybdenum is oxophilic, causing it to be very sensitive to moisture in the air¹² and intolerable to functional groups such as alcohols. Therefore, use of the 'Schrock catalyst' is not a suitable option if the monomer contains sensitive functional groups. Furthermore, the reaction must be conducted under very controlled, dry conditions.



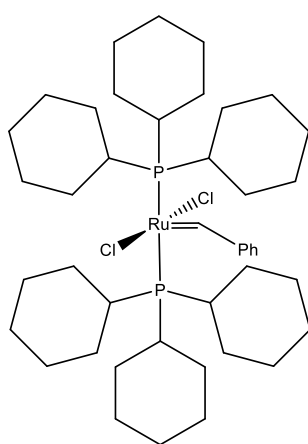
Schrock catalyst



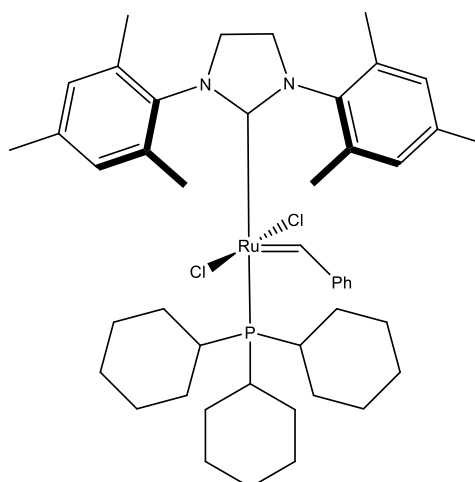
Grubbs 3rd generation catalyst

Figure 1 Common catalysts for Ring-Opening Metathesis Polymerisation (ROMP).

Nowadays, the preferred choice is the 'Grubbs catalyst' which uses the metal ruthenium as opposed to molybdenum in the alkylidene moiety. Ruthenium is much less oxophilic than molybdenum, meaning that it is easier to handle and can tolerate a greater range of functional groups¹³, allowing the design of monomers that can be used for a wider variety of applications. There are several iterations of the Grubbs catalyst, but the one most commonly used is Grubbs 3rd generation catalyst (Figure 1). Grubbs 1st generation^{13,14} and 2nd generation^{15,16} catalysts are shown in Figure 2 and explained below:



Grubbs 1st generation catalyst



Grubbs 2nd generation catalyst

Figure 2 Chemical structures for Grubbs 1st and 2nd generation catalysts.

Grubbs 1st generation catalyst was one of the first ruthenium based alkylidene catalysts to be widely used for ROMP. It was much more tolerant to different functional groups compared to the sensitive Schrock catalyst. However, the increased tolerance came with a decreased activity towards metathesis. Furthermore, it tended to produce polymers with a polydispersity index (PDI) of around 1.2^{13,17} which is good, but lower values closer to 1 are preferred.

PDI values are important as they show that ROMP is a controlled process that produces well defined polymers of similar weights and chain lengths. This control is dominated predominantly by kinetic effects where a fast rate of initiation compared to propagation leads to narrower PDI values.

Due to the decreased activity of Grubbs 1st generation catalyst compared to the Schrock catalyst, attempts were made to increase the activity of the ruthenium complexes which lead to the design of Grubbs 2nd generation¹⁵ catalyst. Grubbs 2nd contains the nitrogen based heterocyclic carbene ligand instead of the phosphane ligand used in Grubbs 1st. The nitrogen-based ligand is more electron donating and this was expected to result in the observed increase in activity of Grubbs 2nd. Although Grubbs 2nd provided greater activity towards metathesis, it was found to produce polymers with PDI values around 2.0¹⁶ for strained alkenes such as norbornene and oxanorbornene derivatives. This is due to the slow rate of initiation seen in Grubbs 2nd compared to its fast rate of propagation which can lead to chain-transfer reactions, affecting the PDI of the resulting polymer.

Table 1 Typical Polydispersity Index (PDI) values for common ROMP catalysts.

Catalyst	Typical PDI
Schrock	≈1.1 ¹⁸
Grubbs 1 st generation	≈1.2 ¹⁷
Grubbs 2 nd generation	≈2.0 ¹⁶
Grubbs 3 rd generation	<1.1 ¹

Grubbs 3rd was discovered¹⁹ after many attempts to improve catalyst activity. It was found to have initiation rates significantly greater than any other prior catalysts as well as a high rate of initiation/rate of propagation ratio. This makes Grubbs 3rd such a powerful catalyst as it is very tolerant, active and produces almost

monodisperse polymers with PDI values very close to 1¹. Approximate typical PDI values for polymers obtained by the various catalyst are shown in Table 1.

Although Grubbs 3rd is tolerant, it still must be treated with care, used quickly and kept under a nitrogen atmosphere whilst stored. If not stored correctly the catalyst will become oxidised and change from a green colour to a brown as shown in Figure 3 below:



Figure 3 Grubbs 3rd generation catalyst which is green when good (left vial) and brown when oxidised (right vial).

Grubbs 3rd generation catalyst is the most widely used catalyst for ROMP for the reasons mentioned above and was therefore the catalyst of choice for this project.

Monomer Design

ROMP monomers typically consist of three main components which are the polymerisable unit, linker and functional unit. This is depicted in Figure 4 below:

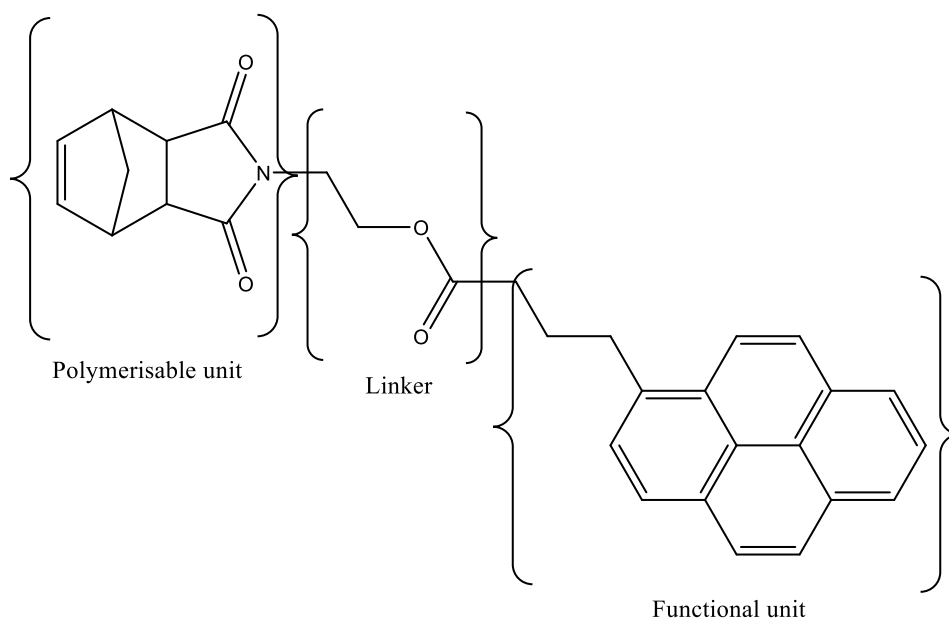


Figure 4 The three distinguishable sections of a typical monomer for ROMP - The Polymerisable unit, Linker and Functional unit.

Note: The monomer in Figure 4 above is not designed randomly but was in fact designed by Mukherjee *et al.*²⁰ and used as part of a copolymer. In this case the functional unit is pyrene which would make the monomer fluorescent and upon polymerisation could produce a fluorescent imaging probe.

Polymerisable unit

Norbornene is not very useful on its own as the only reactive functional group on the compound is the alkene, which is required for ring-opening. Thus, norbornene-based derivatives are used instead which contain reactive groups other than the alkene for further functionalisation. The most common norbornene and oxanorbornene based derivatives are shown in Figure 5.

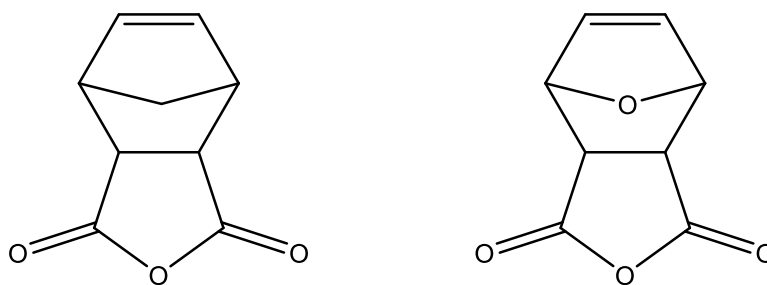
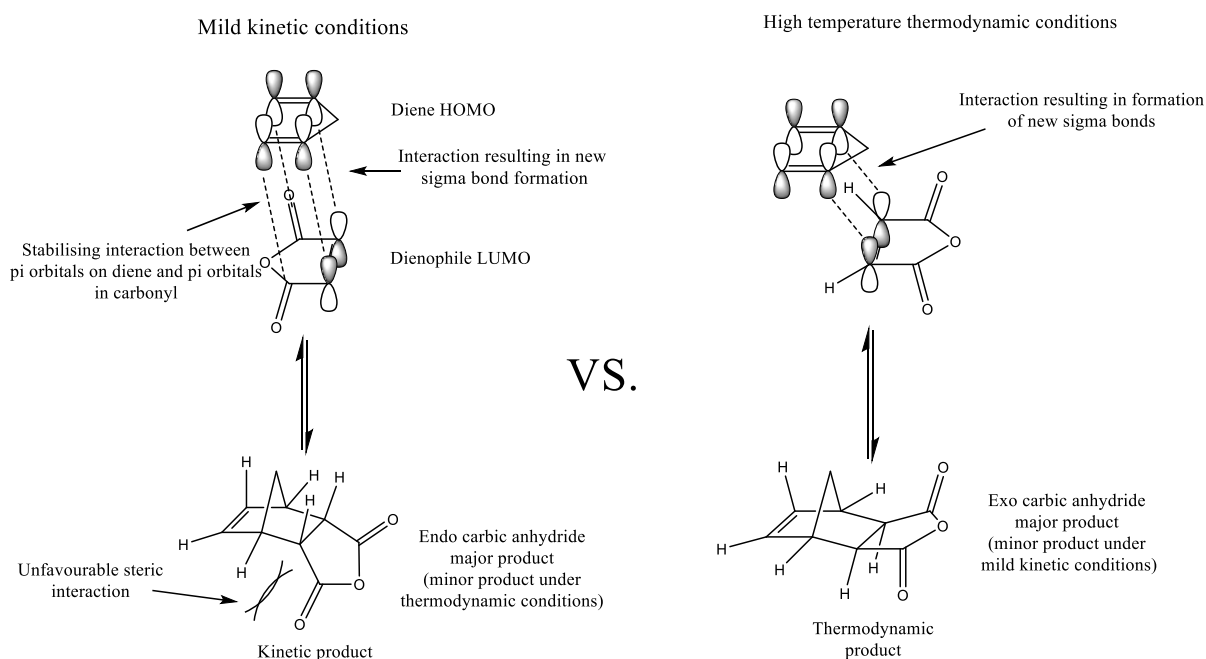


Figure 5 Carbic anhydride (left) and its oxygen-containing analogue (right).

The norbornene and oxa-norbornene derivatives in Figure 5 are key building blocks in the design of an effective monomer⁶. However, the stereochemistry of these derivatives is very important and hence the stereochemical control of their synthesis is crucial. These adducts are synthesised by a Diels Alder (DA) reaction that can give rise to both *endo* and *exo* isomers²¹⁻²³. The general conditions under which the isomers of the norbornene derivative, carbic anhydride, are formed is shown in Scheme 3 below:



Scheme 3 Frontier molecular orbital interactions leading to the kinetic (left) and thermodynamic (right) products for the Diels-Alder reaction between cyclopentadiene and maleic anhydride.

The *endo* adduct is favoured under mild conditions but due to the reversibility of the reaction via a retro-Diels Alder (rDA) pathway, the *exo* adduct can be favoured as the major product under thermodynamic conditions.

The *endo* isomer is favoured under mild conditions due to the lower activation energy compared to the *exo* as a result of the stabilising interactions between π orbitals on the diene and the π orbitals in the carbonyl bond. However, the steric interactions in the *endo* adduct mean that the *exo* adduct is lower energy and can therefore be formed preferentially despite its greater activation energy under thermodynamic conditions. This is contradicted by previous studies^{23,24} which claim that the *endo* adduct is slightly lower in energy. However, results from this project do not agree with these studies and therefore in this project, the *exo* isomer is considered the thermodynamic product.

It is imperative to isolate the *exo* adduct as the *endo* adduct does not polymerise well, mainly due to steric effects. This was demonstrated by Biagini *et al.*²⁵ and is shown in Figure 6 below which was adapted from the paper:

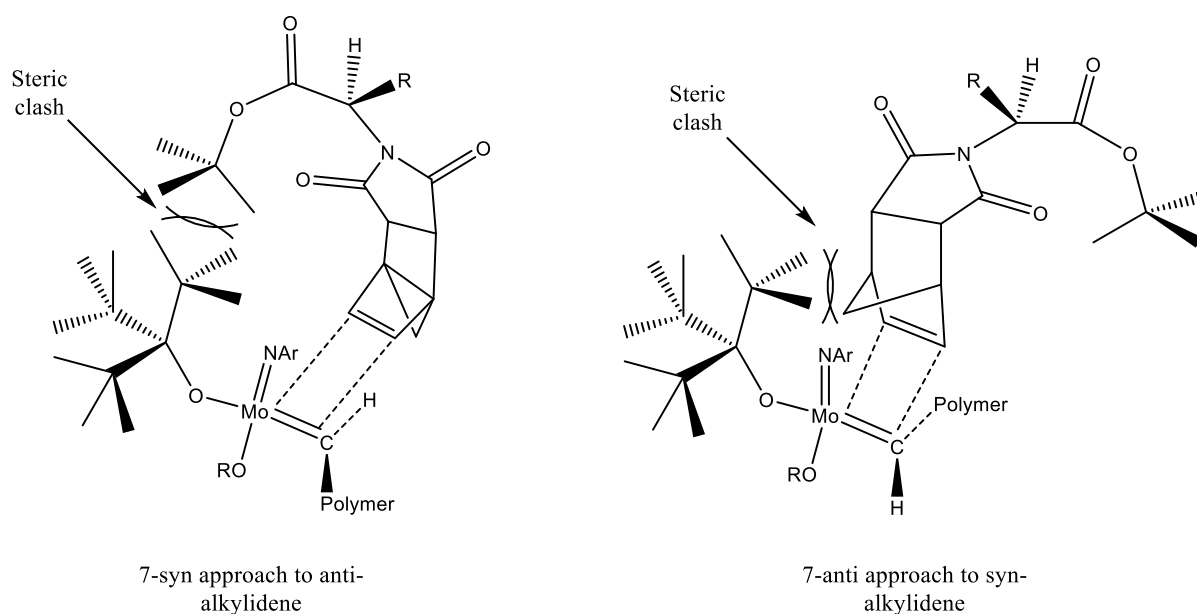


Figure 6 Representation of the steric clashes which result in poor reactivity for *endo* isomers.

From Figure 6 above it can be seen that polymerisation of an *endo* adduct can lead to some unfavourable steric clashes that result in very slow polymerisation rates²⁵ and in some cases no polymerisation. It is important to note that the specific catalyst used will have implications on the ability to polymerise an *endo* adduct¹. Grubbs 3rd generation catalyst has been shown to polymerise certain *endo* adducts due to its extremely high activity.¹ However, yields tend to be lower and adducts with bulkier linkers and functional units will still likely polymerise very slowly, if at all. Therefore, it is essential to build monomers from *exo* adducts. Although the *endo* adducts

do not undergo ROMP readily, it can be very useful to initially perform reactions on the *endo* adduct in order to avoid wasting the more precious *exo* adducts in failed attempts. This strategy was employed during this project in most cases, but polymerisations were only attempted using the *exo* adducts.

Although in the retro-Diels Alder equilibration reaction under thermodynamic conditions the *exo* adduct is the major product, it is still only present in a ratio of approximately 60:40 in terms of the *exo* and *endo* adducts respectively. Therefore, the isomerisation from *endo* to *exo* carbic anhydride and its subsequent isolation and purification is very important. Thus, an optimisation of the reaction was performed as part of this project and is detailed extensively.

The oxa-norbornene based derivative in Figure 5 above is also synthesised by a DA reaction but in contrast to the synthesis of carbic anhydride, the *exo* adduct is obtained under much milder conditions^{24,26}. The derivative is synthesised from the DA reaction between furan and maleic anhydride. Maleic anhydride is the starting material in the synthesis of carbic anhydride and so the stereochemical differences in the reactions stems from the difference in diene, which in this case is furan. Furan is a planar, heterocyclic and aromatic compound which is explained in Figure 7 below:

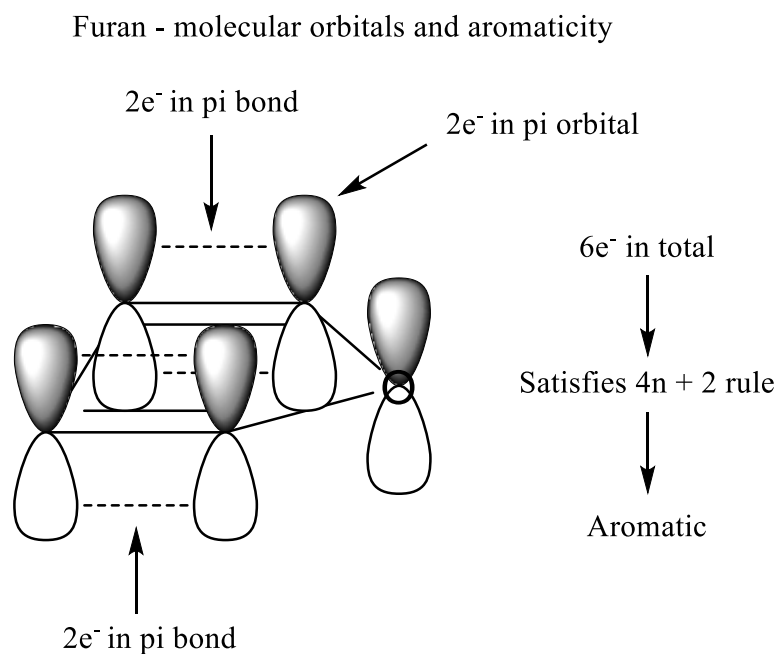


Figure 7 Representation of the pi orbitals in furan which result in its aromaticity.

The aromaticity in furan impacts its reactivity quite drastically as the stabilisation brought about by an aromatic system can be unfavourable to break. However, furan does still react with dienophiles such as maleic anhydride with relative ease. In fact, it favours the *exo* product under relatively mild conditions as the activation barriers for *endo/exo* are very similar but the final energy of the *exo* product is significantly lower and therefore more stable²⁴.

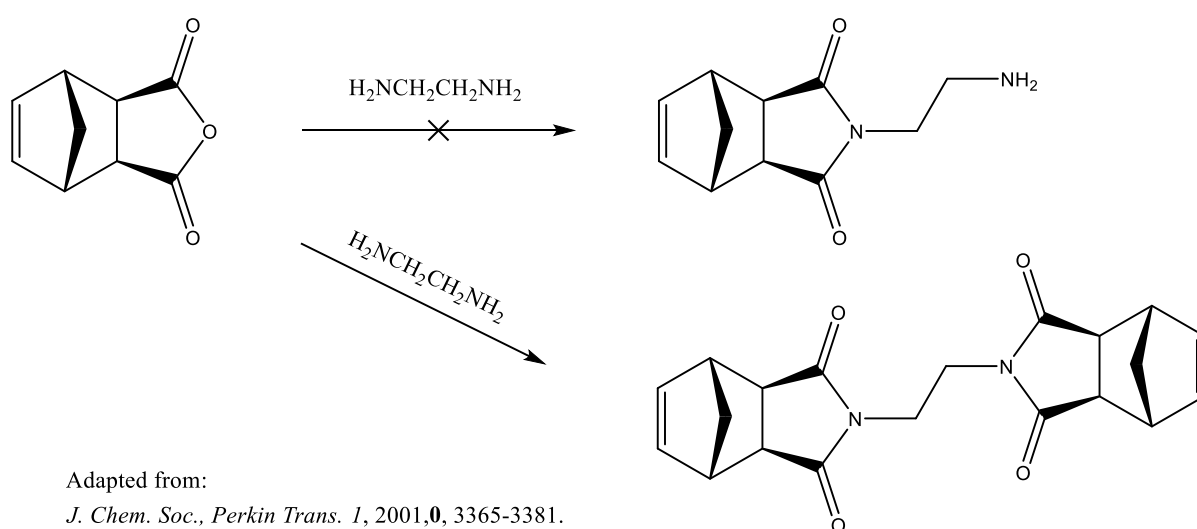
The synthesis and isolation of *exo* carbic anhydride may appear unnecessary when the *exo* oxa-norbornene adduct can be synthesised more easily²⁴. However, the energy of *exo* carbic anhydride is much lower than that of the oxa-norbornene adduct compared to their relative starting materials. This is significant as *exo* carbic anhydride is much more stable under harsher reaction conditions, making it suitable for a wider range of reaction conditions in subsequent reactions. The oxa-norbornene is much less stable and will undergo a rDA under much milder conditions due to the favourable aromatic stability of furan. Therefore, the importance of an efficient and effective synthesis and isolation of *exo* carbic anhydride is even more relevant and explains why it was worth exploring in this study.

Linkers

Linkers are key components in the design of functional monomers as they connect the norbornene polymerizable unit and the functional unit whilst providing some separation. Linkers can be quite long for flexibility or short to provide some increased density. There are many important decisions that must be made when choosing a linker for polymer design, especially in more complex cases when the linker has impactful implications on the properties of the polymer²⁰.

In this study several different linkers were synthesised for specific purposes including amino acid linkers, amino alcohols and diamines. Amino acid norbornene derivatives have been studied extensively^{6,27} in the past and therefore the synthesis and sometimes ROMP of these adducts are well detailed. The synthesis of derivatives utilising amino alcohol linkers are also well detailed in the literature^{4,28,29}. However, the synthesis and purification of derivatives containing diamine linkers are less well defined in the literature^{8,27,30-34}. Several procedures report vague descriptions for the purification of these adducts, whilst other procedures state that certain synthetic routes, such as the one shown in Scheme 4 below, were unsuccessful²⁷. Hence, the synthesis

and purification of a derivative containing an ethylenediamine linker was studied as part of this project to provide a greater understanding of this area.



Scheme 4 The reported reactivity of exo carbic anhydride with ethylenediamine where only the bis product was found to form.

Adding functionality

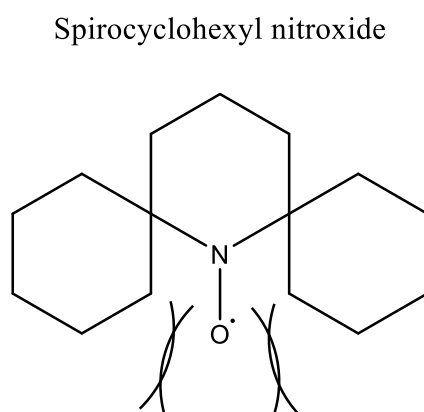
If there is compatible reactivity between the functional unit and the linker, the functional unit can be attached. This makes ROMP extremely versatile and opens the possibility of ROMP polymers to be used in a whole host of applications. These applications vary in breadth and scope however in relation to this project we were interested in the imaging capabilities of ROMP polymers *in vitro* and *in vivo*^{9,35}. Additionally, more ambitious studies into ROMP copolymers containing 2 or more imaging modalities have been conducted. Furthermore, polymers containing therapeutic functionalities have been employed. Some of these studies are described in further detail below.

Organic-Radical based Contrast Agents (ORCAs) for MRI

Gadolinium complexes are used as contrast agents because the paramagnetic gadolinium causes the relaxation time of the protons in the target tissue to shorten, making the tissue appear brighter. However, gadolinium is not the only paramagnetic substance that can be used as a contrast agent and there have been toxicity concerns regarding gadolinium³⁶ and its accumulation in organs and tissues such as the brain³⁷.

Organic radicals such as nitroxide radicals (NRs) can be used as a metal-free alternative, although a lot more design is required to make them a feasible option compared to gadolinium-based agents. Organic radicals such as NRs are paramagnetic due to their single unpaired electron. They can be used as positive contrast agents for T_1 images, shortening the relaxation time and causing the target tissue to appear brighter. There is a drawback to NRs in their sensitivity to redox in biological environments as they are easily reduced, rendering them useless as MRI contrast agents. However, ROMP copolymers have been employed to minimise the sensitivity of NRs, allowing them to become a feasible option as an MRI contrast agent.

Sowers *et al.*⁹ developed a nitroxide radical based ORCA through ROMP that can be used *in vivo*. The group were able to reduce the sensitivity of the ORCA to redox in two main ways. The first way involved incorporating the nitroxide radical into the ROMP macromonomer as spirocyclohexyl nitroxide (Figure 8).



Steric hindrance provides some protection
for the nitroxide radical.

Figure 8 General structure of the spirocyclohexyl nitroxide moiety.

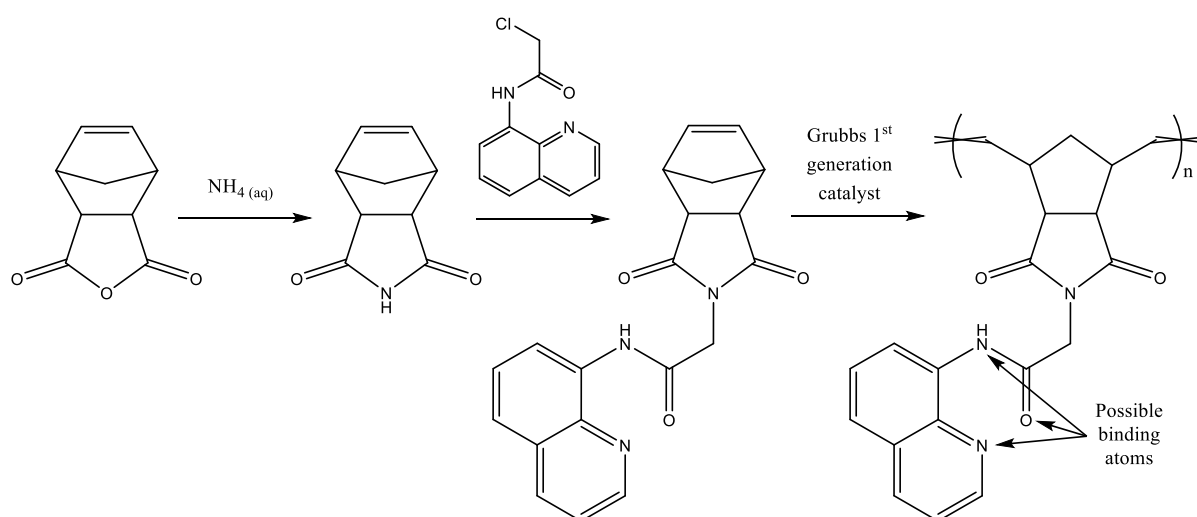
In this form, the nitroxide radical is harder to access as a result of the steric hindrance induced by the cyclohexyl rings. The use of ROMP created a branched-bottlebrush polymer architecture through self-assembly. Therefore, the longevity of the radical was also enhanced by the fact it was hidden at the core of the architecture, amongst long PEGylated branches.

Furthermore, by introducing the NR into a large polymer, they inherently increased the concentration of the NR significantly, resulting in an ORCA with an increased lifespan for MRI. These findings show that NRs, despite their sensitivity to redox, can be made into contrast agents that are tolerant to biological environments *in vivo*. Enhancement of contrast in MRI images were seen in certain organs of mice such as the aorta, renal pelvis, renal artery, renal vein and inferior vena cava. The enhancement was significant and reportedly not dissimilar to enhancement shown by other classes of completely organic MRI contrast agents.

Fluorescence imaging

Fluorescence imaging is one of the most popular imaging modalities utilized for ROMP polymers and there are many examples in the literature. This is due to the large variety of fluorophores that are commercially available and relatively cheap.

Yao *et al.*³⁸ wanted to find a fluorophore which would show noticeable changes in its fluorescence upon binding metal ions *in vivo*, specifically Hg^{2+} , Zn^{2+} and Cu^{2+} . They decided to use quinoline which was known to bind metal ions through several different binding modes. Norbornene based quinoline monomers were synthesised and homo-polymerised by ROMP (Scheme 5).



Scheme 5 Reaction scheme for the synthesis of a metal ion binding homopolymer as synthesised by Yao *et al.*³⁸, which starts from exo carbic anhydride.

These polymers were found to bind the desired metal ions with very noticeable fluorescent responses, where binding to Hg^{2+} resulted in a green emission, whilst Zn^{2+} and Cu^{2+} resulted in blue emission. This allowed the toxic

Hg²⁺ ion to be distinguished from the common non-toxic Zn²⁺ and Cu²⁺ ions. Further work on this area, developing copolymers could allow for these quinoline based monomers to be used *in vivo*.

Feng *et al.*³⁹ have designed co-polymers that can target specific organelles and simultaneously provide fluorescence imaging. This was achieved by synthesising several monomers which include a rhodamine-b based fluorescent monomer, a PEGylated monomer and a targeting peptide-based monomer. Statistical copolymerisation of the monomers in different ratios gave rise to well-defined copolymers (Figure 9).

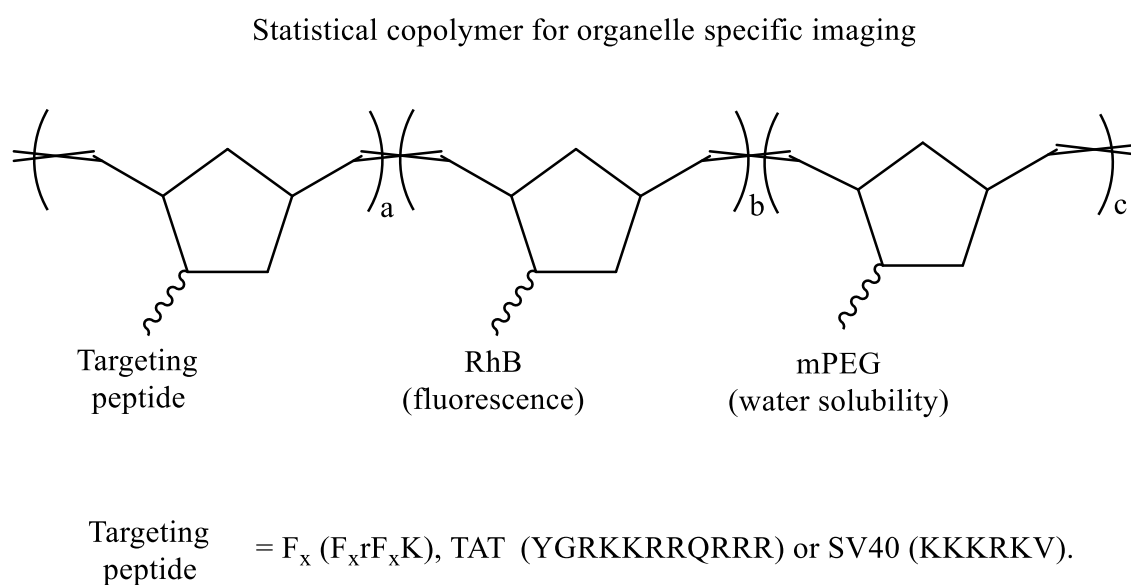


Figure 9 General structure of the statistical copolymers synthesised by Feng *et al.*³⁹ for organelle specific imaging.

The PEGylated monomer was essential to allow for water solubility of the polymers and rhodamine b is a very strong fluorophore. The targeting peptides varied depending on the organelle to be targeted and generally showed good targeting towards the desired organelles. This example shows how the ease of copolymerisation of ROMP monomers makes the synthesis of complex polymers a reality through careful design.

Multi-modal imaging

ROMP is a very versatile tool and as such, allowed Sowers *et al.*⁴ to develop the ORCA into a dual-modality imaging agent, which they coined an 'ORCAFluor'. As well as being an MRI contrast agent, the ORCAFluor, OF1, contained 1% Cy5.5 – MM, a macromonomer containing the dye Cy5.5 for Near-Infrared (NIR) fluorescent imaging. This design is incredibly powerful as it gives a much deeper insight into the body than MRI can provide independently. As previously discussed above, NRs are sensitive to redox (reduction) and *in vivo* this process usually occurs because of ascorbate. During the *in vivo* MRI imaging studies, it was found that no enhancement was seen in the liver and brain, both of which are organs in mice known to have high ascorbate concentrations, therefore quenching OF1 for MRI. However, upon reduction of the NRs in OF1, fluorescence increased significantly, allowing organs with high ascorbate concentrations that were previously not enhanced in MRI, to be viewed by NIR fluorescence imaging *in vivo*. This demonstrates the power of ROMP for imaging purposes, as two different modalities were employed to complement each other. This allowed for enhancement of MRI images, provided information on redox processes *in vivo* and gave full body NIR fluorescent images of live mice; and all of this done with a completely organic, metal-free ROMP polymer with low toxicity and good circulation time.

Theranostics

The example by Feng *et al.*³⁹ described above already shows how copolymers can target specific organelles and allow them to be seen by fluorescence imaging. The same research group took this concept further by deciding to introduce another monomer into the copolymer with the ability to induce apoptosis in cancer cells.⁴⁰ The monomers involved in the copolymer are norbornene derivatives and include rhodamine b for fluorescence, PEG for improved solubility, a peptide sequence for cell membrane penetration and the [KLAKLAK]₂ (KLA) peptide which induces apoptosis of cancer cells. In this case a targeting moiety was not required as the enhanced permeation and retention (EPR) effect⁴¹ provides sufficient accumulation in cancer cells, and the KLA peptide causes apoptosis through disruption of the mitochondrial membrane once within the cell, so no additional organelle targeting is required.

These examples show how complex and interesting ROMP polymers can become through clever design. Hence, these examples provided the motivation for this project which will investigate certain aspects at each stage of

monomer design and the synthesis of complex monomers that could be used for similar purposes as those described above in future work.

DNA Intercalation

A large proportion of studies on ROMP polymers, as discussed above, have been conducted with the aim of using the polymers for *in vivo* applications. Therefore, it is essential to understand how these polymers may behave when inside the body. When it comes to the use of planar, aromatic fluorophores such as rhodamine-b and proflavine, it is important to consider the interactions that these compounds may have with DNA. Proflavine and its derivatives are well known as DNA intercalators^{42,43}, which results in these compounds having antibacterial and anticancer properties. Rhodamine-b has also been shown to bind to DNA through intercalation^{44,45}, however there are far fewer studies compared to the case of proflavine and its derivatives. Whilst DNA intercalation can lead to beneficial antibacterial and anticancer properties, for the same reasons, it can also potentially be very harmful. Iverson *et al.* showed that polymers can intercalate DNA, however, similar studies on ROMP polymers containing potential DNA intercalators have not been reported. Therefore, if ROMP polymers containing potential DNA intercalators are synthesised, then determination of its intercalating ability may be necessary. This was the case for this project as rhodamine-b was selected as a functional unit to be incorporated into a monomer, and as described above, it is known to intercalate DNA.

Aims and Objectives:

Aims:

- To optimize the isomerisation of carbic anhydride along with a rigorous analysis of the product and its purity.
- To use the optimized isomerisation of carbic anhydride to produce the *exo* isomer in a sufficient quantity for subsequent reactions.
- To attach a selection of linker moieties to the *exo* carbic anhydride
- To identify and attach a suitable functional unit with imaging properties to one or more of the synthesized linker monomers, creating a complex monomer.
- To analyse and characterize the synthesized complex monomers, providing evidence to prove its existence.
- To polymerize the synthesized complex polymer as a homopolymer and potentially as a co-polymer.
- To analyse the synthesised polymer(s) using a variety of techniques.

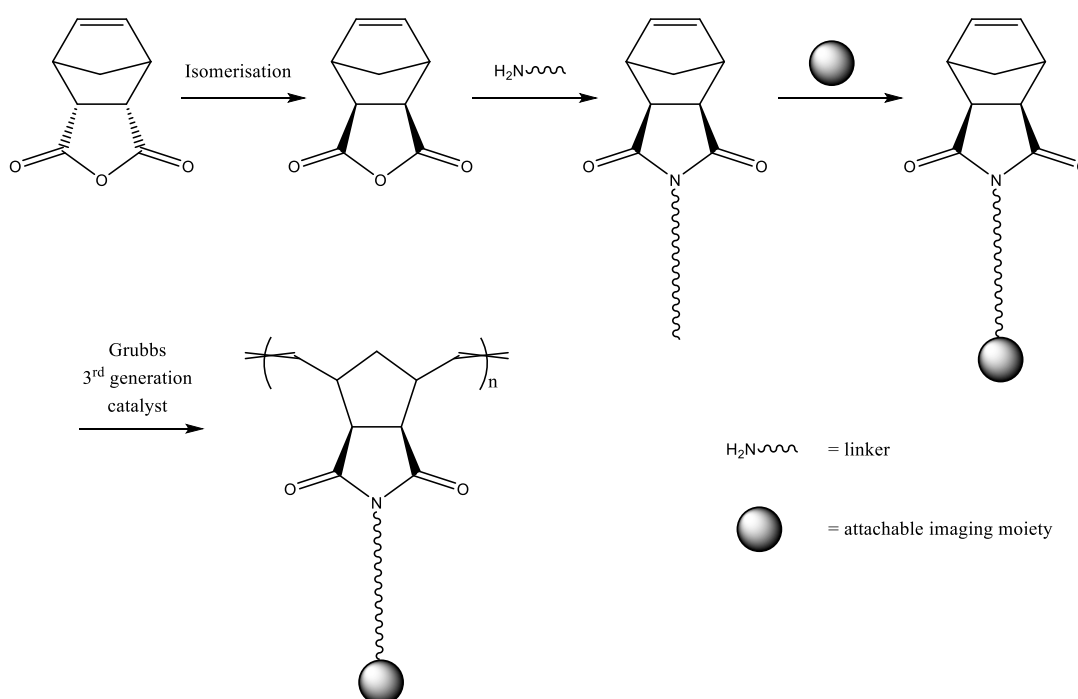
Objectives:

- To compare literature procedures used for the synthesis of carbic anhydride, identifying reaction conditions, solvents and purification steps used. To repeat experimental procedures and identify which aspects can be improved upon or detailed more thoroughly. To use various techniques such as ^1H NMR and GC-MS to distinguish between the *endo* and *exo* isomers, allowing for quick and easy product analysis.
- To use the optimized procedure, using a large amount of starting material, in order to yield a sufficient quantity of *exo* carbic anhydride and show that the procedure can work on a large scale.
- To identify linker moieties that are suitable for attachment to *exo* carbic anhydride. To attach the various linkers to carbic anhydride using suitable reactions obtained from the literature.
- To search the literature for examples of imaging moieties, particularly identifying one that is attachable to the synthesized linkers through compatible reactivity. To use *endo* isomers to obtain practice with

before attempting reactions with *exo* isomers which are much more precious. To provide a route from the *exo* carbic anhydride to a complex monomer which should have imaging capabilities.

- To use ^1H , COSY, ^{13}C and HSQC NMR techniques to make reasonable arguments that prove the complex monomers were synthesized. To obtain crystal structures of the complex monomers where possible to provide more decisive evidence.
- To use Grubbs 3rd generation catalyst to polymerise the complex monomers after first practicing with a less precious monomer. To copolymerize the complex monomers if more than one complex monomer is synthesized, using both/either, statistical or block copolymerization techniques.
- To utilize ^1H NMR to initially determine if polymerization has occurred and perform end group analysis if possible. To use gel permeation chromatography (GPC) techniques to determine polydispersity index (PDI) values for the polymers as well as M_n and M_w values for approximate determination of chain length. To use dynamic light scattering (DLS) to determine the size of the polymers in solution which may hint towards the occurrence of self-assembly.

A general reaction scheme for the synthesis of complex monomers, used during this project is shown below:



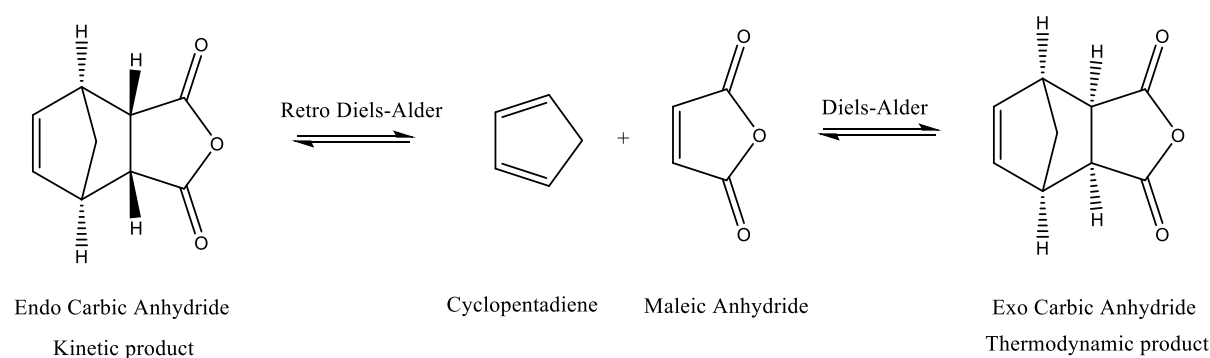
Scheme 6 General reaction scheme for the synthesis of complex monomers containing imaging moieties to be used for ROMP.

Results and Discussion:

Optimising the thermal isomerization of carbic anhydride:

Carbic anhydride is an important compound which is used as the starting point in the synthesis of many interesting monomers for ROMP. The *endo* isomer of carbic anhydride, which is commercially available and very cheap, does not perform well in ROMP as previously reported²⁵. However, it is non-trivial to isomerise to the *exo* isomer as the reaction is low-yielding and typically involves toxic solvents such as benzene for recrystallisation. The lack of a reliable, easy to follow procedure for this isomerization has prompted many groups^{20,38} to purchase the expensive *exo* isomer commercially (Sigma Aldrich – *cis*-5-norbornene-*exo*-2,3-dicarboxylic anhydride 95%) rather than performing the isomerization themselves.

Endo carbic anhydride is the kinetic product of the Diels-Alder reaction between cyclopentadiene and maleic anhydride. It is preferentially formed during the standard Diels-Alder reaction due to the frontier molecular orbital interaction and stabilisation between the p-orbitals in the C=O of maleic anhydride and those in the C=C bonds of cyclopentadiene. Although the *endo* isomer is formed as the major product under standard Diels-Alder reaction conditions, it is slightly less thermodynamically stable than its *exo* counterpart due to steric interactions. Therefore, the thermodynamically more stable *exo* isomer can be formed as the major product in the reversible thermal isomerisation of *endo* carbic anhydride. The *endo* undergoes a retro Diels-Alder reaction, giving the starting materials cyclopentadiene and maleic anhydride, which then go through a higher energy Diels-Alder pathway to form the thermodynamic product as shown in Scheme 7.



Scheme 7 Reaction scheme for the isomerisation of *endo* carbic anhydride to *exo* carbic anhydride. The cyclopentadiene and maleic anhydride exist temporarily, as the Diels-Alder reaction occurs very readily under the reaction conditions.

Due to the reversible nature of the isomerisation, *exo* is formed as the major product but a large amount of *endo* persists. A study²³ into the thermodynamics of the *endo/exo* isomers estimates that the *endo* is more stable by only 0.7 kcal/mol whereas the transition state for the *endo* is 2.5 kcal/mol more stable than the *exo*. However, experimentally the estimated greater stability of the *endo* isomer is contradicted by an equilibrium ratio of 55%:45% *exo:endo* respectively under thermodynamic conditions (170 °C). If the *endo* isomer were to be the thermodynamically more stable as estimated, even only by 0.7 kcal/mol, then at equilibrium it should be the major product, which is not the case experimentally. Regardless of which product is most stable, the close similarity in thermodynamic stability of both products explains why the thermal isomerisation is low yielding.

As a result of having such similar energies and the thermal isomerisation producing ratios of only around 55%:45% *exo:endo* respectively; the real challenge is the isolation of the *exo* isomer from the crude reaction mixture. Previously reported procedures such as the one from Matson and Grubbs⁴⁶ have used solvents such as benzene for the recrystallisation of the *exo* isomer. Cole *et al.*⁴⁷ also used benzene as the recrystallisation solvent but more interestingly performed the reaction in 1,2-dichlorobenzene. This reaction solvent is a practical choice, as its boiling point (179 - 180 °C) is sufficiently high for the isomerisation to take place compared to other solvents of similar structure, such as toluene (Boiling point: 110 - 111 °C). However, both benzene and 1,2-dichlorobenzene are undesirable solvents in terms of their toxicity and their environmental impact. Therefore, an optimized method should avoid such solvents and make use of safer and cleaner alternatives.

The first reported procedure by Craig²¹ for the isomerisation of carbic anhydride used no solvent and heated the *endo* neat in an oil bath (190 °C), followed by recrystallisation with benzene. Subsequent research, such as that by B. Shin *et al.*⁴⁸ utilized a slightly modified method where the *endo* was heated neat (185 °C) for 4 hours and the crude product was recrystallized using ethyl acetate.

Analysis procedure and examples

Before describing the optimized procedures developed, it is necessary to describe how the data recorded from the NMR & GC-MS were interpreted; as the data collected using these techniques played an important part in the optimization process.

¹H NMR analysis

The annotated ¹H NMR and COSY of commercial *endo* carbic anhydride are shown below:

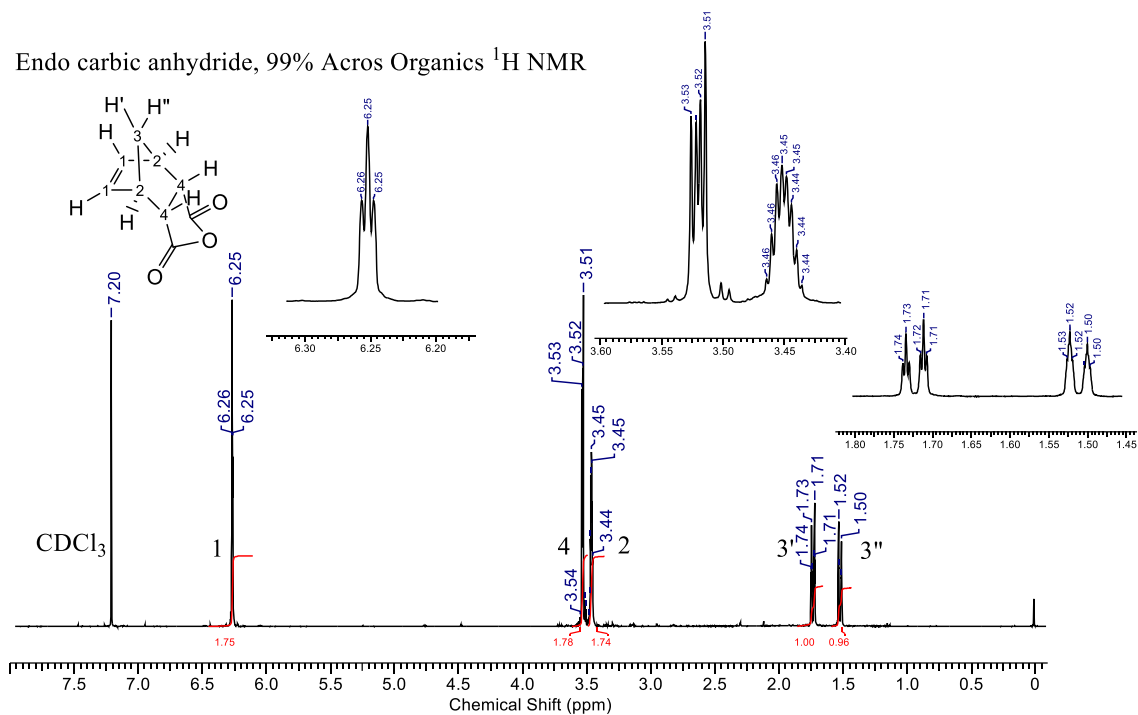


Figure 10 Annotated ¹H NMR of *endo* carbic anhydride as bought from Acros Organics.

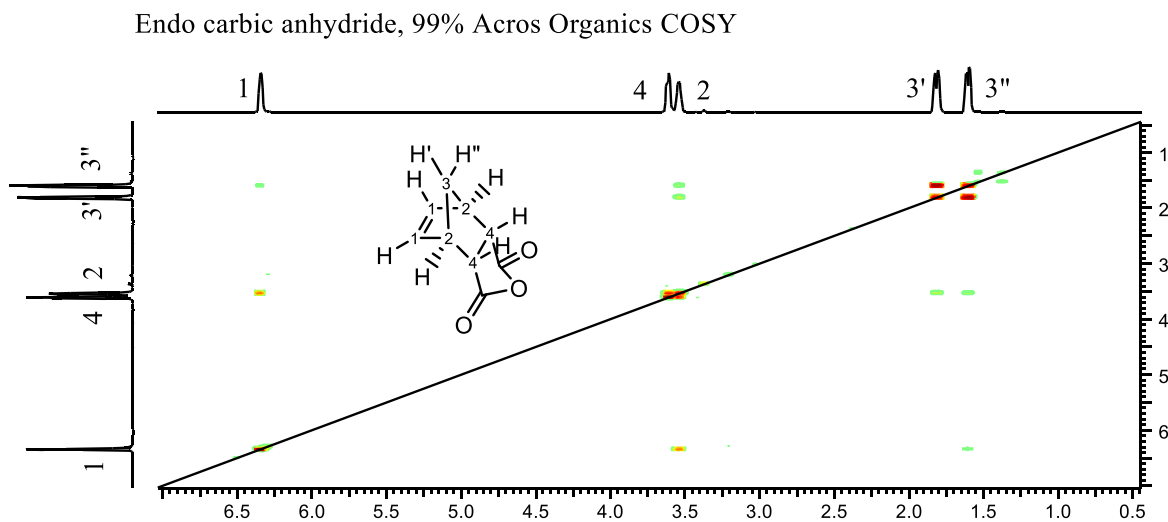


Figure 11 Annotated COSY NMR of *endo* carbic anhydride as bought from Acros Organics.

The easiest peak to assign for carbic anhydride is peak 1 as the hydrogens on the alkene are deshielded as a result of the pi-bond and it is well documented that hydrogens on an alkene appear within this ppm range. Therefore, it is a good starting point for piecing the molecule together using COSY NMR. From the COSY, 1 is coupling to peak 2 as well as a weak coupling to peak 3". From this we can deduce that 2 is the hydrogen on the adjacent carbon as three bond coupling is strong and long-range coupling is not normally observed. However, in this rare case, long-range coupling between the alkene hydrogen and the bridgehead hydrogen, 3", is observed due to w-coupling. W-coupling is seen in rigid systems like carbic anhydride where the four bonds (H – C – C – C – H) are stuck in a 'W-like' arrangement where there is weak overlap between the anti-bonding orbitals of both C-H bonds. This phenomenon allows the bridgehead hydrogens to be distinguished, which are in chemically different environments due to the rigidity of the compound.

In non-rigid compounds where free rotation is allowed, what is seen on the ^1H NMR is an average value associated with the environment felt by all the protons attached to a specific carbon atom. In rigid compounds such as carbic anhydride where free rotation cannot occur, the hydrogens are in chemically distinct environments and second-order effects are observed. If peaks 3' and 3" were chemically equivalent, then only one average peak would be observed in the middle of peaks 3' and 3". As the two hydrogens are not in chemically equivalent environments, their peaks separate from the average mid-point and they couple with each other, resulting in the two observed doublet peaks, 3' and 3". As a result, they exhibit a 'roofing effect' (Figure 12 below) which is distinctive for systems that exhibit second order effects. The extremity of this 'roofing effect' depends on the similarity in the chemical environments of the protons. In systems where the protons are very close to being equivalent the 'roofing effect' is more pronounced. In the case of *endo* carbic anhydride, the roofing is less drastic, showing that the hydrogens are less close to being equivalent.

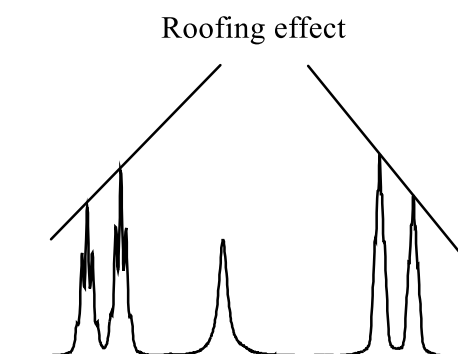


Figure 12 Representation of the 'Roofing effect' seen in ^1H NMR spectra as a result of second order effects.

The assignment of peak 3'' is confirmed further by its three-bond coupling to peak 2 which is shown by the COSY but is too weak to be seen on the ¹H NMR. This weak coupling can be explained by the Karplus equation⁴⁹ which describes the relationship between the dihedral angle in a three-bond coupling and the expected magnitude of the coupling. According to the Karplus equation, a dihedral angle of 90° will give the lowest possible coupling constant, *J*. Deviation from 90° towards 180° gives the greatest coupling constants due to the antiperiplanar conformation of the bonds that provides the best overlap of antibonding orbitals. Deviation towards syn-periplanar at 0° also provides greater coupling constants compared to 90°, but the overlap is not as good as an antiperiplanar system. Using Crystal Maker software and the crystal structure of *endo* carbic anhydride⁵⁰, the dihedral angle between hydrogens 3'' and 2 was calculated to be 65.2°. This dihedral angle is closer to 90° than 0° and explains why the coupling constant, *J*, is so small that it is not observable by ¹H NMR under the conditions used.

Since peak 3'' was assigned, peak 3' can consequently be assigned as it has the two-bond coupling with peak 3'' and the three-bond coupling with peak 2 which are shown by the COSY. Unlike with hydrogen 3'', the coupling between hydrogen 3' and 2 is strong enough to be seen by ¹H NMR, resulting in peak 3'' being a doublet of triplets. This is further confirmed by calculations from the crystal structure which shows the dihedral angle between hydrogen 3' and 2 to be 61.7°. Despite it only getting closer to 0° compared with the dihedral angle between hydrogen 3'' and 2 by only 3.5°, it is enough to increase the strength of the *J* coupling, making it visible by ¹H NMR. However, the *J* coupling is still weak at *J* = 1.58 Hz.

Unlike with hydrogen 3'' where it exhibits some long-range w-coupling with hydrogen 1, hydrogen 3' does not exhibit the same long-range coupling as there is not a hydrogen in the w-coupling arrangement. This is due to the fact that it is the *endo* hydrogen and therefore the four bonds (H_{3'} – C – C – C – H₄) are not in a 'W-like' arrangement.

Finally, peak 4 can be assigned as it is coupled only to peak 2 in the COSY which agrees with expectation as hydrogen 2 is the only hydrogen three bonds away for it to couple with. Furthermore, as described above, there is no long-range coupling between hydrogen 4 and 3'. Despite the COSY only showing hydrogen 4 coupling with hydrogen 2, which would expect to result in a triplet, according to the 'n+1' rule, the ¹H NMR shows a quartet of peaks exhibiting 'tilting' like you would expect with the 'roofing effect'.

This hasn't been fully understood but is likely the result of long-range coupling within the norbornene that is not entirely obvious. This issue does not affect the ability to assign the peaks to the structure correctly. On the other side of the molecule, hydrogen 1 does exhibit the triplet from the three-bond coupling as expected by the 'n+1' rule. The magnitude of the coupling is $J = 1.83$ Hz and the dihedral angle between the coupling protons 1 and 2 is 21.4° as calculated from the crystal structure. As expected, the coupling is greater than that between 2 and 3' which had a dihedral angle of 61.7° . However, even with such a large change in dihedral angle the coupling is not much greater in magnitude. This can be put down to the *syn* relationship not providing good orbital overlap, even at an angle like 21° .

Having assigned the ^1H NMR of the *endo* isomer, the ^1H NMR of the *exo* isomer can be looked at and compared:

Exo carbic anhydride ^1H NMR

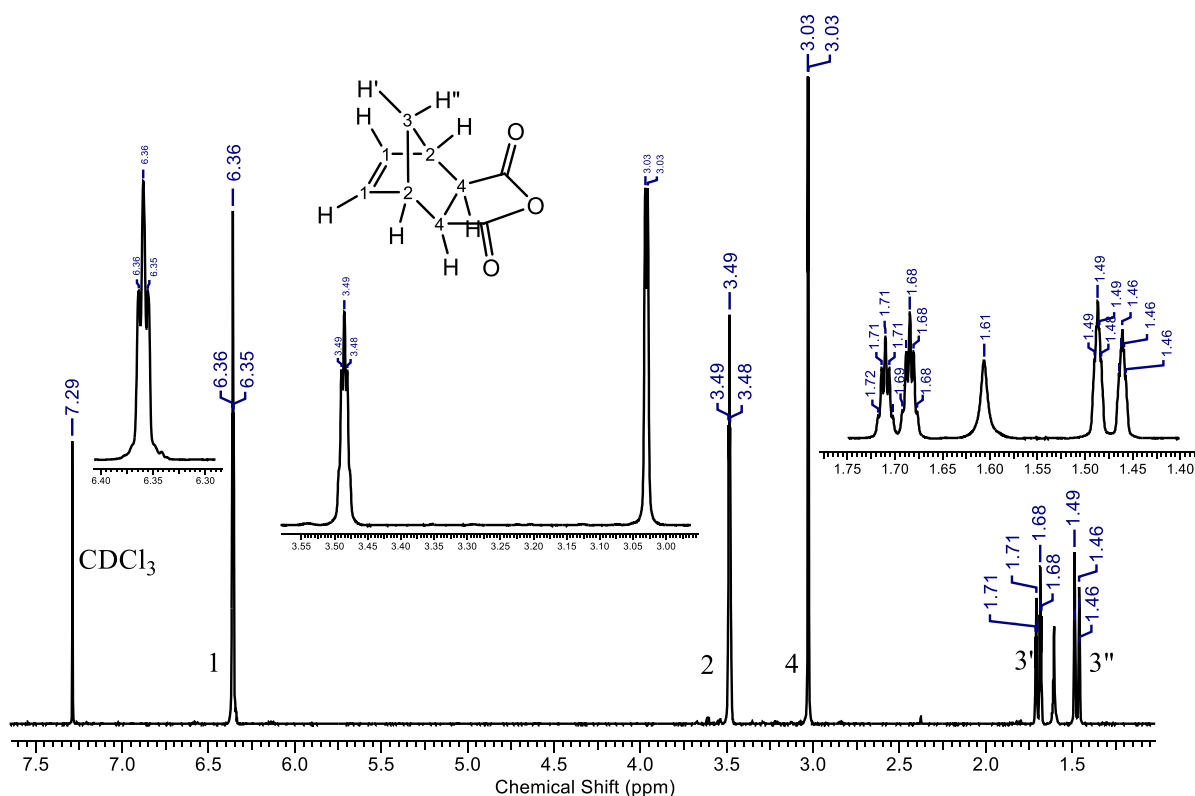


Figure 13 Annotated ^1H NMR spectrum of exo carbic anhydride.

Exo carbic anhydride COSY

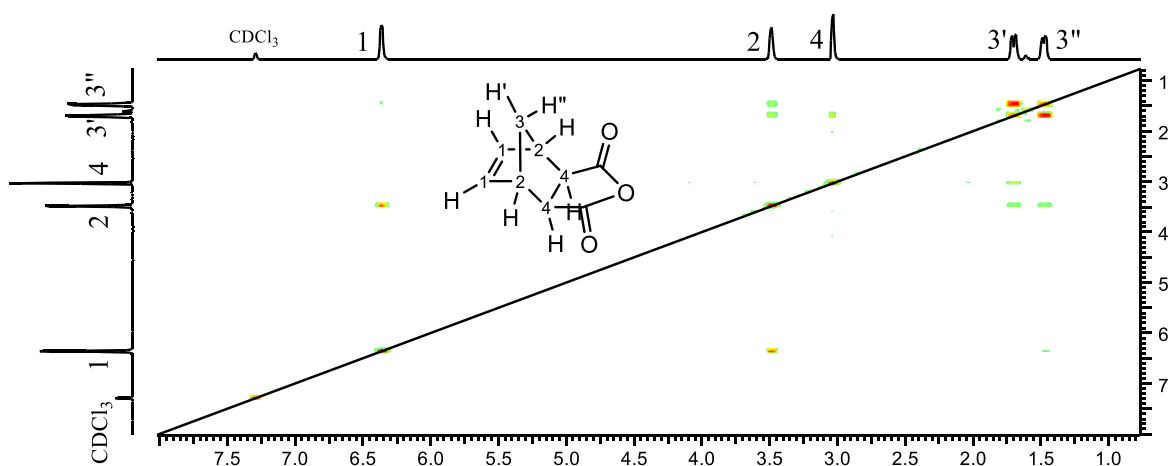


Figure 14 Annotated COSY NMR spectrum for exo carbic anhydride.

As with the *endo* isomer, the protons on the alkene are easiest to assign as peak 1 for the same reasons and therefore can be used as a good starting point to assign the ^1H NMR using COSY. From the COSY, peak 1 is coupling to peak 2 and peak 3'', with peak 2 being the strongest coupling. As with the *endo*, 2 must therefore be the proton environment on the carbon adjacent to 1 due to the three-bond coupling. Furthermore, some very weak W-coupling is present with proton 3'', which distinguishes proton environment 3'' from 3' on the bridgehead. Having assigned peak 3'', peak 3' can be assigned as the other bridgehead proton, which can further be confirmed by its coupling to peak 4 on the COSY.

This coupling to peak 4 is another example of W-coupling, although this W-coupling is stronger than the example between 1 and 3'', due to the less distorted 'W-like' arrangement. This is different from the *endo* isomer where there was no W-coupling with the bridgehead proton closest to the alkene. This provides strong evidence for the *exo*, as the 'W-like' arrangement for W-coupling is only possible in the *exo* isomer. Having deduced the assignment of peak 4 through process of elimination and its W-coupling to peak 3', it is interesting to note that the COSY shows no sign of 4 coupling to 2 through a common three-bond coupling. This seems strange at first but using the crystal structure of the *exo* which was collected (Figure 15), the dihedral angle between 2 and 4 was found to be 75° . This 75° angle provides very little orbital overlap for coupling to occur, therefore explaining why none was seen on the COSY. Furthermore, it makes sense why peak 4 is a doublet, as it is only visibly coupling to peak 3' through the W-coupling as described, with $J = 1.46$ Hz.

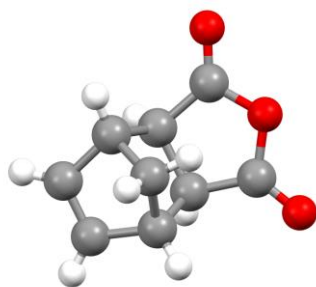
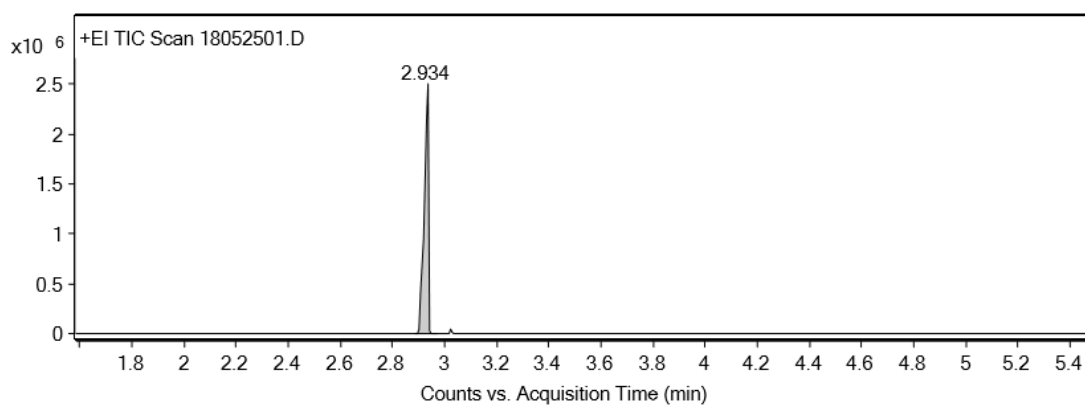


Figure 15 Crystal structure of the exo isomer of carbic anhydride.

The only unassigned peak at $\delta = 1.61$ was thought to possibly be some solvated water in the crystal structure. This was dismissed as a single crystal x-ray diffraction experiment was conducted on the sample which found no water in the crystal structure. Therefore, it is expected to instead be a small trace of water absorbed onto the surface of the crystals. The same deuterated solvent was used to analyse other samples and no peak at $\delta = 1.61$ was present, thereby dismissing the possibility of it being a result of wet solvent.

GC-MS analysis

Having confirmed the presence of exo by single crystal XRD and ^1H NMR, GC-MS measurements were run on the same sample, providing the following results:



Integration Peak List

Peak	Start	RT	End	Height	Area	Area %
1	2.887	2.934	2.97	2507099	2714883.13	100

Figure 16 GC trace of purified exo carbic anhydride.

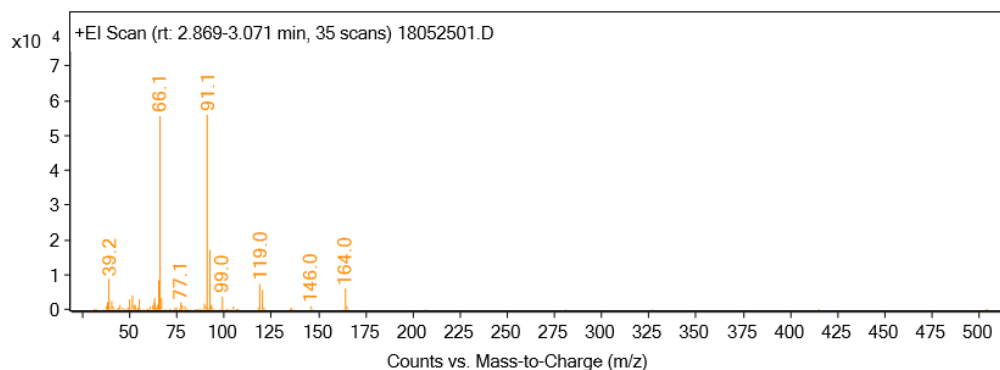
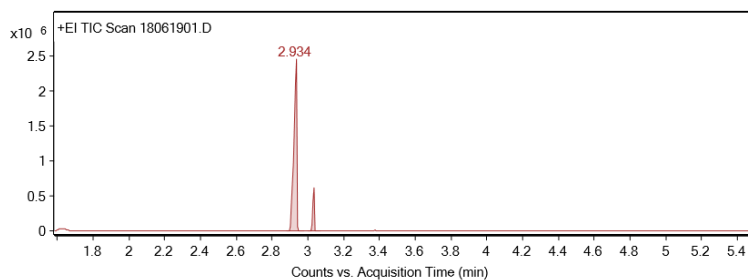


Figure 17 Mass spectrum of purified *exo* carbic anhydride.

Looking at the GC trace above, the main peak at 2.943 min must be indicative of the *exo* isomer as its presence was confirmed by NMR and XRD. The main peak was present at 100% as calculated from the integration of peaks determined by the software. A very small peak is visible just after 3 min which must be a small trace of *endo*, however it was not considered large enough by the software to be integrated. Therefore, it is reasonable to say that this sample is >99% pure. Further evidence of the peak at 2.943 min being carbic anhydride is the MS spectrum shown above, where the parent ion peak is at $m/z = 164$, the monoisotopic mass of carbic anhydride. The peak at $m/z = 66.1$, which is one of the most abundant and therefore most stable fragments is indicative of cyclopentadiene.



Integration Peak List						
Peak	Start	RT	End	Height	Area	Area %
1	2.881	2.934	2.976	2464920.79	2701316.16	100
2	3	3.035	3.071	614918.3	412472.8	15.27

Figure 18 GC trace of a crude sample containing both *exo* and *endo* carbic anhydride.

Having obtained GC-MS results from a sample of pure *exo*, a crude sample was run on the GC-MS in order to ensure that the *exo* and *endo* isomers were not coming off at exactly the same time. The results of the GS-MS analysis of the crude sample along with a ^1H NMR of the same sample are shown below:

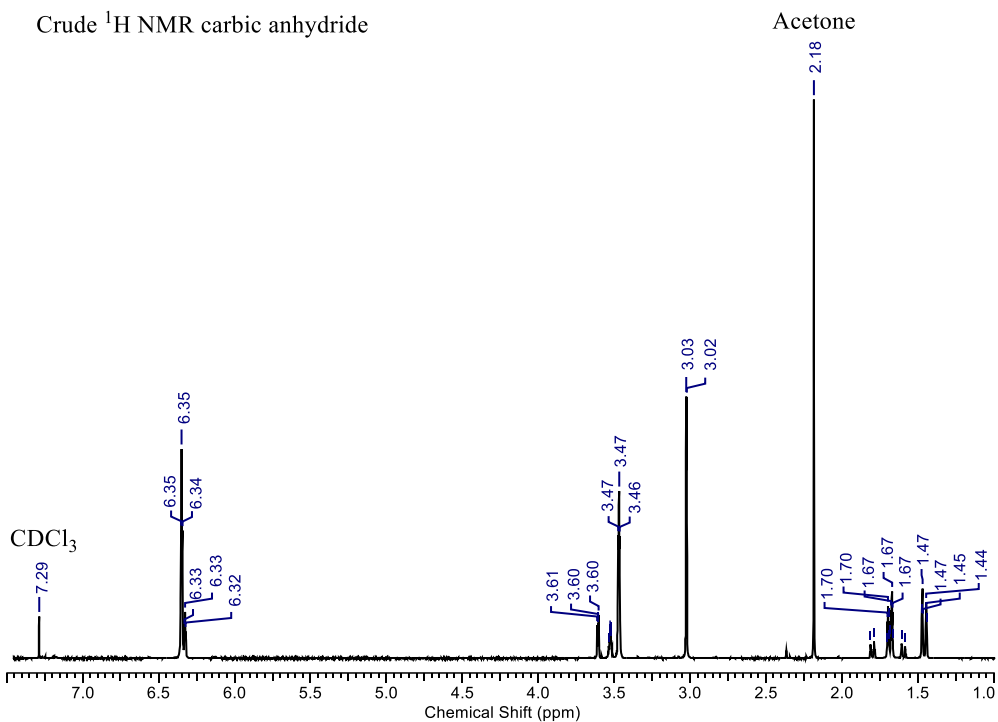


Figure 19 ^1H NMR spectrum of a crude sample containing both *exo* and *endo* carbic anhydride.

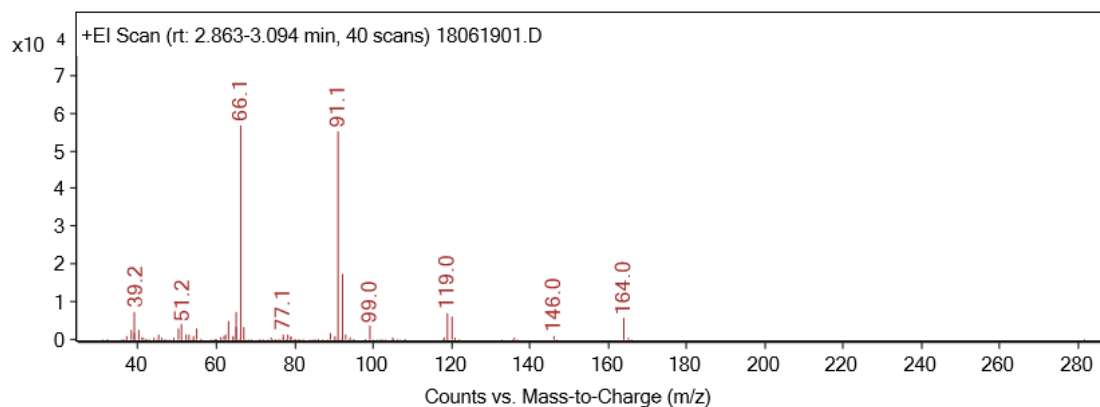


Figure 20 Mass spectrum of the crude sample containing both *exo* and *endo* carbic anhydride.

From the ^1H NMR of the crude mixture (Figure 19), it is possible to see that there is more *exo* present than *endo*. The most distinctive peak that indicates *exo* is the peak at $\delta = 3.03$ as it is the environment that changes the most when comparing *endo* to *exo*. The alkene peak is in almost the identical place and the bridgehead peaks are shifted slightly upfield in the *exo* compared to the *endo*. By looking at the GC trace (Figure 18), the peak at

3.035 min is much larger in the crude sample, compared to the pure sample which is expected. The ratios of the peaks in the NMR are also similar, indicating that the peak at 3.035 min in the GC is in fact the *endo*. This was further confirmed by the MS (Figure 20) which contained the parent ion peak for carbic anhydride at $m/z = 164.0$. It is also worth noting that upon inspection of a crude crystalline mixture containing both *endo* and *exo* under microscope, the isomers can be distinguished by their morphology. A plate-like crystal from the crude was screened by single crystal XRD and gave parameters indicative of the *endo*. A needle-like crystal was then screened by single crystal XRD and gave parameters indicative of the *exo*.

Using the GC-MS integration values calculated by the software for the crude mixture above as an example, the % of *exo* in the sample can be determined as shown below:

$$\begin{aligned} \text{Exo}\% &= \frac{\text{Area \%}_{RT=2.934(\text{Exo})}}{\text{Area \%}_{\text{Total}}} \times 100 = \frac{\text{Area \%}_{RT=2.934(\text{Exo})}}{\text{Area \%}_{RT=2.934(\text{Exo})} + \text{Area \%}_{RT=3.035(\text{Endo})}} \times 100 \\ &= \frac{100}{100 + 15.27} \times 100 = 86.8\% \end{aligned}$$

Equation 1 Calculation of purity of exo carbic anhydride using GC analysis.

T₁ analysis and GC-MS comparison

T_1 analysis was conducted on a crude mixture so that the integration values from ^1H NMR could be used to determine an approximate ratio of *exo:endo*. Peaks from the *endo* that have very similar T_1 values to peaks in the *endo* can be used to determine the better approximate ratios. Peaks with very dissimilar T_1 values will not give very accurate ratios and should not be used. Some results from the T_1 measurements are shown below:

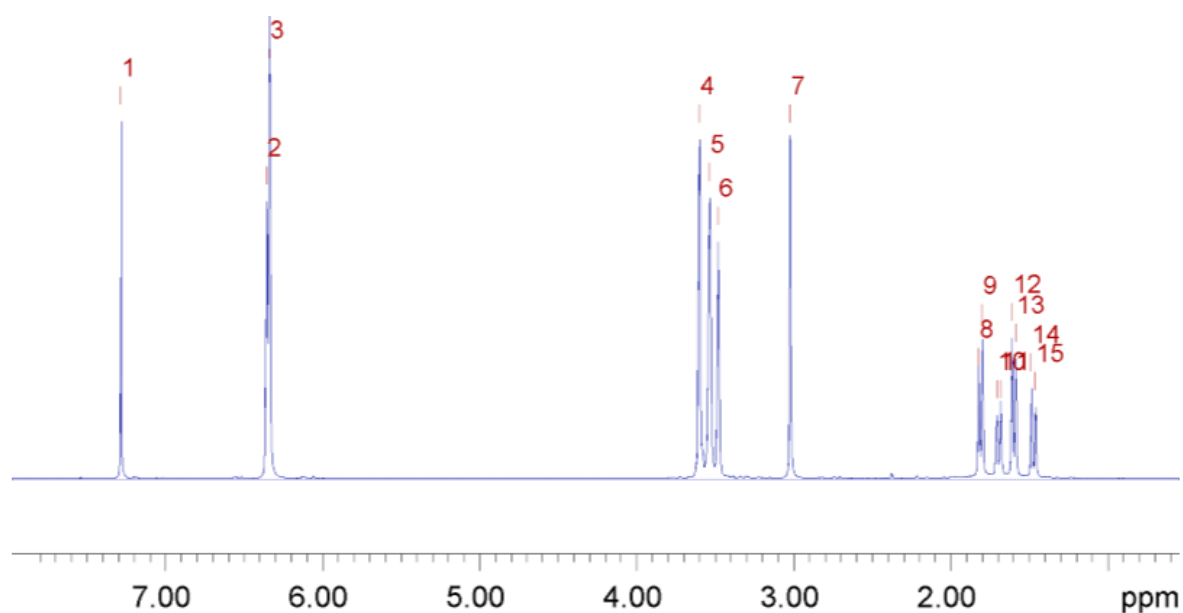


Figure 21 Annotated ^1H NMR of a crude sample containing both *exo* and *endo* carbic anhydride for T_1 analysis.

Table 2 T_1 values for each individual peak that is labelled in Figure 23 along with their respective error values.

Peak name	F2 [ppm]	T1 [s]	error
1	7.284	7.78	0.1368
2	6.355	5.10	0.02613
3	6.338	5.50	0.02732
4	3.600	5.01	0.02700
5	3.535	4.83	0.01921
6	3.481	4.96	0.02585
7	3.021	5.40	0.02017
8	1.820	2.89	0.01266
9	1.798	2.88	0.01205
10	1.705	2.57	0.007416
11	1.679	2.59	0.008450
12	1.607	2.74	0.01236
13	1.586	2.74	0.01720
14	1.486	2.70	0.01505
15	1.460	2.72	0.01432

From the T_1 results (Table 2), the peaks that can be compared to give the best approximate ratio are peaks '12 & 13' (2.74 & 2.74) and '14 & 15' (2.70 & 2.72) which are both representative of the same bridgehead proton environment in the *endo* and *exo* respectively. The difference in T_1 between 12 and 14 is only 0.04 s and between 13 and 15 only 0.02 s. Therefore, comparing the ^1H NMR integration values of 13 and 15 from the crude sample measured by GC-MS above, which are 0.09 and 0.44 respectively, results in an *exo* content of 83 %.

The values for the % of *exo*, determined both by GC-MS (86.8 %) and from the NMR integration calculations (83 %) are only different by around 4 %. Therefore, it is possible to use the integration of the peaks mentioned above to quickly calculate an approximate *exo* %. This allows people who don't have access to GC-MS, the ability to obtain an approximate value for the purity of their sample using this method.

Assigning the ^{13}C NMR:

The ^{13}C NMR spectra for compounds synthesized during this project were assigned using a combination of fundamental NMR concepts as well as HSQC and DEPT NMR techniques. An example of how these techniques were used is shown and described below in Figure 22 for *exo* carbic anhydride. However, explanations for other compounds will not be provided and instead assignments are shown in the experimental section.

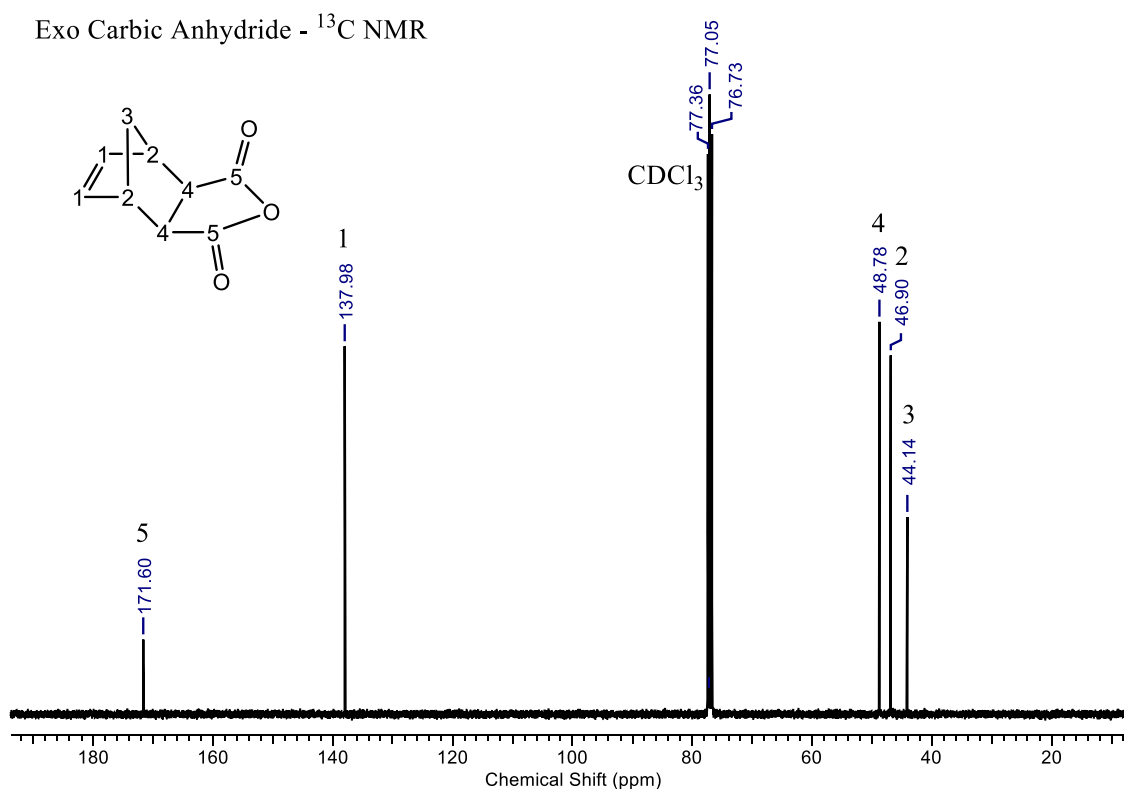


Figure 22 Annotated ^{13}C NMR spectrum of *exo* carbic anhydride.

Exo carbic anhydride - HSQC NMR

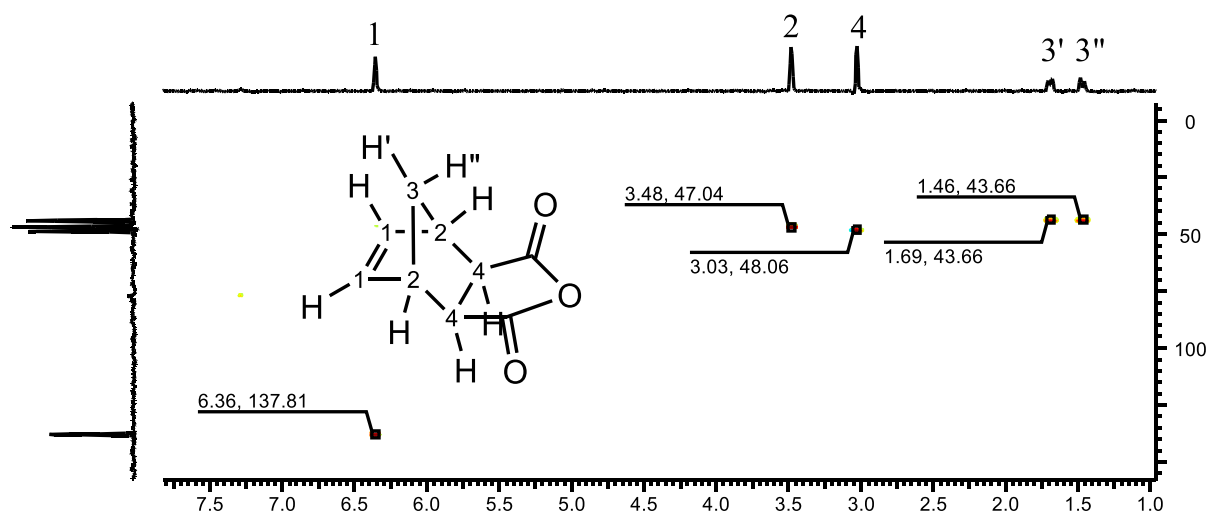


Figure 23 Annotated HSQC NMR spectrum for exo carbic anhydride.

Having already assigned the ^1H NMR for exo carbic anhydride, the assignment of the ^{13}C is simple using the HSQC NMR (Figure 23) which correlates the ^1H and ^{13}C signals. The signals on the HSQC spectrum are labelled as ' δ ^1H signal, δ ^{13}C signal' as some of the ^{13}C peaks are very close together and difficult to tell apart. HSQC NMR does not give very accurate peak values compared to the ^1H NMR and ^{13}C NMR but it does show which signals correlate.

The bridgehead protons are bound to the same carbon which is confirmed by the HSQC values and the bridgehead carbon is shown to be the most upfield of the ^{13}C NMR signals. The next most downfield carbon signals are shown to couple to proton environments 2 and 4 respectively. The alkene carbon environment is much more downfield as expected due to its sp^2 hybridisation and can be confirmed by its coupling to the alkene proton environment in the HSQC spectrum.

The only remaining carbon signal is the most downfield peak at δ 171.60. The HSQC NMR experiment was only set up to a certain range for the ^{13}C NMR and δ 171.60 is outside of that range. However, it would not provide a signal anyway as carbon associated with that signal is not attached to any protons. It is in fact the carbon on the carbonyl group as shown by the assignment above which can be explained by the fact that the carbon is sp^2 hybridised and bound to the electronegative oxygen atom. The oxygen atom attracts the electron density

away from the carbon atom, making it more deshielded compared to a standard alkene sp^2 carbon and causing it to appear much more downfield on the ^{13}C NMR.

Infrared Spectroscopy:

As with the ^{13}C NMR spectra, an example IR assignment will be explained for *exo* carbic anhydride but the IR assignments for the remaining products will be shown in the experimental section. The IR spectrum for *exo* carbic anhydride is shown below in Figure 24:

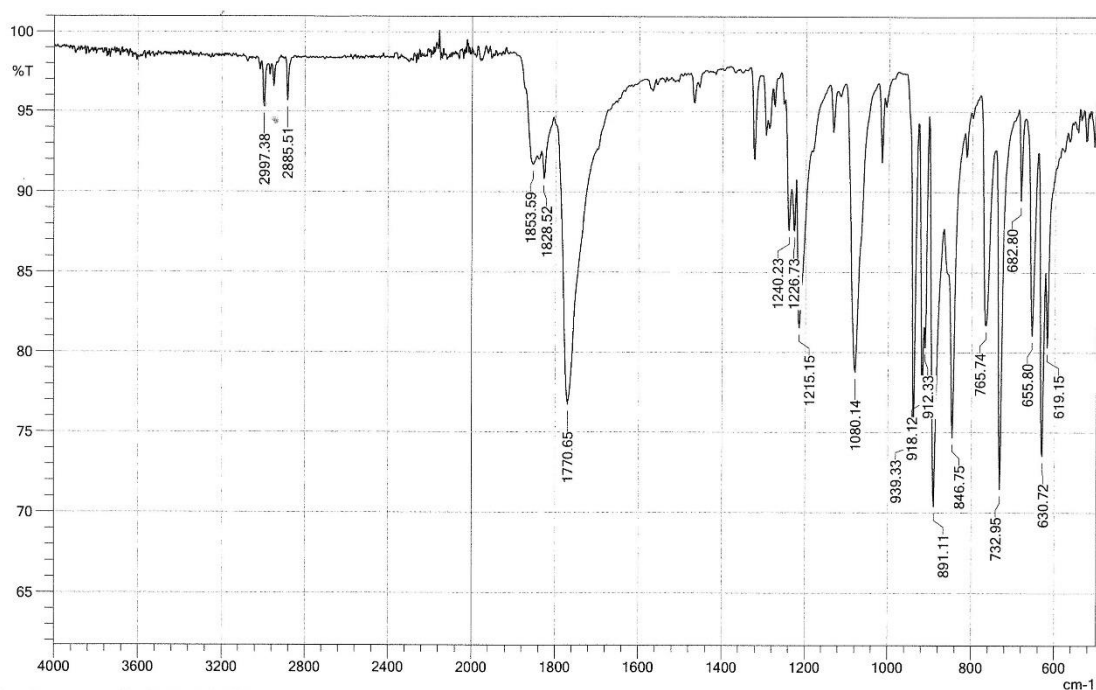


Figure 24 Infrared spectrum for *exo* carbic anhydride.

Exo carbic anhydride contains several functional groups that are reasonably identifiable by IR spectroscopy which include the alkane, alkene and carbonyl (anhydride) groups. The peaks at 2997.38 cm^{-1} and 2885.51 cm^{-1} are indicative of sp^3 alkane C-H stretching. The peaks at 1853.59 cm^{-1} and 1828.52 cm^{-1} are identifiable as weak C=O stretches for anhydrides. The peak at 1770.65 cm^{-1} can be assigned as the strong C=O stretch which is seen for anhydrides. A weak peak is expected in the region of approximately $1600 - 1680\text{ cm}^{-1}$ for the C=C alkene stretch; however, this is not seen. It is possible that the alkene C=C stretch is hidden by the very strong C=O stretch but it may also not be visible due to the nature of the norbornene moiety which is very strained and rigid and therefore may not allow for much stretching.

Melting points:

Melting points were recorded wherever possible for solids and were compared to literature values. Although melting points can provide some degree of evidence of purity, more rigorous analytical techniques such as NMR, XRD and GC-MS were considered much better indicators of purity than melting point values. This is due to the number of variables that can affect melting point values such as the degree of crystallinity, the presence of solvent, the solvent used for crystallisation, the equipment used for measurement and the ability of the scientist to determine accurate values. A brief comparison of the recorded melting point values to the literature values is given where appropriate and where literature values are available. If literature values were not available, then no comparison was made, and the melting point values were recorded in the experimental section. An example comparison between the recorded values and literature values for *exo* carbic anhydride is shown below:

Recorded melting point: 141-144 °C

Literature values: ^{51,52}140-142 °C

The recorded melting point range fits quite well to the literature values but does slightly extend outside of the range recorded in the literature. This could be a result of a high degree of crystallinity as the sample used for melting point measurements was found to be >99% pure by GC-MS.

Neat heating method:

The aim of this study was to develop an optimized method for the isomerisation of *endo* carbic anhydride to the *exo*-adduct that is robust, easily repeatable and cleaner (i.e. avoiding solvents such as benzene and 1,2-dichlorobenzene). Therefore, following on from prior studies, a modified neat heating method was developed. Toluene was chosen as the recrystallisation solvent due to its similarity to benzene, as well as its much lower toxicity, making the reaction safer and more accessible.

Initially, the procedure reported by Craig²¹ which involved heating the *endo* neat in an open flask was repeated although using a heating mantle rather than an oil bath. However, the setup was not optimal as the solid was evaporating from the flask and crystallising on the rim. Upon further investigation, it became apparent that the *endo* was subliming well below its melting point. A search among the literature revealed that Rogers and Quan²³ sublimed *endo* carbic anhydride at 88-90 °C. Therefore, the equipment setup used by Craig needed to be modified. For this optimization the solid was heated in a round bottom flask with a condenser attached to avoid loss of the product/reactant. During the reaction, some solid was condensing on the top half of the round bottomed flask. Rather than forcing the condensed solid to melt using a heat gun, the reaction was left alone. Towards the end of the reaction the top half of the flask had become hot enough that the solid was no longer condensing.

In order to recover the crude product from the thermal isomerisation, it is not practical to simply allow the crude mixture to fully solidify. The solid resulting from this would be a big solid lump rather than crystals which are easier to handle. It would also be a completely crude solid with none of the *exo* product isolated. Moreover, it would be difficult to re-dissolve and therefore make it difficult to isolate the product by recrystallisation.

Ideally the product would be isolated exclusively by adding a solvent whilst still quite hot, dissolving the solid and then crystallising the pure product. Unfortunately, it is not possible for this crude mixture due to the similarity of the two components to be separated. As they are isomers, their solubility is so similar that it makes it very difficult to selectively crystallise the *exo* product from the crude. Despite there not being much difference between their solubilities, there is still a slight difference. Therefore, rather than allowing the molten crude mixture to solidify, toluene was added at a ratio of 1:1.9 in g:ml, heated to reflux until all solid dissolved and was

then allowed to crystallise. This process produced crystals with an *exo* composition of around 75%, rather than a solid lump that would have an *exo* composition of the equilibrium composition at around 55%.

As part of the optimization process, the solubility of both the *endo* and *exo* isomers in toluene at room temperature was measured. The results from the solubility measurements are shown below:

Endo/Exo solubility:

Solubility of Endo:

The stock carbic anhydride from Acros organics which exists as the *endo* isomer contains some impurities that do not dissolve in toluene.

Therefore, firstly it was necessary to obtain pure *endo* carbic anhydride. This was achieved by dissolving *endo* carbic anhydride in a large excess of toluene (approx. 1:10 ratio in g:ml worked well).

Once dissolved, the solution still looked slightly cloudy as it contained the insoluble impurity. This solution was filtered by gravity through filter paper, leaving a clear colourless solution which was put on the rotary evaporator to remove the solvent. Fluffy white residue of pure *endo* carbic anhydride was obtained and used in the solubility measurements.

Measurements:

Measurements were obtained by adding known quantities of toluene to a round-bottomed flask containing *endo* carbic anhydride (0.5 g) at room temperature. The toluene was added via pipette and the round-bottomed flask was agitated after every addition.

1st measurement: 4 ml + 1 ml + 0.5 ml = 5.5 ml (This was a rough measurement to determine when smaller amounts of toluene should be added.)

2nd measurement: 4 ml + 0.5 ml + 0.5 ml = 5.0 ml (All solid dissolved but required a lot of swirling)

3rd measurement: 4 ml + 0.5 ml + 0.2 ml + 0.1 ml + 0.1 ml = 4.9 ml (A lot of swirling was required)

Therefore, between 4.9 ml and 5.0 ml was required to dissolve 0.5 g of *endo* carbic anhydride.

$$\text{Solubility of Endo}_{\text{Toluene,RT}} = \frac{0.5 \text{ g}}{5.0 \text{ cm}^{-3}} = 0.1 \text{ g cm}^{-3}$$

Equation 2 Calculation of the solubility of endo carbic anhydride in toluene at room temperature.

Solubility of Exo:

The *exo* carbic anhydride used for these measurements was obtained in a prior experiment and the sample was >96% *exo* (calculated by GC). There were no insoluble impurities present that needed to be removed beforehand like for the *endo*.

Measurements:

Measurements were obtained by adding known quantities of toluene to a round-bottomed flask containing *exo* carbic anhydride (0.25 g) at room temperature. The toluene was added via pipette and the round-bottomed flask was agitated after every addition.

1st measurement: 1 ml + 0.5 ml + 0.2 ml + 0.2 ml + 0.1 ml + 0.1 ml = 6.1 ml

$$\text{Solubility of Exo}_{\text{Toluene,RT}} = \frac{0.25 \text{ g}}{6.1 \text{ cm}^{-3}} = 0.041 \text{ g cm}^{-3}$$

Equation 3 Calculation of the solubility of exo carbic anhydride in toluene at room temperature.

Endo vs. Exo solubility:

$$\frac{\text{Endo}_{\text{Solubility}}}{\text{Exo}_{\text{Solubility}}} = \frac{0.1 \text{ g cm}^{-3}}{0.041 \text{ g cm}^{-3}} = 2.44$$

Equation 4 Calculation of how much more soluble endo carbic anhydride is compared to the exo isomer in toluene at room temperature.

Therefore, the *endo* isomer is 2.44 times more soluble than the *exo* isomer in toluene at room temperature. It is important to note that these measurements are at room temperature and do not necessarily represent the solubilities of the isomers at higher temperatures. Although no measurements were recorded for their solubilities at high temperatures, it was clear during recrystallisation experiments that crude mixtures containing a greater percentage of *exo* required a larger volume of hot toluene to fully dissolve.

Previous procedures report using several recrystallisations to purify the *exo*^{21,46}. A standard recrystallisation involves dissolving the crude material in the minimal amount of hot solvent. When trying to repeat this with the

crude product of thermal isomerisation, both the *endo* and *exo* crash out from solution, resulting in very little further purification of the product. Despite the *exo* being less soluble in toluene at room temperature, the difference in solubility compared to the *endo* is not great enough to result in the *exo* crystallising selectively using a standard recrystallisation. In order to selectively recrystallize the *exo* from the crude mixture of isomers, the recrystallisation procedure had to be changed slightly. Although, it should be noted that once the purity of the *exo* was over approximately 90%, a standard crystallization using minimal hot solvent was suitable and did not result in both *endo/exo* 'crashing out'.

Instead of using the minimal amount of hot solvent, differing ratios of 'crude:hot solvent' were tested to determine which ratio resulted in the greatest increase in *exo* purity while maintaining a good yield. Ratios of 1:2, 1:2.5 and 1:3 in g:ml were tested numerous times and the best results came from the ratio of 1:2. However, occasionally when a high percentage of *exo* was present in the crude mixture, 1:2 was not enough to fully dissolve the solid. Also, when there was a large amount of *endo* in the mixture, a 1:2 was not enough to avoid both *endo/exo* from 'crashing out'. Therefore, it seemed reasonable to set a 1:2 ratio as a starting point and increase the volume by small increments if necessary. By doing this, the yield remains as high as possible whilst purifying the *exo* significantly.

As previously mentioned above, the commercial *endo* carbic anhydride contains some insoluble impurities which can affect the recrystallisation process during the isomerisation. To avoid this issue, if the insoluble impurities are present when performing the recrystallisation, then the hot solution is filtered to remove the insoluble impurities. It is also possible to remove the insoluble impurities before starting the isomerisation as described above for the solubility measurements. However, if any traces of toluene remain in the *endo* carbic anhydride then it can severely inhibit the thermal isomerisation as the presence of toluene doesn't allow the carbic anhydride to get hot enough. Therefore, for this optimized procedure, it is recommended to remove the insoluble impurities once heating is complete, during the first crystallization.

This optimized procedure was used by a selection of around 10 third year undergraduate students, most of which obtained an *exo* product of >95% purity within 3 recrystallisations and a yield of approximately 15% on average. A yield of 15% is good for this reaction and one undergraduate student managed to achieve a yield of around 25%. Common issues experienced by the undergraduate students are listed below:

- Overheating: Either the solid was heated for too long or at a temperature that was too high, resulting in a dark brown solid which did not recrystallize well.
- Low yield: Some students tried to force crystallization by agitating the crystallization flask. This resulted in less selective recrystallisation, meaning that more recrystallizations had to be done in total, therefore lowering their yield.

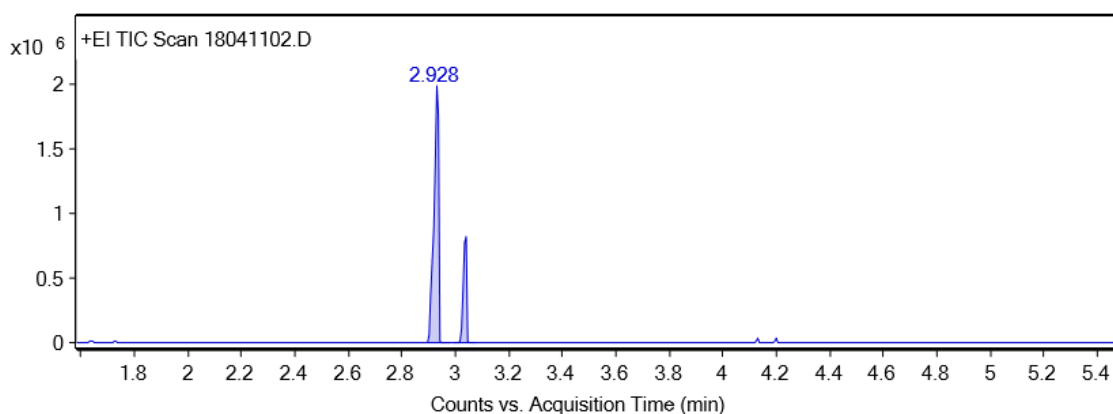
A very important part of the reaction is the crystallization which was evident when some undergraduate students didn't allow the *exo* to crystallize naturally, affecting their purity and yield. Due to the sensitivity of the recrystallisation, it is essential to allow the crystals to grow on their own, without agitation or seeding. Even seeding with pure *exo* (>98%) resulted in lower *exo* selectivity than allowing the *exo* to crystallize itself.

The results from the undergraduate experiments show that the optimized method is robust, reliable and easy to follow. The method also contains additional information, provided to avoid common issues involved with the reaction. If followed correctly, the reaction proceeds well and can be completed in approximately a day to a day and a half. Due to the long heating period and several recrystallisations, the reaction can be performed alongside other reactions with ease.

Research groups wanting to get involved with ROMP can use this optimized method which gives clear instruction and utilizes mild chemicals as opposed to the previously used 1,2-dichlorobenzene. This method was used on several different scales and works well. A 100g scale should yield approximately 15g of pure *exo* (>95%) which is plenty for developing interesting monomers for ROMP and works out to be considerably cheaper than purchasing *exo* carbic anhydride from chemical retailers.

Small scale microwave method:

Since carbic anhydride is the starting point for building monomers for ROMP, a small quantity of carbic anhydride can result in a reasonable amount of monomer as linkers and functionality are added. Therefore, a large-scale preparation is not always necessary, and a small-scale method could be preferred with some advantages. Following a search through the literature, a patent⁵³ describing a method using microwave radiation was found that claimed to have optimized the method; although some parts of the procedure seemed strange and unnecessary. Initially, the 'optimized' method from the patent was repeated fully, resulting in a product that was analysed by GC-MS and found to contain 75% *exo* (GC trace shown in Figure 25 below) at a yield of 74%. These results differ a lot from the reported values of 98% *exo* and 80% yield. Importantly, the microwave method was successful, but improvements to the method were necessary. Therefore, many aspects of the method were optimised and unnecessary steps were removed.



Integration Peak List

Peak	Start	RT	End	Height	Area	Area %
1	2.893	2.928	2.976	1987945.24	2305777.43	100
2	2.994	3.041	3.078	822449.13	763123.53	33.1

Figure 25 GC trace of the crude product obtained using the optimised procedure from the patent.

The patented microwave method tried several different solvents such as 1,4-dioxane, xylene, butyl acetate and toluene. Recrystallisation using 1,4-dioxane was attempted during initial isomerisation experiments and was found to be more selective towards the *endo* than *exo*. Xylene was also attempted during initial experiments for the thermal isomerisation, resulting in poor conversion and proving to be difficult to remove due to its high

boiling point (137 – 140 °C). Butyl acetate wasn't tested but is slightly more expensive than toluene, which was already shown to be more selective to the *exo* during recrystallisations. Therefore, toluene was chosen to be the reaction solvent for the microwave reaction.

No solvent was used during the large-scale neat heating method as the solvent would not get hot enough to allow effective conversion to occur. A solvent such as 1,2-dichlorobenzene, which has been used in the past⁴⁷ has a high enough boiling point that it would allow good conversion to take place. However, the toxicity of 1,2-dichlorobenzene has already been discussed and is therefore undesirable for an optimised process. Conversely for the microwave reaction, a solvent is necessary with a stirrer so that the carbic anhydride is irradiated evenly. Due to the mechanism in which heating occurs through microwave irradiation, where the bonds in carbic anhydride are irradiated directly, the low boiling point (110°) of the solvent (toluene) does not affect the conversion. However, the choice of solvent is important as the converted product is crystallised from solution after irradiation takes place. Therefore, it must be selective towards the *exo* to provide a good crude purity and yield.

Certain aspects of the microwave method were kept the same as reported in the patent. For example, the ideal temperature in the patent was stated as 200 °C. During standard neat heating isomerisation at 180 °C, the conversion is good, but the product can darken through charring over the reaction time (1.5 h) at higher temperatures. However, the short reaction times in the microwave method can allow higher temperatures of 200 °C without charring and may provide a greater ratio of *exo:endo*.

In the patent, differing ratios of starting material:solvent were tried and they found that a ratio of 1:3 was best. However, after some initial microwave experiments, it was found that results from a 1:2 ratio were not so different to those from a 1:3 ratio. 1:2 is preferable as the microwave vials are small and therefore a 1:2 ratio will allow more starting material to be used.

One of the strangest parts of the procedure from the patent is the crystallization procedure used after irradiation takes place. It was stated that stirring the solution at 100 °C for around 30 min after irradiation would result in a greater purity of the crude product. This was put to the test by taking an aliquot of the reaction mixture straight after irradiation had finished and analyzing it by GC-MS. The same reaction mixture was transferred to a conical

flask and stirred (100 °C, 30 min) and afterwards an aliquot was taken to analyse by GC-MS and compare. This was repeated to give two sets of results, and the GC traces are shown in Figure 26 below:

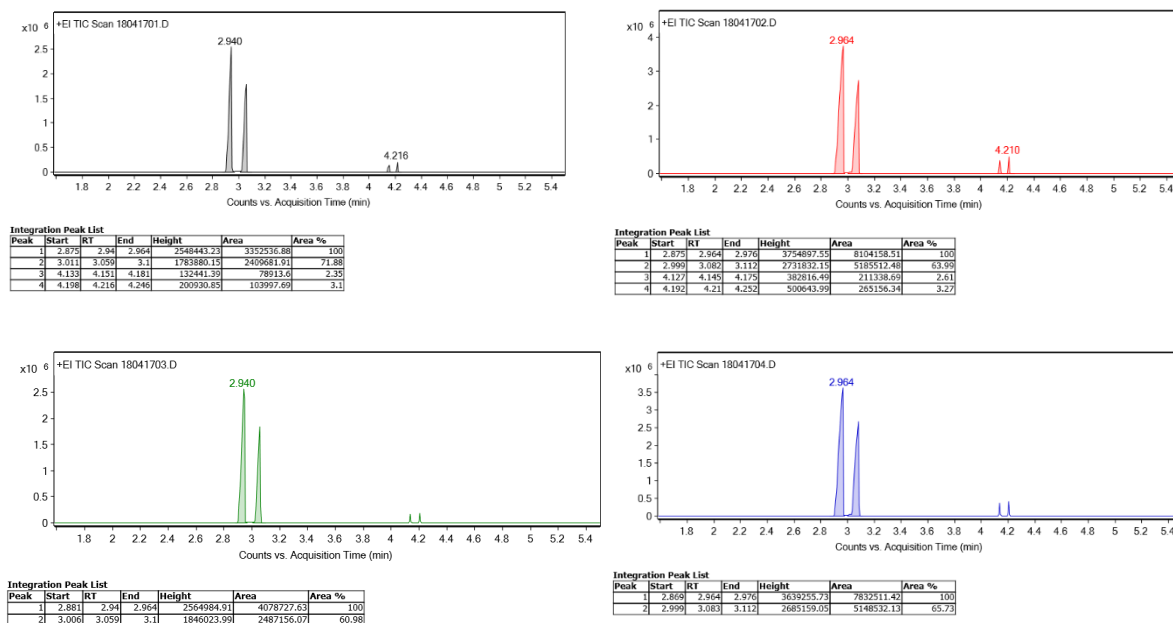
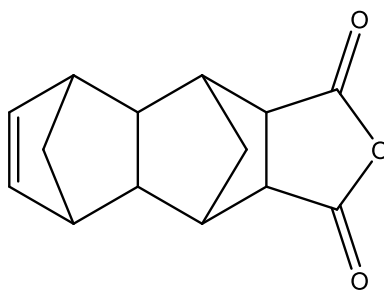


Figure 26 GC traces used to analyse the effect of stirring after heating on the endo/exo composition in solution. Top left: Before stirring, exo = 58 %. Top right: After stirring (100 °C, 30 min), exo = 61 %. Bottom right: Repeat measurement before stirring, 62 %. Bottom right: Repeat measurement after stirring (100 °C, 30 min), exo = 60 %.

In the first measurement we can see that there was a 3 % increase in the ratio of *exo:endo* after stirring, which is not a significant increase. Furthermore, the results from the repeat measurements show a 2 % decrease in the *exo:endo* ratio after stirring, which shows that the additional stirring essentially makes no difference to the *exo* % and is therefore unnecessary. As a result, this step was not included in the optimized procedure.

Interestingly in the GC traces in Figure 26, there are two peaks either side of 4.2 min which are impurities. These impurities were detected predominantly in samples where aliquots were taken from a reaction mixture as opposed to samples that were made up using the crystallized product. This shows that these impurities mostly remain in solution during crystallization and therefore do not appear in the crude crystallized product. Having looked at the MS of the identified peaks, a parent-ion was identified at $m/z = 230$, which corresponds to the Diels-Alder adduct of cyclopentadiene (CPD) and carbic anhydride (CA), shown in Figure 27 below, and was tentatively assigned on that basis:



RMM = 230.26 g mol⁻¹

Figure 27 Suspected by-product of the isomerisation of *endo* to *exo* carbic anhydride which was detected by GC-MS.

Due to the very small amount of impurities present it was not possible to isolate and characterize them, however, it is highly likely that the structure shown above is representative of the impurities. The GC trace shows two peaks, signifying that two isomers of the impurity are present out of a possible four (*exo* of CPD & *endo* CA, *endo* of CPD & *endo* CA, *exo* of CPD & *exo* CA and *endo* of CPD & *exo* CA). It is expected that CPD will only form the *exo* adducts of the *endo/exo* CA, because the *endo* adducts (Figure 28) will have a lot of steric hindrance. However, this is just speculative as there is no evidence to back it up. In order to prove this, the Diels-Alder adduct of CPD and CA could be synthesized purposefully using the literature procedure^{54,55}, and full characterization of the compound and the isomers could be done.

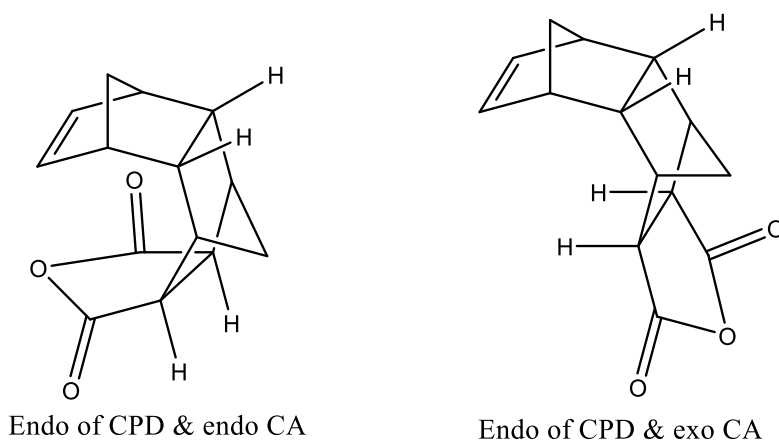


Figure 28 Expected configuration of the *endo* adducts formed from the Diels-Alder reaction between cyclopentadiene and carbic anhydride.

Having decided on the parameters that would remain constant (1:2 ratio of starting material:solvent in g:ml, 200 °C) during the optimization, it was necessary to find the ideal reaction time. In order to find the ideal reaction time, an experiment was designed to determine the percentage of *exo* in the reaction mixture at different reaction times. It takes time for the isomerisation to reach an equilibrium, at which point the reaction is complete and ready for work-up. This experiment therefore shows when the equilibrium has been reached. A 1:2 ratio of *endo*:toluene was heated at 200 °C by microwave irradiation over a range of 2-22 minutes at 2-minute intervals. The reaction mixture was cooled to 60 °C and an aliquot was taken to analyse by GC-MS. The reactions were repeated twice more for an overall three measurements at each time interval, which were averaged and plotted as a graph in Figure 29.

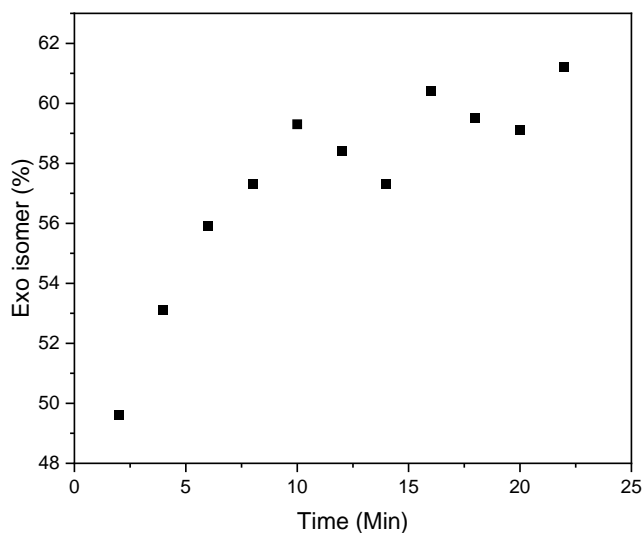


Figure 29 Change in *exo* isomer composition in the reaction mixture as a function of reaction time.

It is important to note that the data in Figure 29 above does not take into account any impurities. Therefore, the *exo* isomer % is not the % composition of *exo* in the entire reaction mixture but the % of *exo* when comparing the two isomers only.

From the graph in Figure 29 it is clear to see that the reaction time does affect the conversion of *endo* to *exo*. At 2 minutes the conversion is below 50 % and at 10 minutes the conversion is up to 59%. This shows that the reaction hasn't reached equilibrium at 2 minutes and demonstrates why it is necessary to find an ideal reaction time as part of the optimization. From the data collected, 10 minutes was chosen to be the ideal reaction time

and the point at which the equilibrium is reached. Despite there being some slightly greater conversions at 17 and 22 minutes, the increase was minimal (<2% at most) and the results for times after 10 minutes were much less consistent. This lack of consistency is suspected to result from the amount of impurity that can form at longer reaction times, which was seen in the raw GC traces (Example shown in Figure 30 below). Further reason to choose 10 minutes is to make the reaction quick and therefore greener, which is an important aspect of an optimized procedure in modern chemistry.

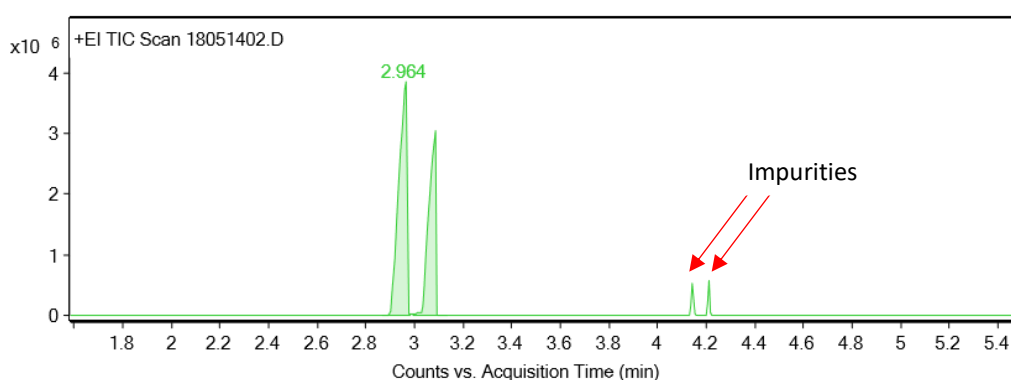


Figure 30 GC trace of the first measurement at reaction time = 20 minutes (LTB-16-110). Impurity peaks are annotated.

The final part of the microwave method left to be optimized was the work-up once the reaction is complete. Initially the solution was transferred to a conical flask while still hot (60 °C) and left to crystallise. This method worked but the crystals were typically of a purity around 80 % and required two or three recrystallisations to purify above 97%. Note that the recrystallisations were completed in the same way as they were in the neat heating method.

Instead of transferring to a conical flask for crystallization to occur, the stirrer was removed when the solution was at 60 °C and the solution was then left to crystallise in the microwave vial. After 3 days, crystals had formed, and they were collected by filtration. The crystals were found to be >90% pure and after one recrystallisation the purity of the crystals was 97%. 3 days is a long time for crystallization to occur, but it was repeated and again took 3 days. Although this is a long time, it is easy to do alongside other experiments and provides high purity *exo* in a single recrystallisation. The alternative method of transferring to a conical flask can be used by people who are in a rush and do not mind performing several recrystallizations to obtain high purity *exo*. Further work

could be done to see if changing the ratio of *endo*:solvent from 1:2 to 1:1.9 could speed up the crystallization. However, this may also affect the purity of the first batch of crystals.

In conclusion, two optimized methods for the isomerisation of *endo* carbic anhydride to *exo* carbic anhydride have been developed. These methods have used milder chemicals compared to previously reported procedures, making them more accessible. Finer details such as the recrystallisation have been studied and found to require more than the 'minimal hot solvent' to get good selectivity. Both a large-scale and small-scale method have been developed and the characterization of the compounds has been discussed in detail. This includes discussion on how the *exo* % can be determined; accurately through GC-MS and approximately through ^1H NMR. This isomerisation is very important for researchers working in the area of ROMP, given that *exo* carbic anhydride is one of the most commonly used starting points for monomer development.

Romp monomers – adding linkers

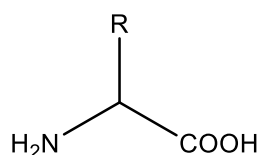
The importance of linkers

Linkers are an important part of designing a monomer for ROMP and can play many roles in the final polymer. A linker is typically an organic-based chain that is connected to the polymerizable norbornene-based unit as well as the functional unit as shown previously in Figure 4. The length of the linker chain can vary significantly and will have implications on the properties of the final polymer. A short linker can hide sensitive functional groups among long linker chains in a co-polymer as demonstrated by Mukherjee *et al.*²⁰ with their multimodal imaging polymer. Long PEGylated chains can be employed in polymers to provide improved polymer solubility. The end group of the linker is also an important factor as it must be reactive towards whichever functional unit is to be attached to. Typically, the end group of the linker will be a functional group with the ability to form an ester or amide with a compatible group on the functional unit. However, if the linker end group has compatible reactivity with the desired functional unit, it does not matter what functional groups are used.

Amino acid linkers

Amino acids such as glycine are fantastic short linkers when designing monomers. They are typically cheap and their reactions with carbic anhydride and *exo*-3,6-Epoxy-1,2,3,6-tetrahydrophthalic anhydride are well documented⁶. The general structure of an amino acid is shown below (Figure 31) and consists of an amine, a carboxylic acid and an 'R-group' which varies from, for example, a simple alkyl group in alanine to a heterocyclic ring system in tryptophan.

Amino acid general structure:



Alanine: R = Me

Tryptophan: R =

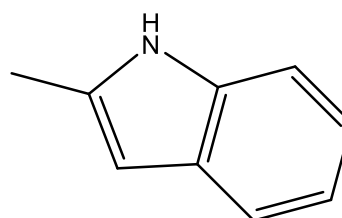


Figure 31 General structure of amino acids. Example R-groups are shown for the amino acids known as alanine and tryptophan.

The amine group is typically reacted with the norbornene-based compound, leaving a reactive carboxylic acid as well as a possible second reactive site depending on the nature of the 'R-group'. This opens the possibility of adding two functional units to a single monomer, allowing for a homopolymer with very interesting properties. For example, a PEG chain could be reacted with the carboxylic acid, and a fluorophore reacted with the R-group, resulting in a water-soluble fluorescent homopolymer after ROMP.

In the case of this project, glycine was reacted with *exo* carbic anhydride to produce a product of high analytical purity in a yield of 48%. It was synthesised as part of the project to gain experience in the synthesis and characterisation of carbic anhydride derivatives. It was also later used to practice the ROMP procedure as opposed to practicing with the more precious monomers that were synthesised.

A reported procedure⁶ for the reaction was modified slightly and produced large crystals through recrystallisation. The crystals grew slowly over the period of a day, after which they were collected and analysed by ¹H NMR (Figure 32) which is shown and explained below along with the COSY (Figure 33).

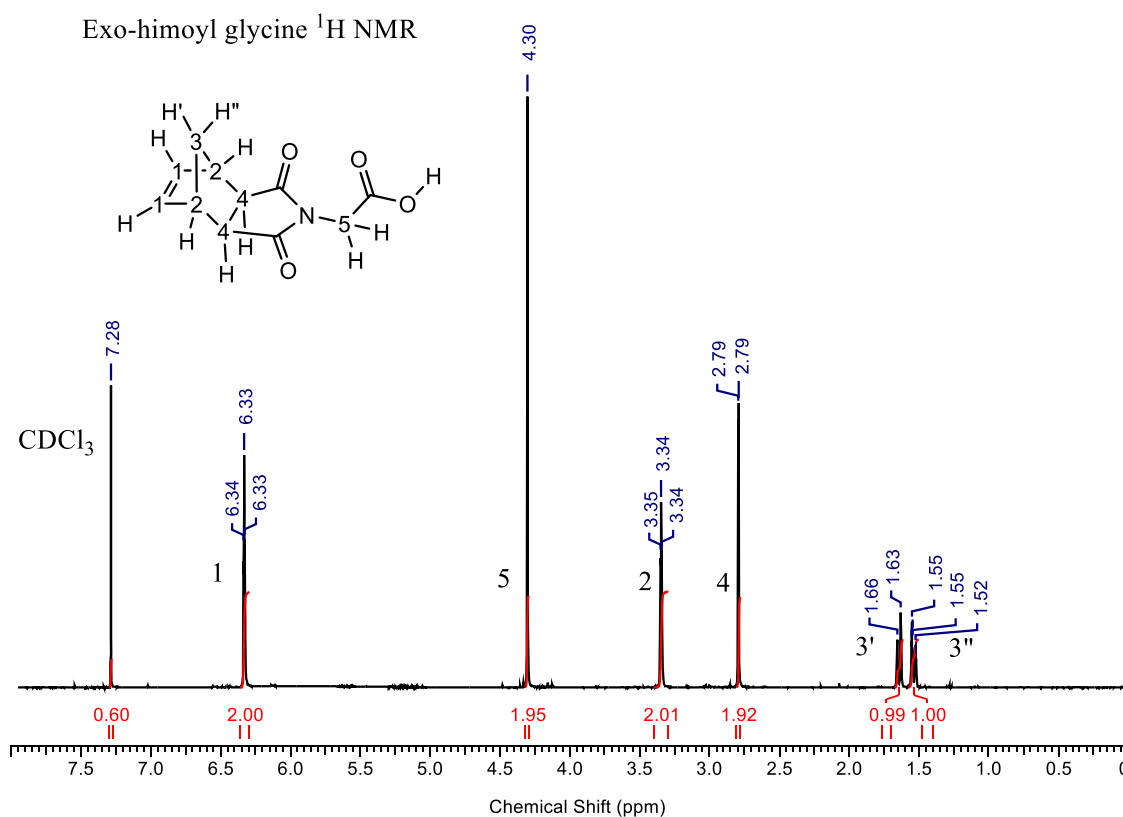


Figure 32 Annotated ¹H NMR spectrum for *exo*-himoyl glycine.

Exo himoyl glycine COSY NMR

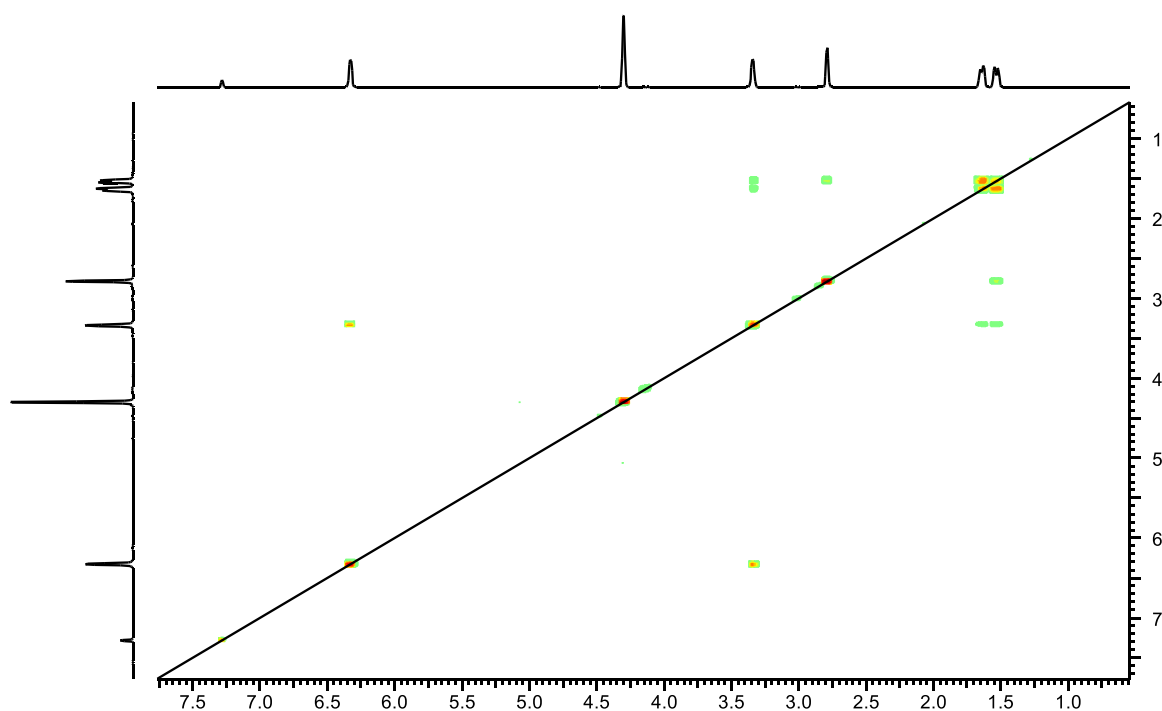


Figure 33 COSY NMR spectrum for *exo*-himoyl glycine.

The ^1H NMR was assigned in the same way as for *exo* carbic anhydride as the peaks are very similar in both their shape and position. The additional singlet peak at δ 4.30 that was not present in the starting material, *exo* carbic anhydride, is indicative that a reaction has occurred. This new peak has been assigned to the environment 5 in the molecule as shown. The proton on the carboxylic acid is not present in the spectra as it could be involved in an exchange process and therefore no peak has been assigned to that environment.

A feature of the NMR which may go unnoticed is what happened to the peaks corresponding to the bridgehead environments. In the starting material, *exo* carbic anhydride, the bridgehead proton that was w-coupling to the alkene proton was the most upfield of the two bridgehead protons. However, in the product, *exo* himoyl glycine, the same bridgehead proton coupling to the alkene is the most downfield of the two bridgehead protons. This isn't particularly important and does not affect the possibility to assign the compound, but it is not entirely clear what caused the environments to essentially flip. What makes it more interesting is that this phenomenon only occurred in this product out of all the compounds synthesised during the project.

Having searched the literature, it was found that the crystal structure of the *endo* glycine derivative had been solved, but the *exo* adduct had not. Therefore, single crystal XRD was performed on the crystals and the crystal structure was solved (Figure 34), confirming that the *exo* adduct had been successfully synthesised. GC-MS analysis (Figure 35 and Figure 36) was conducted for the product and the results are shown and explained below.

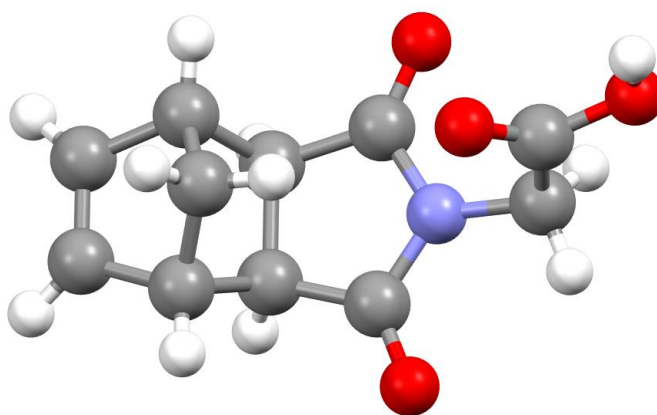
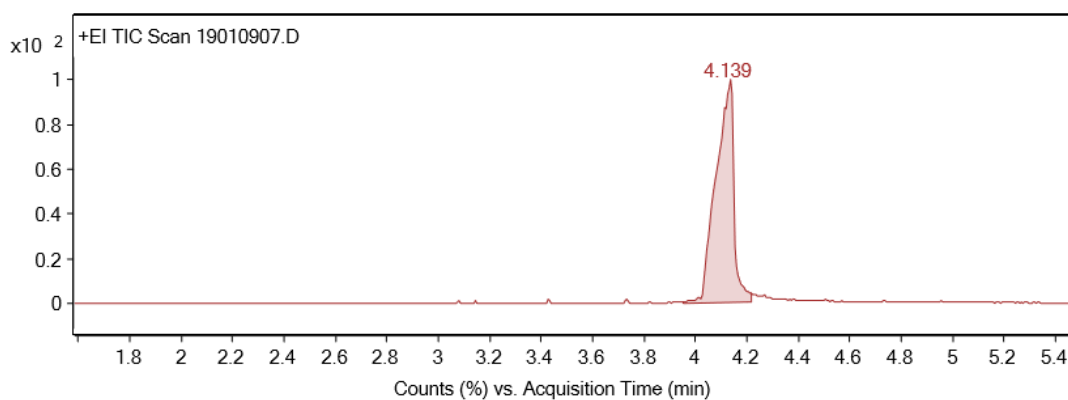


Figure 34 Structure of *exo*-himoyl glycine as determined by single crystal XRD.



Integration Peak List

Peak	Start	RT	End	Height	Area	Area %
1	3.949	4.139	4.216	723505.86	3474294.21	100

Figure 35 GC trace for *exo*-himoyl glycine.

The GC trace (Figure 35) shows one major peak at RT = 4.139 which can almost certainly be assigned as the product. There are some very small minor peaks, but these were not large enough to be integrated by the

software. Therefore, the trace shows that the product has an analytical purity of 100%. However, this is not realistic, and it can be said that the product has an analytical purity >99%.

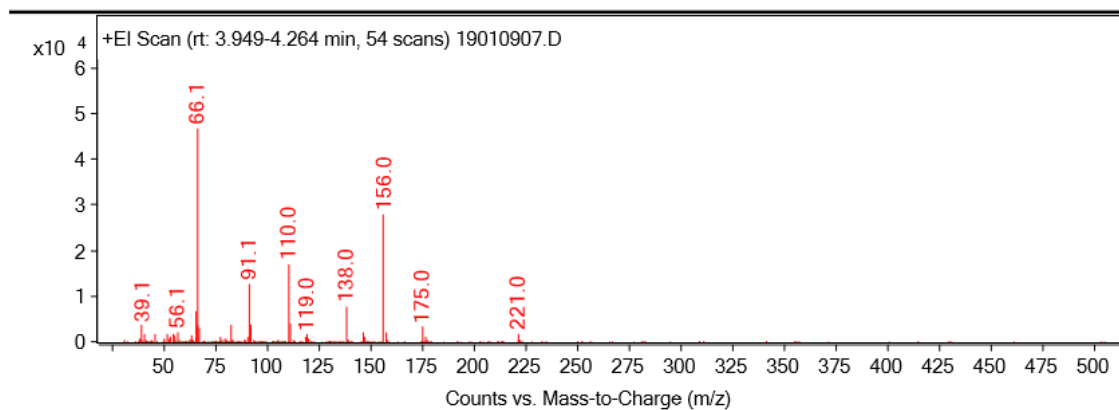


Figure 36 Mass spectrum for *exo*-himoyl glycine.

The MS spectrum above (Figure 36) corresponds to the major peak on the GC trace at RT = 4.139 and contains a parent ion peak at $m/z = 221.0$. This mass of the parent ion peak corresponds with the monoisotopic mass of the product and further confirms that the peak on the GC trace is indicative of the product.

Recorded melting point: 160 – 162 °C.

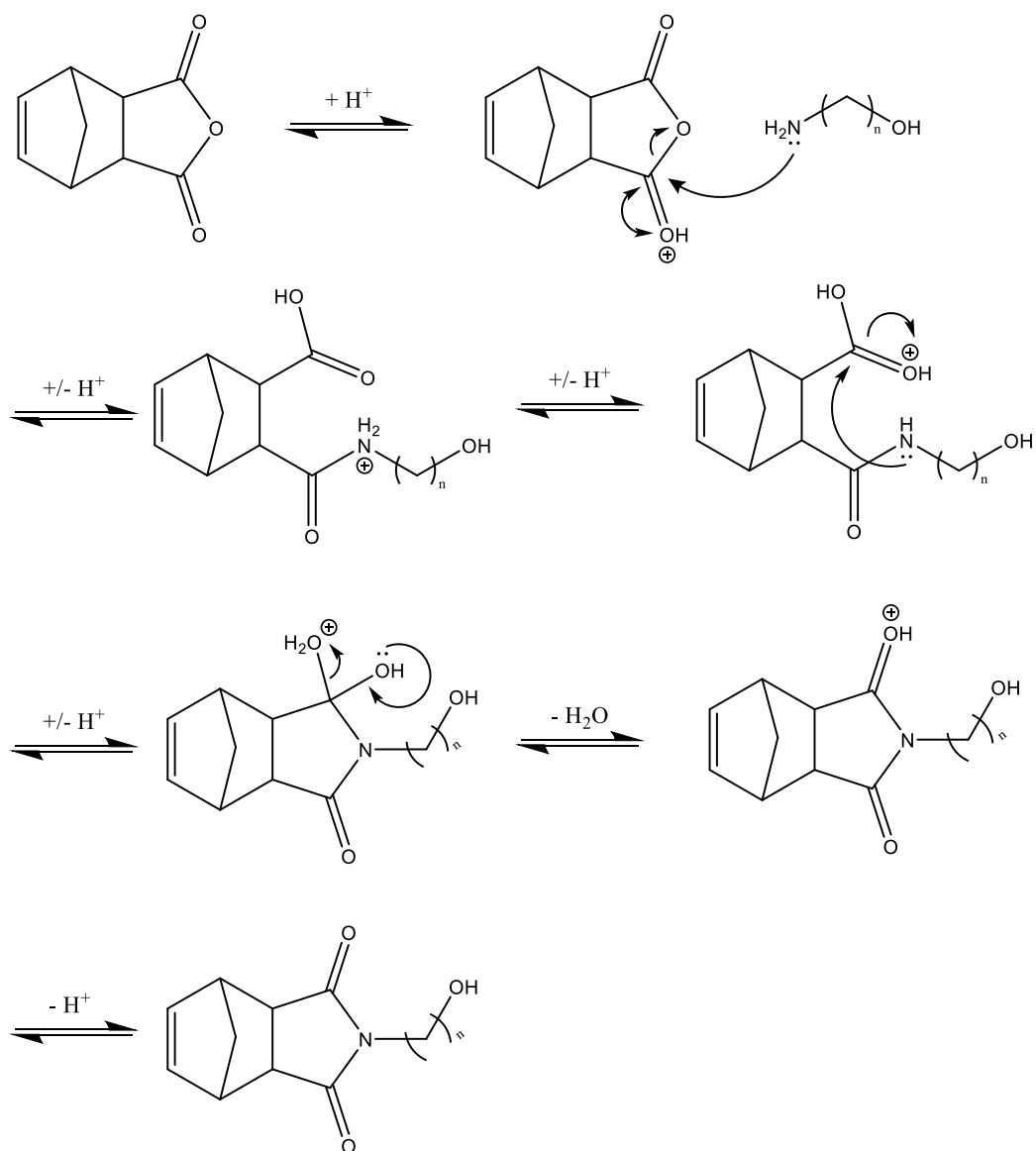
Literature melting point values: ⁵⁶120 – 122 °C, ⁵⁷129.5 – 130.5 °C, ⁶149 – 150 °C.

The melting point values differ quite noticeably from the literature values. However, the ¹H NMR is very clean, the XRD results correspond to the expected structure and the GC-MS shows that the product is pure. The disparity between the recorded values and the literature values is most likely due to the high degree of crystallinity of the recorded sample as the crystals grown were mostly large single crystals.

No further reactions were performed with the glycine derivative apart from ROMP which will be discussed in later. However, previous work⁵⁸ has used *exo*-himoyl glycine to yield a PEGylated monomer. In future work, this monomer could be synthesised and copolymerised with other monomers to produce a water-soluble polymer. Furthermore, a small amount of the PEG monomer could be used in a homo-polymerisation and essentially become a water-soluble ROMP catalyst that could allow polymerisation to occur in aqueous conditions.

Amino alcohol linkers

Amino acid linkers can typically only act as short linkers in ROMP monomers and are therefore limited by their length. Amino alcohols are a very good alternative for amino acids as linkers due to the additional versatility in possible chain length²⁹ that limit natural amino acids. Amino acids can however be more versatile in that they can link to two different functional units depending on the R-group as discussed above. An amino alcohol contains two functional groups of differing reactivity, where the amine group is more reactive than the OH group towards the anhydride of carbic anhydride. This allows for the facile selective reaction of the -NH₂ group with the anhydride, yielding a monomer which can be linked to a functional unit through reaction with the primary -OH group. The general reaction mechanism for this transformation is shown in Scheme 8.



Scheme 8 Mechanism for the reaction between carbic anhydride and aminoalcohols.

As the reaction between carbic anhydride and an amino alcohol yields a monomer with a reactive primary -OH group, the functional unit is typically attached via an ester where the -OH group reacts with a carboxylic acid. Therefore, when designing a monomer, it is important to decide which reactivity the linker will need for several reasons. Firstly, if the functional unit does not contain a carboxylic acid or another group that can react with a primary -OH, then it is not sensible to use an amino alcohol linker. Secondly, the bond between the linker and functional group can be important for the overall properties of the polymer. For example, if someone wished to design a polymer that could release a drug through hydrolysis of the linker – functional unit bond; an ester would be easier to hydrolyse than an amide. Lastly, an ester is not always easy to create due to factors such as steric hindrance on the functional unit for example. Therefore, amides which tend to be easier to produce as a result of their greater stability when compared to esters; could be employed to overcome reactivity issues.

During this project, both *endo* and *exo* carbic anhydride were reacted with 5-amino-1-pentanol following a literature procedure⁴, which produced *N*-(hydroxypentanyl)-*cis*-5-norbornene-*endo/exo*-2,3-dicarboximide in high yield. The reaction worked well as demonstrated by the high yield and is easy to perform. The products for both *endo* and *exo* were viscous yellow oils and therefore could not be analysed by XRD. They were however analysed by GC-MS. The GC trace of the *exo* adduct (Figure 37) contained a large peak at RT = 4.353 and using the integration areas as calculated by the software, the analytical purity of the sample was found to be >94 %. The MS spectrum (Figure 38) relating to the peak at RT = 4.353 showed a small parent ion peak at $m/z = 249.1$ which corresponds with the monoisotopic mass of the product. The GC-MS analysis indicates that it is highly likely that the product was indeed synthesised, however NMR was also used to provide further evidence.

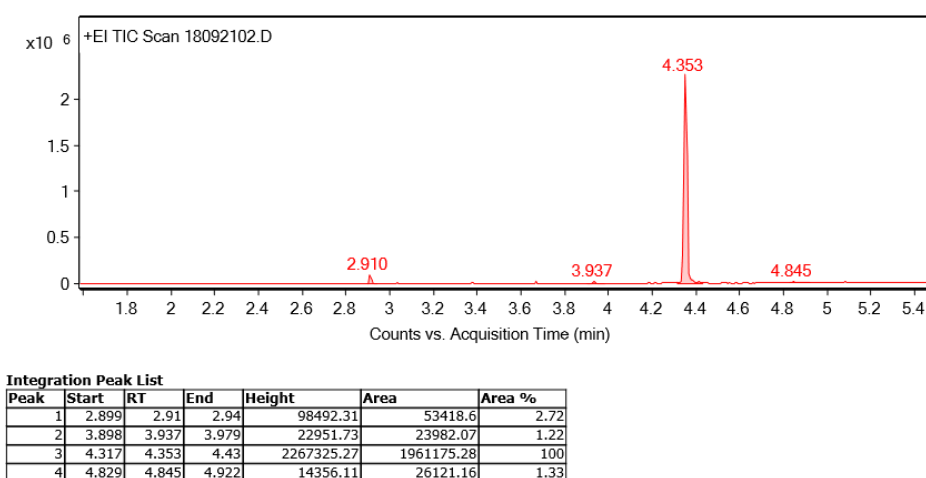


Figure 37 GC trace for the product formed from the reaction between *exo* carbic anhydride and 5-amino-1-pentanol.

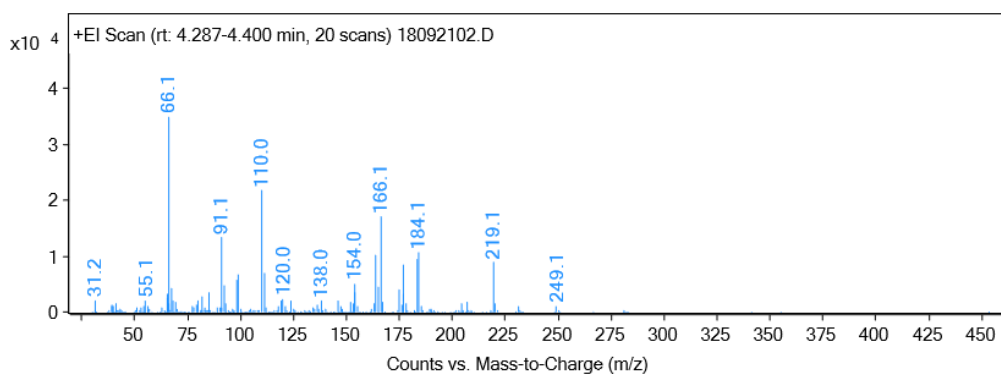


Figure 38 Mass spectrum for the product formed from the reaction between *exo* carbic anhydride and 5-amino-1-pentanol (*N*-(hydroxypentanyl)-*cis*-5-norbornene-*exo*-2,3-dicarboximide).

Endo amino alcohol product (*N*-(hydroxypentanyl)-*cis*-5-norbornene-*endo*-2,3-dicarboximide)

The ^1H NMR of the *endo* adduct was not entirely clean, but the product could be assigned using the ^1H (Figure 39) and COSY (Figure 40) NMR as shown and explained below.

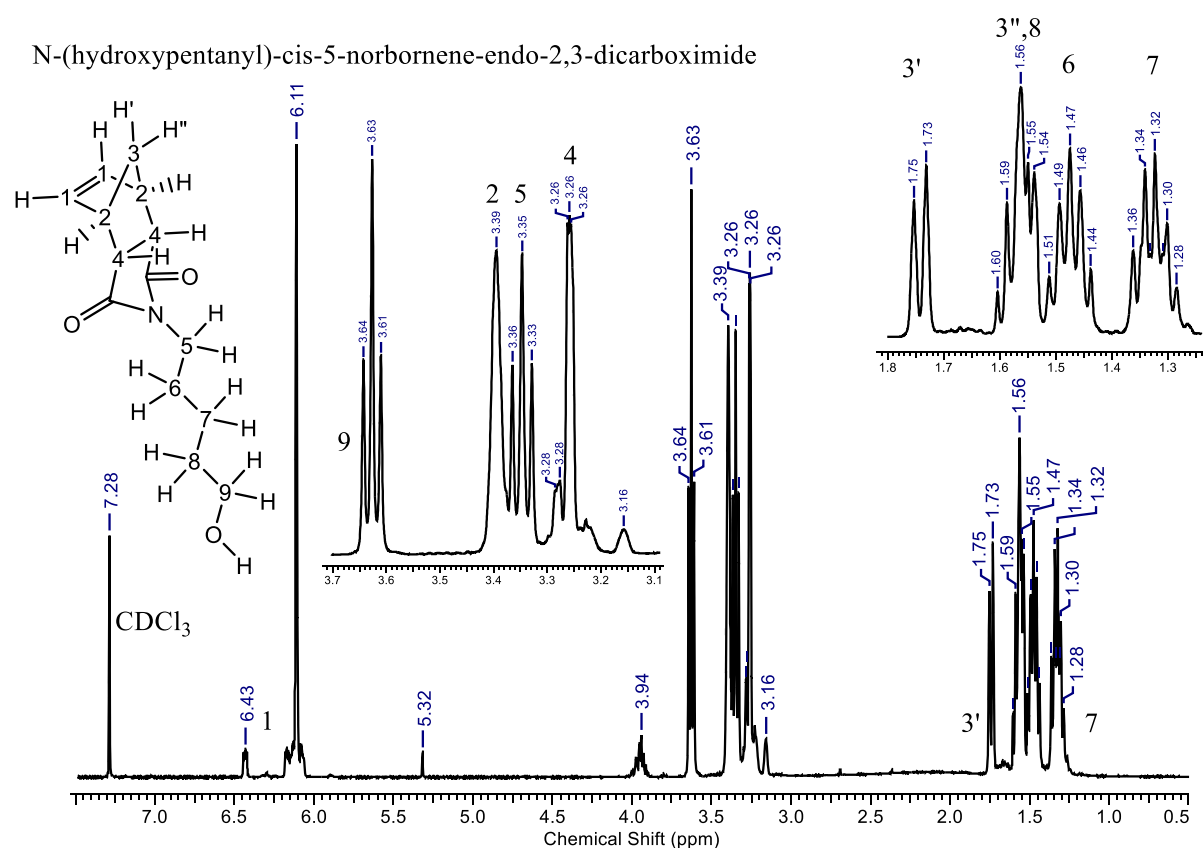


Figure 39 Annotated ^1H NMR spectrum of the product formed from the reaction between *endo* carbic anhydride and 5-amino-1-pentanol (*N*-(hydroxypentanyl)-*cis*-5-norbornene-*endo*-2,3-dicarboximide).

N-(hydroxypentanyl)-cis-5-norbornene-endo-2,3-dicarboximide

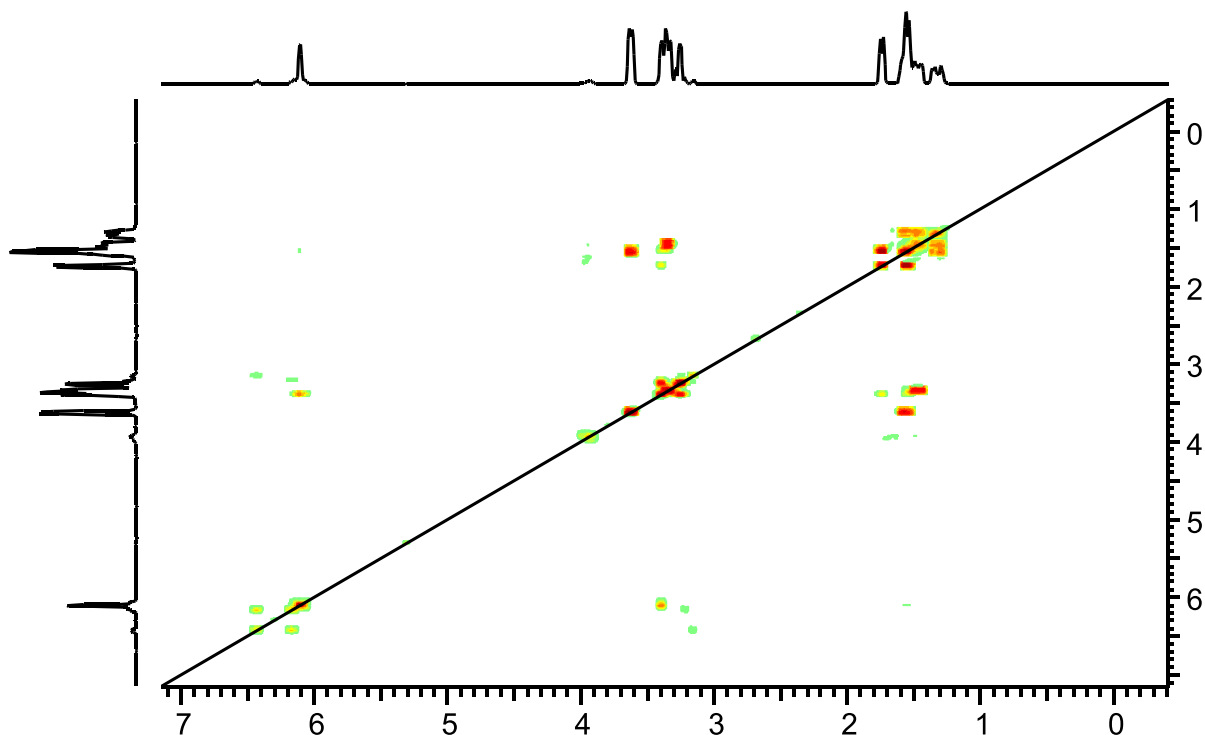


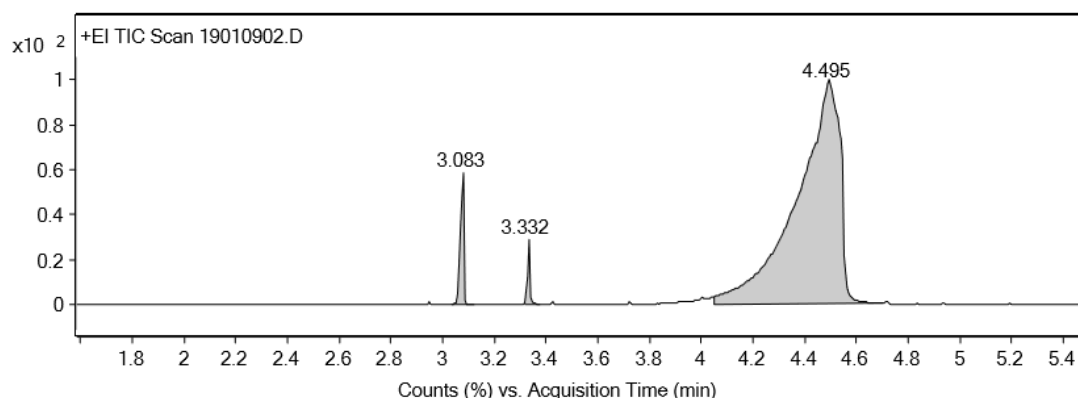
Figure 40 COSY NMR spectrum of the product formed from the reaction between *endo* carbic anhydride and 5-amino-1-pentanol (*N*-(hydroxypentanyl)-*cis*-5-norbornene-*endo*-2,3-dicarboximide).

Despite the ^1H NMR of the *endo* adduct not being entirely clean, when looking at the expanded regions, the relevant peaks are clear and generally well defined. The norbornene peaks were assigned as before, starting from the alkene peak at δ 6.11 and piecing the rest of the norbornene together through a combination of COSY analysis and long-range coupling analysis in the ^1H NMR. The protons in the amino alcohol part of the molecule are not close enough to the norbornene protons to show coupling visible on the COSY. Therefore, it is not possible to easily find a starting point for assigning this part of the molecule and it must be done from first principles.

The easiest environment to assign on the amino alcohol section is 7, as it is most weakly affected by the dicarboximide and the alcohol and therefore will be the most upfield peak, δ 1.33, as assigned. However, it does not provide a good starting point to figure out the remaining environments as they are difficult to differentiate between. Therefore, it is necessary to start from the outermost protons, closest to the dicarboximide and alcohol functional groups. Using the differences in electronegativities of the nitrogen and oxygen atoms on the

dicarboximide and alcohol respectively, where oxygen has a greater electronegativity, the environment closest to the alcohol can be assigned to the most downfield of the remaining peaks. The peak, 9, is at δ 3.63 and is a triplet, which agrees with expectations based on the 'n +1' rule. Having assigned the environment next to the alcohol, the environment adjacent to the dicarboximide can be assigned as the most downfield of the remaining peaks. This peak, 5, is at δ 3.35 and is a triplet as expected. Using COSY analysis, the remaining peaks can be determined as 9 shows to be coupling with 8, and 5 is coupling to 6. Both 8 and 6 are also coupling to 7, further confirming the assignment. Peak 6 is a quintet as expected based on the 'n + 1' rule but peak 8 looks more like a multiplet due to it overlapping with the peak from the bridgehead proton. All of the peaks apart from the OH peaks were therefore assigned. The OH peak did not appear to be present; this could be due to proton exchange processes.

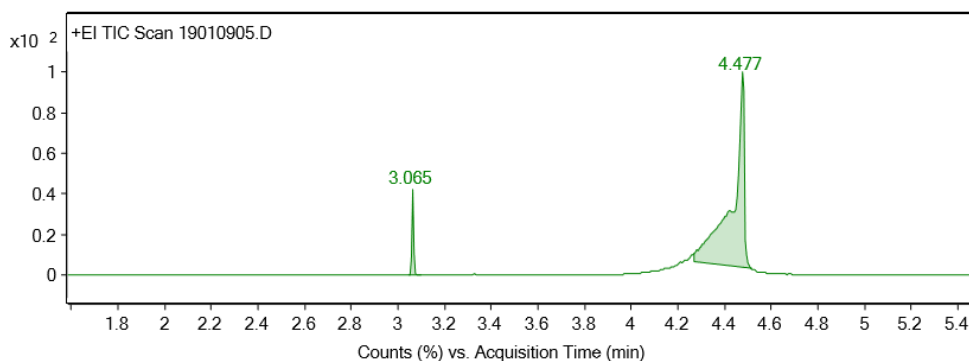
As the environments from the amino alcohol section on the molecule were assigned independently from the norbornene section, it could be argued that what is present on the ^1H NMR are the peaks for the unreacted starting materials, *endo* carbic anhydride and 5-amino-1-pentanol. However, the integrations match up to the number of protons expected for all assigned peaks. Furthermore, all of the norbornene peaks apart from those of the bridgehead protons are shifted upfield in the product compared to the starting material, *endo* carbic anhydride. This shows that a reaction had occurred, and the starting material had not remained the same. Further evidence for the product is shown and explained below using the results from GC-MS analysis.



Integration Peak List

Peak	Start	RT	End	Height	Area	Area %
1	3.035	3.083	3.123	849547.78	871892.41	5.23
2	3.314	3.332	3.373	418477.75	250509.13	1.5
3	4.05	4.495	4.703	1432373.82	16683231.63	100

Figure 41 GC trace (1) for the product formed from the reaction between *endo* carbic anhydride and 5-amino-1-pentanol (*N*-(hydroxypentanyl)-*cis*-5-norbornene-*endo*-2,3-dicarboximide).



Integration Peak List						
Peak	Start	RT	End	Height	Area	Area %
1	3.047	3.065	3.1	180685.04	96775.8	6.7
2	4.27	4.477	4.516	413290.04	1445144.4	100

Figure 42 GC trace (2) for the product formed from the reaction between *endo* carbic anhydride and 5-amino-1-pentanol (*N*-(hydroxypentanyl)-*cis*-5-norbornene-*endo*-2,3-dicarboximide).

The GC traces shown above are both of the *endo* adduct. The GC trace (1, Figure 41) contained too much analyte and therefore gave rise to a very broad peak. The amount of analyte used was reduced in the GC trace (2, Figure 42) but still gave quite a broad peak and it is not entirely obvious why this has occurred. However, the broad peak in both traces at around RT = 4.4 appears to be the product due to it being the dominant peak. The other peak present in the GC trace (2), which is also present in (1), appears to be the starting material when comparing it to traces from the *endo/exo* isomerisation. There is a third small peak in (1) at RT = 3.332, which must be showing up due to the large amount of analyte used and is representative of another impurity, however, the identity of this impurity could not be determined. Although, in both traces, the composition of the product compared to the impurities was calculated to be 94%, which shows that there is still only a small amount of overall impurity present.

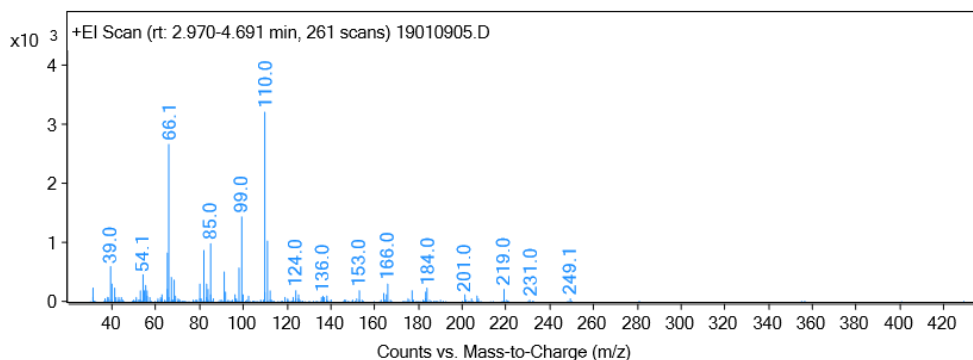


Figure 43 Mass spectrum for the product formed from the reaction between *endo* carbic anhydride and 5-amino-1-pentanol (*N*-(hydroxypentanyl)-*cis*-5-norbornene-*endo*-2,3-dicarboximide).

The MS spectrum shown above (Figure 43) contains a parent ion peak at $m/z = 249.1$ which aligns with the monoisotopic mass of the expected product and shows that it is highly likely that the product was synthesised successfully.

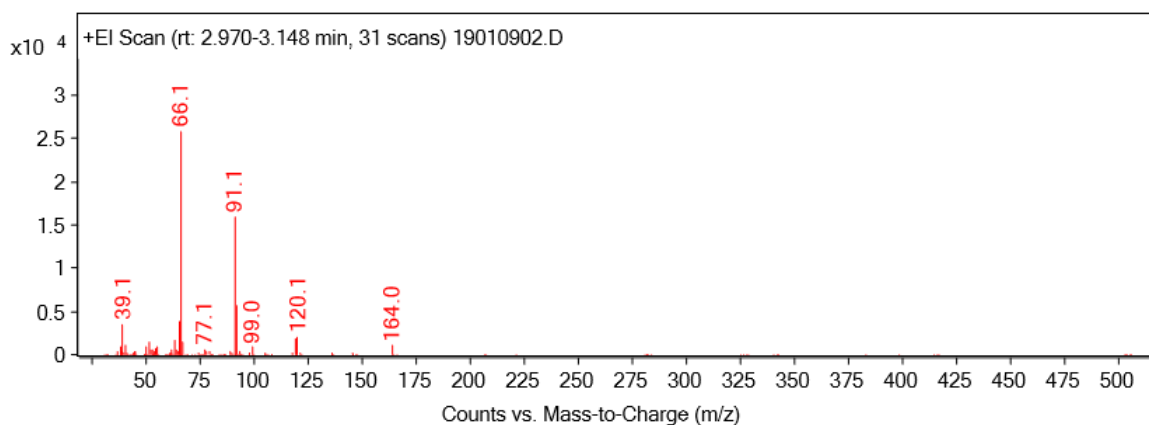


Figure 44 Mass spectrum of the expected residual starting material in the sample.

The MS spectrum above (Figure 44) corresponds to the peak at RT = 3.083 in the GC trace (1) which contains a parent ion peak at $m/z = 164.0$. This is consistent with the monoisotopic mass of the starting material, *endo* carbic anhydride. This confirms that the main impurity present in the product is the starting material.

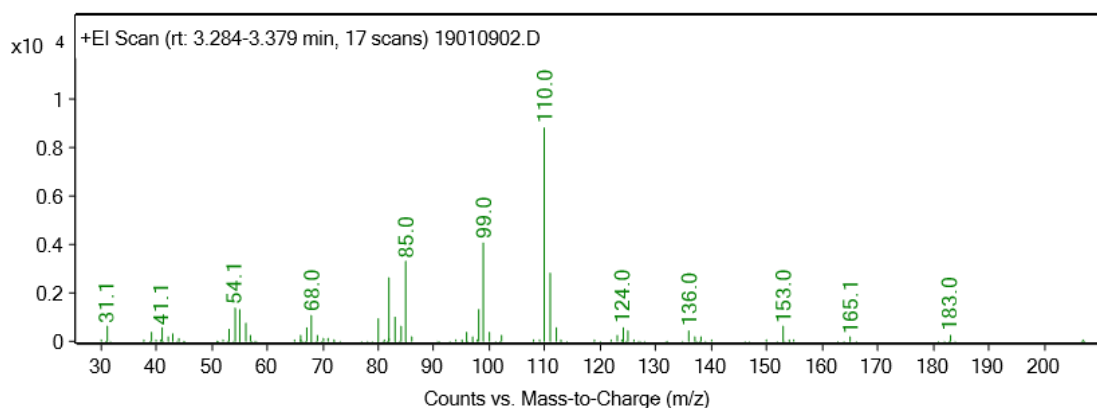


Figure 45 Mass spectrum of an impurity detected in the GC trace in Figure 41 at RT = 3.332.

The MS spectrum shown above (Figure 45) corresponds to the unknown peak at RT = 3.332 on the GC trace (1). There is a parent ion present at $m/z = 183.0$. This mass corresponds to the monoisotopic mass of the compound shown below:

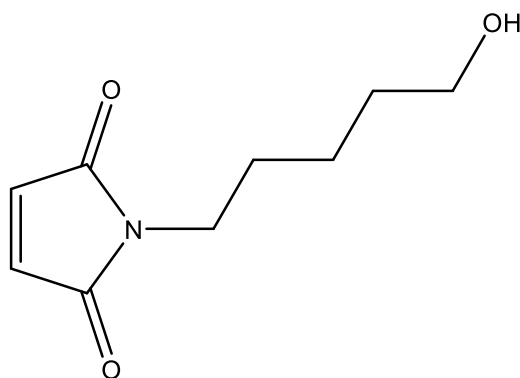


Figure 46 Structure of the suspected impurity detected on the GC trace in Figure 41 and corresponds to the mass spectrum in Figure 45.

Therefore, it is highly likely that this compound is the unknown impurity from the GC trace (1). This compound could have been formed by a retro-Diels-Alder reaction that occurred alongside the main reaction. However, it is important to note that this impurity was present in a very small amount.

Exo amino alcohol product (N-(hydroxypentanyl)-cis-5-norbornene-exo-2,3-dicarboximide)

N-(hydroxypentanyl)-cis-5-norbornene-exo-2,3-dicarboximide

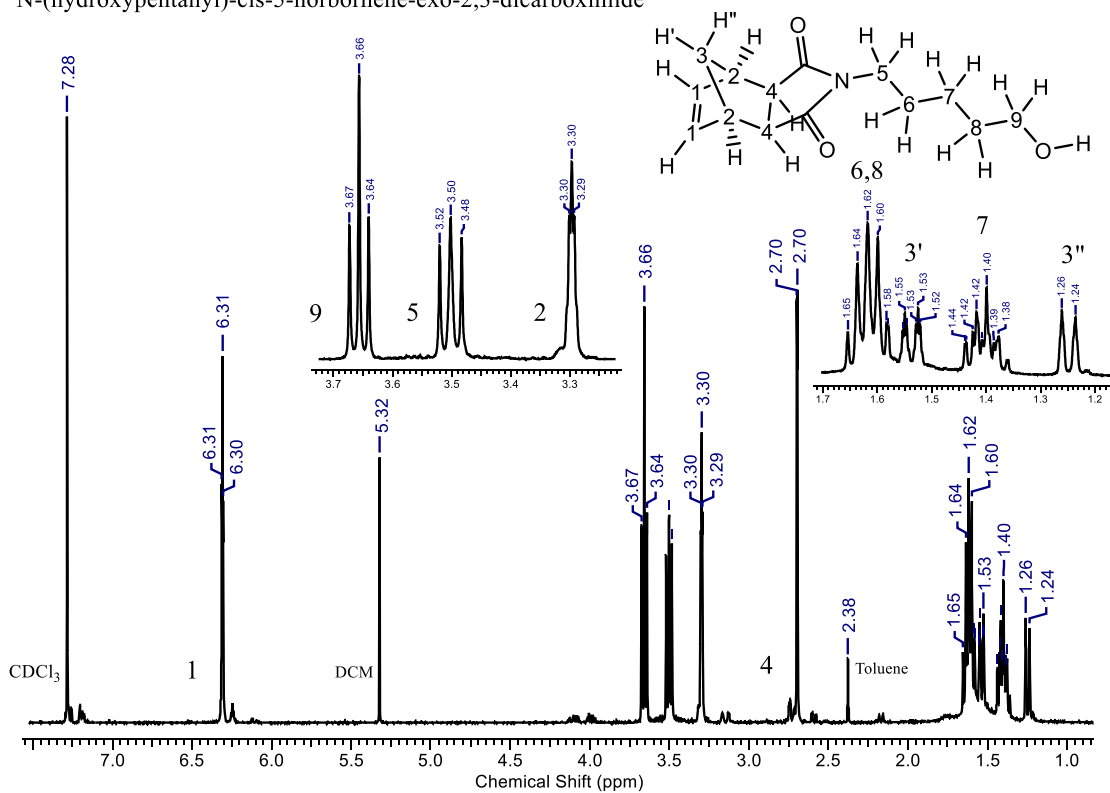


Figure 47 Annotated ^1H NMR spectrum of the product formed from the reaction between *exo* carbic anhydride and 5-amino-1-pentanol (*N*-(hydroxypentanyl)-*cis*-5-norbornene-*exo*-2,3-dicarboximide).

N-(hydroxypentanyl)-cis-5-norbornene-exo-2,3-dicarboximide

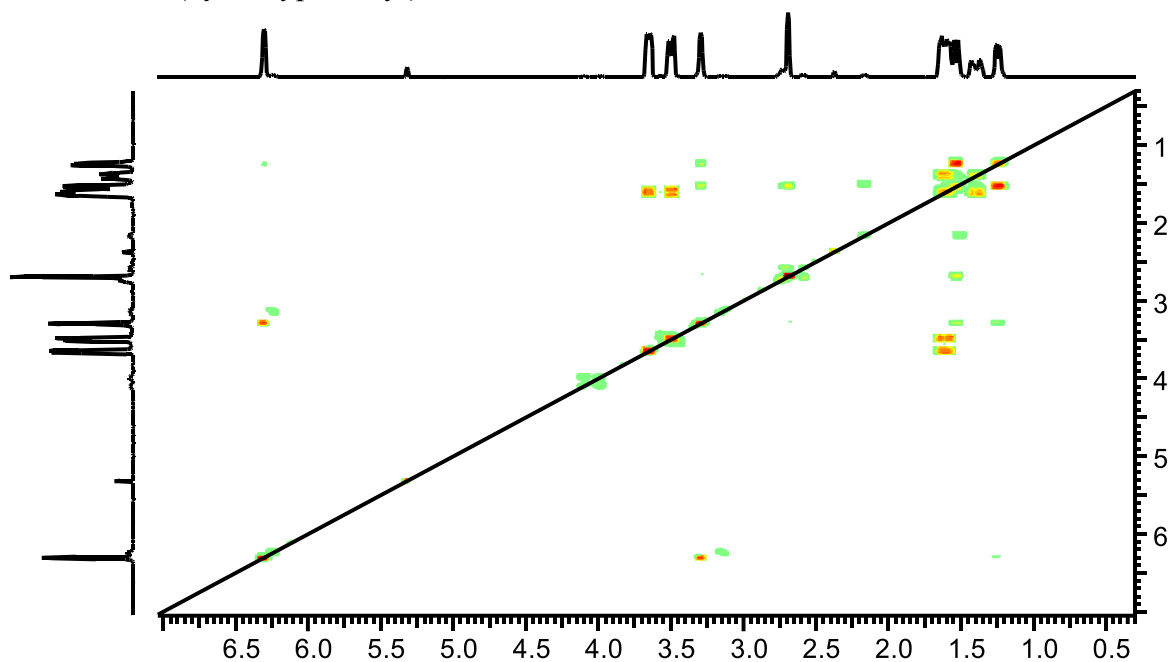


Figure 48 COSY NMR spectrum of the product formed from the reaction between *exo* carbic anhydride and 5-amino-1-pentanol (*N*-(hydroxypentanyl)-*cis*-5-norbornene-*exo*-2,3-dicarboximide).

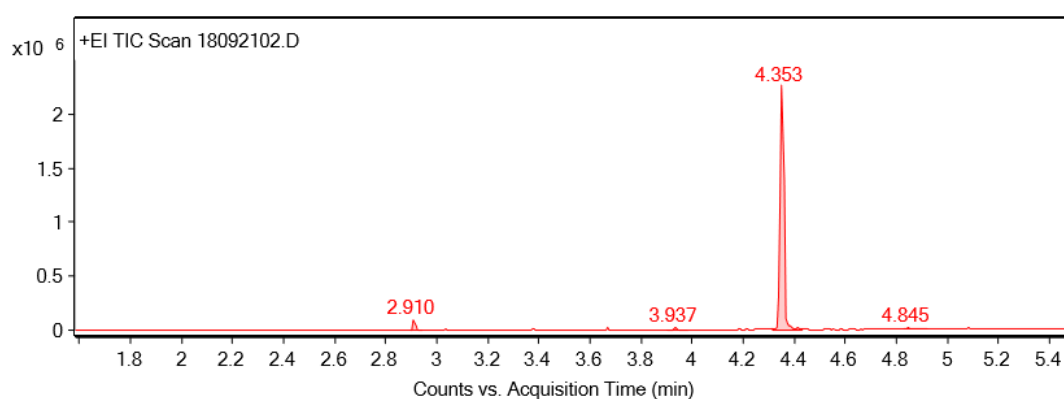
As with the *endo* adduct, the norbornene section of the *exo* adduct can be assigned very similarly to the *exo* carbic anhydride in starting with the alkene peak and using the COSY (Figure 48) and ^1H (Figure 47) NMR spectra to assign the remaining peaks. When looking at the expanded regions, the overall shapes of the peaks for the norbornene part of the adduct are very similar to the *exo* carbic anhydride and are all just shifted slightly upfield with the addition of the dicarboximide.

In the *endo* adduct the amino alcohol section had to be assigned almost independently from the norbornene section and this is the same for the *exo* adduct. Using the same logic for the *exo* adduct, the most downfield of the remaining peaks was assigned to the environment next to the -OH group. The next most downfield peak at δ 3.50 was then assigned to the environment adjacent to the dicarboximide. Using the COSY, it was seen that these two triplet peaks were coupled to the same peak at δ 1.62. Interestingly it seems as though the environments labelled 6 and 8 are in the exact same environment as the peak is showing to be a quintet. The expected splitting pattern would be a quintet for these protons, but more likely a multiplet due to overlapping where they are in similar environments but not the same environment. However, a quintet is seen and therefore

must be overlapping with almost identical coupling constants. This is confirmed by integration of the peak which showed that 4 protons were present in that peak.

The only remaining unassigned peak at δ 1.40 was assigned to environment 7. It was the most upfield peak besides the bridgehead proton on the norbornene as expected, due to it being the central environment on the amino alcohol section and therefore the least de-shielded. The proton on the -OH group was not present on the ^1H NMR in the same way and for the same expected reasons that it was not present in the *endo* adduct.

As with the *endo* adduct, it could be questioned that the starting materials are present in the ^1H NMR in their unreacted states. However, the peaks in the product, especially those for the norbornene section, are shifted upfield compared to the starting material, *exo* carbic anhydride. This indicates that the carbic anhydride has reacted and caused the peaks to shift upfield. Further evidence for the formation of the product is shown and explained below using GC-MS analysis.



Integration Peak List

Peak	Start	RT	End	Height	Area	Area %
1	2.899	2.91	2.94	98492.31	53418.6	2.72
2	3.898	3.937	3.979	22951.73	23982.07	1.22
3	4.317	4.353	4.43	2267325.27	1961175.28	100
4	4.829	4.845	4.922	14356.11	26121.16	1.33

Figure 49 GC trace of the product formed from the reaction between *exo* carbic anhydride and 5-amino-1-pentanol (*N*-(hydroxypentanyl)-*cis*-5-norbornene-*exo*-2,3-dicarboximide).

The GC trace above (Figure 49) shows one major peak at RT = 4.353 and a minor peak at RT = 2.910 which are expected to be the product and the starting material, *exo* carbic anhydride respectively. The minor peak is of a very similar RT to the RT of *exo* carbic anhydride in the many GC traces done during the isomerisation optimisation. There are some very small additional minor peaks, but this can be put down to column bleed as

the sample is weak. The analytical purity of the sample, assuming the major peak is the product, is >95%, and the starting material appears to be the only main impurity present in the GC trace.

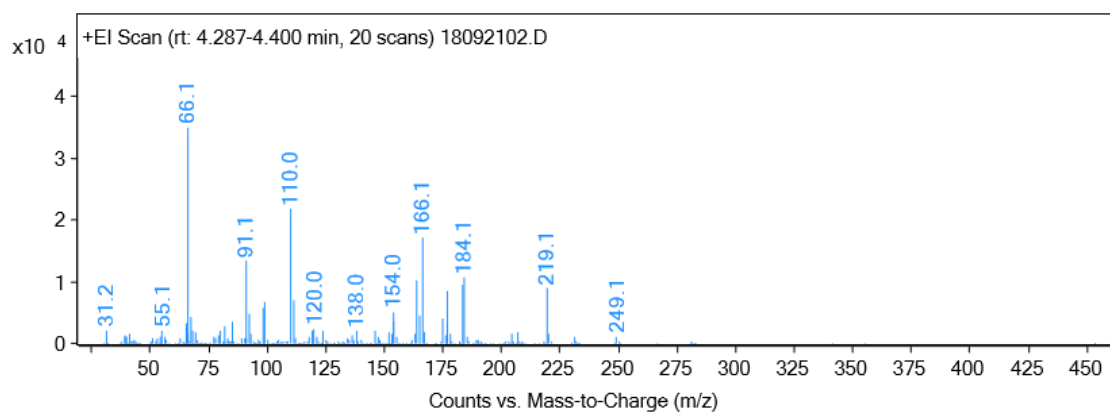


Figure 50 Mass spectrum of the product formed from the reaction between *exo* carbic anhydride and 5-amino-1-pentanol (*N*-(hydroxypentanyl)-*cis*-5-norbornene-*exo*-2,3-dicarboximide).

The MS spectrum above (Figure 50) corresponds to the major peak in the GC trace at RT = 4.353 and contains a parent ion peak at $m/z = 249.1$. This parent ion peak is in line with the monoisotopic mass of the expected product, *N*-(hydroxypentanyl)-*cis*-5-norbornene-*exo*-2,3-dicarboximide. This evidence, along with that from the ^1H NMR, strongly suggests that the product was synthesised successfully and provides additional proof that the ^1H NMR does not just show the unreacted starting materials.

N-Diamine linkers

As discussed above, amides are more stable to hydrolysis than esters and are typically easier to synthesise. Therefore, diamines can be used instead of aminoalcohols to produce a monomer with a primary $-\text{NH}_2$ group that can react with a carboxylic acid on the functional unit. However, diamines tend to be more toxic than their amino alcohol counterparts and therefore care must be taken. The fact that both functional groups on a diamine are primary $-\text{NH}_2$ groups causes issues which must be overcome. Unlike with aminoalcohols where the difference in reactivity between the $-\text{NH}_2$ and $-\text{OH}$ groups is substantial so that their reaction with carbic anhydride is

selective, the -NH_2 groups on diamines have equal reactivity. Consequently, both -NH_2 groups can react with the carbic anhydride, yielding a monomer (Figure 51) which cannot act as a linker as desired.

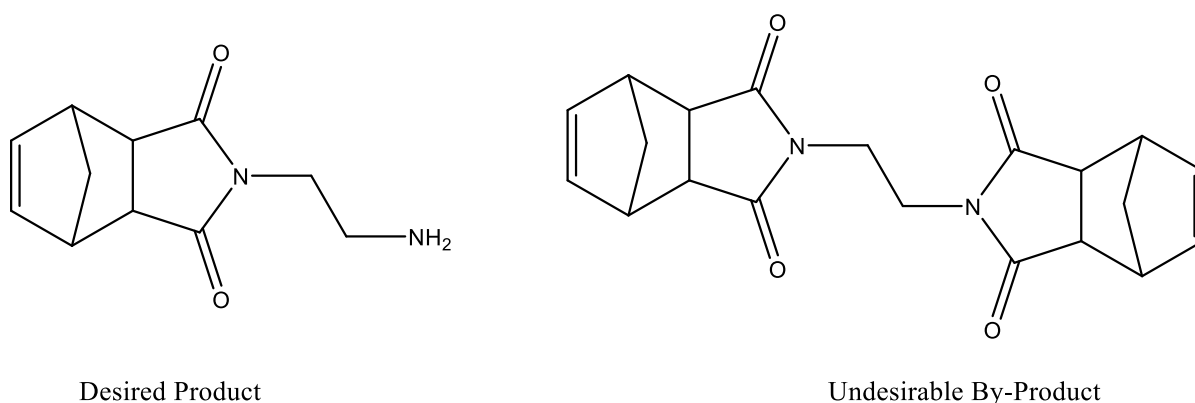


Figure 51 Possible products from the reaction between carbic anhydride and ethylenediamine.

Endo-N-(2-aminoethyl)-5-norbornene-2,3-dicarboximide

In this project, ethylenediamine was chosen as the diamine linker because it is a simple, cheap compound and the longer chain diamines tend to be more toxic. Having searched the literature for a procedure to follow, it became apparent that the reaction was not trivial as had been expected. One paper²⁷ reported that the reaction with *endo* carbic anhydride was possible using an excess of ethylenediamine but stated that attempts with the *exo* isomer had failed. Other literature procedures have reported successful reactions with the *exo* isomer, but the purification procedures varied drastically from column chromatography^{8,31,32} to no work-up explanation at all³⁰. One paper³³ stated that the product was obtained but not properly purified as its purity would not affect subsequent steps. However, for the purposes of this project, it was necessary to develop a work-up procedure to isolate and characterise the purified product.

Initially the reaction between *endo* carbic anhydride and ethylenediamine was attempted following a procedure²⁷ where 4 equivalents of the diamine were used. *Endo* carbic anhydride was dissolved in toluene which required some gentle heating and agitation. Once fully dissolved and the solution had cooled slightly, ethylenediamine was added slowly, causing a white precipitate to form which dissolved once the solution was heated under reflux and stirred. The identity of the white precipitate is not known, and although the precipitate

could be the product, the reaction was left to proceed to reach an equilibrium and therefore maximise conversion.

After the solution had been heated under reflux for 18 hours, the solution was left to cool and then the solvent was removed *in vacuo*, leaving a solid residue. The procedure was followed in adding ethyl acetate, but a vast majority of the residue did not dissolve. The mixture was then filtered, and the ethyl acetate was removed *in vacuo*, yielding a yellow-orange oil which later solidified after additional drying. The solid was analysed by ^1H NMR which is shown below in Figure 52.

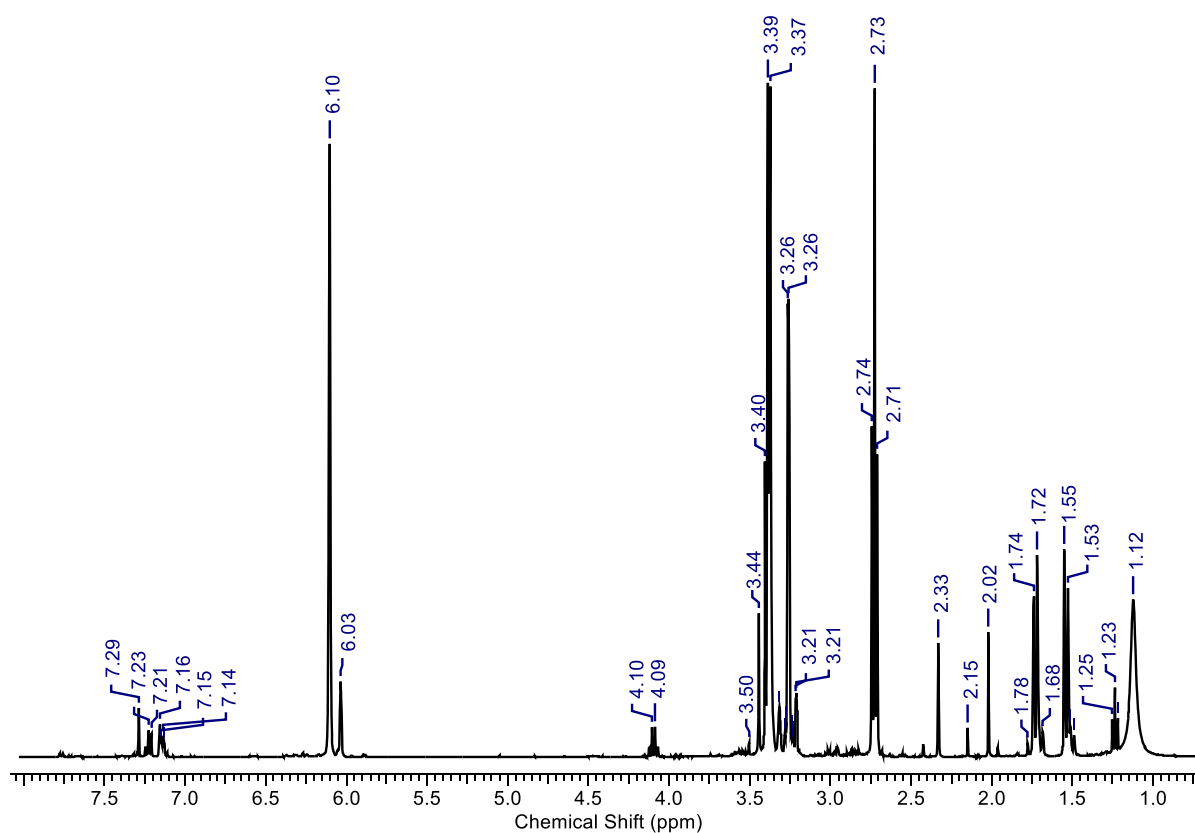


Figure 52 ^1H NMR spectrum of the crude product from the reaction between *endo* carbic anhydride and ethylenediamine (*endo-N*-(2-aminoethyl)-5-norbornene-2,3-dicarboximide) after initial work-up with ethyl acetate.

From the ^1H NMR in Figure 52, it is apparent that the work-up procedure from the literature was not successful. The peaks at δ 6.10 and δ 6.03 are indicative of the alkene environments on the norbornene and clearly these represent two different environments. These two environments were suspected to represent the product and the by-product, but further analysis of the spectrum is required to distinguish between them. Another large, well-defined peak on the spectrum is the triplet at δ 2.73. This triplet is not present in the spectrum of the

starting material, carbic anhydride. Therefore, it was suspected to be indicative of the CH_2NH_2 environment on the product which would have a three-bond coupling to the adjacent CH_2 group, giving rise to the triplet seen.

It is important to note that the triplet peak at δ 2.73 cannot be representative of the by-product as the alkane peak would not be a triplet. The by-product is symmetrical and thus the alkane environments, $\text{NCH}_2\text{CH}_2\text{N}$, are equivalent and would be represented by a large singlet on the ^1H NMR. Integration of the peaks at δ 6.10 and δ 2.73 showed that 2 hydrogens were present in each environment as expected. Therefore, the peak at δ 6.10 was suspected to represent the product and the peak at δ 6.03 was suspected to represent the by-product. Looking at the relative intensities of these two peaks and their integrations, it can be deduced that there is significantly more product present and the integration suggests a ratio of 10:1 for product:by-product.

Knowing from the initial reaction conditions that the residue is soluble in toluene, the residue was taken up in toluene and washed with water. The organic layer was then dried over MgSO_4 , filtered and the solvent removed *in vacuo*. The resulting solid was analysed by ^1H NMR, and the spectrum is shown below in Figure 53.

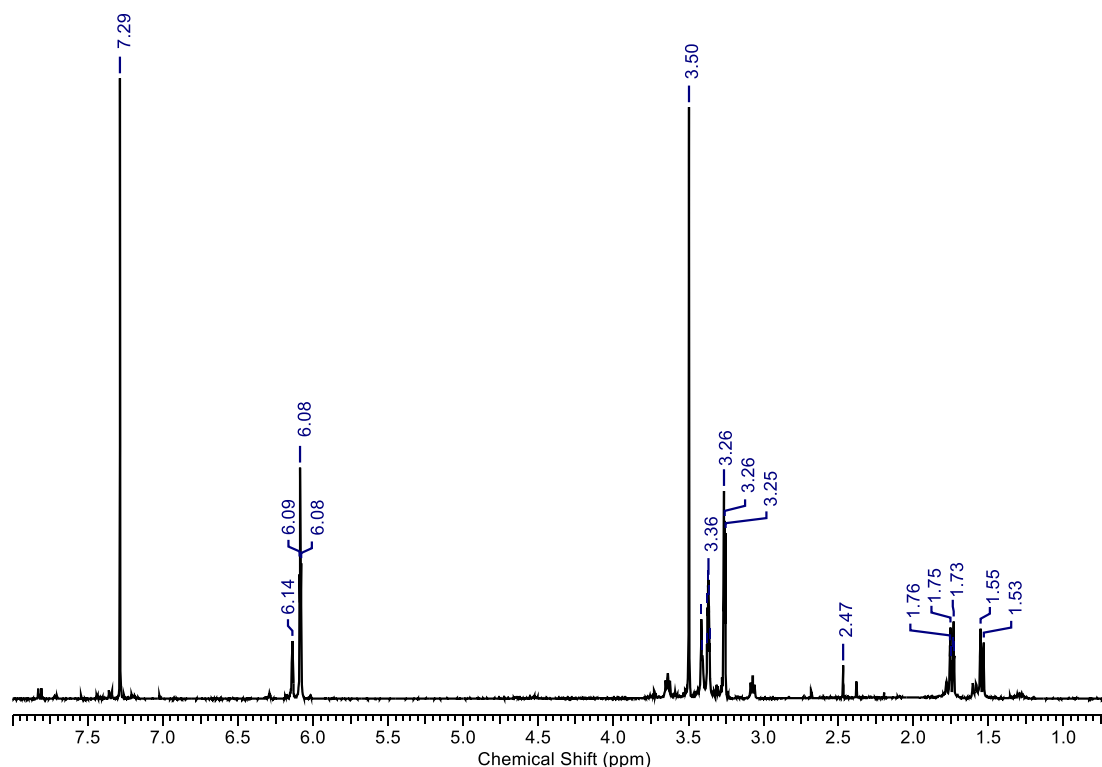


Figure 53 ^1H NMR spectrum of the crude product from the reaction between *endo* carbic anhydride and ethylenediamine (*endo-N*-(2-aminoethyl)-5-norbornene-2,3-dicarboximide) after extraction with toluene and water. Suspected to mostly contain the undesired bis product.

Looking at the ^1H NMR spectrum after the toluene/water wash it is clear to see that there are still two alkene environments present at δ 6.14 and δ 6.08, supposedly representing the product and by-product respectively. The peak at δ 3.50 is a large singlet which is suspected to represent the equivalent alkane environments that were previously mentioned. The integration of the peaks at δ 6.08 and δ 3.50 showed 4 protons in each environment. This is expected, as the by-product has two alkene norbornene environments which are equivalent by symmetry, giving 4 protons. The alkane environments are also equivalent by symmetry as discussed and explains why the peak at δ 3.50 contains 4 protons. Therefore, it can be deduced that the wash with toluene most likely separated the by-product from the crude residue.

The toluene wash can be rationalised retrospectively as the by-product contains two norbornenes and no $-\text{NH}_2$ group, making it unlikely to stay in the aqueous phase and more likely to go into the toluene layer. On the other hand, the desired product contains only one norbornene and an $-\text{NH}_2$ group, making it likely to compete between the two phases due to the hydrogen bonding capabilities of the $-\text{NH}_2$ and the organic nature of the norbornene. This explains why a small amount of the product, represented by the peak at δ 6.14, is present in the spectra after washing with toluene. However, comparing the crude NMR spectra to the spectra after the toluene wash, it is clear to see that only a small amount of the product is present after the toluene wash, and therefore most of the desired product remained in the aqueous phase.

Having deduced that the product had remained mostly in the aqueous phase, it was necessary to find a suitable solvent to separate the product from it. Previous experience with the reaction between carbic anhydride and 5-amino-1-pentanol showed that the work-up involving DCM and HCl/brine was able to successfully isolate the product into the organic layer. The product in that reaction is not too different from the amine product as both contain the norbornene as well as a group that is capable of hydrogen bonding. Using this logic, DCM was washed with the aqueous layer along with brine several times. The organic layer was then dried over MgSO_4 , filtered and the solvent was removed *in vacuo*, affording a yellow solid which was analysed by ^1H NMR. The NMR spectrum is shown below in Figure 54.

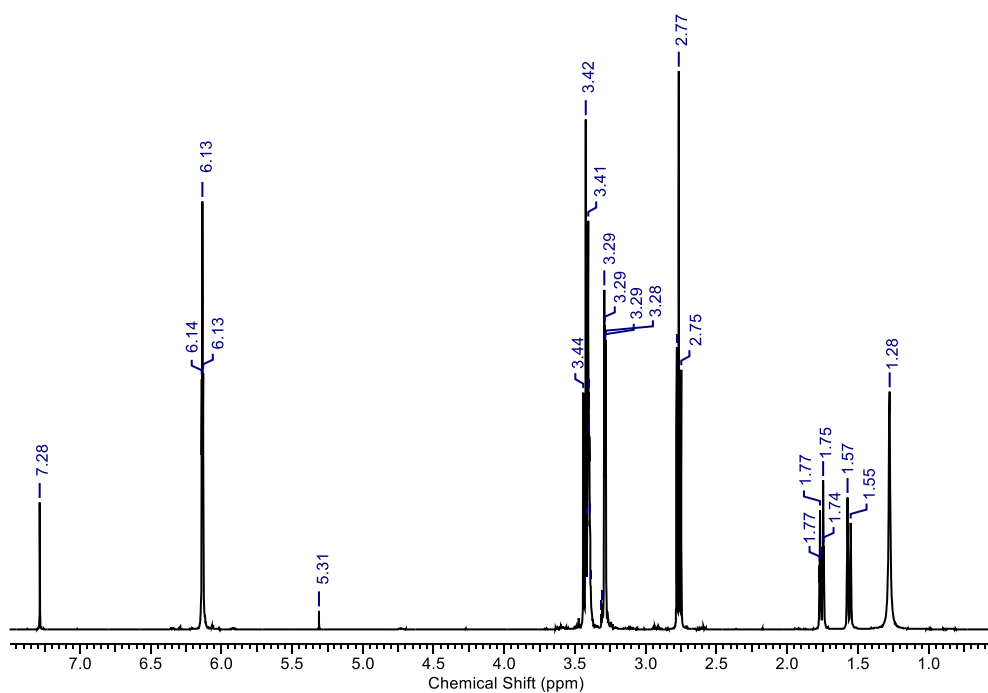


Figure 54 ^1H NMR spectrum of the purified product from the reaction between *endo* carbic anhydride and ethylenediamine (*endo*-*N*-(2-aminoethyl)-5-norbornene-2,3-dicarboximide) after extraction from water with DCM.

From the NMR spectrum after the DCM/water wash, it can be seen that there is only one alkene norbornene environment present at δ 6.13, hinting to the successful isolation of the product. The triplet at δ 2.77, which was present in the crude NMR, can be seen in the spectra above, which is further indication of the product. The CH_2 bridgehead region is clean and contains only one set of second-order peaks as expected, exhibiting the 'roofing' effect. There is a broad singlet peak at δ 1.28, that integrates to 2 protons, which should represent the $-\text{NH}_2$ group. Without COSY NMR the peaks at δ 3.42 and δ 3.29 cannot be distinguished easily, but in total they integrate to 6 protons which corresponds to the number of unassigned protons for the product. The NMR spectrum is very clean, apart from a very small amount of residual DCM at δ 5.31 and therefore shows that the product was successfully isolated and purified.

Having discovered how to isolate the pure product, the reaction was repeated without the unnecessary ethyl acetate step. Instead the reaction solvent, toluene, was removed and the residue was taken up in toluene and washed with water. Although it may seem counterintuitive to remove the toluene and then dissolve it again in toluene, it was done purposefully. When removing the reaction solvent, toluene, *in vacuo* the excess ethylenediamine is also removed. This means that there is one less component to deal with during the washing

process. The full repeated procedure resulted in a yield of 33% and is described in the experimental section.

Characterisation of the product is shown and explained below.

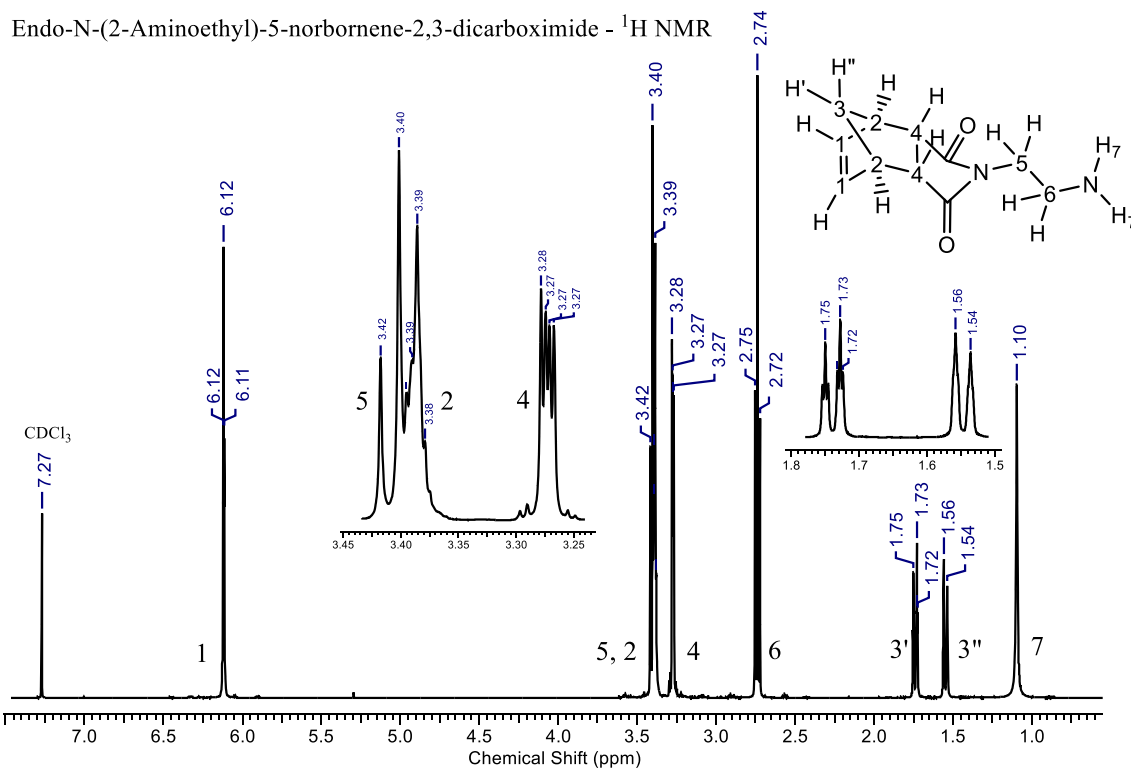


Figure 55 Annotated ^1H NMR spectrum of the purified product from the reaction between endo carbic anhydride and ethylenediamine (endo-N-(2-aminoethyl)-5-norbornene-2,3-dicarboximide) with expanded regions included.

Endo-N-(2-Aminoethyl)-5-norbornene-2,3-dicarboximide - COSY NMR

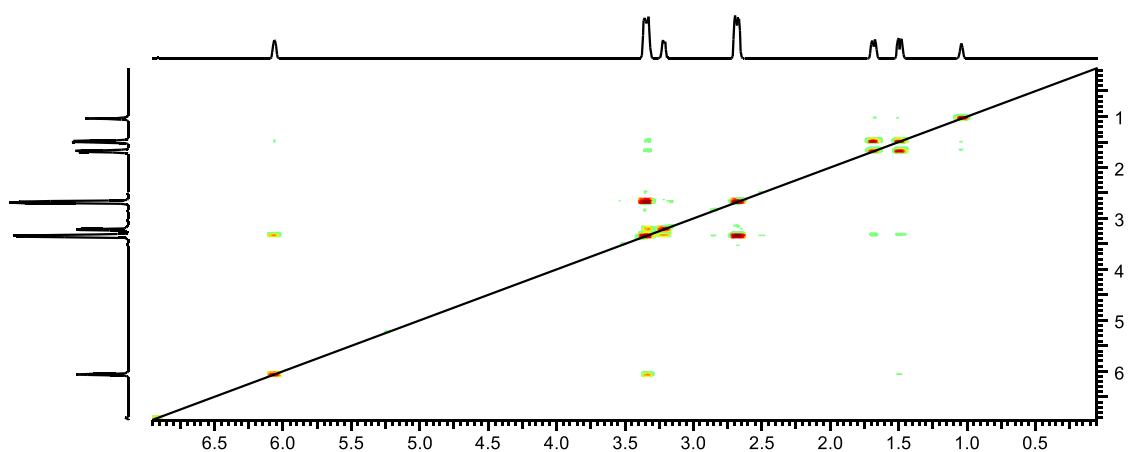
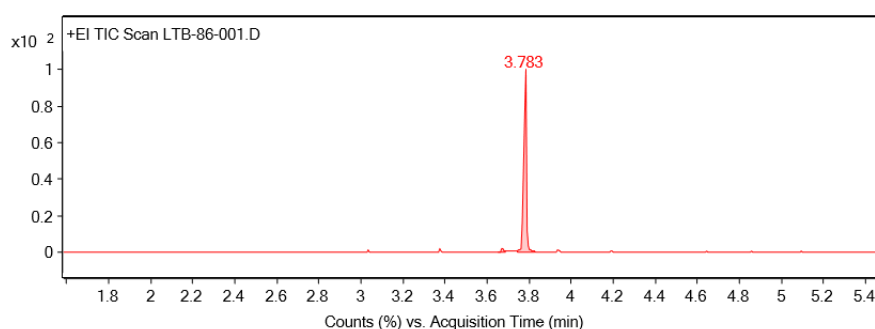


Figure 56 COSY NMR spectrum of the purified product from the reaction between endo carbic anhydride and ethylenediamine (endo-N-(2-aminoethyl)-5-norbornene-2,3-dicarboximide).

As with the assignment of *endo* carbic anhydride, the peak at δ 6.12 is easiest to assign as 1 because it is indicative of the alkene protons on the norbornene. Using the COSY NMR (Figure 56), the peak at δ 3.39 can be assigned as 2, due to the presence of its expected three-bond coupling with 1. It is important to note here that environments 5 and 2 overlap lightly, where 5 appears to be a triplet, and 2 appears to be a multiplet. Environment 1 is also seen to be coupling very weakly to peak 3", which, as before can be explained by W-coupling. Having assigned peak 3", peak 3' can be assigned as the other bridgehead proton, which shows no long-range coupling on the COSY. This provides some evidence towards the *endo* conformation as explained previously due to the lack of a 'W-like' arrangement needed for long-range coupling.

Peak 2 shows some moderate coupling with peak 4, indicative of a 3-bond coupling and therefore 4 must be representative of the only other unassigned adjacent environment, 4. The peak at δ 1.10 is a broad singlet, shows no coupling on the COSY, and integrates for 2 protons, and is therefore indicative of the NH₂ environment.

The remaining two unassigned environments are the alkane environments between the dicarboximide and the amine which cannot be distinguished using COSY NMR as they are both adjacent to a nitrogen atom. However, the environment adjacent to the dicarboximide is expected to be more deshielded than the environment adjacent to the amine. This is due to the greater electron withdrawing strength of the dicarboximide compared with the amine. There are two unassigned triplet peaks, 5 and 6, at δ 3.40 and δ 2.74 respectively. Peak 5 can be assigned as the environment adjacent to the dicarboximide as it is the most deshielded and therefore most downfield of the two triplet peaks. Peak 6 can therefore be assigned as the environment adjacent to the amine which is more shielded and upfield than peak 5.



Integration Peak List							
Peak	Start	RT	End	Height	Area	Area %	
1	3.652	3.67	3.688		30861.04	28689.63	2.17
2	3.741	3.783	3.824		1411453.96	1320416.7	100

Figure 57 GC trace of the purified product from the reaction between *endo* carbic anhydride and ethylenediamine (*endo*-N-(2-aminoethyl)-5-norbornene-2,3-dicarboximide).

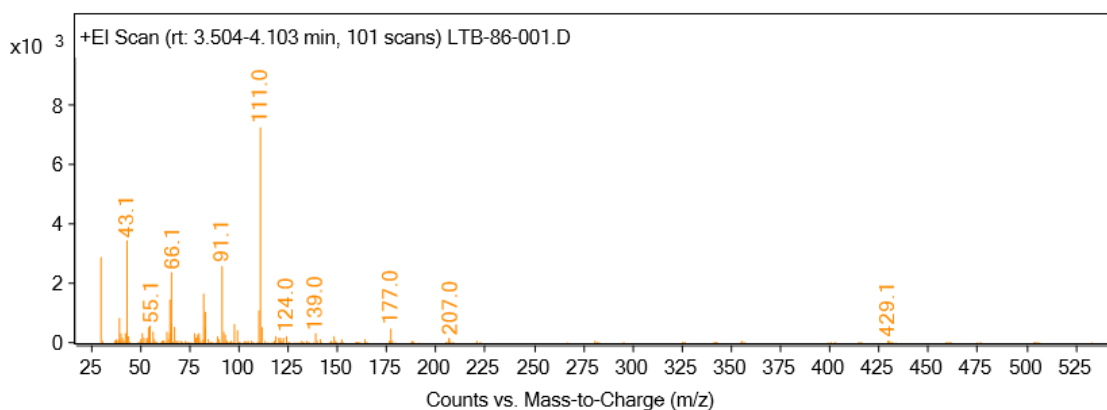


Figure 58 Mass spectrum of the crude product from the reaction between *endo* carbic anhydride and ethylenediamine (*endo*-*N*-(2-aminoethyl)-5-norbornene-2,3-dicarboximide).

The GC trace (Figure 57) shows a large peak at RT = 3.783 which should be indicative of the product. There are some very small peaks present but these most likely represent normal column bleed due to a low mass of analyte. Using the integrations determined by the software, the analytical purity of the product can be calculated as 98%. The MS spectrum shows a very small peak at 429.1 which can be attributed to a column bleed ion. There is a very small parent ion peak at $m/z = 207.0$. This does not correspond directly with the monoisotopic mass of the product which is 206.1 g mol^{-1} . However, it may be representative of the protonated product or perhaps the isotope ion peak which may be more stable than the monoisotopic ion peak. It is also worth mentioning that there is a peak at $m/z = 177.0$ which is 30 g mol^{-1} less than the peak at $m/z = 207.0$. A fragmentation loss of 30 g mol^{-1} is indicative of the breakdown of some primary amines where the fragment lost is $\text{CH}_2=\text{NH}_2^+$. Overall, the GC-MS and NMR results indicate that the product, *endo*-*N*-(2-aminoethyl)-5-norbornene-2,3-dicarboximide, was successfully synthesised with a high analytical purity.

Recorded melting point: 76 – 78 °C

Literature melting point value: ²⁷60 – 62 °C

There is disparity between the recorded melting point values and the literature values. However, there is no evidence of purity such as GC-MS provided alongside the literature value. The purity of the product synthesised in this project was found to be 98% by GC-MS and the ¹H NMR was very clean. Therefore, it may be the case that the product synthesised in this project is purer than the literature example, causing disparity in the values.

Exo-N-(2-aminoethyl)-5-norbornene-2,3-dicarboximide

Despite claims in the literature that the analogous synthesis of the *exo* adduct results only in the formation of the undesirable by-product, the reaction was attempted. Having successfully synthesised *endo*-N-(2-aminoethyl)-5-norbornene-2,3-dicarboximide and developed a method to isolate the analytically pure product, the same method was used in the reaction between *exo* carbic anhydride and ethylenediamine. Contrary to the literature report²⁷, the *exo* adduct was synthesised and isolated successfully (38%) using the same procedure as for the *endo* adduct. Analysis and characterisation of the product is shown and explained below.

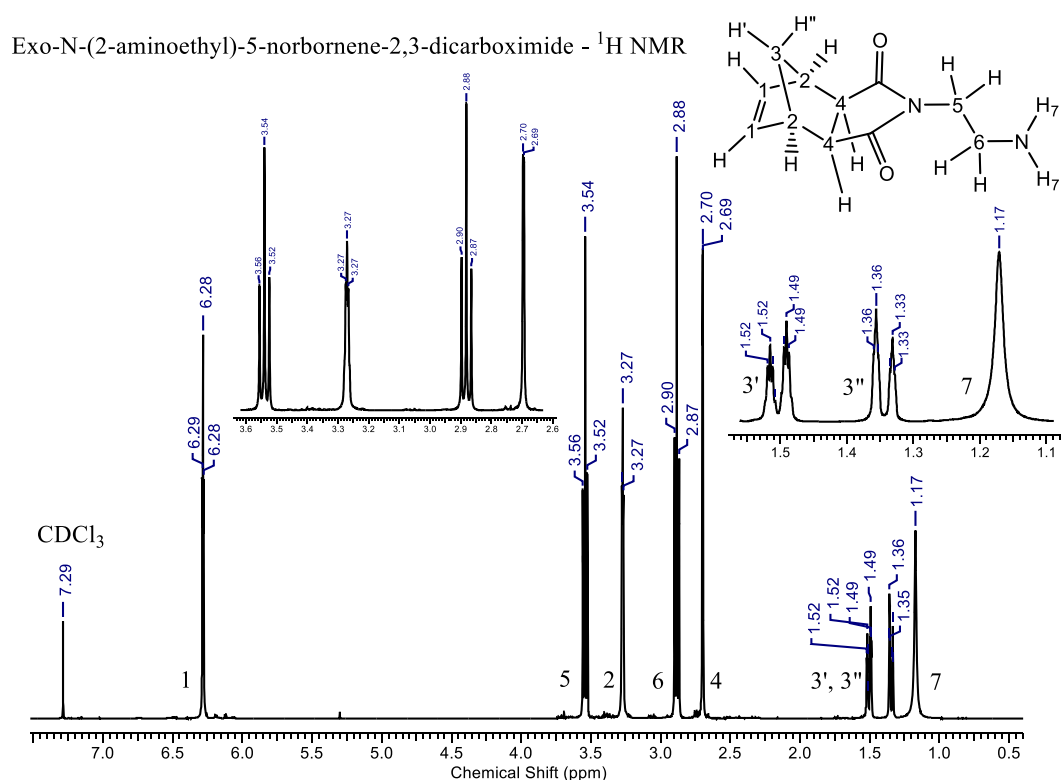


Figure 59 Annotated ¹H NMR spectrum of the purified product from the reaction between *exo* carbic anhydride and ethylenediamine (*exo*-N-(2-aminoethyl)-5-norbornene-2,3-dicarboximide) with expanded regions included.

Apart from the introduction of peaks 5, 6 and 7, the ¹H NMR (Figure 59) is extremely similar to that of *exo* carbic anhydride except that all of the peaks are shifted slightly upfield. The upfield shift can be attributed to the lower electronegativity of nitrogen compared to oxygen, meaning that electrons are withdrawn from the norbornene environments less strongly. Other than the upfield shift, the splitting patterns and coupling are almost exactly the same and thus these peaks can be assigned as they were for *exo* carbic anhydride.

Exo-N-(2-aminoethyl)-5-norbornene-2,3-dicarboximide - COSY NMR

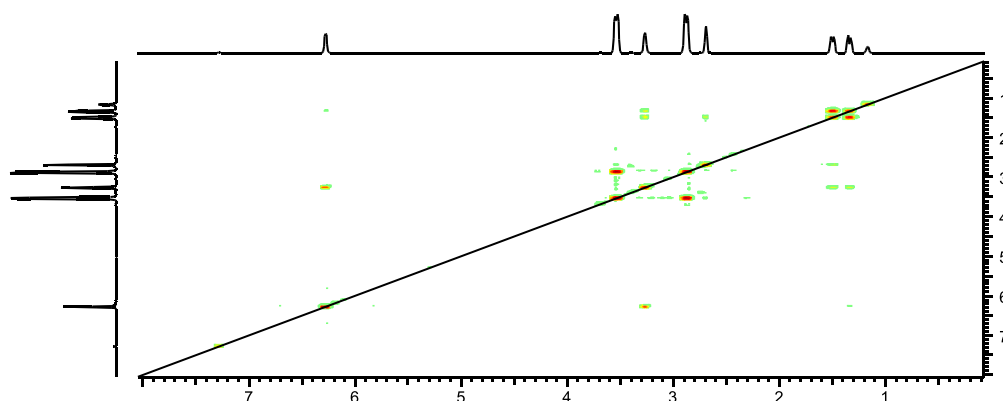
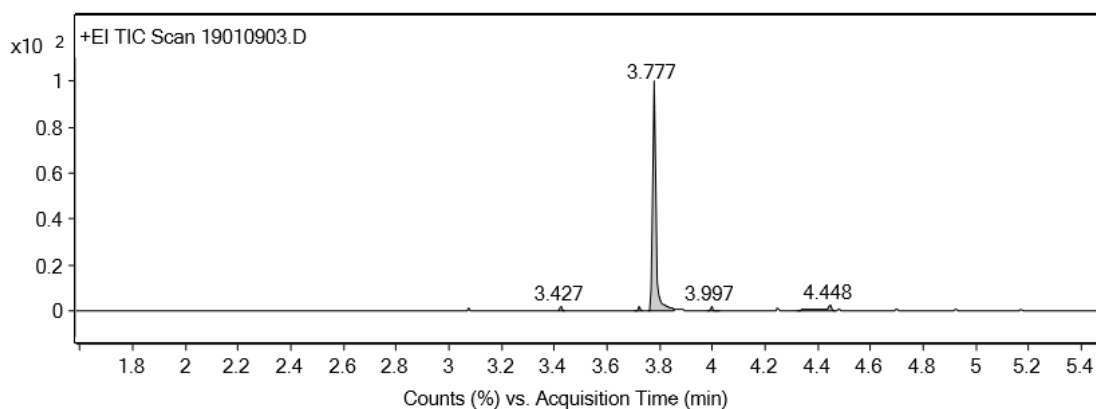


Figure 60 COSY NMR spectrum of the purified product from the reaction between *exo* carbic anhydride and ethylenediamine (*exo*-N-(2-aminoethyl)-5-norbornene-2,3-dicarboximide).

A noteworthy coupling is that between peak 3' and 4 which is indicative of W-coupling that is only present in the *exo* isomer. In terms of the new peaks, peak 7 is a broad singlet with an integration of 2 protons, indicating that it is the NH₂ environment, which along with OH environments are typically broad. The remaining two triplet peaks, 5 and 6, were assigned by the same logic as with the *endo* adduct. Overall the ¹H NMR is mostly clean, indicating a high degree of analytical purity. This is further confirmed by the GC-MS results which are shown and explained below.



Integration Peak List

Peak	Start	RT	End	Height	Area	Area %
1	3.415	3.427	3.438	17511.67	8303.07	1.1
2	3.706	3.724	3.735	16084.51	7654.89	1.02
3	3.753	3.777	3.854	800908.36	753931.18	100
4	3.979	3.997	4.026	15160.87	8924.97	1.18
5	4.323	4.448	4.464	21501.45	37905.33	5.03

Figure 61 GC trace of the purified product from the reaction between *exo* carbic anhydride and ethylenediamine (*exo*-N-(2-aminoethyl)-5-norbornene-2,3-dicarboximide).

From the GC trace (Figure 61), there is predominantly one main peak, which when compared to the ^1H NMR (Figure 59) can almost certainly be attributed to the product. The small peaks which are present again are most likely a result of column bleed due to the small amount of analyte used. Another noteworthy feature of the GC trace is that the large product peak shows some slight tailing. This is indicative of amines and carboxylic acids in GC traces, in this case though it is a result of the amine. Assuming that the small regular peaks in the GC trace are a result of the column bleed, and the presence of only one major peak, the purity of the product can be approximated as >99%.

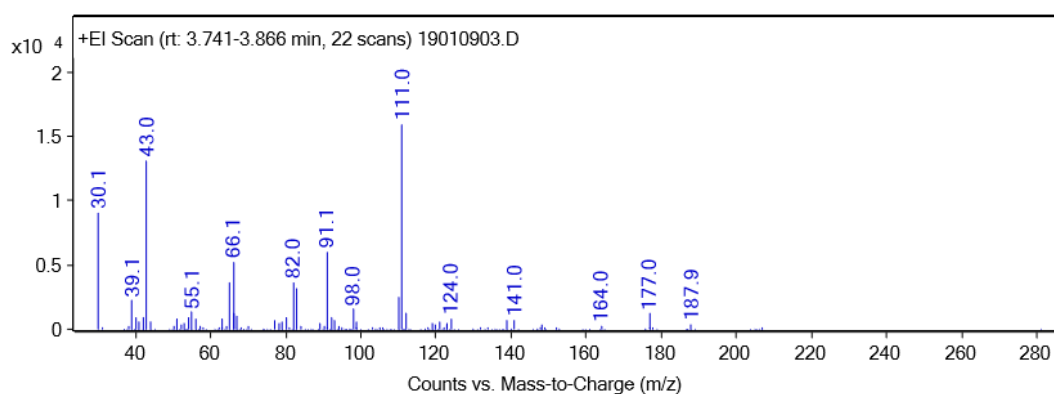
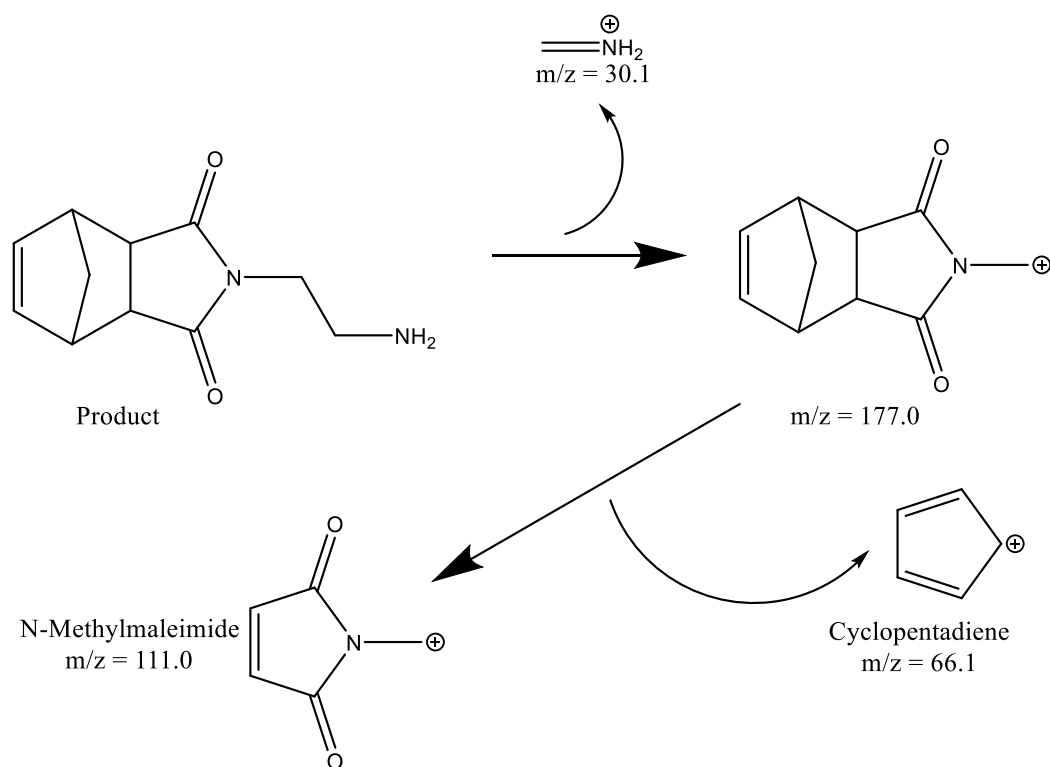


Figure 62 Mass spectrum of the purified product from the reaction between *exo* carbic anhydride and ethylenediamine (*exo*-*N*-(2-aminoethyl)-5-norbornene-2,3-dicarboximide).

The MS spectrum (Figure 62) does not show a parent ion peak at $m/z = 207$, as with the *endo* adduct. This does not mean that the product is not present, just that the molecular ion is not stable. The peaks at $m/z = 177.0$ and $m/z = 30.1$ are more indicative of the product as they represent the 'product minus fragment' and the 'fragment' respectively, where the fragment is $\text{CH}_2=\text{NH}_2^+$. The most abundant molecular ion peak on the MS is at $m/z = 111.0$. This peak can most likely be attributed to the *N*-methylmaleimide molecular ion (Scheme 9) which shows the nitrogen must have reacted with the anhydride, thus forming the product. This is further supported by the peak at $m/z = 66.1$, which can be attributed to cyclopentadiene, showing a retro Diels-Alder type fragmentation could have led to the *N*-methylmaleimide fragment. The suggested fragments (omitting charges where unknown) are shown in Scheme 9.



Scheme 9 Possible fragmentation pattern of the product from the reaction between carbic anhydride and ethylenediamine (*endo/exo*-*N*-(2-aminoethyl)-5-norbornene-2,3-dicarboximide) based off fragments detected in the mass spectra.

Although it is not entirely clear why the MS spectrum of the *endo* and *exo* diamine derivatives have higher than expected parent ion peaks, even if only by >1 Dalton, there is a lot of evidence indicating that they were successfully synthesised. Protonation of the ion to give the [M + H] ion peak is highly unlikely, as the ionisation used was EI (Electron Ionisation). The evidence for the products will be summarised below:

- The ^1H NMR spectra are clean, and all peaks were assigned using both the COSY NMR and scientific logic. Importantly, the broad singlet peaks on the ^1H NMR's integrated for 2 protons, as expected, which wouldn't be seen if an OH group was present.
- One of the most abundant fragmentation peaks in the MS spectra is the peak at $m/z = 30.1$ which is indicative of the fragmentation of primary amine, as shown in Scheme 9.
- Crystal structures of products that were synthesised from these diamine derivatives are shown in Figure 82 and Figure 87 below. These provide very strong evidence for the successful synthesis of the diamine derivatives.

Functional unit addition

As previously mentioned, monomers can gain useful properties when certain functional units are attached to the linker. These functional units can be anything that is attachable via a suitable reaction and provides the monomer with a desirable property.

Due to the size of polymers, they tend to self-assemble under certain conditions, forming structures such as micelles, which are nanoparticles. Assemblies of this size are known to benefit from the enhanced permeability and retention (EPR) effect⁴¹, meaning they are more likely to accumulate in tumour cells than healthy cells. As a result of this phenomenon, it is common and desirable to design polymers that could be utilised for *in vivo* applications such as diagnostic imaging and therapy. Hence, the functional units of ROMP monomers are commonly tailored towards imaging such as fluorescence and MRI by incorporating fluorophores and/or contrast agents.

ROMP is a relatively recent area of research, especially in terms of finding desirable uses for the polymers, as initial studies focused mainly on understanding ROMP and improving catalysts. However, in recent years, several studies have highlighted the potential of ROMP. Simple studies have been carried out where fluorophores such as 7-hydroxycoumarin⁵⁹ and fluorescein⁶⁰ (Figure 63) have been incorporated into monomers and the fluorescence properties of the resulting polymers have been investigated.

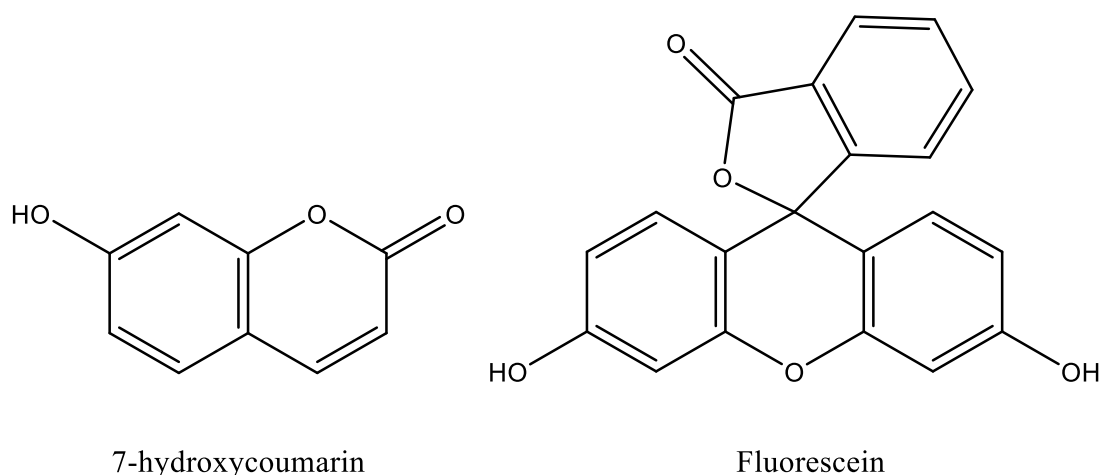


Figure 63 Chemical structures of 7-hydroxycoumarin and fluorescein.

More complex studies have investigated the copolymerisation of functional monomers, allowing for improved solubility, targeting and/or imaging potential^{39,61}. However, the most complex study has investigated copolymers consisting of monomers that complement each other and have been tested for *in vivo* applications.

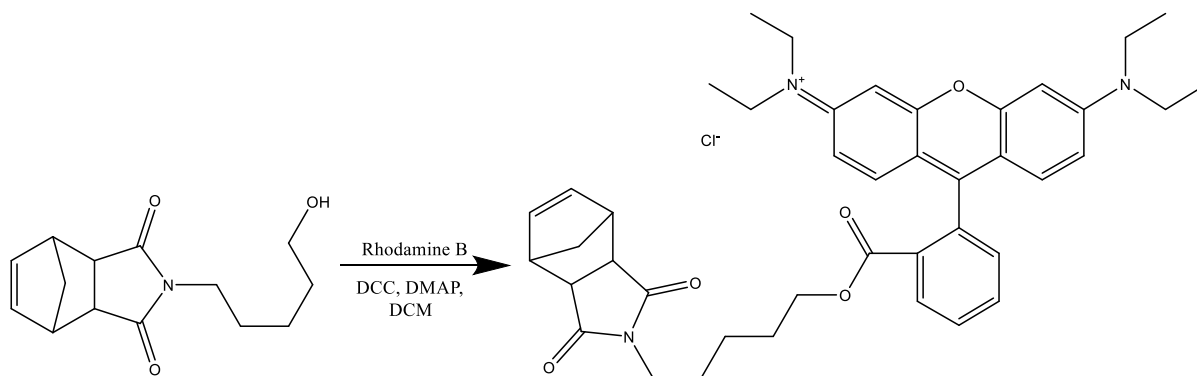
The study by Sowers *et al.*⁹ took monomer design to another level where two functionalities were incorporated into a single monomer. Their monomer Chex-MM contains a nitroxide radical species which acts as a good Gd-free contrast agent for MRI and a PEG chain for solubility and biocompatibility. The other monomer Cy5.5-MM contains the fluorophore Cy5.5, allowing for fluorescence imaging to occur, as well as a PEG chain. These are known as macromonomers and reduced the total number of different monomers needed in the copolymer.

These macromonomers were copolymerised by a statistical copolymerisation and have shown positive results in *in vivo* studies. This is a great example showing how the careful design of ROMP monomers can lead to incredible polymers with numerous interesting properties.

Due to the limited length of this project, only one functional unit was attached to the linker at a time. Reported procedures^{35,39,40} have demonstrated that the fluorescent dye rhodamine B could be attached to a suitable linker via a Steglich esterification. As rhodamine B is a relatively cheap fluorophore and the 5-amino-1-pentanol derivative had been synthesised during this project, it was decided that they would be reacted together. This was decided to provide an alternative RhB based monomer that could be incorporated into copolymers for fluorescence imaging. Due to the *exo* linker being precious, the reaction was initially attempted using the *endo* linker.

Endo ester RhB

A Steglich esterification can be performed using several different reagents, but the reaction mixture typically consists of a carboxylic acid (Rhodamine B (RhB)), an alcohol (*N*-(hydroxypentanyl)-*cis*-5-norbornene-*endo*-2,3-dicarboximide), a carbodiimide (dicyclohexylcarbodiimide (DCC)), an acyl-transfer reagent (DMAP) and a suitable solvent (DCM). A common issue with this reaction is the urea by-product dicyclohexylurea (DCU) which is difficult to remove during work-up. The scheme for the reaction that was conducted is shown below (Scheme 10).



Scheme 10 Reaction scheme for the Steglich esterification between N-(hydroxypentyl)-cis-5-norbornene-endo/exo-2,3-dicarboximide and rhodamine B, using DCC as the carbodiimide, DMAP as the base and DCM as the solvent.

The reaction itself is a simple procedure that requires stirring the reagents together overnight in the solvent, DCM, at room temperature. However, as previously mentioned, the DCU by-product is difficult to remove. It was decided that the best way to remove the by-product and obtain a pure product was to use column chromatography. Several TLC plates were run to determine a suitable solvent system. The best system found was DCM:Methanol 15:1, where the expected product had an $R_f = 0.26$.

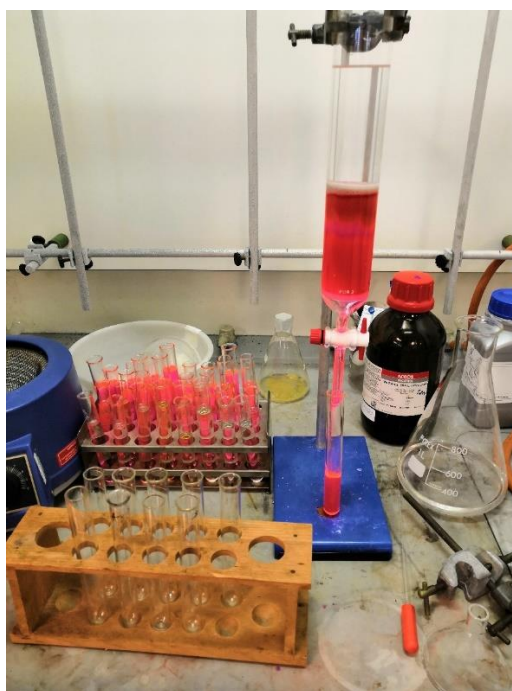


Figure 64 Image depicting the column used to purify the endo ester RhB monomer which shows some of the fluorescent fractions obtained.

The solvent, DCM, was removed from the reaction mixture *in vacuo*, leaving a shiny brown crude residue. 300 mg of the crude residue was run on a column using the DCM:Methanol 15:1 system described above. The colour of the fractions very clearly changed as more fractions came off the column, going from a very faint yellow to a more fluorescent pink/orange colour which can be seen in Figure 64.

Many of the initial fractions contained several spots on the TLC plate, but as the fractions became more and more pink/orange, the number of spots decreased to a single spot, indicating a single component had been isolated. After a few days, once some solvent had evaporated from the fractions, some white needle-like crystals had grown in many of the initial fractions. These white crystals were expected to be the DCU by-product. Fraction 6 was filtered, and the crystals were collected to be analysed by ^1H NMR which is shown below in Figure 65.

Endo ester RhB column - Fraction 6 - white needle crystals

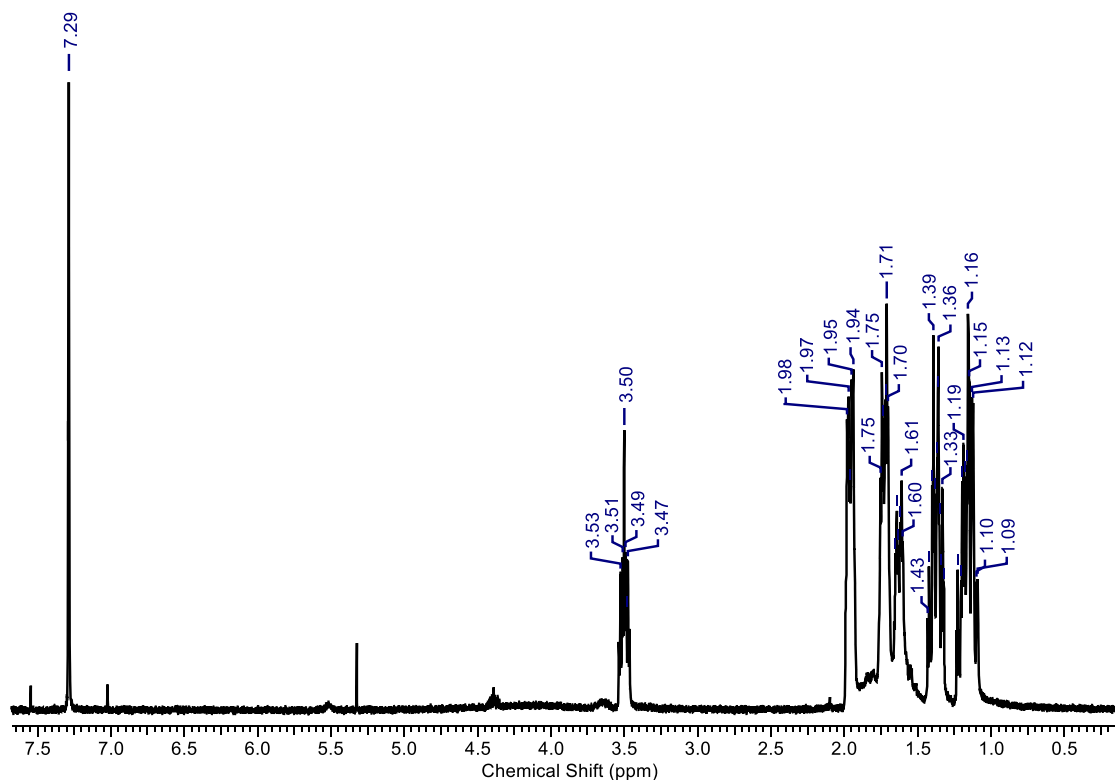


Figure 65 ^1H NMR spectrum of the white needle-like crystals collected in the initial column fractions during the purification of the endo ester RhB monomer. Expected to be the by-product dicyclohexylurea (DCU) based off comparison to literature examples.

The spectrum was not analysed in detail but was instead compared to literature spectra⁶² for the by-product, DCU. It was found to match the spectrum well and can almost certainly be attributed to the DCU impurity. The

DCU crystals persisted through many of the fractions, however, upon combining the fractions of the product, it was ensured that some space was left between the DCU fractions and the clean fractions to avoid any DCU contamination. To obtain an analytical sample, only a couple of fractions containing 1 spot were combined. The solvent was then removed *in vacuo*, yielding the resulting product (6%), which was dissolved in CDCl₃ for ¹H NMR analysis. The ¹H NMR spectrum and its expanded regions are shown below in Figure 67 and Figure 68 respectively.

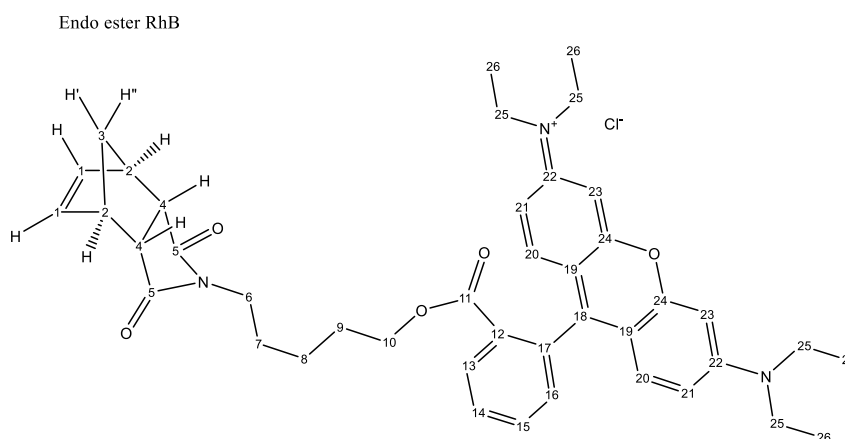


Figure 66 Representation of the chemical structure of the product endo ester RhB with the carbon atoms numbered for easy assignment of NMR spectra.

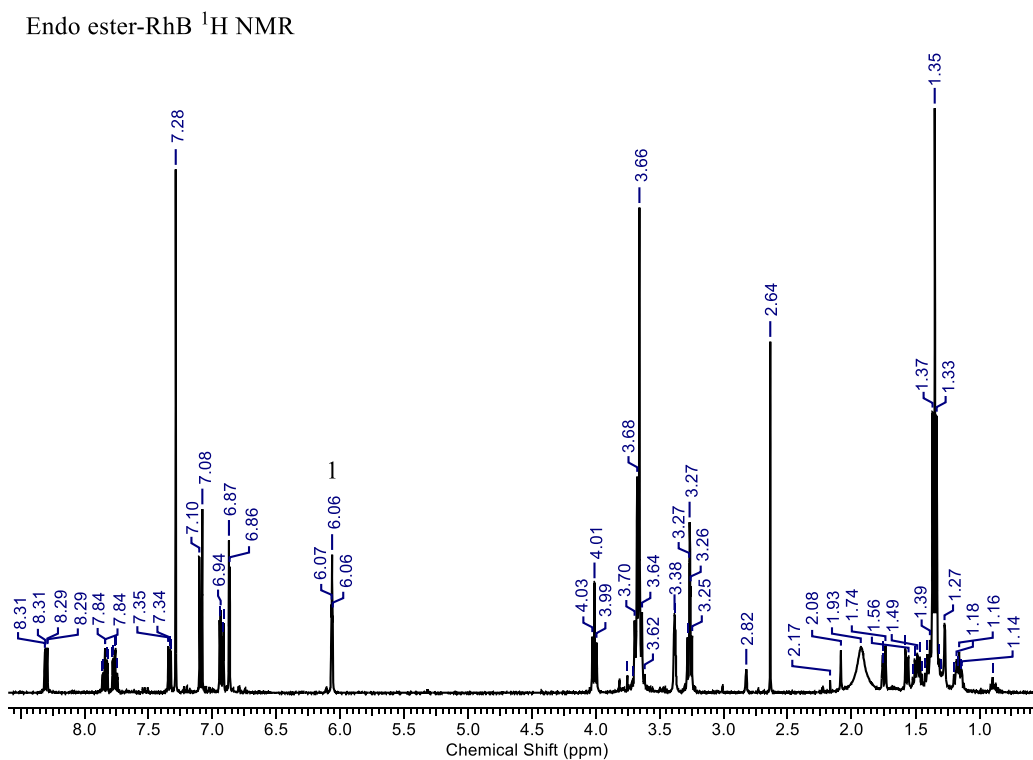


Figure 67 Partially annotated ¹H NMR spectrum for the product between *N*-(hydroxypentanyl)-*cis*-5-norbornene-endo-2,3-dicarboximide and rhodamine B (endo ester RhB).

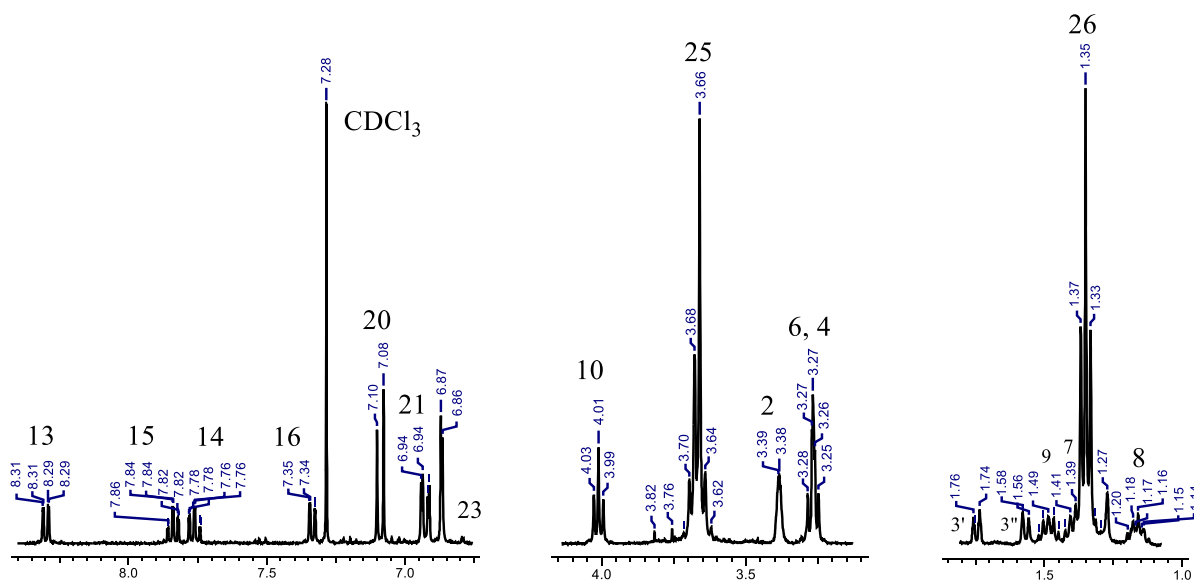


Figure 68 Annotated expanded regions from the ^1H NMR spectrum for the product between *N*-(hydroxypentanyl)-*cis*-5-norbornene-*endo*-2,3-dicarboximide and rhodamine B (*endo* ester RhB).

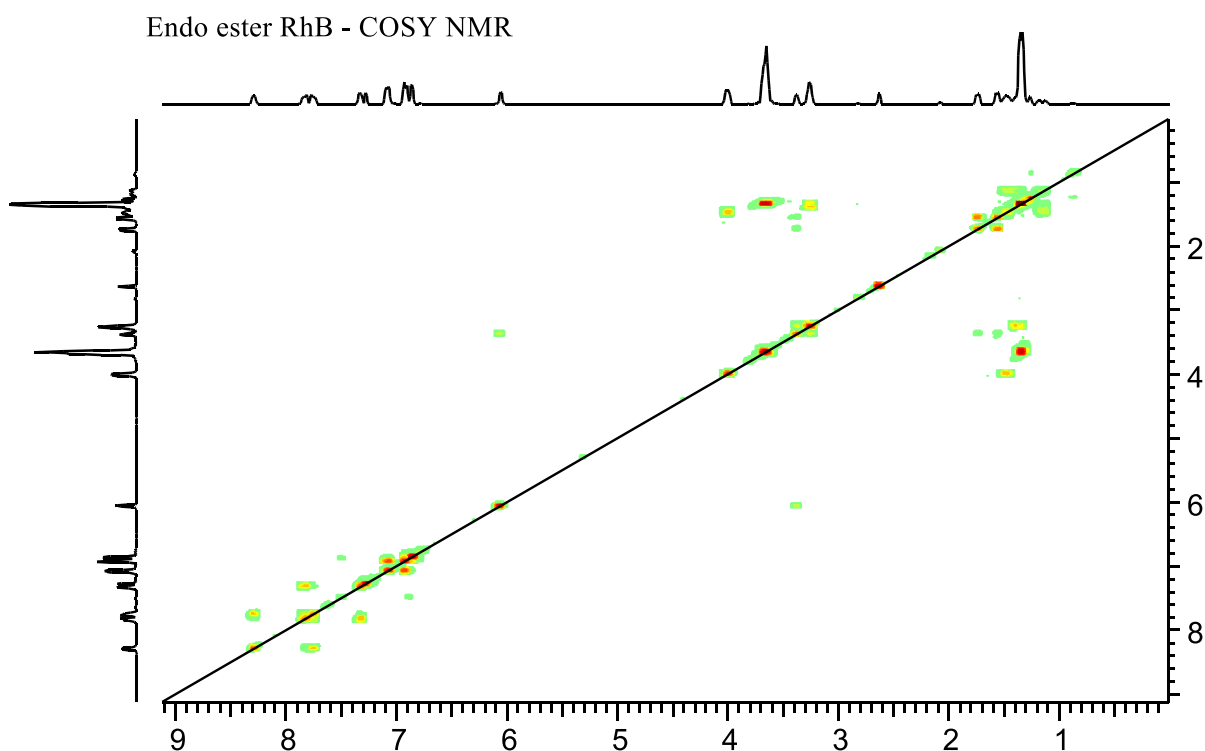


Figure 69 COSY NMR spectrum for the product between *N*-(hydroxypentanyl)-*cis*-5-norbornene-*endo*-2,3-dicarboximide and rhodamine B (*endo* ester RhB).

There are many environments present in the *endo* ester RhB compound and as a result there is some peak overlap between environments. Although the norbornene section was assigned in the same way as it was for

the previous products, it is less obvious in this case due to the peak overlap and will therefore be explained in detail. Furthermore, the ^1H NMR spectrum for the product above in Figure 67 is not completely clean and therefore a cleaner sample obtained from a single column fraction is shown below in Figure 70.

Starting from peak 1 at δ 6.06, indicative of the alkene peak, it can be seen to couple with peak 2 at δ 3.39 which must be the adjacent environment. Upon zooming in on the COSY in ACD NMR software, peak 1 can also be seen to couple very weakly (w-coupling) to the bridgehead peak 3", which was used to distinguish it from the other bridgehead peak 3'. Peak 2 is shown to couple with the peak at δ 3.27, but the integration shows 4 protons and the environment is also coupling to a peak at δ 1.39. This can be explained by the fact that there is a direct overlap of two environments, and therefore environment 4 can be assigned as one of the two environments present in that peak.

The linker was the next section of the product to assigned, starting with the most downfield (ignoring the aromatic region) triplet peak (10) at δ 4.01, which can be attributed to the CH_2 environment adjacent to the oxygen of the ester. The peak that was overlapping with environment 4 of the norbornene environment is the other expected triplet and can be assigned as the environment (6) adjacent to the nitrogen of the dicarboximide. Peak 9 was assigned as a result of its coupling to peak 10. Peak 7 is less clearly visible as it is overlapping slightly with the very large peak at δ 1.35, however it was assigned at δ 1.39 which shows coupling with environment 6. Both peaks 9 and 7 can be seen coupling to the peak at δ 1.17, which is most upfield as expected and can therefore be assigned to the central environment (8) of the linker.

There were no NMR peaks in the aromatic region of the starting material, *N*-(hydroxypentanyl)-*cis*-5-norbornene-*endo*-2,3-dicarboximide. Therefore, the peaks present in the aromatic region of the product NMR provide an indication that a transformation has occurred. The assignment of the RhB section of the product was relatively simple and achieved by looking at couplings as well as electron-donating and electron-withdrawing effects in aromatic systems.

The RhB section of the product was assigned in three parts. The peaks between δ 8.31 and δ 7.34 belong to the protons on the aromatic ring that is connected to the carbonyl of the ester. The ester is an electron withdrawing group (EWG) which leaves the protons deshielded and results in them being more downfield. The remaining peaks in the aromatic region that are more upfield can be attributed to the other aromatic rings, which are

symmetric and connected to the NEt_2 groups. The NEt_2 groups are electron donating groups (EDGs) which increase the electron density in the aromatic rings and cause the protons to be more shielded, resulting in them being more upfield. Finally, the protons on the NEt_2 groups were assigned separately as they do not fall within the aromatic region on the NMR.

The first peak of the RhB section to be assigned was the doublet at δ 8.30 as environment 13. Electron-withdrawing groups de-shield the ortho and para positions strongly and de-shield the meta positions weakly. However, the ortho position is deshielded most strongly of all due to its close proximity to the EWG and explains why 13 was assigned as the most downfield peak. Peak 13 is shown to couple with the triplet peak at δ 7.76 and can therefore be assigned to environment 14 which is adjacent to 13. Peak 14 is also shown to be coupling with the triplet peak at δ 7.84 which can be assigned to the adjacent environment 15. The fact that peak 15 is more downfield than peak 14 here is consistent with the fact that 15 is ortho to the EWG. Environment 15 is more strongly deshielded than environment 14 despite the closer proximity of 14 to the EWG as a result of EWG effects. On the COSY NMR (Figure 69), peak 15 can be seen to couple with the peak at δ 7.35 which can be assigned as environment 16. Environment 16 is in the meta position relative to the ester EWG and is therefore least deshielded. Furthermore, environment 16 is also closer to the connected aromatic system which can weakly donate electrons. This explains the disparity between the NMR shifts of environments 14 & 16 which are both meta to the ester EWD but 16 is closer and ortho to the weak EDG that is the connected aromatic system.

In the xanthene section of the RhB moiety, the aromatic rings are equivalent due to the symmetry despite there being a charge on one of the NEt_2 groups. This is because the electrons can move through the entire xanthene aromatic system through resonance forms. Therefore, on average, the electron density across both rings is equal, resulting in the observed symmetry.

Environment 23 can be assigned to the peak at δ 6.87 because it shows very little coupling as expected. Although it is not adjacent (ortho) to any other protons, aromatic rings can allow for long range coupling, mostly between proton environments that are meta to each other. This explains why the peak assigned to environment 23 is a doublet, as it can couple weakly (2.27 Hz) to environment 21. This assignment can also be explained by the fact that it is ortho to the oxygen and NEt_2 EDGs, making it the most shielded environment and therefore most upfield as observed. Environment 21 can be assigned as the peak at δ 6.93 using multiple arguments. Firstly, it is a doublet of doublets, resulting from its ortho coupling to environment 20 (9.41 Hz) and its meta coupling to

environment 23 (2.43 Hz). Secondly, it is more upfield than the other remaining aromatic peak (δ 7.09). This agrees with the fact that environment 21 is ortho to the NEt_2 EDG and is therefore shielded more strongly than environment 20 which is meta to the EDG. This essentially leads to the assignment of environment 20 as the peak at δ 7.09, as it is the least shielded as explained and appears as a doublet due to its ortho coupling (9.41 Hz) to 21.

The remaining environments to be assigned were those on the two NEt_2 groups which were equivalent by symmetry as explained above. Environment 25 was expected to be much more downfield than 26 as it is much closer to the electronegative nitrogen. It is also expected to be an intense quartet due to the 'n + 1' rule and the fact that there are 8 protons in that environment. These expectations were observed in the peak at δ 3.67 which was therefore assigned to environment 25. This peak was shown to couple on the COSY with the intense triplet peak at δ 1.35, which integrated for 12 protons as expected and was therefore assigned to the adjacent environment, 26.

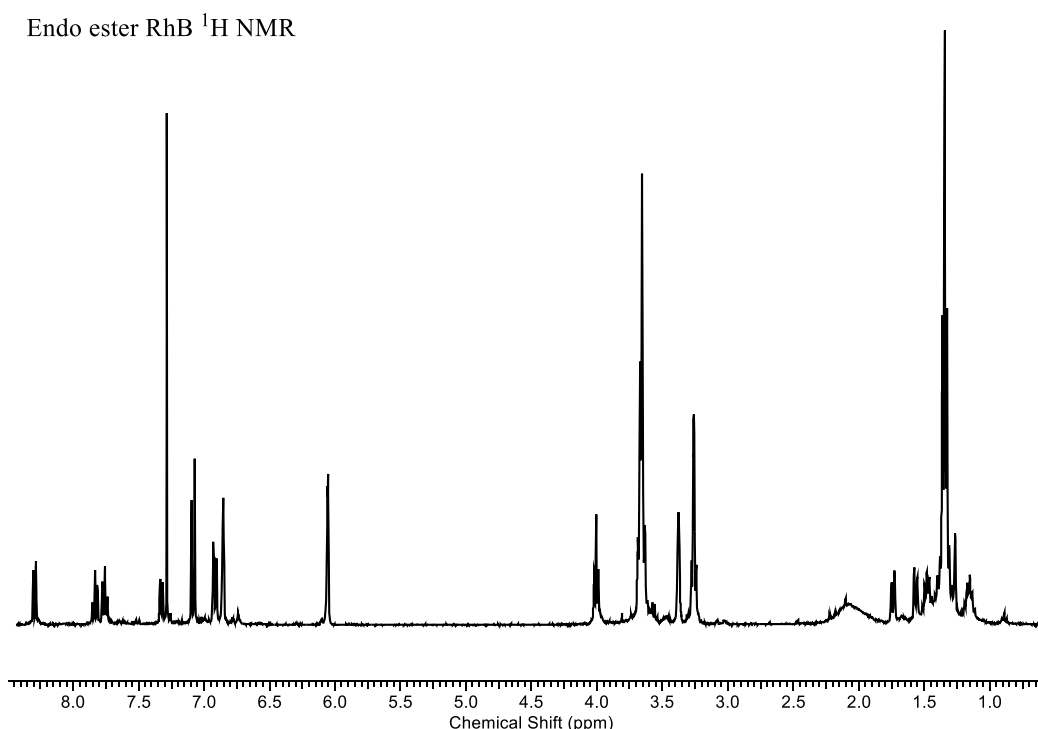


Figure 70 ^1H NMR spectrum for the product between *N*-(hydroxypentanyl)-*cis*-5-norbornene-endo-2,3-dicarboximide and rhodamine B (endo ester RhB). This sample was obtained from a single column fraction and is therefore cleaner than the spectrum in Figure 67.

Exo ester RhB

Having successfully isolated and characterised the *endo* ester RhB adduct, the same reaction was attempted using *N*-(hydroxypentanyl)-*cis*-5-norbornene-*exo*-2,3-dicarboximide. Despite successfully isolating the *endo* ester RhB adduct, it was only isolated in a very low yield as the product persisted across many column fractions. As more fractions were combined, more impurities appeared on the NMR that were not visibly present on the TLC. Therefore, in order to maximise the yield and purity, the crude product was purified twice by column chromatography. Due to the large crude yield of 4.396 g, the crude product was split approximately in half and purified separately before being recombined for a second column purification. The fractions containing only one spot by TLC were combined to obtain the final product (32%).

As with the *endo* adduct, an analytical sample was obtained by analysing a single fraction obtained from the final column. The ^1H NMR spectrum (Figure 72) for the *exo* adduct, along with expanded regions (Figure 73) and COSY NMR (Figure 74) are shown below.

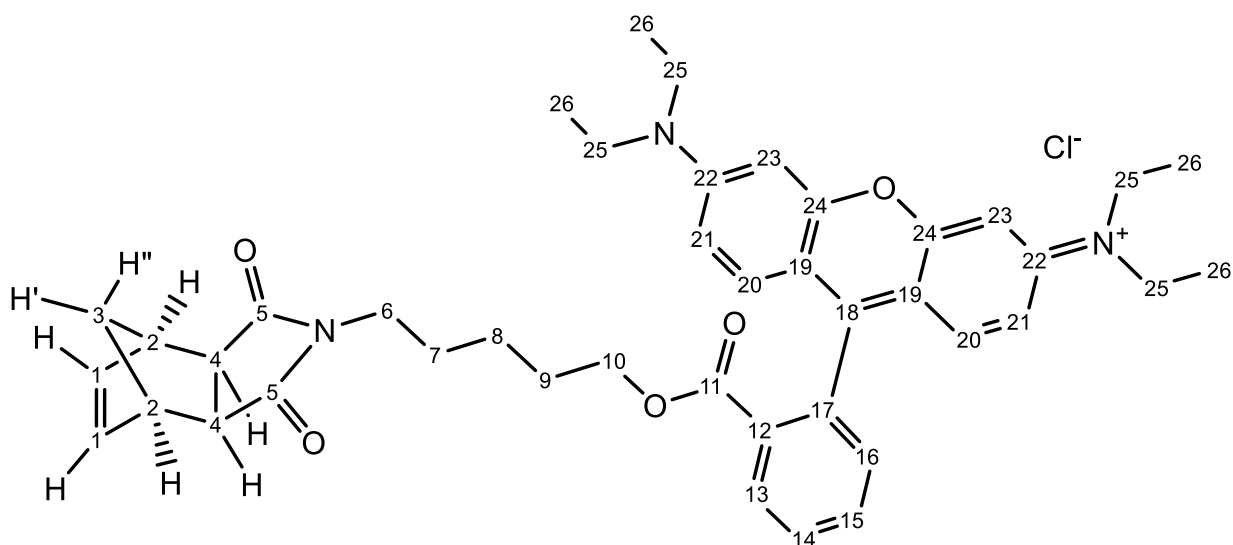


Figure 71 Representation of the chemical structure of the product *exo* ester RhB with the carbon atoms numbered for easy assignment of NMR spectra.

Exo ester-RhB ^1H NMR

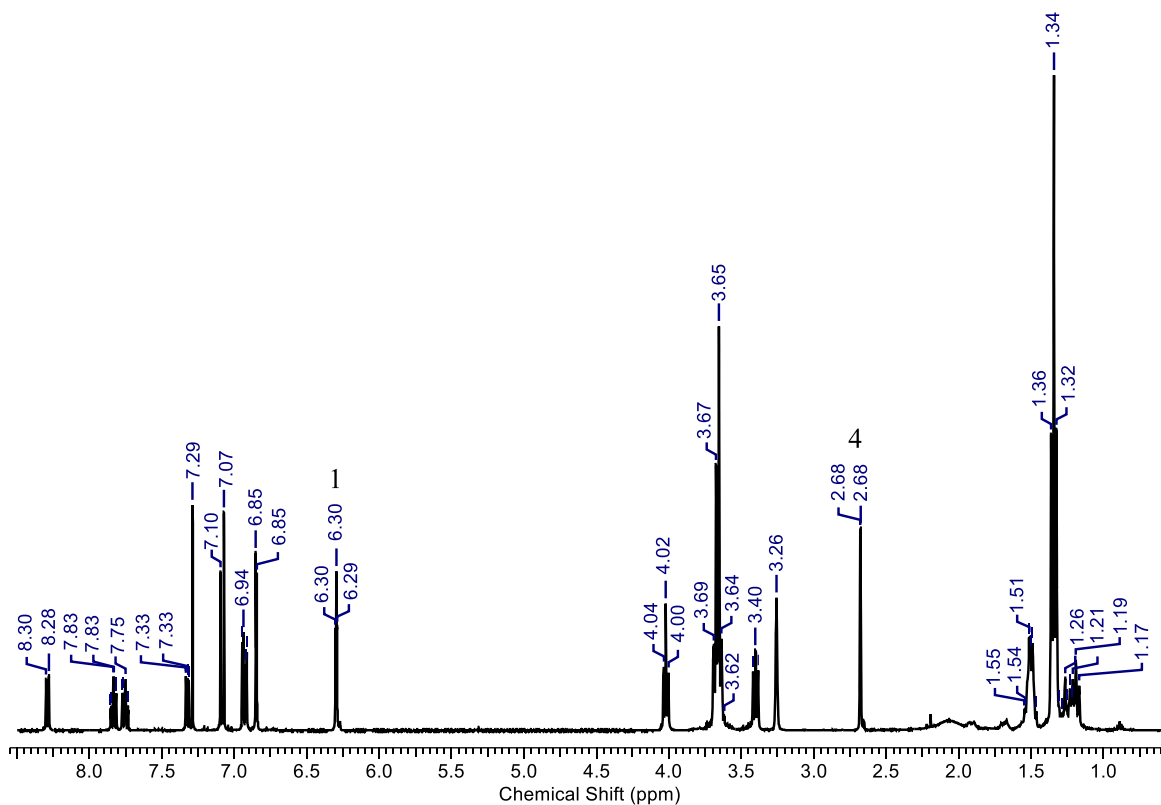


Figure 72 Partially annotated ^1H NMR spectrum for the product between *N*-(hydroxypentanyl)-*cis*-5-norbornene-*exo*-2,3-dicarboximide and rhodamine B (*exo* ester RhB).

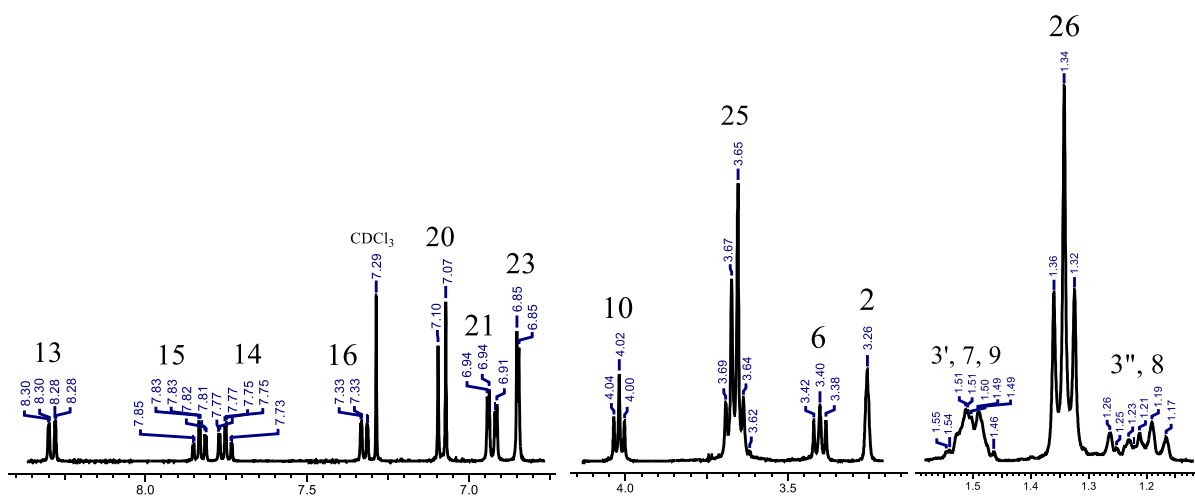


Figure 73 Annotated expanded regions from the ^1H NMR spectrum for the product between *N*-(hydroxypentanyl)-*cis*-5-norbornene-*exo*-2,3-dicarboximide and rhodamine B (*exo* ester RhB).

Exo ester RhB - COSY NMR

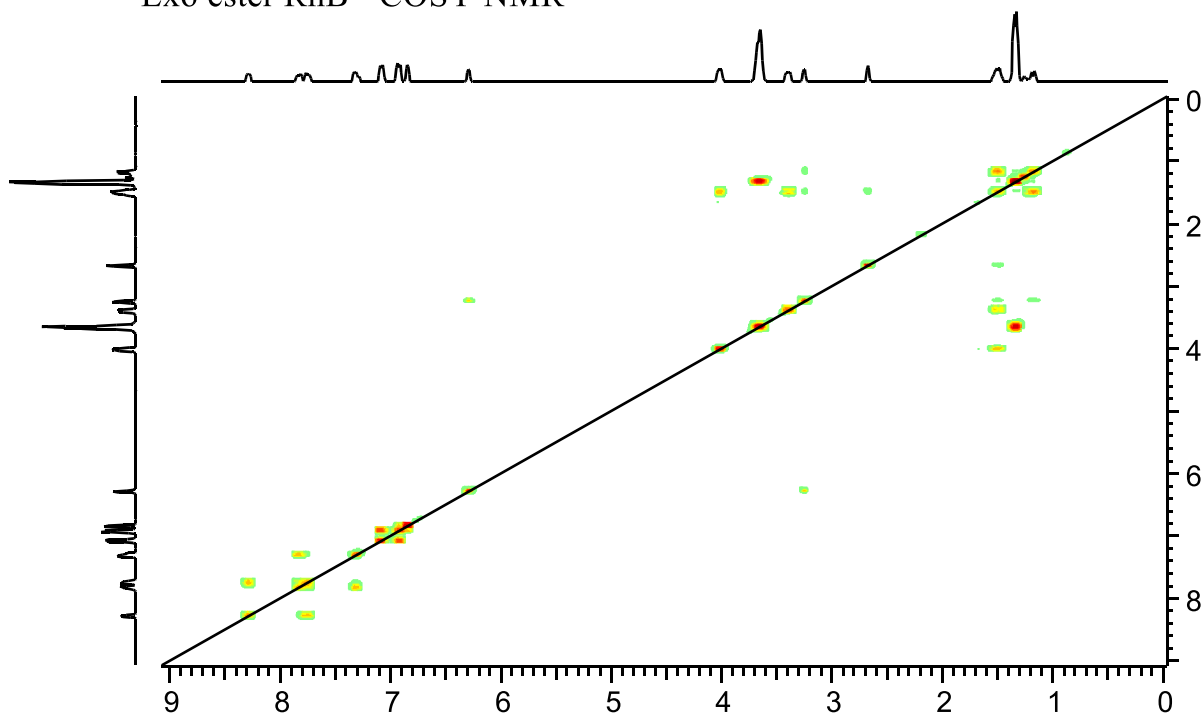


Figure 74 COSY NMR spectrum for the product between *N*-(hydroxypentanyl)-*cis*-5-norbornene-*exo*-2,3-dicarboximide and rhodamine B (*exo* ester RhB).

The aromatic region in the ^1H NMR is almost identical to that of the *endo* adduct and was assigned in exactly the same way. The NEt_2 groups were also assigned as they were for the *endo* adduct as the peaks are very distinctive due to their intensity and shape.

Although the norbornene and linker sections of the compound were assigned using the same principles as before, there were some cases where there was overlap between peaks, making it less straightforward to assign. Environments 1, 2 and 4 on the norbornene were simple to assign and well defined as they were in the starting materials. However, the bridgehead protons overlap with some of the linker proton environments, making them hard to distinguish. Using the COSY, it can be seen that environment 2 is coupling to the peaks at δ 1.50 and δ 1.22, showing that the bridgehead protons are present under the two multiplet peaks mentioned. Furthermore, environment 4 is coupled to the peak at δ 1.50, which is explained by *w*-coupling which has been explained previously and allows the bridgehead protons to be distinguished as δ 1.50 (3') and δ 1.22 (3'').

In terms of the linker section, environments 6 and 10 are very similar to the starting materials and the *endo* adduct in that they are the outer environments closest to the nitrogen of the dicarboximide and the oxygen of

the ester respectively. As seen in the starting material, N-(hydroxypentanyl)-*cis*-5-norbornene-*exo*-2,3-dicarboximide, environments 7 and 9 were so similar that they overlapped and formed part of the multiplet at δ 1.50. This was confirmed by the observed coupling between the multiplet and the two environments, 6 and 10, seen on the COSY. Finally, the most central environment on the linker was assigned to the multiplet peak at δ 1.22, which was the most downfield peak, and coupled with the peak at δ 1.50 (containing 7 and 9) as expected.

All environments on the compound were therefore assigned with good reasoning, indicating the high probability that the product was successfully synthesised. Overall the spectrum was clean, apart from the broad peak around 2 ppm which was also present in the *endo* adduct and could possibly be a small amount of water, from the methanol solvent used on the column, or a result of the fact that the compound exists as a salt.

However, as mentioned, this spectrum was obtained from an analytical sample obtained from a single column fraction. The final product was obtained by combining 49 fractions, all containing one spot on the TLC at the same R_f . The final yield was 0.736 g (32 %) and its ^1H NMR spectrum is shown in Figure 75 below.

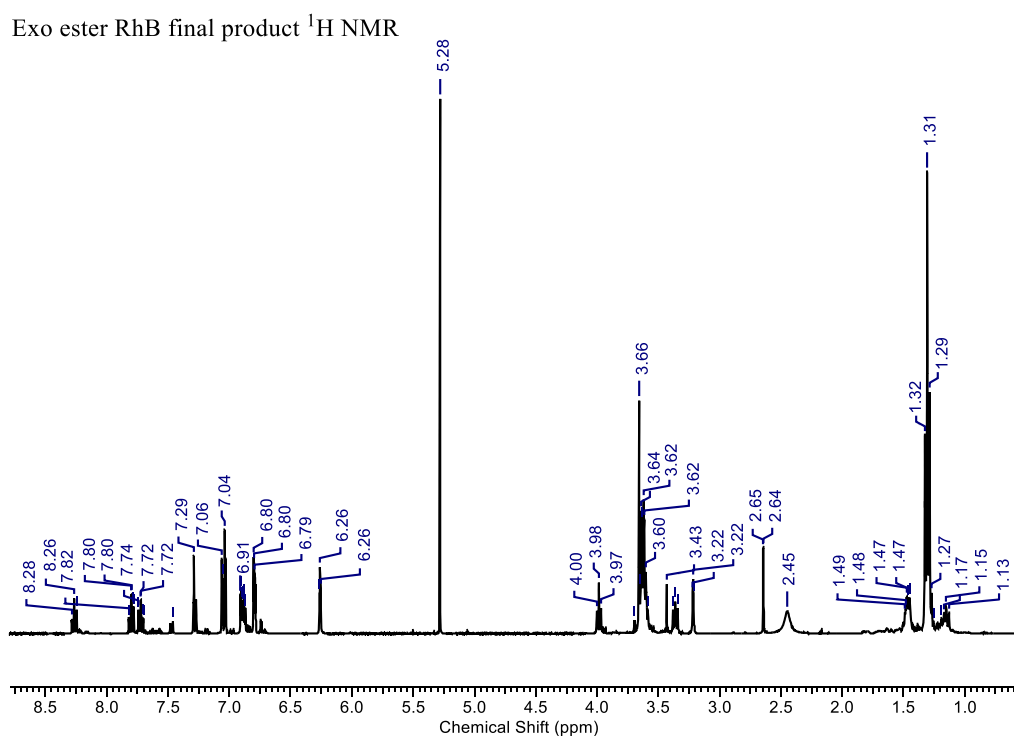


Figure 75 ^1H NMR spectrum for the product between N-(hydroxypentanyl)-*cis*-5-norbornene-*exo*-2,3-dicarboximide and rhodamine B (exo ester RhB). This is the final combined product after multiple columns where fractions containing only one spot were combined.

Upon initial inspection, the ^1H NMR spectrum looks very similar to the spectrum of the analytical sample in Figure 72 above, apart from some suspected solvent peaks at δ 5.28 (DCM), δ 3.66, δ 3.43 (possibly MeOH) and δ 2.45. However, upon closer inspection, it becomes apparent that the product is not as clean as it appears to be. The expanded regions of the ^1H NMR spectrum are shown (Figure 76) and analysed below.

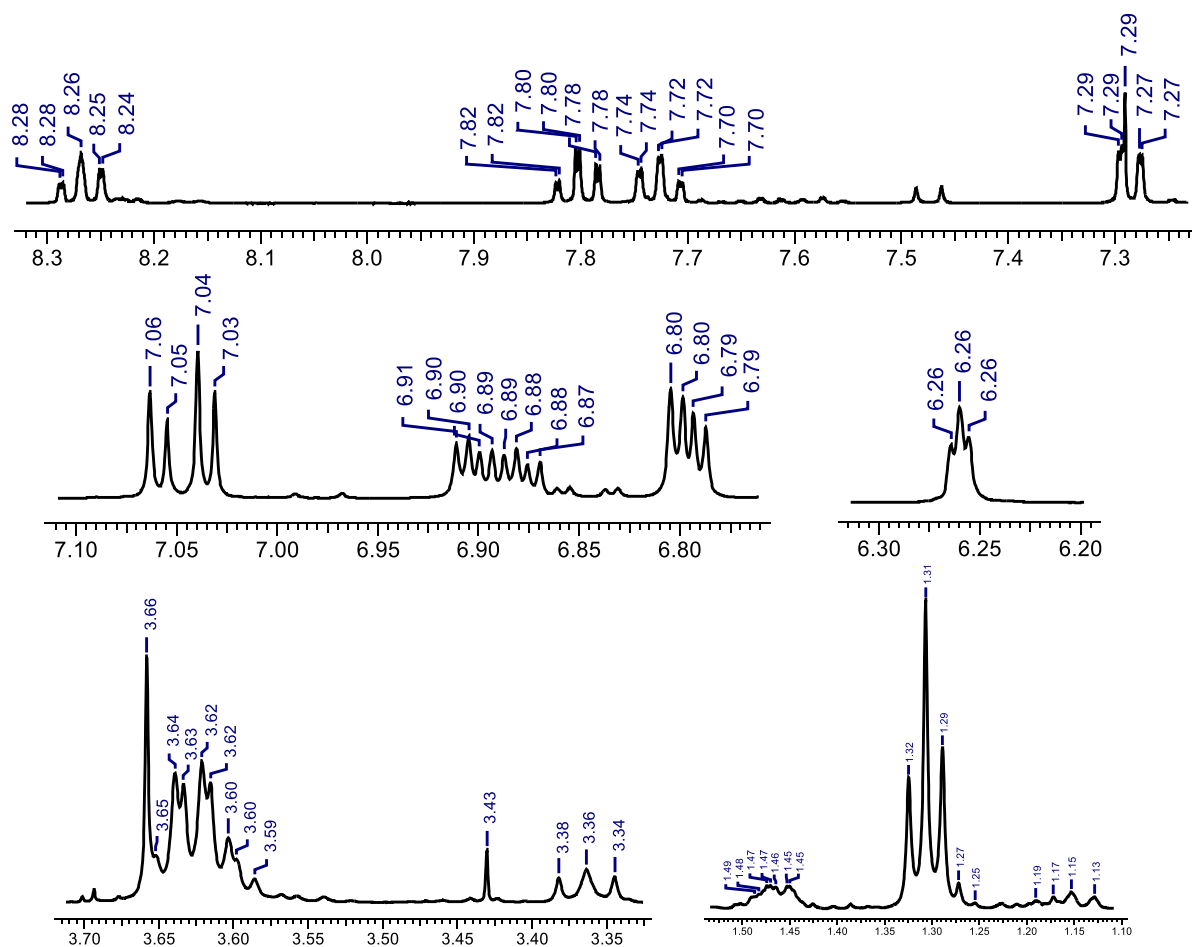


Figure 76 Expanded regions from the ^1H NMR spectrum for the product between *N*-(hydroxypentanyl)-*cis*-5-norbornene-*exo*-2,3-dicarboximide and rhodamine B (*exo* ester RhB). This is the final combined product after multiple columns where fractions containing only one spot were combined. Comparing to Figure 73 shows that this product contains impurities.

Looking at the expanded regions, the peaks that are most clearly different compared to the analytical sample are those between 6.7 – 7.1 ppm. The peaks in this region are showing two compounds containing RhB that are visibly distinct by a separation of 0.01 ppm. This is echoed in different regions such as the quartet at δ 3.63 which shows a second quartet overlapping with it. However, looking at the peaks at δ 6.26 and δ 3.36, which belong to the norbornene section and linker section respectively, there is no sign of duplication in these peaks. In fact,

the only duplicate peaks that appear to be present are peaks that can be assigned to RhB. TLC of the RhB starting material shows that the RhB has a very similar R_f to the product under the conditions used for the column, further indicating the likelihood of the impurity being RhB. The spectrum of the starting material, RhB, is shown below (Figure 77) for comparison.

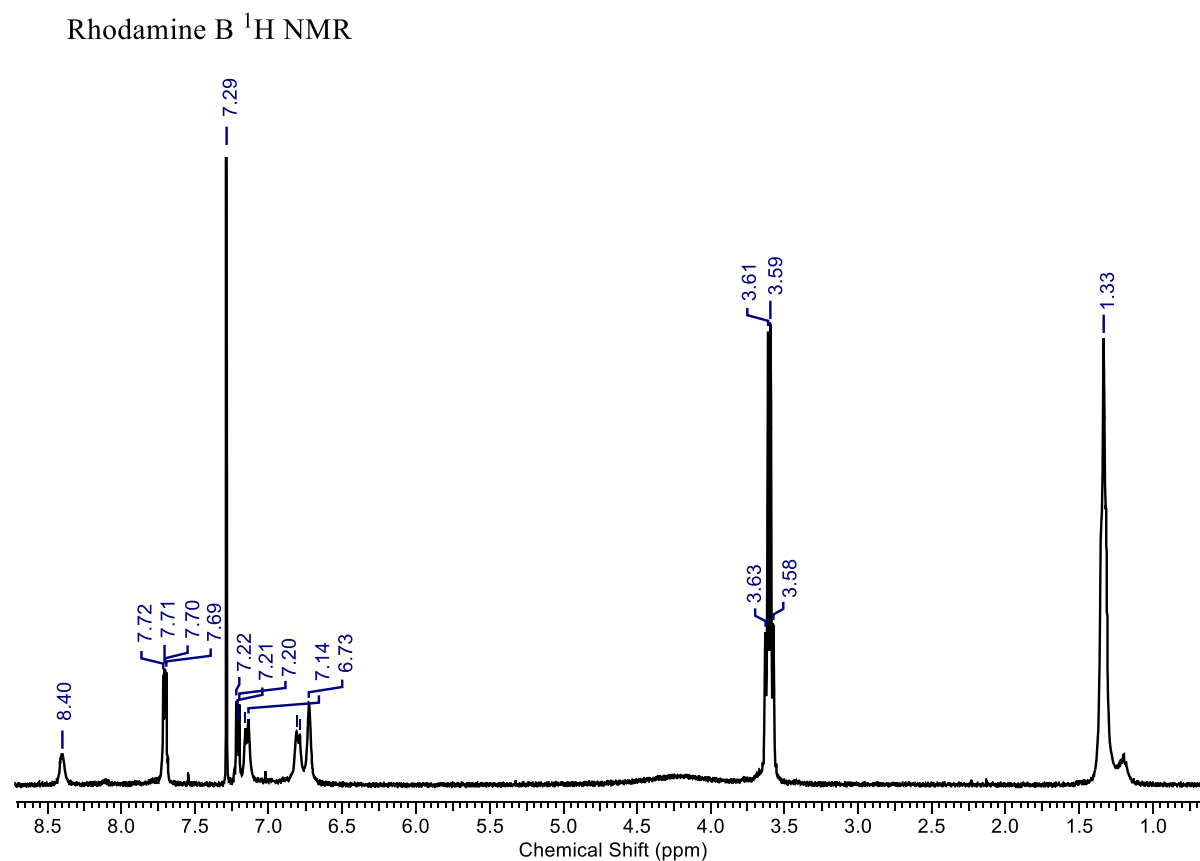


Figure 77 ^1H NMR spectrum of Rhodamine B as bought from Sigma Aldrich.

Although the chemical shifts are slightly different when comparing the spectrum of the starting material RhB and the suspected RhB present in the final product, it is quite possible that π -stacking and other intermolecular interactions could be affecting the chemical shift. Furthermore, there is no other evidence to make the case for the presence of a different impurity. Unfortunately, looking at the intensity of the peaks and their integrations, it appears that the impurity and the product are present in almost equal ratios. Thus, the yield of the final product is probably half of the reported value. Despite the unfortunate presence of impurity, it is still clear to see that the product was successfully synthesised. Furthermore, the impurity did not appear to involve the norbornene or linker, hinting that no unexpected monomer side products were formed.

If this reaction were to be repeated, there are several things that could be tried in order to improve the overall yield and purity of the final product. For example, instead of running a second column, a work-up involving washing could be attempted once the DCU by-product was removed by the first column. Alternatively, a different stationary phase could be used on the column, such as aluminium oxide, which may be able to better separate the product from the RhB starting material. Another change that could be made to the reaction is the carbodiimide that is used. For example, using EDC as opposed to DCC would result in the easier to remove EDU by-product, which may remove the need to run a column altogether.

Endo amide RhB

Having synthesised the *endo/exo* ester RhB derivatives, it showed that the carbodiimide coupling worked to form the ester. However, the reaction was not without its complications and overall the yield was very low. It was decided that rather than repeating the reaction between the amino alcohol derivative and RhB, it would make sense to try a carbodiimide coupling between the *endo* amine derivative and RhB. This was decided since amides are typically easier to form and more stable than esters, which may result in better yields. Furthermore, it was decided that EDC would be used as the carbodiimide, rather than DCC to make the work-up process easier and give a cleaner product in greater yield.

Apart from using EDC rather than DCC, the rest of the reaction conditions (reagent equivalents and reaction time/temperature) were left mostly unchanged besides some small changes as a result of scaling.

Unlike DCU which is very difficult to remove from reaction mixtures, EDU is much simpler due to its solubility in water. However, it is known that EDU is also slightly soluble in DCM and therefore in order to best remove it, ethyl acetate is more appropriate to use for the organic phase as EDU is insoluble in ethyl acetate. Thus, upon reaction completion, it was first necessary to remove the reaction solvent, DCM, *in vacuo*. The reaction residue was then taken up in both ethyl acetate and water and a separating funnel was used to isolate the organic layer. The organic layer was then dried over MgSO₄, filtered by gravity and the ethyl acetate was removed *in vacuo*. ¹H NMR was used to analyse the product which clearly showed some residual ethyl acetate peaks. Thus, the product was taken up in DCM several times and the solvent removed *in vacuo*, in order to remove the residual EtOAc

peaks from the ^1H NMR spectrum. After the product was left to dry, it was analysed again by ^1H NMR (Figure 79) which is shown and explained below along with the COSY (Figure 81) and expanded regions (Figure 80).

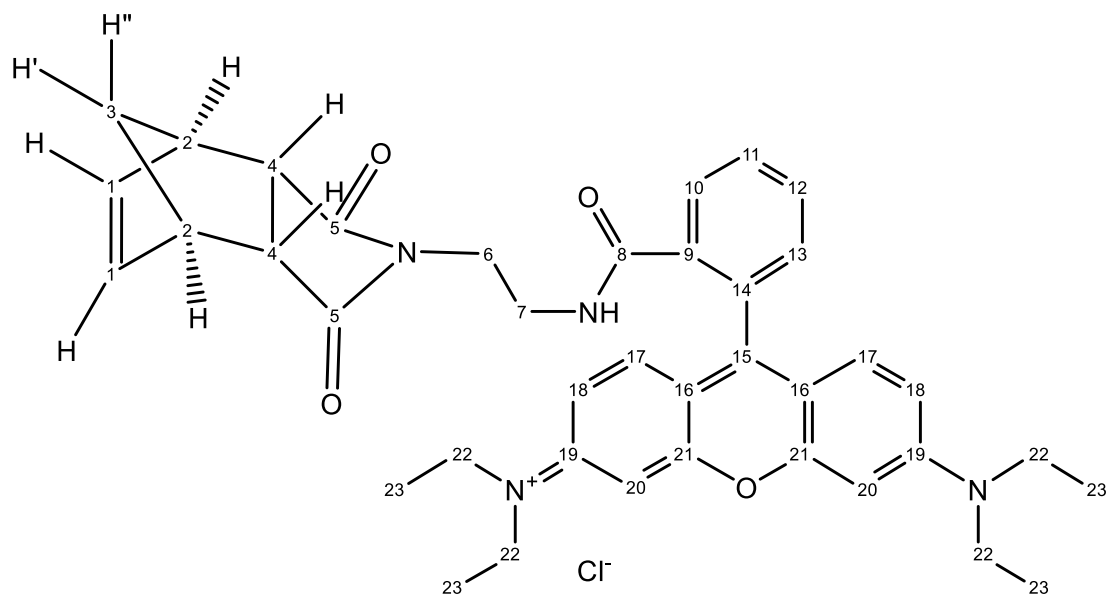


Figure 78 Representation of the product endo amide RhB where the carbon atoms are labelled for easy assignment of NMR spectra.

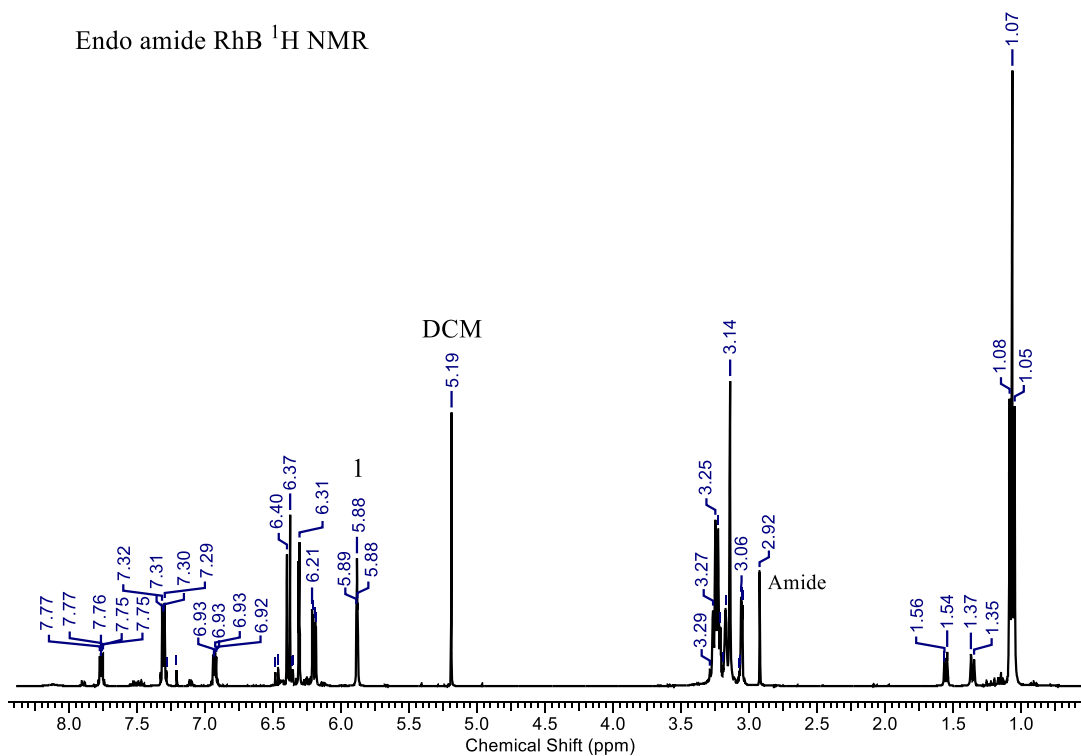


Figure 79 Partially annotated ^1H NMR spectrum for the product from the reaction between endo-N-(2-aminoethyl)-5-norbornene-2,3-dicarboximide and Rhodamine B (endo amide RhB).

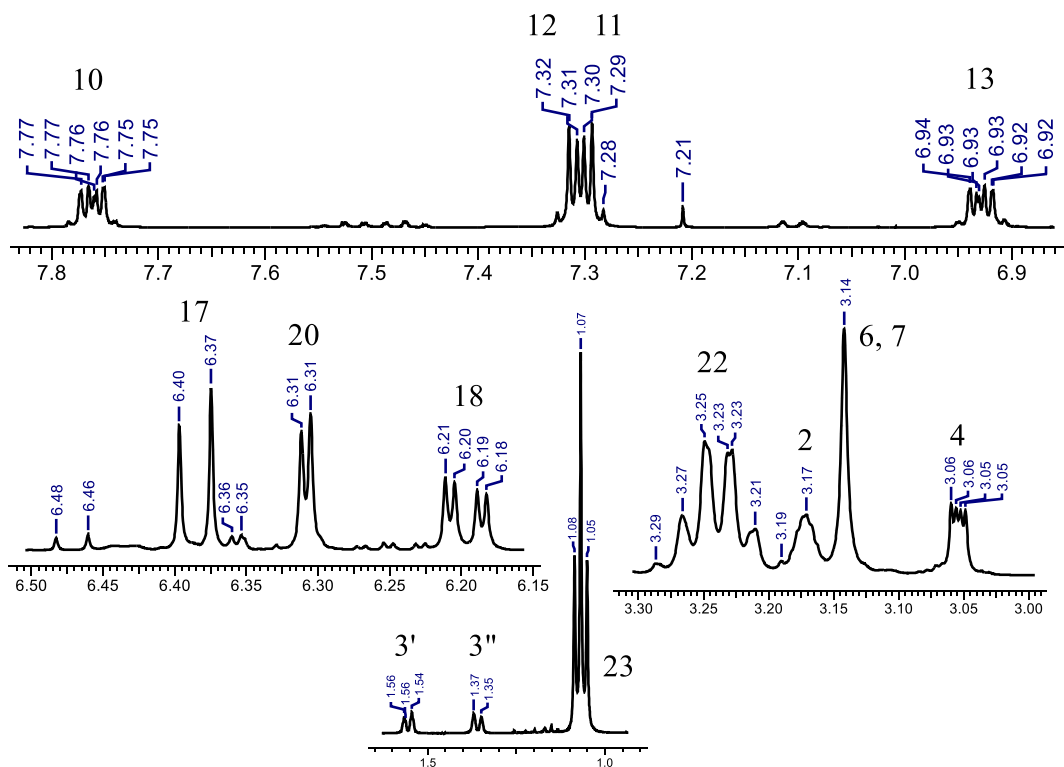


Figure 80 Annotated expanded regions from the ^1H NMR spectrum for the product from the reaction between *endo*-N-(2-aminoethyl)-5-norbornene-2,3-dicarboximide and Rhodamine B (*endo* ester RhB).

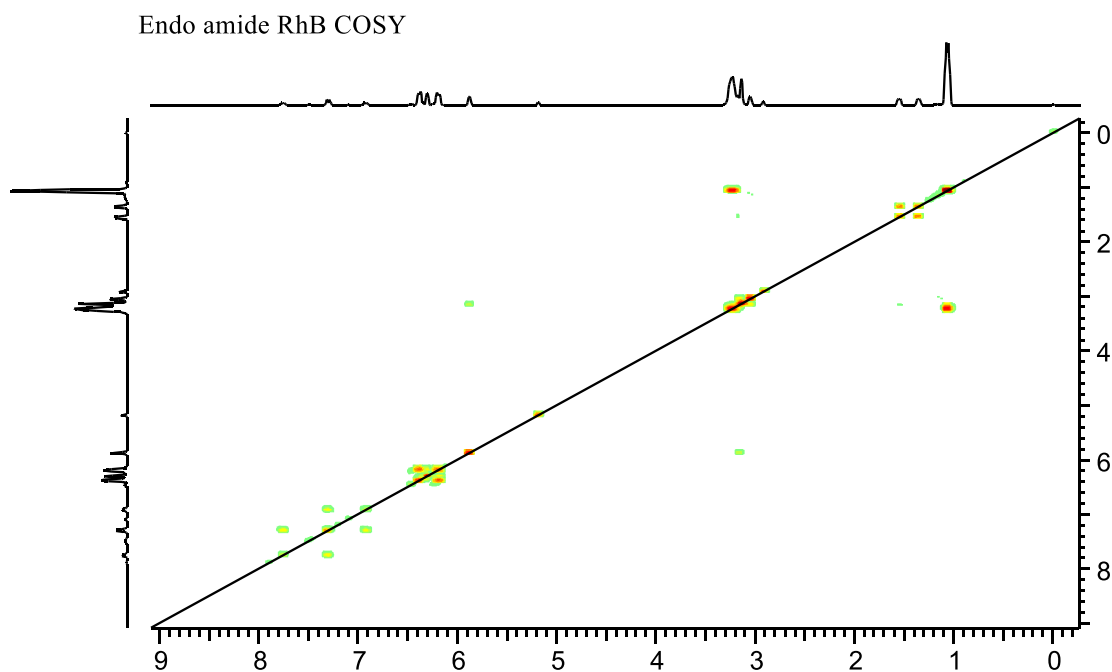


Figure 81 COSY NMR spectrum for the product from the reaction between *endo*-N-(2-aminoethyl)-5-norbornene-2,3-dicarboximide and Rhodamine B (*endo* ester RhB).

Having already assigned the *endo/exo* ester RhB derivatives, the ^1H NMR spectrum for the *endo* amide RhB can be assigned using similar logic and explanations. The rhodamine section was assigned first as it is very distinct, and the explanations used for the aforementioned derivatives can be directly applied to assign this product. The only slight difference with this adduct is that protons 11 and 12 cannot be distinguished using the COSY NMR as they were for previous adducts because these environments are very similar and almost overlap. As they are so similar, a very distinctive roofing effect can be seen due to second order effects. This gives rise to what appears to be a single peak, where in fact, there are two distorted triplets (roofing effect) that are overlapping. Despite not being distinguishable by COSY NMR, it is expected that the same effects that allowed these environments to be distinguished in previous adducts are present here. Hence, the environment that is para to the carbonyl EWG is assigned as the most downfield of the two peaks. The protons on the NEt_2 groups can simply be assigned as they were in previous examples, and the peaks do not appear to overlap with other environments.

The norbornene section of this derivative can be assigned using the same explanations as previously assigned adducts, starting with the alkene peak at δ 5.88. However, the bridgehead protons cannot be distinguished using the COSY NMR, as the *W*-coupling between protons 1 and 3'' must be so weak that it is not visible. Although the bridgehead protons cannot be distinguished solely using NMR, a crystal structure of the product was obtained and allows the protons to be assigned. The bridgehead proton peak at δ 1.55 can be seen to couple with proton 2 (δ 3.17) whilst the other bridgehead proton peak at δ 1.36 does not show any coupling. Proton 2 is separated from the bridgehead protons by 3 bonds, and therefore it was expected that looking at the bond angles would provide insight into why only one of the bridgehead protons appears to be coupling on the COSY.

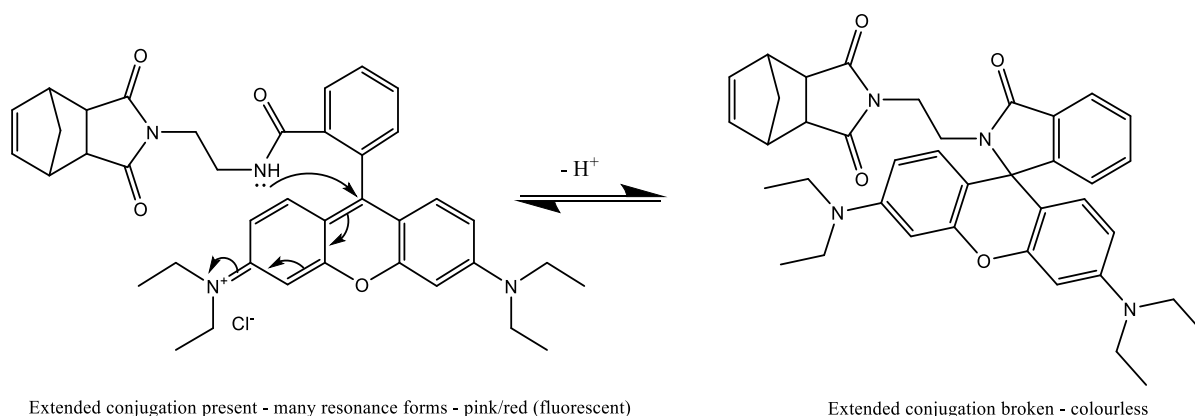
Using the crystal structure and mercury software, the dihedral angle between protons 2 and 3' was found to be 58.2° and the dihedral angle between protons 2 and 3'' was found to be 67.8° . The difference in these dihedral angles is significant and can help to distinguish between the bridgehead protons. 58.2° is closer to 0° than 67.8° , which according to the Karplus equation, gives rise to greater coupling constants. Thus, proton 3' can be assigned to the environment (δ 1.55) which shows coupling to 2 on the COSY and 3'' can be assigned to the other bridgehead environment (δ 1.36). Furthermore, the dihedral angle between 2 and 3'' (67.8°) is closer to 90° and would be expected to couple very weakly.

The remaining unassigned peaks at δ 3.14 and δ 2.92 do not couple with and other peaks and must therefore be assigned using logic and NMR principles. The peak at δ 3.14 integrates to 4 protons and the peak at δ 2.92

integrates to only 1 proton. Therefore, it can be deduced that the protons in environments 6 and 7 must be so similar that they overlap and can be assigned to the peak at δ 3.14. The chemical shift of δ 3.14 is also what could be expected for these protons as the environments are both adjacent to an electronegative nitrogen. The peak at δ 2.92 can tentatively be assigned as the proton on the amide which correlates well with the integration but has a much lower chemical shift than expected.

Apart from a residual solvent peak at δ 5.19 corresponding to DCM, the spectrum is mostly clean, and all peaks have been assigned on the ^1H NMR spectrum. The assignment provides good evidence for the formation of the expected product, which is further clarified by the crystal structure which was obtained.

The crystals were grown from ethyl acetate using slow evaporation and the appearance of the crystals were colourless with some pink colour on the surfaces. The crystal structure showed the ring closed, lactam product which was unexpected and is formed by the process shown in Scheme 11.



Scheme 11 Representation of the open amide and closed lactam structures possible for endo/exo amide RhB. The curly arrows represent the transfer of electrons through the aromatic system.

The disruption of the aromatic system as a result of the ring closure can explain why the crystals were colourless. During crystallisation, the solvent evaporated to dryness and therefore the pink colour on the surfaces can be attributed to the deposition of the ring-opened form on the crystal surface. The structure for *endo* amide RhB as determined by single crystal XRD is shown in Figure 82.

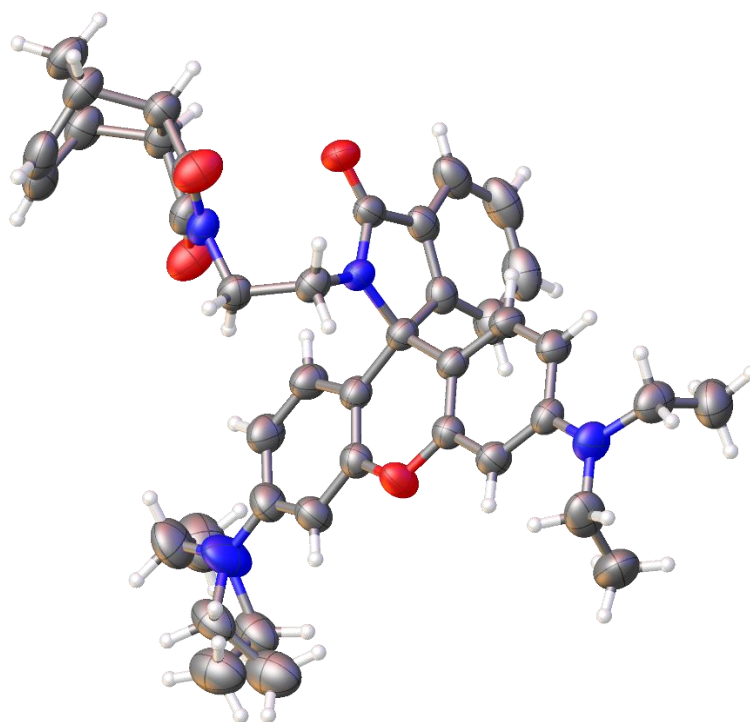


Figure 82 Crystal structure of *endo* amide RhB where one of the Et groups in one of the NEt_2 groups can be in one of two positions approximately 50% of the time.

Not only does the crystal structure provide proof for the formation of the *endo* amide RhB derivative, but also gives further evidence that the starting material *endo* amine was synthesised successfully. Furthermore, crystal structures for the *endo/exo* ester RhB derivatives were not obtained, and therefore were only assigned by NMR. The crystal structure for the *endo* amide RhB adduct and ^1H NMR assignment can be compared to the assignment of the ^1H NMR spectra for *endo/exo* ester RhB adducts to further confirm that these adducts were successfully synthesised.

Having discovered that the product can exist in the ring-opened and ring-closed forms, it could be questioned that the minor aromatic peaks in the ^1H NMR spectrum could possibly represent the ring-closed form. Initially it was expected that the minor impurity peaks in the aromatic region belonged to excess RhB starting material, but it is possible that it belongs to the ring-closed form as explained above. This cannot be proved without further experiments and investigation using varying solvents and NMR techniques which was not possible in the time and not considered a priority for this project.

Overall, the amidation worked very well with the EDC hydrochloride and did not require column chromatography to purify and isolate the product which was obtained in a yield of 59 %. This yield is much greater than the yields for the *endo/exo* ester RhB adducts and the final products are cleaner. Without repeating the ester RhB reactions with EDC hydrochloride instead of DCC, it cannot be deduced whether the reaction improvement can be attributed to the choice of carbodiimide or the fact that an amide was used in place of an ester. However, the simpler work-up procedure can certainly be attributed to the use of EDC hydrochloride instead of DCC. Future work could attempt the ester RhB reaction with EDC hydrochloride to obtain cleaner products in greater yields, but this was not possible during the timeframe of this project. Instead, it was necessary to synthesise the *exo* amide RhB adduct so that it could be used for ROMP.

Exo amide RhB

Given that *endo* amide RhB was successfully synthesised, it was decided that the same procedure should work for the *exo* adduct and therefore the reaction was attempted. The reaction was successful, giving a mostly clean product in a yield of 46%. This yield was not as high as for the *endo* adduct and could perhaps be improved by further extraction of the aqueous layer with EtOAc. Furthermore, optimisation of the reaction could be attempted by varying factors such as reaction time, mass of carbodiimide used, mass of catalyst used and stoichiometry of acid:amine. No optimisation was attempted during this project, as the reaction provided a sufficient yield in order to perform some ROMP experiments. The ¹H NMR (Figure 84) along with expanded regions (Figure 85) and COSY NMR (Figure 86) are shown and explained below:

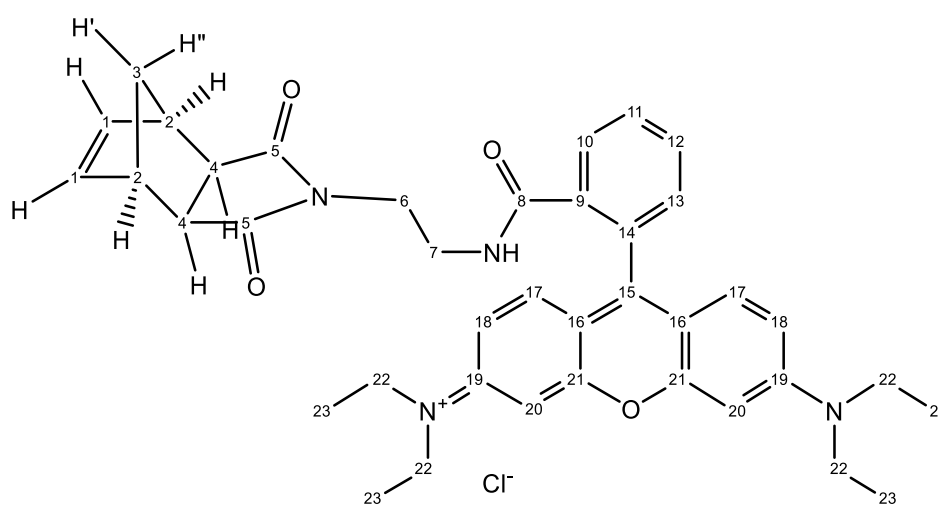


Figure 83 Representation of the product *exo* amide RhB where the carbon atoms are labelled for easy assignment of NMR spectra.

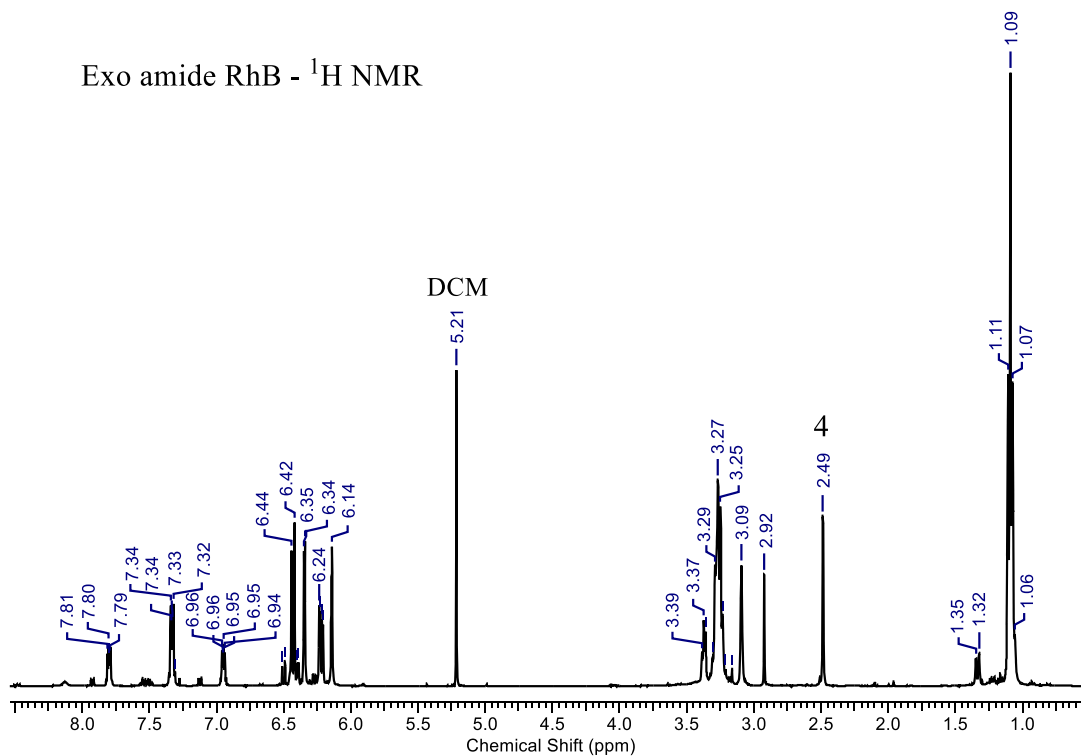


Figure 84 Partially annotated ^1H NMR spectrum for the product from the reaction between *exo*-*N*-(2-aminoethyl)-5-norbornene-2,3-dicarboximide and Rhodamine B (*exo* amide RhB).

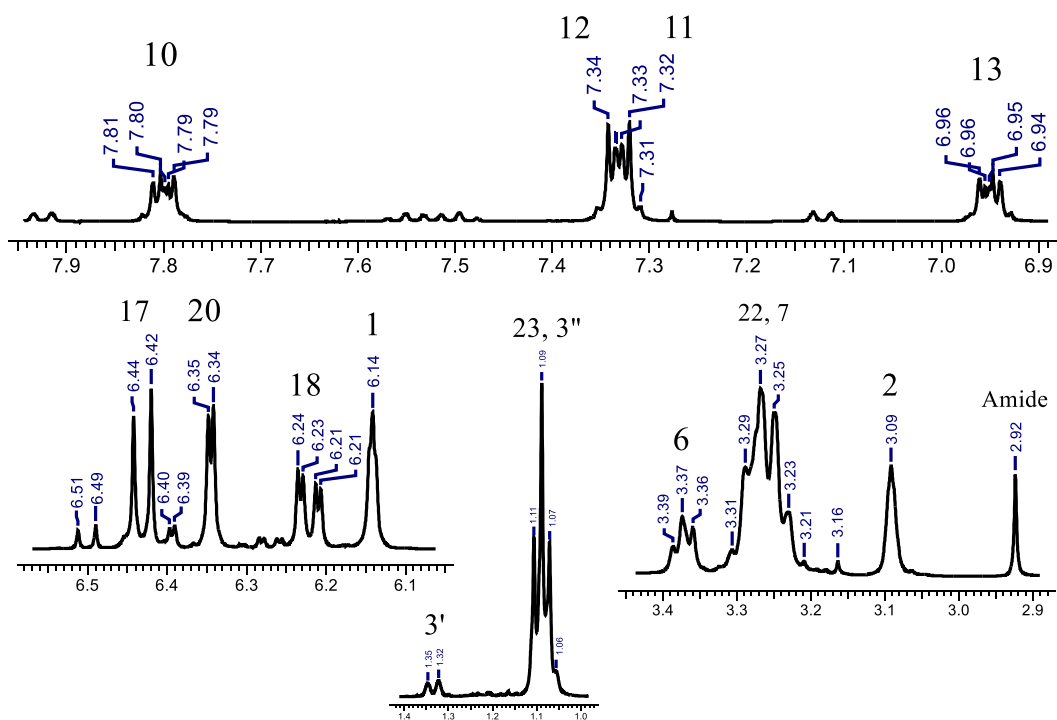


Figure 85 Annotated expanded regions from the ^1H NMR spectrum for the product from the reaction between *exo*-*N*-(2-aminoethyl)-5-norbornene-2,3-dicarboximide and Rhodamine B (*exo* ester RhB).

Exo amide RhB - COSY NMR

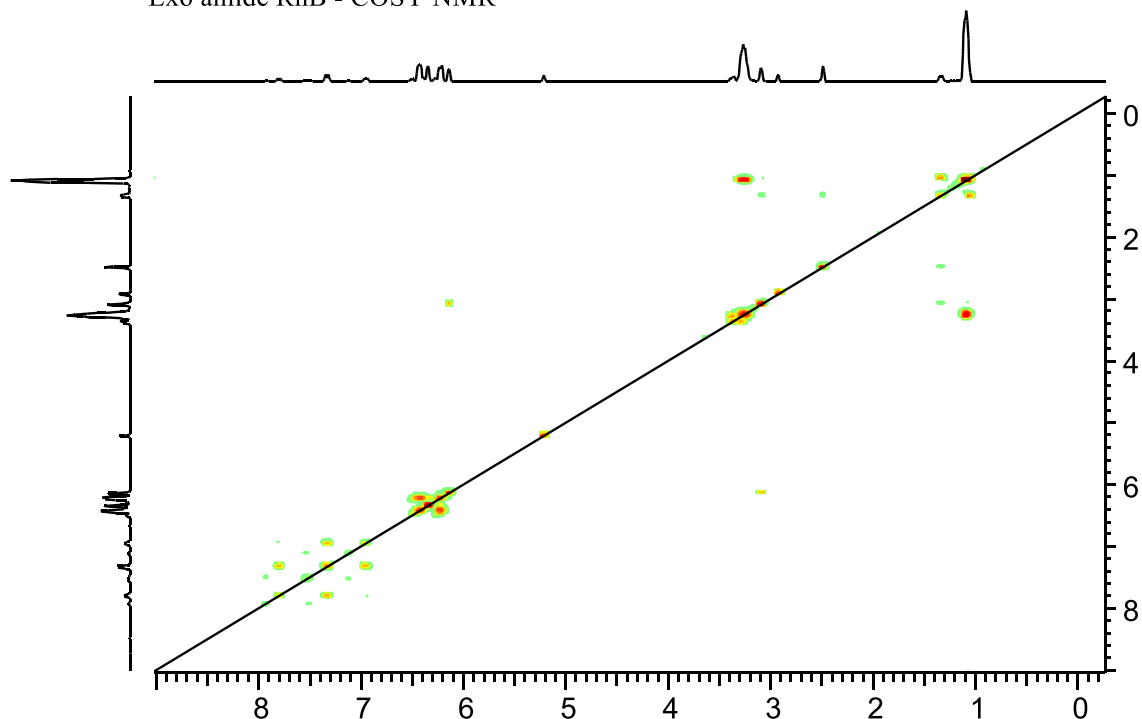


Figure 86 COSY NMR spectrum for the product from the reaction between *endo*-N-(2-aminoethyl)-5-norbornene-2,3-dicarboximide and Rhodamine B (*endo* ester RhB).

The RhB section of the product is very similar to the *endo* adduct and was therefore assigned using the same reasoning. Environment 22 on the NEt_2 group is distorted and does not appear as a quartet as expected. This is due to some overlap with another peak, but the large size of the peak and integration makes it simple to assign as environment 22. Environment 23 is less ambiguous and can be assigned to the triplet peak at δ 1.09. However, one of the bridgehead peaks, 3'', overlaps with this peak which is shown by the COSY NMR as well as the slight distortion of the triplet.

The bridgehead peaks were distinguished by the w-coupling between 3' and 4 which can be seen on the COSY. The rest of the norbornene section was assigned using the same reasoning as used in previous *exo* adducts. The most notable difference in the ^1H NMR spectra of the *endo* and *exo* adducts is in the peaks of the linker section. In the *endo* adduct, environments 6 and 7 overlap completely and appear to be in the same environment but in the *exo* adduct they exist as two separate peaks. One of these peaks is at δ 3.37 and exists as a triplet. This peak is shown to couple on the COSY with the distorted peak at δ 3.27 which was assigned as environment 22. Therefore, the peaks for environments 22 and 7 must overlap on the NMR and no distinction can be made between the signals. The two environments on the linker had been identified as peaks at δ 3.37 and δ 3.27 but

it was difficult to distinguish between them as they are so similar. However, using the logic that environment 6 is adjacent to a dicarboximide which has two carbonyl groups compared to environment 7, which is adjacent to an amide with only one carbonyl, it was decided that environment 6 should be slightly more deshielded and therefore the most downfield of the two peaks. The assignment of these peaks may be wrong as there are other factors such as conformation and conjugation to the aromatic ring (amide) that may affect the shielding of the environments. Despite this ambiguity, the assignment of the peaks as the linker environments is clear and thus the assignment of the overall product is sound.

As with the *endo* adduct, there is a peak at δ 2.92 of similar intensity which can again be assigned as the proton on the amide. The solvents, DCM, EtOAc and Water that were used during the reaction have no signals at δ 2.92 and therefore it is almost certainly the amide as assigned.

Overall the ^1H NMR of the product is clean, apart from some minor peaks in the aromatic region much like with the *endo* adduct. Again, these peaks may be a small amount of residual rhodamine b starting material but may alternatively be the ring closed lactam form of the product. To provide further evidence for the successful synthesis of the product, crystals were grown and analysed by single crystal XRD. The crystallisation process used is described below as it differs from the process used for the *endo* adduct.

Crystallisation of Exo amide RhB

As the *endo* adduct had crystallised by slow crystallisation from EtOAc, it was expected that the *exo* amide RhB may also crystallise under similar conditions. However, after many attempts using varying techniques such as recrystallisation from saturated hot EtOAc and slow evaporation as well as varying product:solvent ratios, no crystals had formed. Different solvents such as methanol, acetone and DCM were used to try to crystallise the product but none of them allowed crystals to form.

An NMR sample of the product in DMSO- d_6 was prepared in a sample vial before being transferred to an NMR tube. However, a small residual amount of solvent remained in the sample vial and after a short time it was noticed that some crystals had formed. These crystals were expected to be the product but were of insufficient quality to be analysed by single crystal XRD. Thus, crystals were grown from a solution in DMSO purposefully. Unfortunately, the crystals that grew from this solution were again of insufficient quality as they were dendritic,

indicating that the crystals had grown too quickly. As DMSO does not evaporate very readily and the temperature of the solution was kept consistent at RT, the growth of the crystals is dependent on the concentration of the solution. Therefore, in order to slow down the rate of crystallisation, a lower concentration solution was prepared in DMSO, giving rise to good quality colourless crystals which were analysed by single crystal XRD. The resulting structure as determined by the XRD experiment, was in the ring closed lactam form and is shown in Figure 87 below:

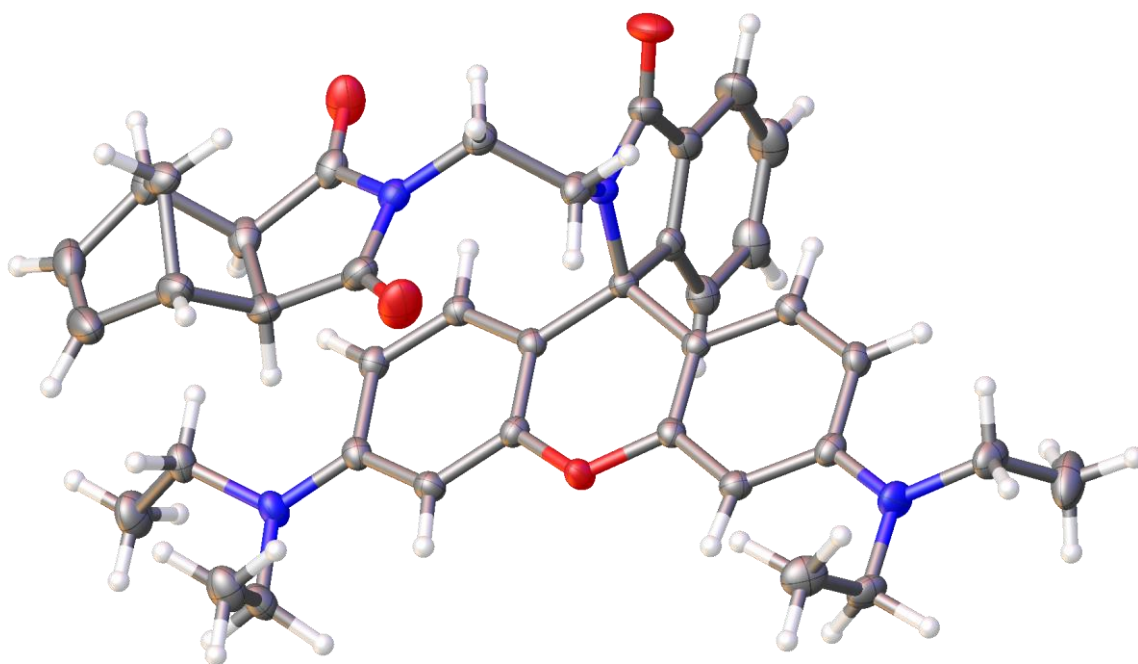


Figure 87 Crystal structure of exo amide RhB in the ring-closed lactam form.

Fluorescence Resonance Energy Transfer (FRET)

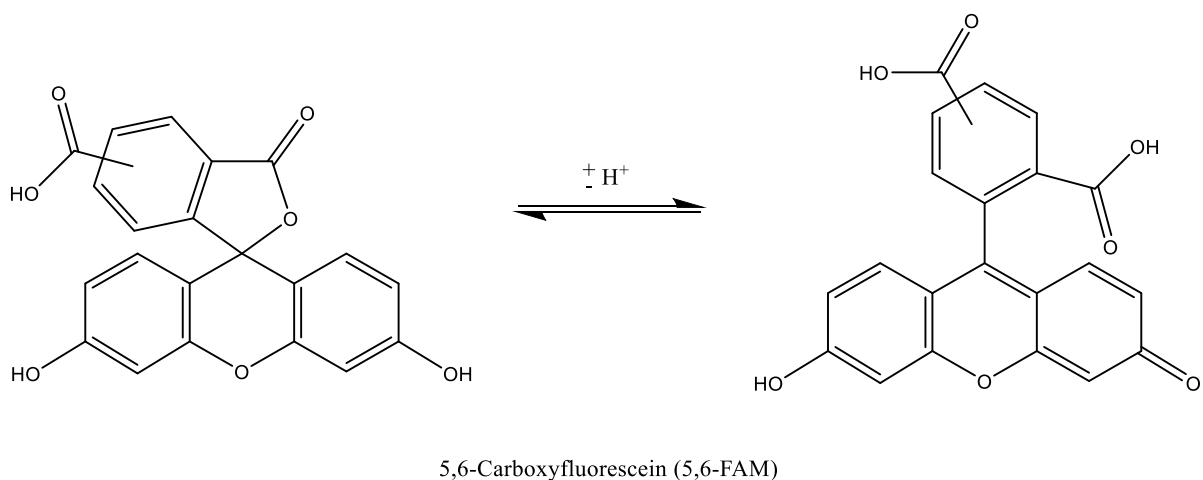
There are numerous examples in the literature of fluorophores being incorporated into ROMP copolymers as previously discussed. Typically, these fluorescent monomers have been copolymerised with monomers that provide different imaging functionalities such as MRI contrast agents^{9,20}. When copolymerised, the fluorescent monomers tend to undergo some quenching of varying amounts and this can be caused by phenomena such as aggregation-caused quenching (ACQ)⁶³ and chemical interactions with other functional groups. If the quenching processes were better understood, then well-informed decisions could be made when designing multimodal imaging ROMP copolymers.

One way to study the factors affecting fluorescence quenching is through fluorescence resonance energy transfer (FRET)⁶⁴. FRET can be used to measure the distance between a pair of donor-acceptor fluorophores and involves a radiation free energy transfer process. For the purpose of this project, the aim was to analyse trends in a FRET process between a compatible donor-acceptor pair of fluorophores at varying copolymer ratios as well as comparing FRET in statistical and block copolymers. In order to achieve this, it was necessary to find a fluorophore that either has an emission wavelength near the excitation wavelength of rhodamine b (553 nm in ethanol⁶⁵) or an excitation wavelength near the emission wavelength of rhodamine b (575 nm in ethanol⁶⁵).

5,6-Carboxyfluorescein

A relatively cheap fluorophore was identified that fits one of these requirements and the monomer could be synthesised using similar carbodiimide coupling as before. 5,6-carboxyfluorescein (5,6-FAM) is a xanthene dye like rhodamine b and has an emission wavelength (515 nm⁶⁶) near the excitation wavelength of rhodamine b. The structure of 5,6-FAM is shown in Scheme 12.

5,6-FAM differs from rhodamine b in that the groups attached to the xanthene moiety in 5,6-FAM are -OH groups (in ring closed form) compared to -NEt₂ groups (in the ring closed form). Furthermore, there are two -COOH groups attached to the lone aromatic ring in 5,6-FAM compared to only one -COOH group in rhodamine b. Although these differences appear to be quite minor, they have implications on things such as reactivity and solubility.



Scheme 12 Representation of the ring closed lactone and ring-opened carboxylic acid forms of 5,6-Carboxyfluorescein.

In the carbodiimide coupling reactions used with rhodamine b, DCM was used as the solvent which is one of the most commonly used. However, the structural differences between 5,6-FAM and rhodamine b mean that 5,6-FAM is mostly insoluble in DCM. Therefore, it was necessary to find an alternative solvent for the reaction. Unfortunately, the best solvents for dissolving 5,6-FAM are ethanol and methanol which are incompatible with the procedure as they would participate in the reaction and form undesirable by-products. 5,6-FAM is also known to be slightly soluble in DMF at approximately 1mg/mL, but this is also undesirable as DMF is very difficult to remove and must be kept dry.

The solubility of 5,6-FAM in THF was not known but a small amount was placed in THF, stirred and found to be slightly soluble. Therefore, a reaction was carried out in the hope that as the product formed, which should be more soluble in THF, the starting material 5,6-FAM would gradually dissolve.

This reaction was attempted with *N*-(hydroxypentanyl)-*cis*-5-norbornene-*endo*-2,3-dicarboximide, DCC as the carbodiimide and was carried out at room temperature like previous coupling reactions. After a short time, it appeared as though most of the solid had dissolved, yielding a yellow solution. The reaction was stirred (24 h), after which time the reaction was stopped and the solvent removed *in vacuo*, yielding a yellow solid which was analysed by ^1H NMR. The ^1H NMR (Figure 88) is shown below:

Endo ester 5,6-FAM - ¹H NMR - crude

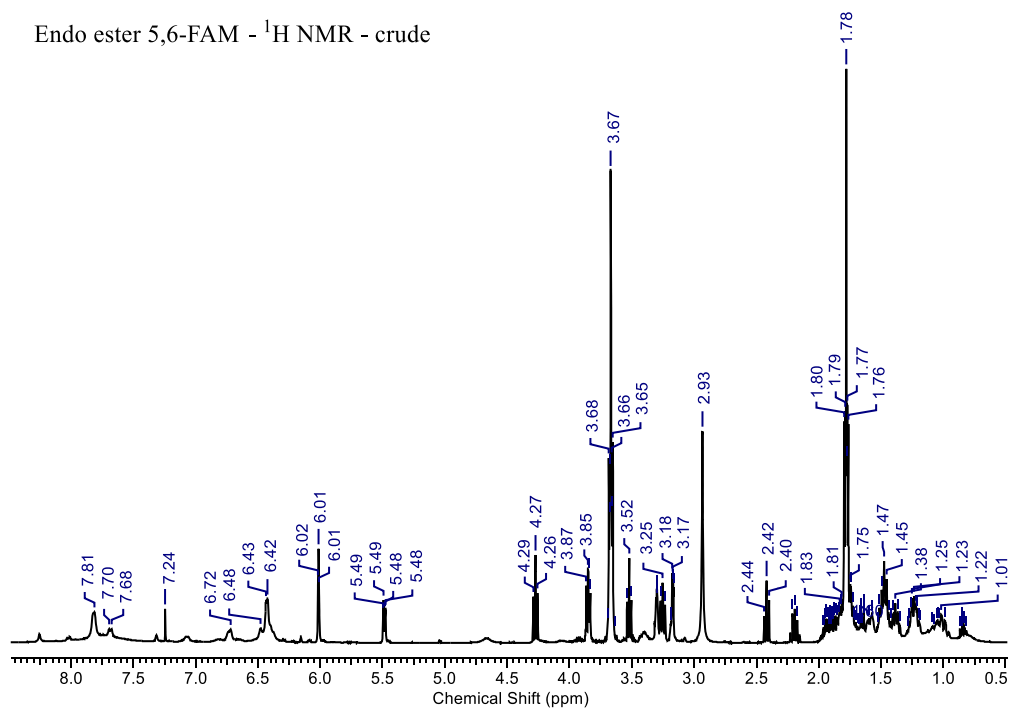


Figure 88 ¹H NMR spectrum of crude product from the steglich esterification between *N*-(hydroxypentanyl)-*cis*-5-norbornene-*endo*-2,3-dicarboximide and 5,6-carboxyfluorescein (*endo* ester 5,6-FAM).

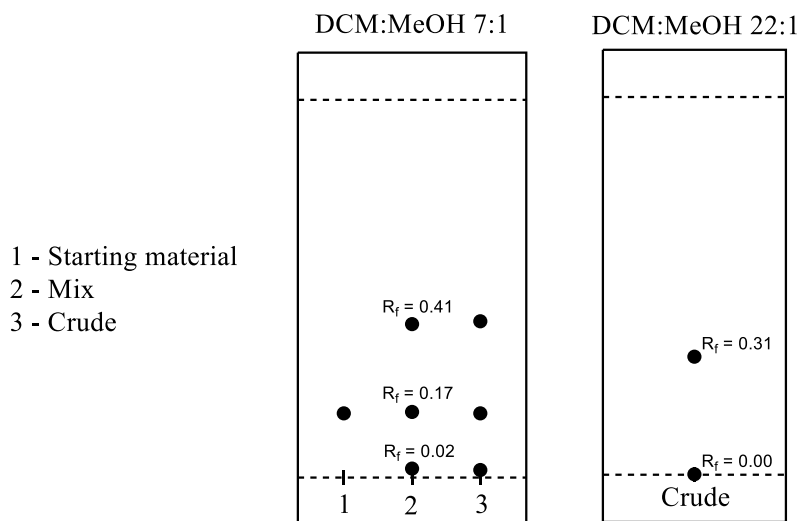


Figure 89 TLC analysis of the crude product *endo* ester 5,6-FAM.

The ¹H NMR of the crude product shows peaks in regions where they would be expected but does not provide evidence that a reaction occurred or that the product was synthesised. However, it was assumed that the product had been successfully synthesised and therefore it was decided that a column would be used to attempt

to isolate the product. Several different solvent ratios of DCM:MeOH were used in the Thin Layer Chromatography (TLC) of the crude product to determine the best conditions for a column. Figure 89 shows the TLC results in two different solvent ratios.

It was decided that the solvent ratio of DCM:MeOH 22:1 was suitable for the column as the spot at $R_f = 0.31$ was expected to be the product. This was because the spot at $R_f = 0.17$ had been identified as the starting material in the solvent ratio DCM:MeOH 7:1 and the spot at $R_f = 0.02$ was expected to be an impurity. Therefore, a column was set up and 80 mg of the crude product was loaded onto it. The column was run, and a single spot was isolated at the expected $R_f = 0.31$. The fractions containing the spot were combined and the solvent was removed *in vacuo*, leaving a very small amount of yellow residue. This residue was taken up in DMSO-d₆ and analysed by ¹H NMR which is shown below in Figure 90:

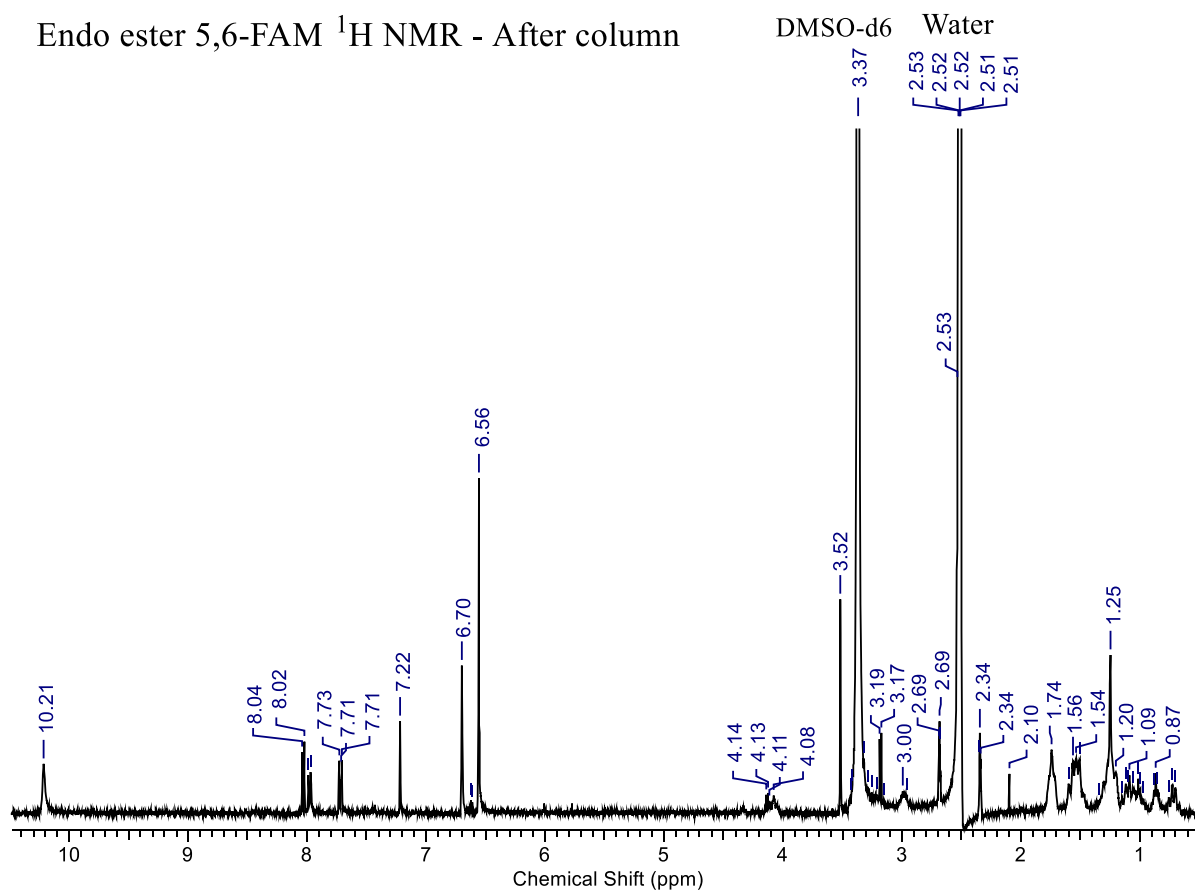


Figure 90 ¹H NMR spectrum of a sample obtained from column fractions containing a single spot after running a column on the crude product from the Steglich esterification between *N*-(hydroxypentanyl)-*cis*-5-norbornene-endo-2,3-dicarboximide and 5,6-carboxyfluorescein (endo ester 5,6-FAM).

The ^1H NMR (Figure 90) of the product isolated by the column does not appear to contain the correct product. This is evident due to the lack of a peak corresponding to the alkene on the norbornene. In fact, it appears to contain more than a single component. The peaks in the aromatic region can almost certainly be attributed to 5,6-FAM or a derivative of it. The peaks in the alkane region could possibly be attributed to DCC or DCU as the lack of a norbornene alkene peak rules out the possibility of the peaks belonging to the monomer linker used. The spectrum could also possibly be a reaction intermediate as a result of the reaction between 5,6-carboxyfluorescein and DCC. However, these possibilities are entirely speculative. The spectrum shown in Figure 90 above is highly zoomed in due to the very small amount of residue isolated. A COSY NMR was run on the sample but only picked up the DMSO and water solvent peaks due to their much greater intensity. Thus, it is extremely difficult to interpret the spectrum above. However, most importantly it does not contain the product and therefore the purification by column chromatography was unsuccessful.

Due to the physical properties of 5,6-FAM, namely its poor solubility, alternative work-up methods such as washing are not suitable. The only solvents that dissolve 5,6-FAM, such as methanol, ethanol, DMF and DMSO are all miscible with water and therefore make it impossible to separate out.

Compared to the reaction between the *endo* alcohol linker and rhodamine b, the reaction between the *endo* alcohol linker and 5,6-FAM appears to be much more difficult and less effective. This coupled with the numerous issues such as poor solubility in the reaction solvent and work-up difficulties makes the reaction very difficult. Hence, it was decided that the reaction would no longer be attempted, and the project would be steered away from the direction of FRET. If more time was available, this reaction could be studied in more depth. It is expected that the additional carboxylic acid group on the aromatic ring of 5,6-FAM negatively impacts its reactivity compared to rhodamine b.

Despite the failure of the reaction with 5,6-FAM, several other monomers had been synthesised during the project as described above, and some of their polymerisations could be investigated.

Ring-Opening Metathesis Polymerisation (ROMP)

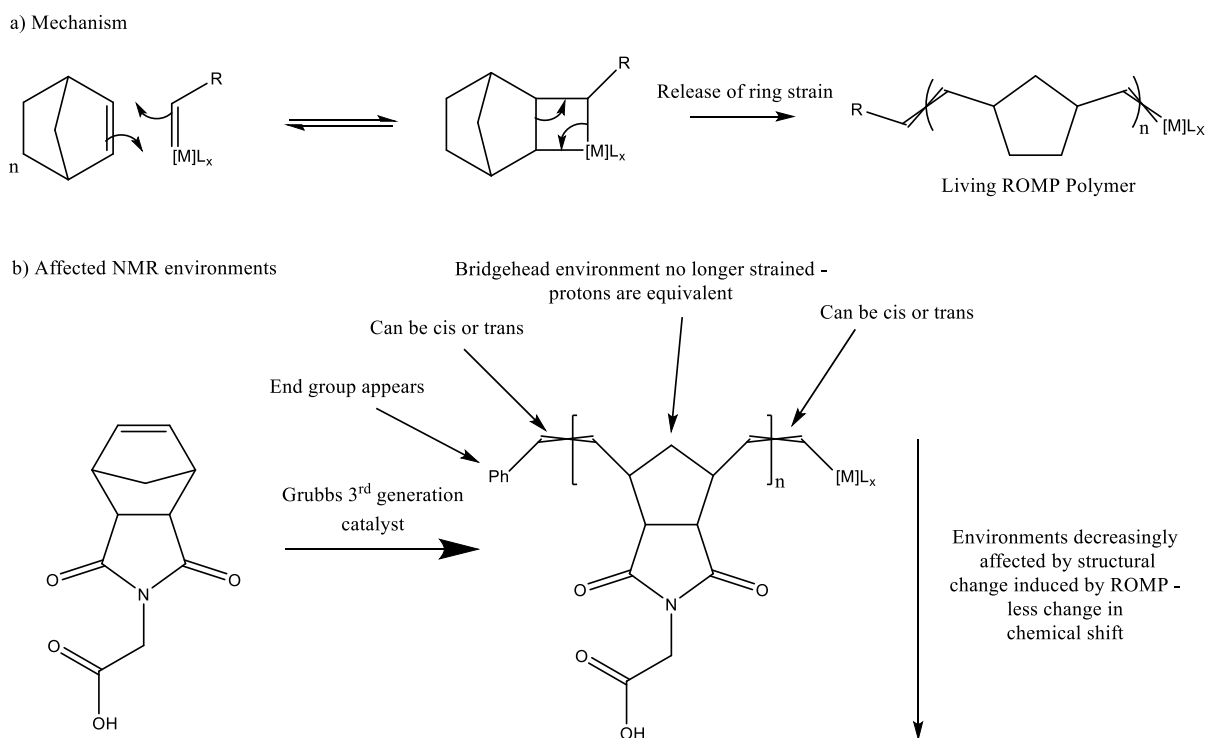
The initial part of this project was to synthesise monomers with norbornene moieties to later be used in ROMP to generate polymers and co-polymers with interesting properties. There are several different catalysts that can be used for ROMP, most of which are air-sensitive and some of which are so sensitive that they must be used within a glove box. However, Grubbs 3rd Generation catalyst is stable enough to be used on the bench, if it is used quickly and stored under the correct conditions.

Despite the catalyst being relatively stable to use, it is still a sensitive reaction that can be affected by things such as the choice of solvent or impurities in the monomer. Furthermore, work-up details in the literature are brief in their description. Therefore, it was necessary to practice the polymerisation procedure with one of the less precious adducts that were synthesised. The monomer used for the practice of ROMP was the *exo* himoyl glycine derivative. This adduct was chosen as the ¹H NMR was very clean, limiting the chance for impurities to impact the reaction and several grams were available to use.

As part of the project, it was decided that a small kinetic study of the ROMP procedure would be carried out to discover how long it may take the reaction to start upon catalyst addition as well as how long the reaction may take to finish. However, first it is important to understand what changes are to be expected in a ¹H NMR spectrum when ROMP takes place.

¹H NMR of ROMP polymers – what is expected?

When a ROMP reaction occurs, there are many expected changes in the ¹H NMR due to the ring opening of the norbornene. This is a drastic change in the molecule that expectedly causes a reduction in intensity or complete disappearance of the alkene peak of the norbornene. Scheme 13 provides a representation of the peaks affected during ROMP due to the ring opening process.



Scheme 13 a) Mechanism for Ring-Opening Metathesis Polymerisation (ROMP) b) Reaction scheme for ROMP that is annotated to show how different ^1H environments are affected in an NMR spectrum when a monomer is polymerised.

From Scheme 13 above it is clear to see the structural changes that occur during ROMP and how it impacts the NMR spectra. The bridgehead protons become equivalent due to the release of ring strain. The initiation step introduces a Ph end group (due to the catalyst) which should appear on the spectra, but in some cases will not be visible due to overlap in the aromatic region or due to low intensity caused by a comparatively long polymer chain. Furthermore, as the reaction takes place on the norbornene, a change in chemical shift may be expected for the other environments on the monomer. This change in chemical shift will be felt most strongly by the environments closest to where the norbornene was ring-opened. Environments further away from the ring-opened alkene are less affected and should therefore experience less of a change in chemical shift.

Scheme 13 above also shows that the alkene bonds that connect the monomers and form the backbone of the polymer can be *cis* or *trans*. In terms of ^1H NMR spectra, this is significant as it results in two new environments for both the *cis* and *trans* environments as shown in Figure 91 below:

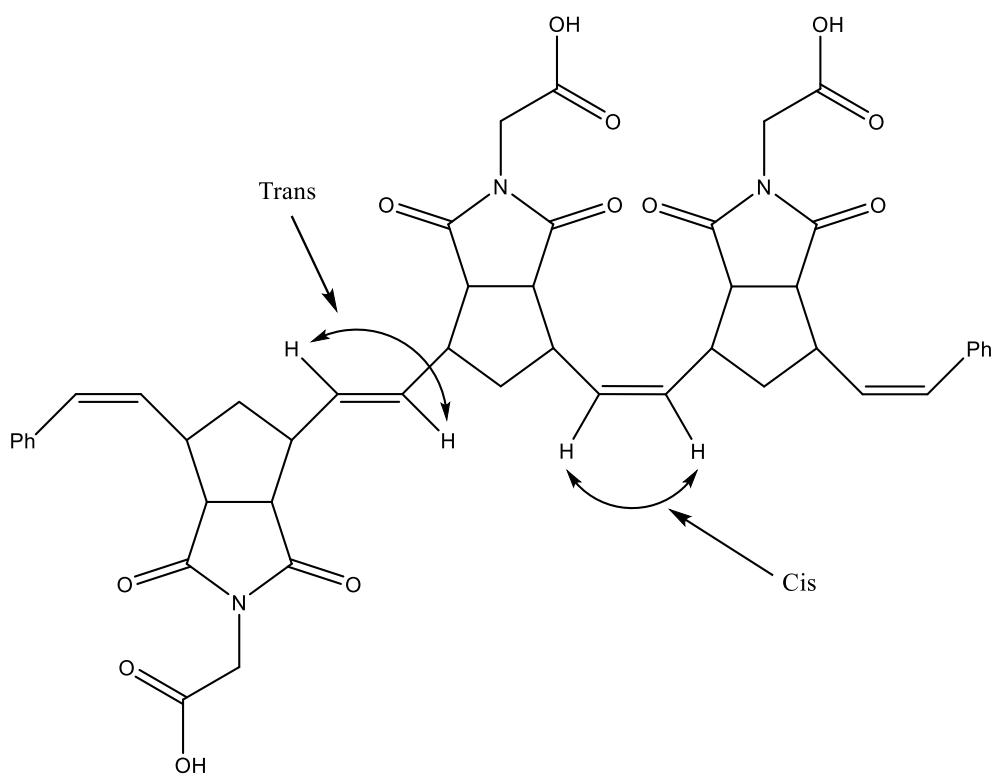


Figure 91 Representation of a ROMP polymer showing the difference between the *cis* and *trans* ^1H environments.

Figure 91 above clearly shows what is meant by the *cis* and *trans* environments that are introduced as a result of ROMP. In the monomers, the alkene environment, typically between δ 6.0 – 6.5 ppm, is very distinctive and easily noticeable. Similarly, once ROMP has occurred, the peaks for the *cis* and *trans* environments are distinctive as they typically appear between δ 5.0 – 6.0 ppm; a region of ^1H NMR spectra that is commonly unoccupied. Furthermore, these peaks along with most of the other peaks in the spectra will be very broad.

Peak broadening is one of the key features in a polymerisation that can occur in both homopolymers and copolymers. Although the monomers making up the polymer may be equivalent, it can be understood that monomer units near the centre of the polymer will feel the effects of the end groups less strongly than those near the end groups. Thus, the chemical shifts of the monomer environments differ slightly in each of the monomers and results in peak broadening. The diagram shown below in Figure 92 provides a more graphical representation of this phenomenon in the example of a homopolymer with equivalent end groups.

Peak broadening in ^1H NMR of homopolymers

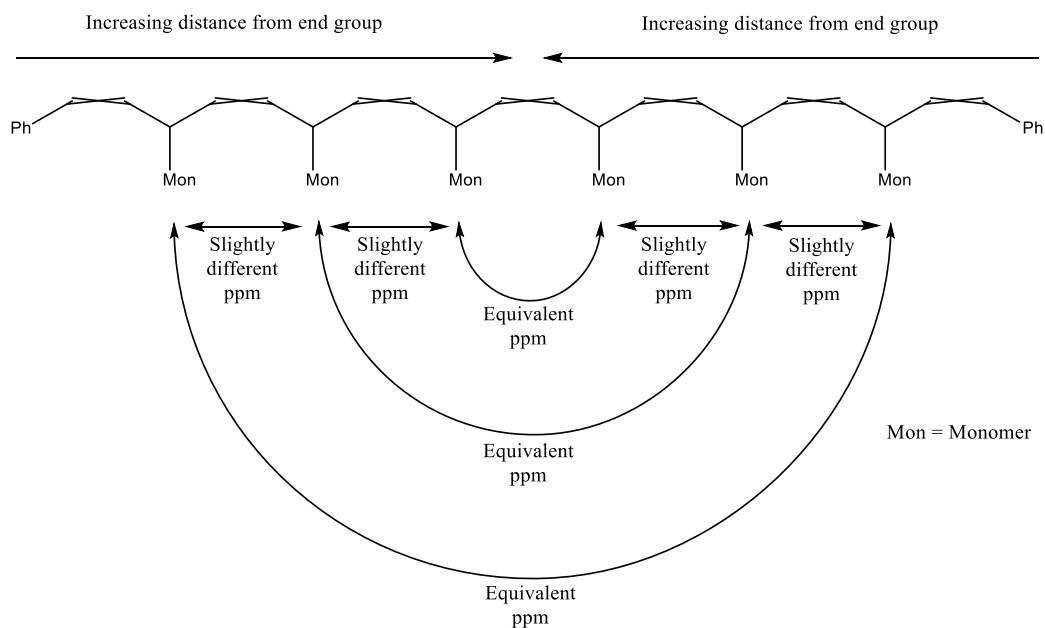


Figure 92 Diagram explaining the origin of peak broadening in the ^1H NMR spectra of polymers.

As with the example in Figure 92, some of the polymers synthesised during this project also had equivalent end groups by terminating the polymerisation with benzaldehyde. By synthesising a homopolymer with equivalent end groups, the ^1H NMR is easier to interpret due to the symmetry of the polymer. End group analysis can be performed to provide insight into the approximate number of monomer units there are within a polymer chain. Although, it assumes that the environments have equivalent relaxation times which is not necessarily the case. The equation below is used to perform end group analysis:

$$n = \frac{I_{c+t} \div NP_{c+t}}{I_{eg} \div NP_{eg}}$$

Equation 5 Calculation of the number of monomer units in a polymer by end group analysis of a ^1H NMR spectrum.

Where n is the number of monomer units in the polymer, I_{c+t} is the sum of the integrals of the *cis* and *trans* peaks, NP_{c+t} is the number of protons in the *cis* or *trans* environments per monomer unit = 2, I_{eg} is the integral value for the end group peak(s) and NP_{eg} is the number of protons in the end group environments = 10. Once this has been calculated, an approximate polymer molecular weight can also be calculated using the molecular

weights of the monomer units and end groups. However, it is important to note that end group analysis is approximate and not always possible due to peak overlap. Therefore, more robust techniques such as GPC analysis should be used to provide more accurate values for molecular weights.

In summary, the key features to look out for when determining if ROMP has been successful are:

- Intensity decrease or disappearance of the alkene peak of the norbornene.
- The appearance of two broad peaks between approximately δ 5.0 – 6.0 ppm which are normally indicative of *cis* and *trans* proton environments.
- Peak broadening.
- Peak shift + broadening for environments closer to the norbornene alkene environment.

ROMP kinetic study

For the kinetic study into ROMP, a ^1H NMR study was carried out in CDCl_3 where the reaction was analysed before addition of the catalyst and then again, several times after catalyst addition at different time increments. A possible concern with this study was that the CDCl_3 may denature the catalyst due to its slight acidity. However, the study was attempted regardless with the ^1H NMR results shown in Figure 93.

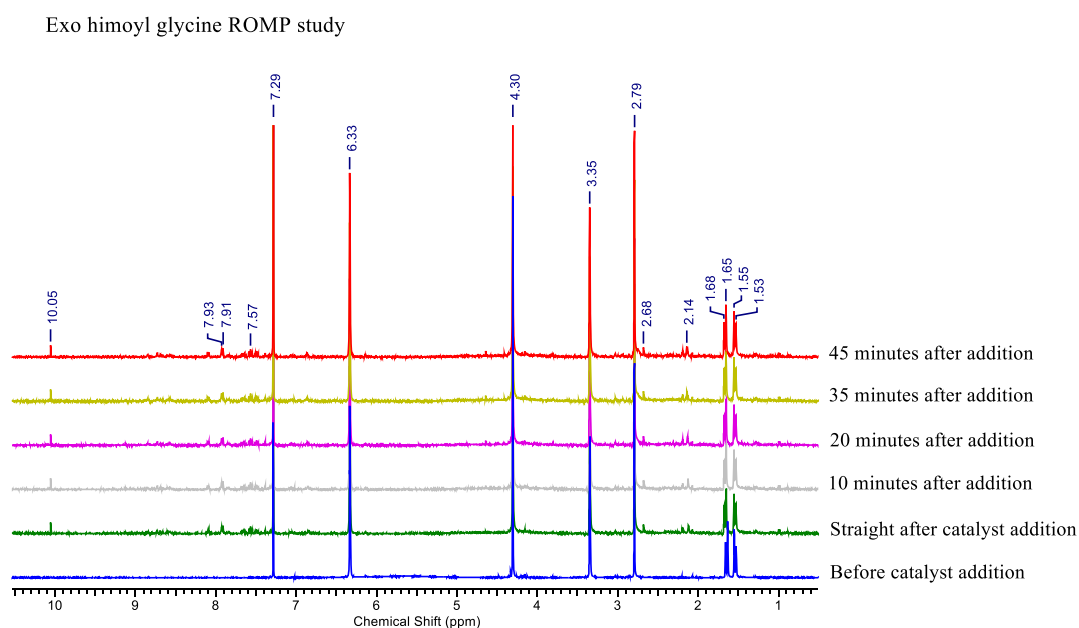


Figure 93 ^1H NMR spectra taken at different time intervals during the ROMP of the exo himoyl glycine monomer (LTB-38 – See Figure 32 for ^1H NMR of monomer) using CDCl_3 as the solvent.

From Figure 93, it can clearly be seen when the catalyst was added to the reaction mixture due to the appearance of several minor peaks, some of which were picked up by the automatic peak picking process. These minor peaks, indicative of the catalyst, appear to remain unchanged over the entire 45 minutes after catalyst addition, hinting towards the fact that the catalyst did not undergo any degradation during this time. However, there also appears to be no change or reduction of peak intensity or broadening in any of the monomer peaks, nor the introduction of any new peaks over the time frame.

Therefore, it seems as though the reaction was unsuccessful, even though the catalyst does not appear to degrade. Despite the catalyst not appearing to degrade, it was expected that the solvent CDCl_3 may have been responsible for the supposedly failed polymerisation.

Exo himoyl glycine ROMP study in DCM (DMSO-d6 capillary)

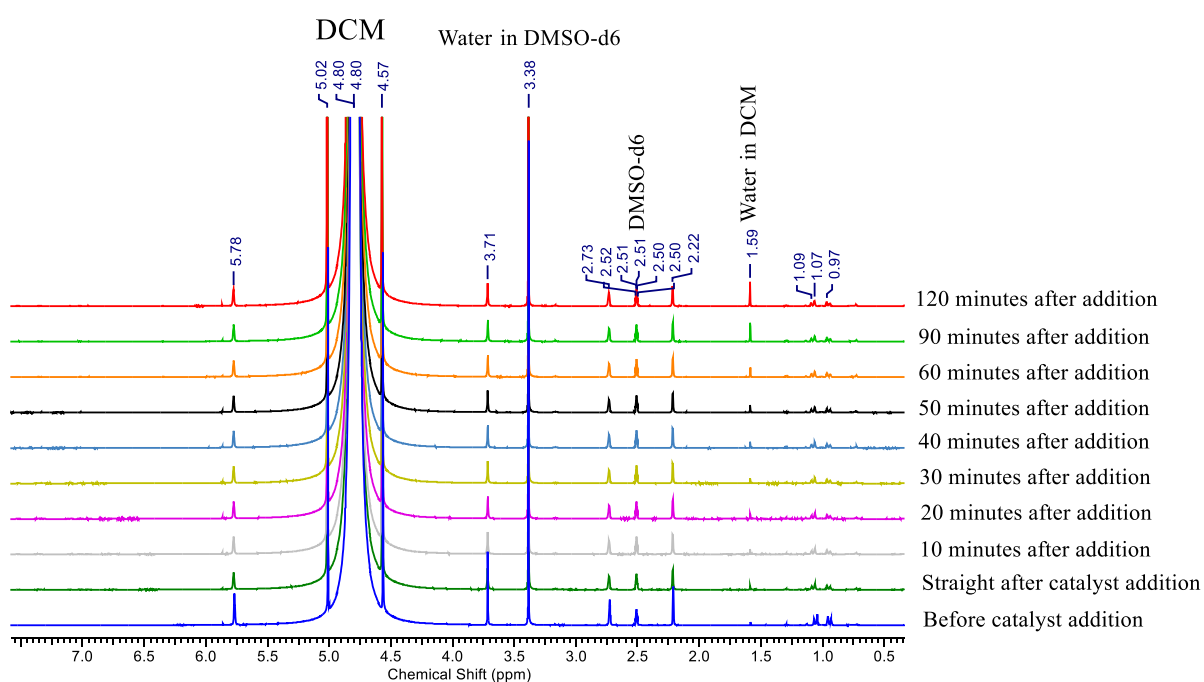


Figure 94 ^1H NMR spectra taken at different time intervals during the ROMP of exo himoyl glycine (LTB-38 – See Figure 32 for ^1H NMR of monomer) using DCM as the solvent where the NMR tube contained a DMSO-d6 capillary.

In order to circumvent the mild acidity issue with CDCl_3 , it was decided that the less acidic solvent DCM could be used. However, deuterated DCM is expensive and so a cheaper system was utilized where the reaction took place in standard DCM which also contained a DMSO-d6 capillary. This system would rule out the issue of the catalyst degrading due to mild acidity. The results of this study are shown in Figure 94.

As with the previous study in CDCl_3 , the ^1H NMR shows no sign of peak broadening, nor the appearance of any new peaks. However, there is a noticeable difference in the peak intensities for the monomer peaks before and after catalyst addition. Although, after the catalyst addition the peak intensities appear to remain consistent as the reaction time increases. This hints that a reaction may have taken place as soon as the catalyst was added and then stopped. Upon inspection of the NMR tube, it was noticed that a precipitate had formed, likely being the polymer. This explains why there is no evidence of line broadening or the appearance of new peaks in the NMR and accounts for the reduction in peak intensity upon catalyst addition. However, it does not explain why a reaction appears to occur upon addition of catalyst and then fails to continue or slows down. Nevertheless, these findings show that *exo* himoyl glycine is not a good choice of monomer for a kinetic study due to the insolubility of the polymer in the reaction solvent.

It is expected that this lack of solubility of the *exo* himoyl glycine polymer can be attributed to the carboxylic acid groups on the monomer. Upon polymerisation, the build-up of $-\text{COOH}$ and potentially $-\text{COO}^-$ groups results in a polymer that is not soluble in non-polar solvents such as CDCl_3 and DCM and is instead more soluble in polar solvents such as DMSO and water. It is quite possible that the polymerisation reactions had worked in CDCl_3 but had precipitated, but this still does not change the fact that the monomer is not suitable for a kinetic study in these solvents.

Due to time constraints, the kinetic study on ROMP was not continued in order to concentrate on progressing with the project. Although the kinetic study was not completed, it allowed for good practice with the ROMP reaction and gave insight into factors that may affect the solubility of a polymer. Moreover, it showed that dry DCM is a suitable reaction solvent.

Exo himoyl glycine polymer

Although the kinetic study allowed for practice of the reaction initiation, it did not allow for practice in the work-up and isolation of the polymer for analysis. *Exo* himoyl glycine was not suitable for the kinetic study but was considered suitable for practice in reaction work-up and product isolation.

Therefore, a ROMP reaction with *exo* himoyl glycine was performed in dry DCM in a capped vial and was terminated by the addition of a few drops of a very dilute solution of benzaldehyde in THF. After terminating

the reaction, the solvent was removed *in vacuo*, leaving a white/grey residue in the vial. This residue was washed twice with diethyl ether, each time the diethyl ether was decanted off and compressed air was blown gently into the vial to remove as much excess solvent as possible. The white-grey residue was dissolved in DMSO-d6 and analysed by ^1H NMR (Figure 95) which is shown and explained below:

Exo himoyl glycine polymer ^1H NMR in DMSO-d6

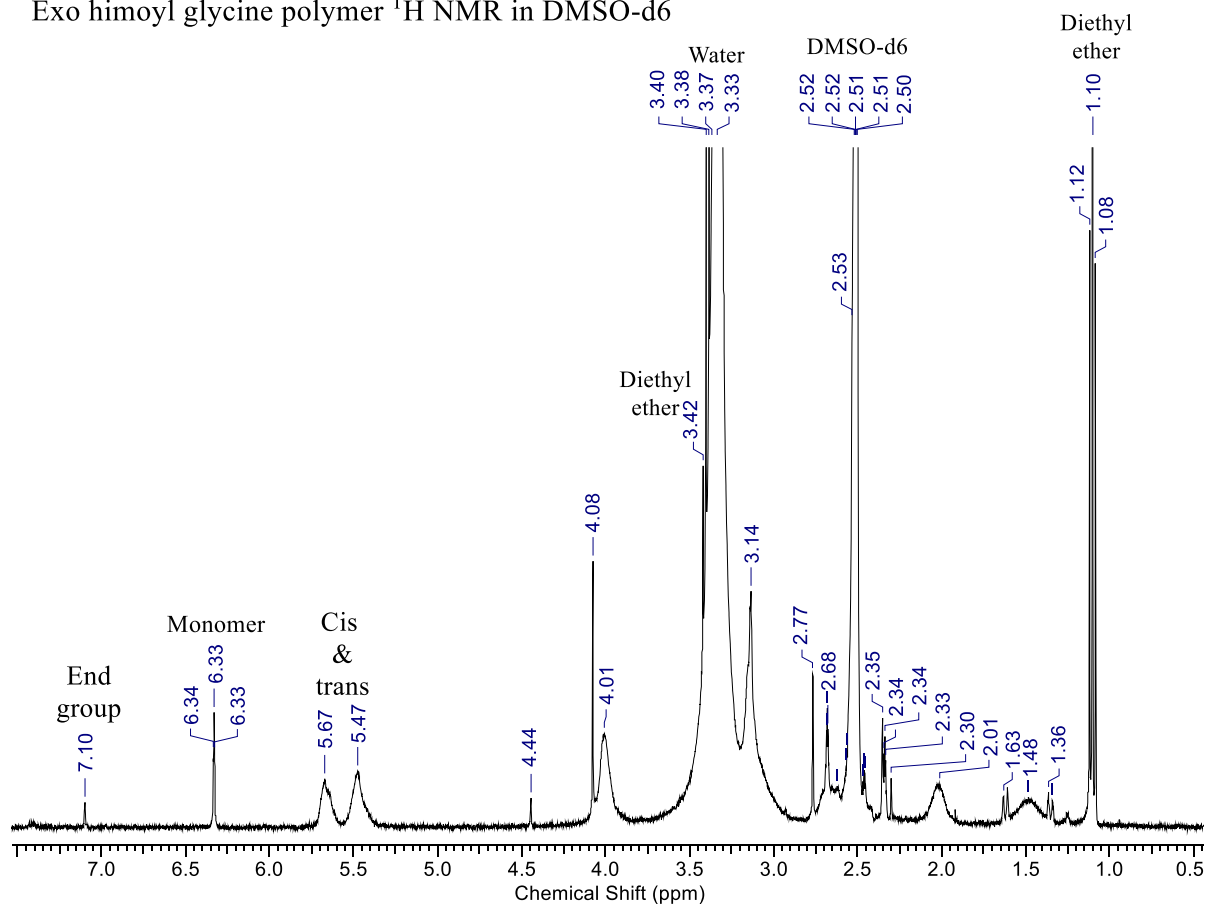


Figure 95 Annotated ^1H NMR spectrum of the polymer of exo himoyl glycine after work-up. Monomer and residual solvent peaks are present.

The ^1H NMR spectrum shows clear signs that polymerisation successfully occurred due to the appearance of broad peaks. The most indicative peaks are those at δ 5.67 and δ 5.47 which are representative of the *cis* and *trans* proton environments on the polymer backbone. However, it is not possible to distinguish between *cis* and *trans* based on this NMR spectrum. If the polymerisation had been performed using Grubbs 1st generation catalyst, the peak for the *trans* environment would be significantly larger than the *cis* environment. This is because the *trans* environment is formed more favourably than the *cis* environment when using Grubbs 1st generation, according to a related study¹³.

Whilst it is clear that the polymerisation occurred successfully, it is also evident that the polymerisation did not go to completion and that the polymer was not isolated successfully during the work-up. The peak at δ 6.33 is indicative of the norbornene alkene environment and it is still present in a significant amount. Unfortunately, since the polymer is not soluble in CDCl_3 , DMSO- d_6 was used as the NMR solvent which results in the large solvent peaks at δ 3.37 (DMSO- d_6) and δ 2.51 (water). Furthermore, there are large solvent peaks at δ 3.42 and δ 1.10, indicative of residual diethyl ether which was used in the reaction work-up. Although there is evidence of residual unreacted monomer, it is difficult to determine whether residual catalyst was removed successfully during the work-up as peak broadening makes it easy for peaks to get hidden by peak overlap.

The *exo* himoyl glycine polymer is suitable for end group analysis as the monomer contains no environments that appear in the aromatic region of the NMR spectra. Thus, there should be no overlap of the end groups with monomer environments. Figure 96 below shows an expanded region of the ^1H NMR of the polymer of *exo* himoyl glycine and contains integration values.

Expanded region of *exo* himoyl glycine ^1H NMR - end group analysis

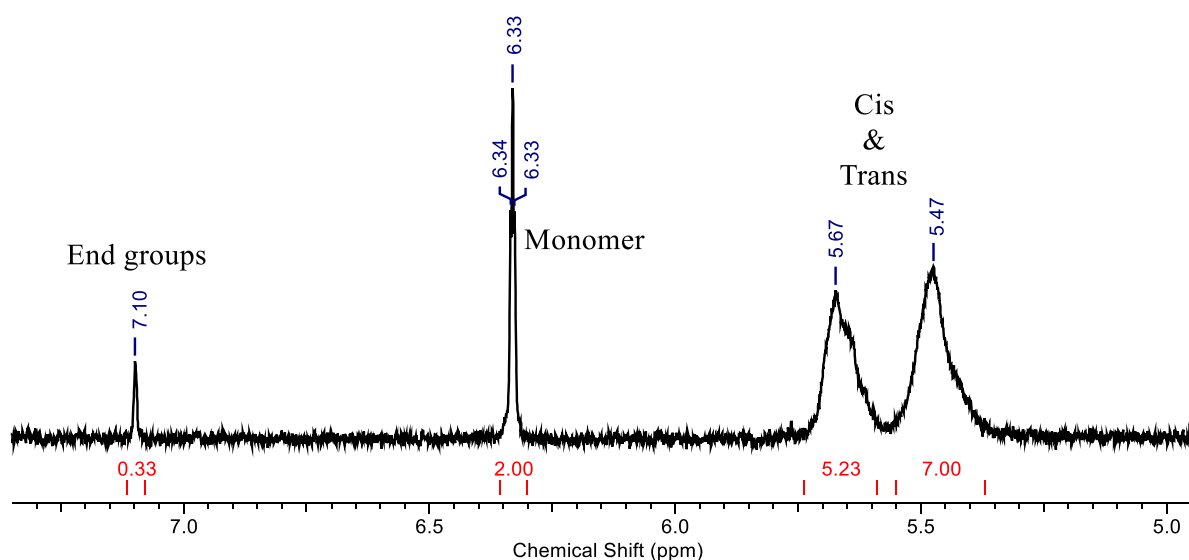


Figure 96 Annotated expanded region of the ^1H NMR spectra of the polymer of *exo* himoyl glycine. Integration values are included for use in end-group analysis.

The expanded region in Figure 96 above contains the peaks for both the end group environments (δ 7.10) and the *cis* & *trans* environments (δ 5.67 and δ 5.47). Along with the integration values, it allows for end group analysis which is performed using Equation 6 shown below:

$$n = \frac{I_{c+t} \div NP_{c+t}}{I_{eg} \div NP_{eg}} = \frac{(5.23 + 7.00) \div 2}{0.33 \div 10} = \frac{6.115}{0.033} = 185.3$$

Equation 6 Calculation of the number of monomer units in the polymer of *exo* himoyl glycine using end group analysis and the integration values obtained from the ^1H NMR spectrum.

It was calculated that the polymer chains were made up of 185 monomer units on average by end group analysis. This value seems very high and Gel Permeation Chromatography (GPC) analysis would have most likely given a very different value, but unfortunately GPC was not available at the time. The high value is probably a result of an incorrect identification of the end groups which is very difficult due to the solvent peaks being so large and the end groups accounting for such a small amount of the polymer.

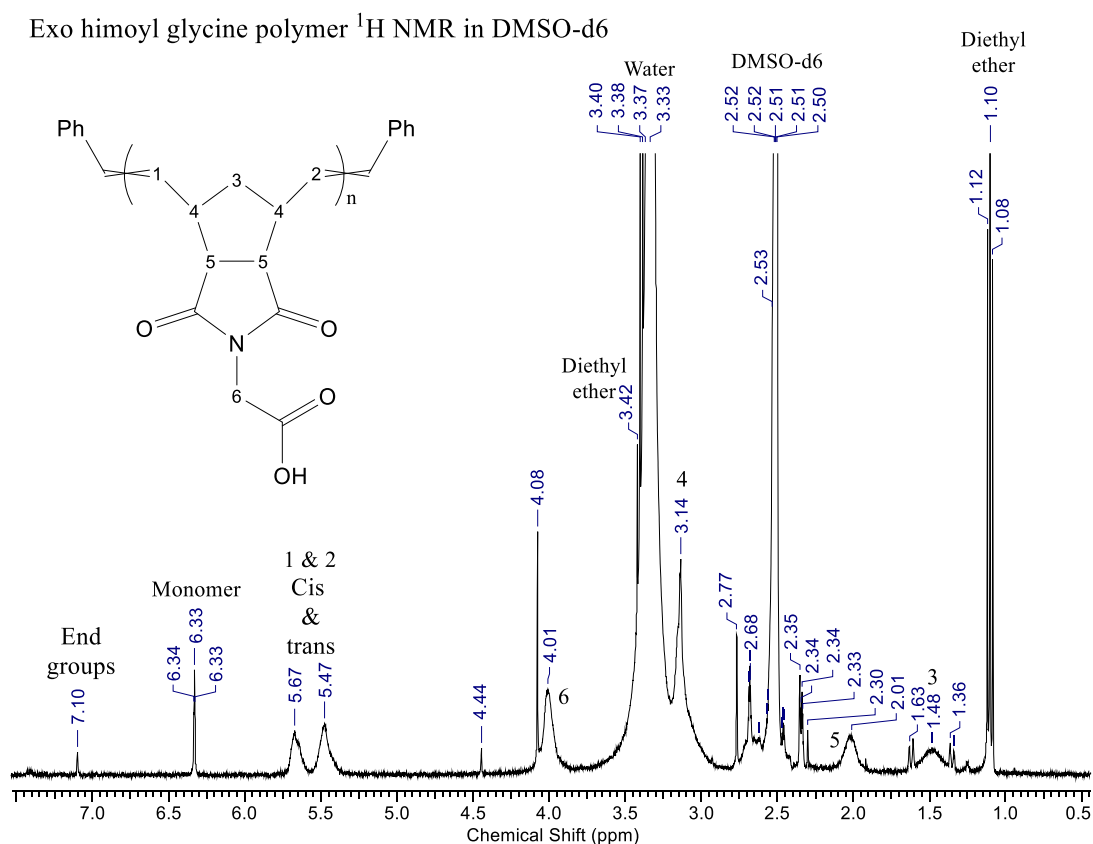


Figure 97 Annotated and assigned ^1H NMR spectrum of the polymer of *exo* himoyl glycine.

Due to the presence of the residual solvent peaks and residual monomer peaks, it is difficult to assign the polymer. However, an assignment of the polymer was attempted and is shown in Figure 97.

The ^1H NMR spectrum in Figure 97 above was assigned based on logic and through comparison to monomer peaks. The *cis* and *trans* peaks which are assigned are the most distinctive as that region of the spectrum is otherwise unoccupied. Despite not being able to distinguish between the *cis* and *trans* environments directly using the NMR spectrum alone, comparison to literature²⁵ suggests that the *trans* environment is the most downfield of the two environments. Therefore, the *trans* can be assigned to the peak at δ 5.67 and the *cis* assigned to the peak at δ 5.47. The broad peak at δ 4.01 can almost certainly be assigned to environment 6 as it is very close to the monomer peak at δ 4.08 as expected due to its distance from the polymer backbone. Due to the proximity of environment 4 to the polymer backbone, it is expected to experience a chemical shift once polymerisation occurs. However, in this case it appears to be in a similar environment to the monomer peak and is therefore assigned as the peak at δ 3.14. Although the presence of the water solvent peak is overlapping with the peak assigned to environment 4, it is still clear to see that it is broad and therefore highly likely to be the correct assignment.

Environment 5 was much more difficult to assign as the monomer peak appears at δ 2.77 but does not have a broad peak in its vicinity. The peak at δ 2.68 is expected to belong to the catalyst but is slightly broad at the bottom. Its proximity to the monomer peak for environment 5 makes it seem possible that it is in fact the peak for the polymer environment 5. However, the peak at δ 2.30 is much more clearly broad and was therefore assigned as environment 5. Despite the disparity in the chemical shifts between the monomer and polymer peak for environment 5, it is not considered too strange due to the ring opening which releases a lot of ring strain and could result in a significant shift in certain environments. Finally, the broad peak at δ 1.48 sits between the monomer peaks for the bridgehead protons. As previously mentioned, once ROMP occurs, these bridgehead protons become equivalent and therefore a single broad peak is expected. Thus, the peak at δ 1.48 was assigned as environment 3 which was previously the bridgehead environment before ROMP.

This assignment may not be entirely correct, but most importantly polymerisation has clearly occurred despite not reaching completion. This may be due to the reaction not being left long enough but is more likely a result of a catalyst that has been denatured. To test this, a new catalyst could be bought, and the reaction repeated to compare reaction progress.

Exo amide RhB polymer

Since finishing in the lab and upon purchase of new catalyst by a colleague (Sara Shehata), it became apparent that the catalyst used during the project period had arrived from the retailer already partially degraded. Hence the polymerisation results in this project were negatively impacted by the degraded catalyst. During the project, the polymerisation of *exo* amide RhB was successfully completed but gave yields that were too low to calculate and even after work-up through centrifugation, the monomer persisted in the ^1H NMR as shown below in Figure 98:

Exo amide RhB polymer - ^1H NMR

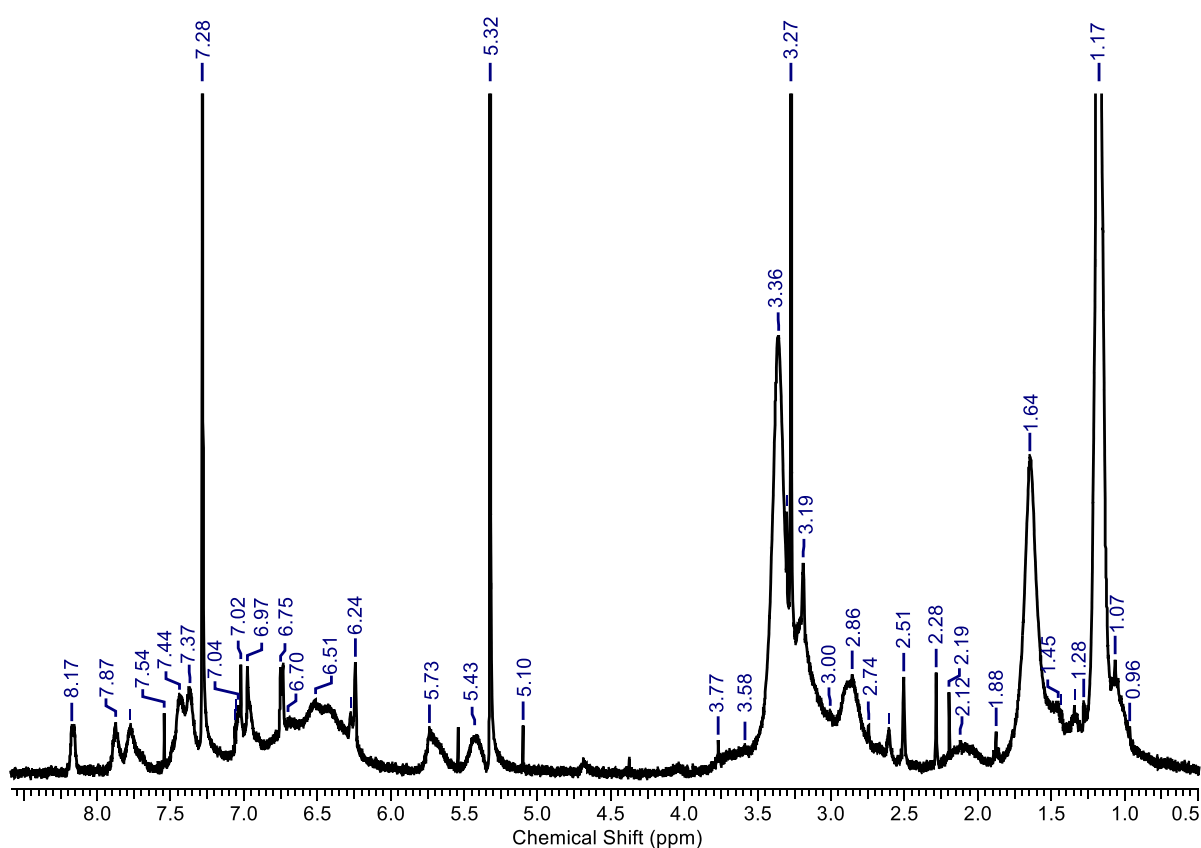


Figure 98 ^1H NMR spectrum of the polymer of *exo* amide RhB. Some monomer is still present in the spectrum.

From Figure 98 above, it is clear to see that polymerisation occurred due to the peak broadening and the appearance of the *cis* and *trans* peaks at δ 5.73 and δ 5.43. However, it is also evident that monomer is still present due to the presence of the alkene norbornene peak at δ 6.24. The presence of the monomer makes it very difficult to assign the polymer peaks in the spectrum. Furthermore, it shows that the polymerisation did not go to completion, which explains the very low yields. Since receiving the new catalyst, a colleague (Sara

Shehata) did a kinetic study on the ROMP of the same *exo* amide RhB used for the polymerisation above. The results of the kinetic study are shown below in Figure 99:

Exo amide RhB ROMP kinetic study - ^1H NMR

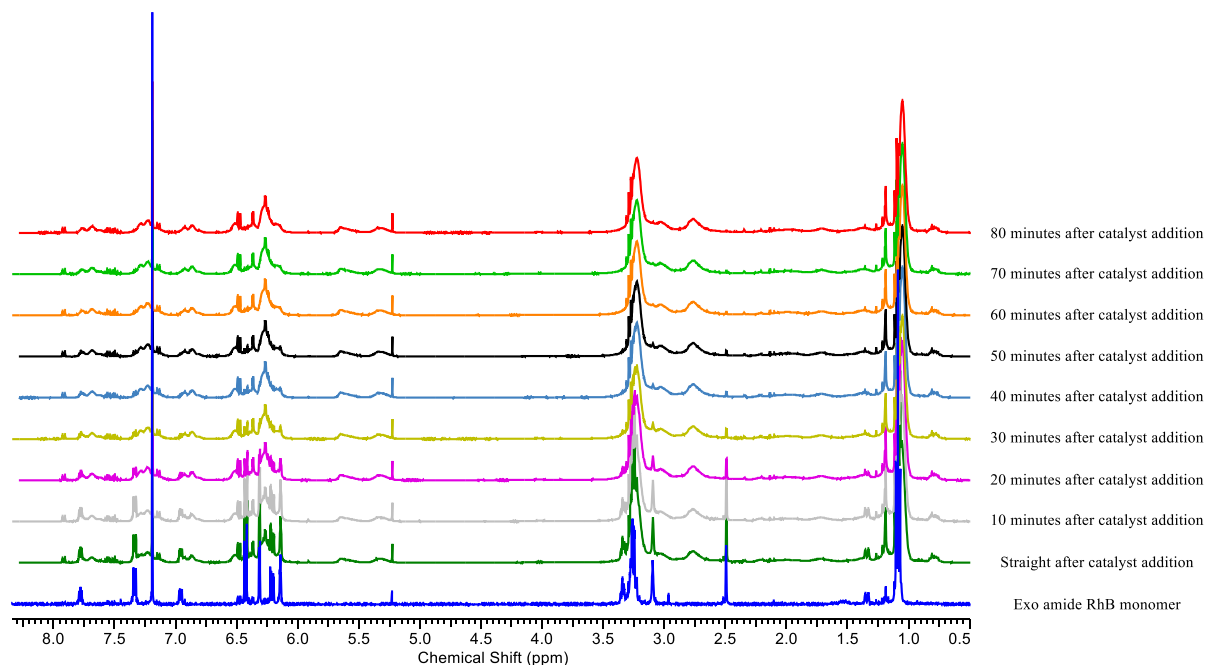


Figure 99 ^1H NMR spectra taken at 10-minute time intervals during the polymerisation of *exo* amide RhB using the new catalyst instead of the old degraded one.

From Figure 99, it can be seen that polymerisation started straight after the catalyst was added and the majority of the monomer had polymerised within 30 minutes. This can be seen through the appearance of the *cis* and *trans* peaks and the decrease in intensity of the monomer peak at approximately δ 2.50. After 30 minutes the polymerisation continued but the intensity of the monomer peak decreased at a slower rate. After 80 minutes the majority of the monomer had reacted which is vastly different to the polymerisation with the old degraded catalyst where the reaction was left overnight, and a large amount of monomer persisted.

The polymerisation was terminated by the addition of ethyl vinyl ether and the polymer was isolated by concentrating the reaction mixture and precipitating the polymer with diethyl ether. The solid was collected by centrifugation and analysed by ^1H NMR (Figure 101) which is shown below:

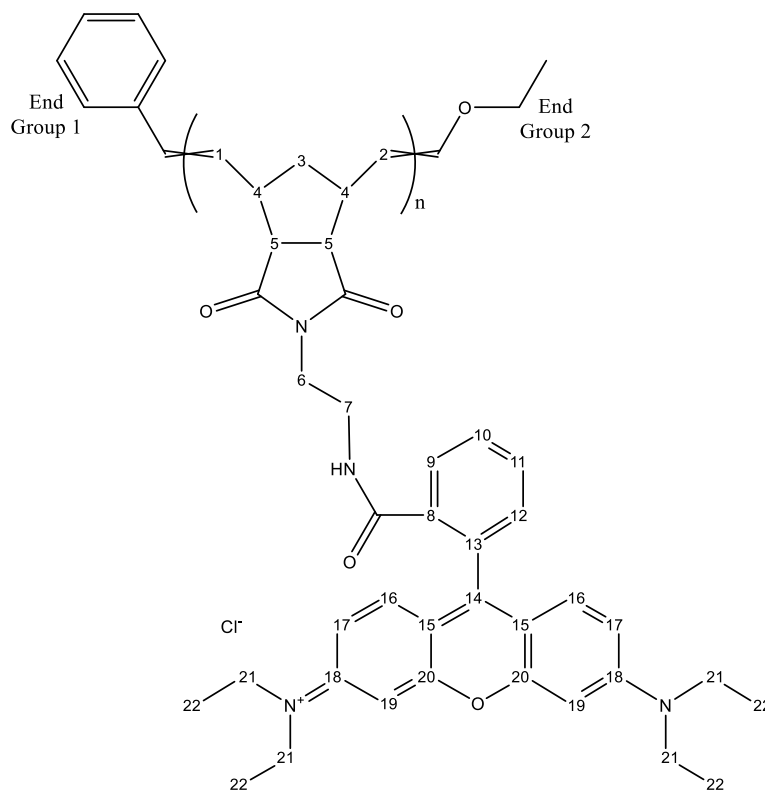


Figure 100 Chemical structure of the repeatable unit in the polymer of exo amide RhB where the carbon atoms are labelled for the easy assignment of NMR spectra.

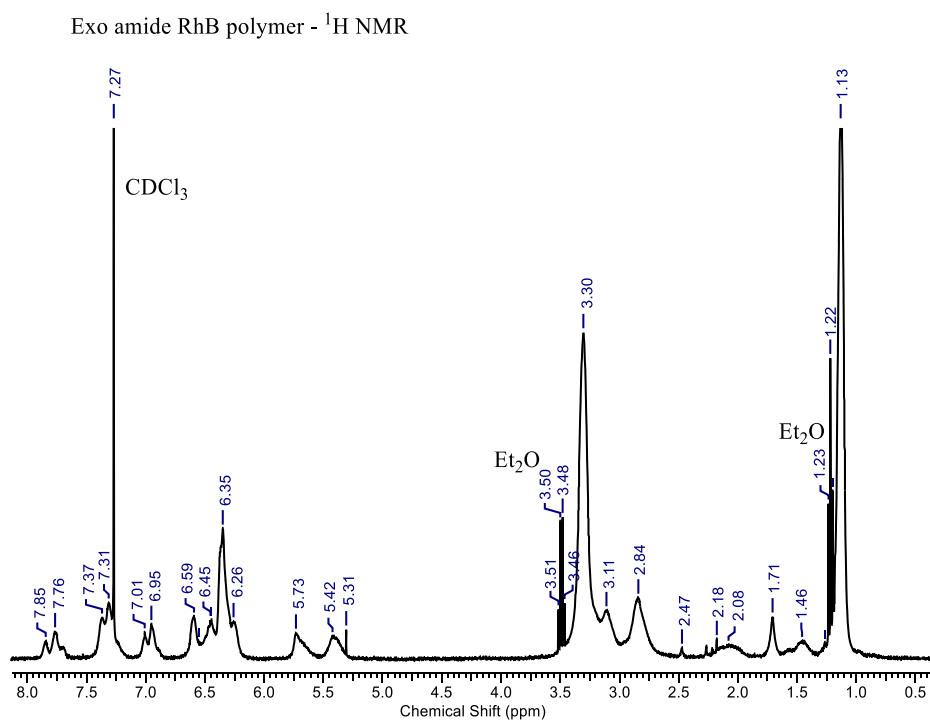


Figure 101 Partially annotated ^1H NMR spectrum for the polymer of exo amide RhB after work-up. Residual solvent peaks are present and labelled.

From the ^1H NMR spectrum shown in Figure 101, it can be seen that the polymer is mostly clean, apart from the diethyl ether solvent peaks which have been labelled and the peak at δ 2.47 which is indicative of a small amount of residual monomer. Expanded regions are shown in Figure 102 below and an assignment of the peaks was attempted.

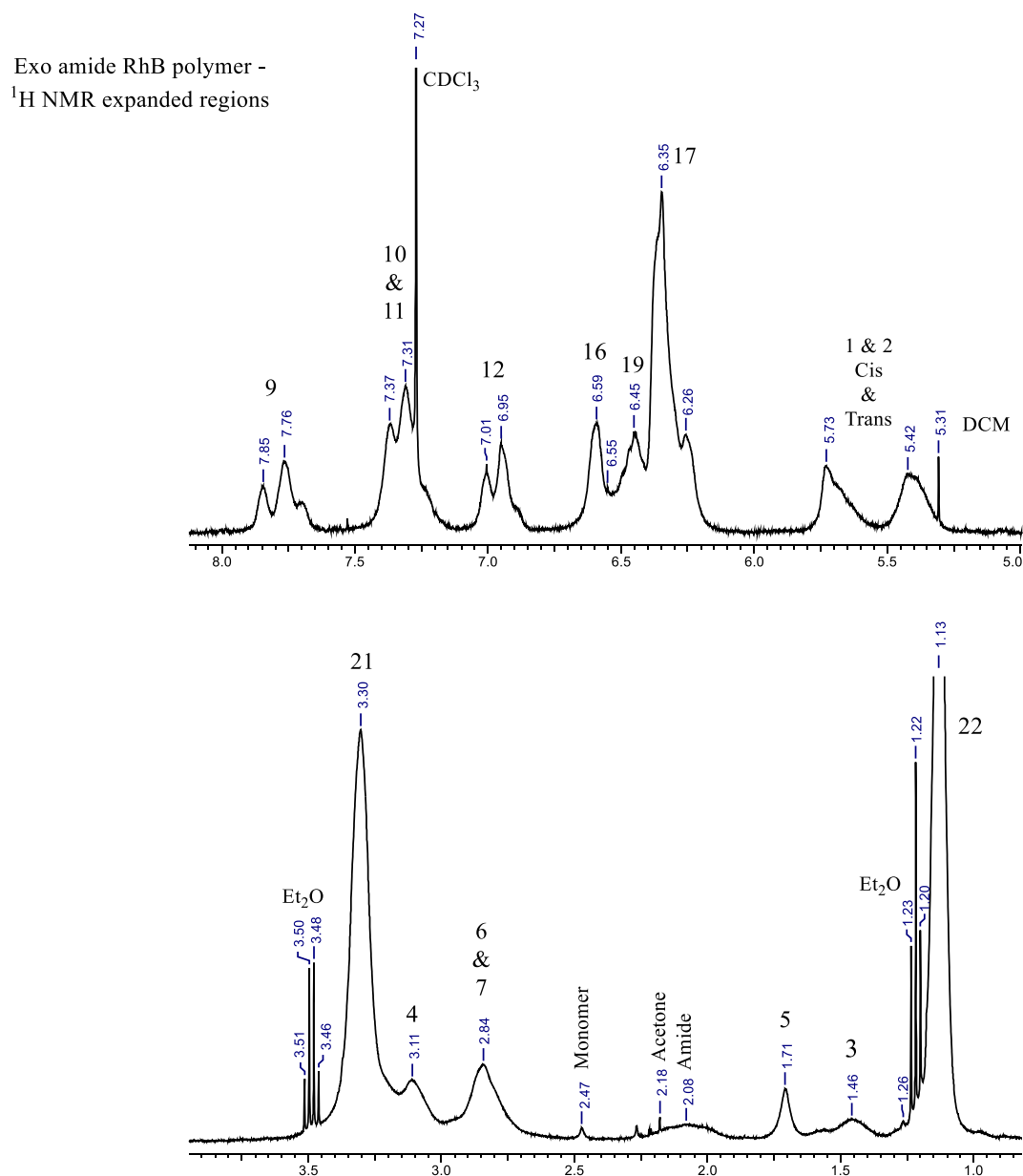


Figure 102 Expanded and annotated regions of the ^1H NMR spectrum for the polymer of exo amide RhB after work-up where the proton environments are tentatively assigned.

The peaks in the aromatic region should be in very similar positions as in the monomer due to the distance of the RhB moiety from the ring-opened norbornene. Hence, the peaks in the aromatic region were assigned as

they were in the monomer. The *cis* and *trans* peaks were assigned but are not distinguishable from each other using this ^1H NMR alone. Although, as with the *exo* himoyl glycine polymer, comparison to literature²⁵ can allow for a tentative assignment of the *trans* peak at δ 5.73 and the *cis* peak at δ 5.42.

The peaks labelled 21 and 22 are part of the RhB moiety and hence have been assigned in the same way as with the monomer. The bridgehead environment from the monomer has been labelled as the peak at δ 1.46 in the polymer as it is directly between where the two bridgehead peaks were in the monomer. Environment 5 has been assigned using similar logic to that used in the assignment of environment 6 in the ^1H NMR of the polymer of *exo* himoyl glycine. Environment 4 was also assigned by similar logic as used in the glycine polymer. Due to the size of the peak at δ 2.84 and the lack of another peak, it was deduced that the protons in the linker appear as the same environment in the polymer, unlike the monomer where they were separate. Finally, it was suspected that the very broad peak at δ 2.08 may be representative of the amide proton in the product, but this is more of a tentative assignment.

Unfortunately, no end group analysis was possible for this polymer as the end group environments appear to be hidden underneath the polymer peaks. Moreover, Gel Permeation Chromatography (GPC) analysis was not possible due to the machine not working at the time.

Furthermore, the success of this polymerisation shows that the monomer was of sufficient purity for ROMP and that the old degraded catalyst was to blame for the lack of successful ROMP reactions during the project.

DNA intercalation

Rhodamine B has been known^{44,45} to intercalate well into DNA due to its planar aromatic moiety that can fit into different grooves in DNA and be stabilised by intermolecular interactions. These intermolecular interactions can cause fluorescence quenching in the RhB which can be studied by fluorescence spectroscopy. Moreover, certain polymers have been shown⁶⁷ to intercalate into DNA but there are no examples of a RhB-based ROMP polymers being used for DNA intercalation.

DNA intercalation has been an important and interesting area of research for many years, especially in areas such as cancer research where certain moieties have been shown to intercalate the DNA of cancer cells and induce apoptosis⁶⁸. Furthermore, developing an understanding of how different species intercalate DNA is important for future research, especially in the areas of polymers where the sizes of polymer self-assemblies are suitable for cancer treatment due to the EPR effect.

Planar aromatic compounds that are fluorescent are particularly good for analysing DNA intercalation. Due to the nature of intercalation where intermolecular interactions hold the self-assembly together, a fluorescence response can be detected that indicates that some interaction has occurred. This technique was utilised, along with DLS measurements using a variety of buffer solutions and different DNA strands. However, it is important to note that the polymer used for the DNA intercalation studies was the lower quality polymer synthesised using the partially degraded catalyst. The higher quality polymer was not synthesised using the fully functioning catalyst until the project was already complete. Table 3 below acts as a key for the results as it shows which buffer, as well as which DNA, if any, was used:

Table 3 Key to be used to determine which buffer solutions were used and whether DNA was present in specifically labelled samples used for DLS and fluorescence measurements.

	Water	TBE 1x	TAMg 1x
No DNA	LTB-120-001	LTB-120-002	LTB-120-003
DNA 1	LTB-120-004	LTB-120-005	LTB-120-006
DNA 2	LTB-120-007	LTB-120-008	LTB-120-009
Mix	LTB-120-010	LTB-120-011	LTB-120-012

DLS is a quick way to see if larger self-assemblies have formed, which would point to the conclusion that some intercalation has occurred. If there is a response in both the fluorescence spectroscopy measurements and DLS measurements for the same set of conditions, then it can be suspected that some intercalation may have occurred. If a set of conditions fitted the criteria above and seemed promising, then further studies such as Atomic Force Microscopy (AFM), Transmission Electron Microscopy (TEM) and Agarose Gel Electrophoresis could be used to provide further insight into the intercalation.

Shown below are the DLS and fluorescence spectroscopy results which have been separated by the buffer solution used. The results present are the size distribution of the particles by intensity, the raw DLS correlation data and the fluorescence spectroscopy results. The particles analysed by DLS were formed simply by combining a solution of the *exo* amide RhB homopolymer in THF with a solution of DNA1, DNA2 or a mixture of DNA1 and DNA2 in the relevant buffer in a PCR tube. The combined solution was mixed using a vortex stirrer and then centrifuged, resulting in particles formed by the self-assembly of the components in the specific THF/buffer system.

Water results:

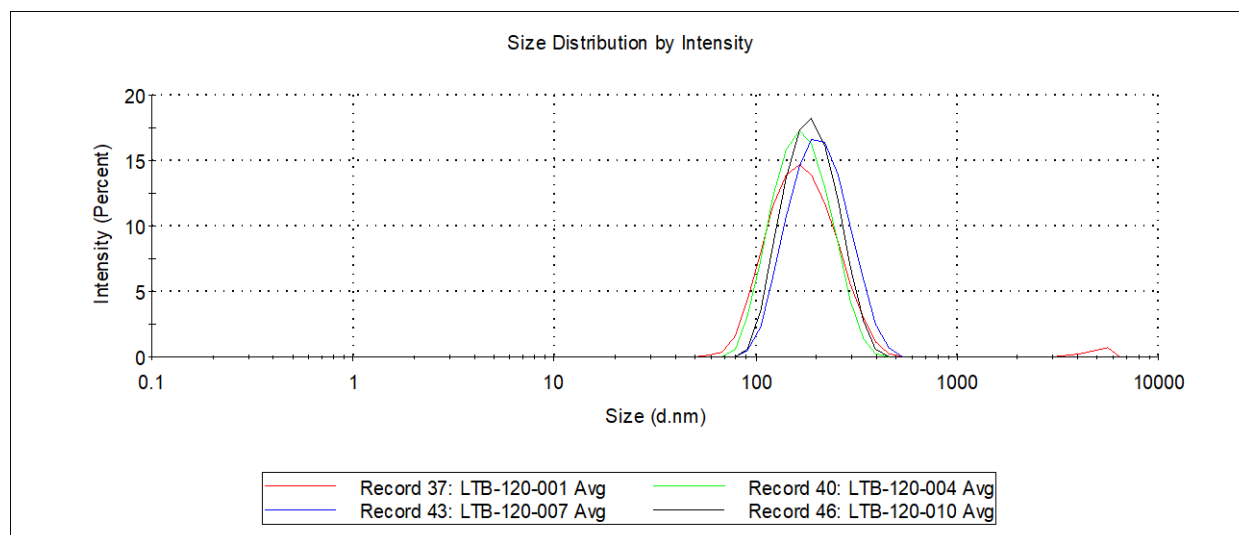


Figure 103 Graph showing the size distribution of particles by intensity in different solutions containing a mixture of the *exo* amide RhB polymer and DNA strands in water. Refer to Table 3 to determine which DNA strands were present, if any, in the samples.

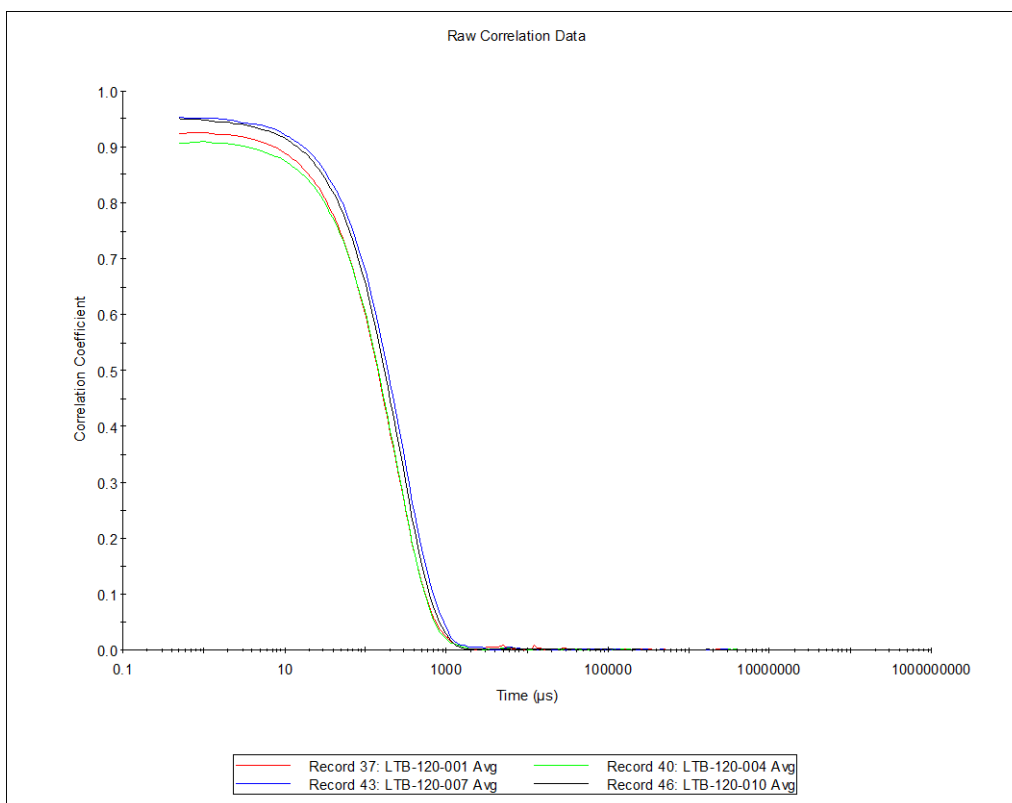


Figure 104 Graph showing the raw correlation data for DLS measurements in different solutions containing a mixture of the *exo amide* RhB polymer and DNA strands in water. Refer to Table 3 to determine which DNA strands were present, if any, in the samples.

From the DLS results, it doesn't appear as though any intercalation occurred due to there being no change in the size distribution of the particles upon DNA introduction, which would be expected when intercalation occurs. The fluorescence results show some differences in the peak intensities for emission. This could be due to a slight interaction between the polymer without intercalation occurring, or a result of another quenching phenomenon such as aggregation-caused quenching. In conclusion, it does not appear that any intercalation occurred in water and therefore no further studies were pursued.

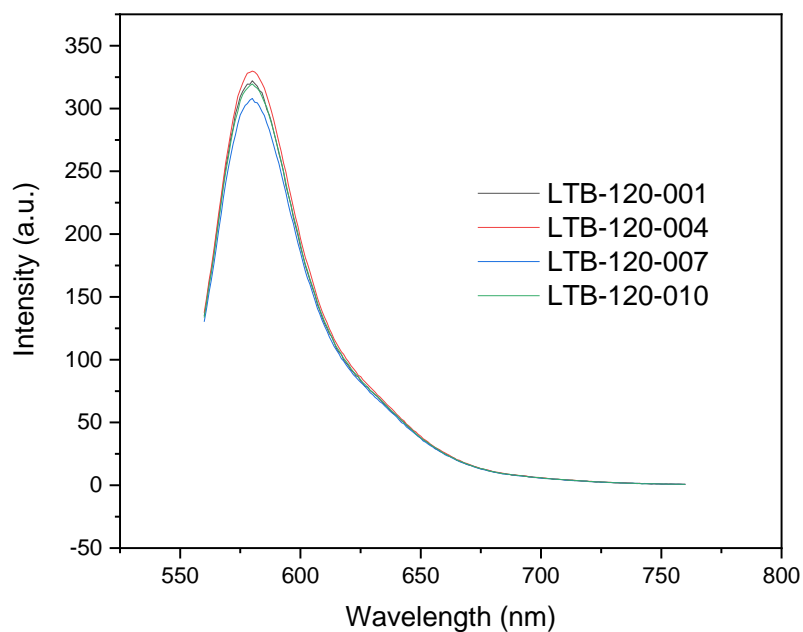


Figure 105 Graph showing the emission spectra recorded using fluorescence spectroscopy for different solutions containing a mixture of the exo amide RhB polymer and DNA strands in water. Refer to Table 3 to determine which DNA strands were present, if any, in the samples.

TBE 1x buffer results:

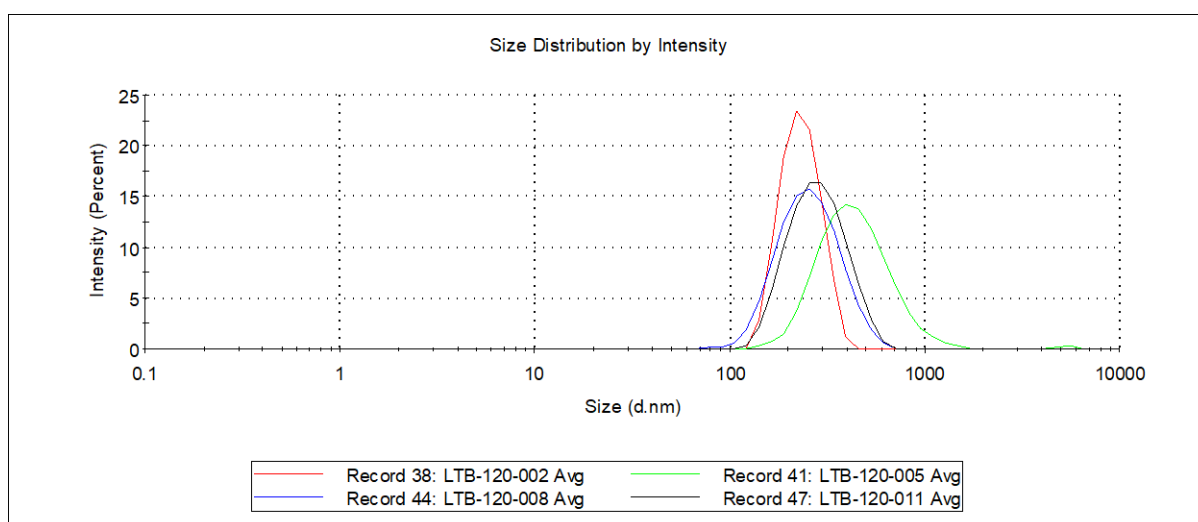


Figure 106 Graph showing the size distribution of particles by intensity in different solutions containing a mixture of the exo amide RhB polymer and DNA strands in TBE 1x buffer. Refer to Table 3 to determine which DNA strands were present, if any, in the samples.

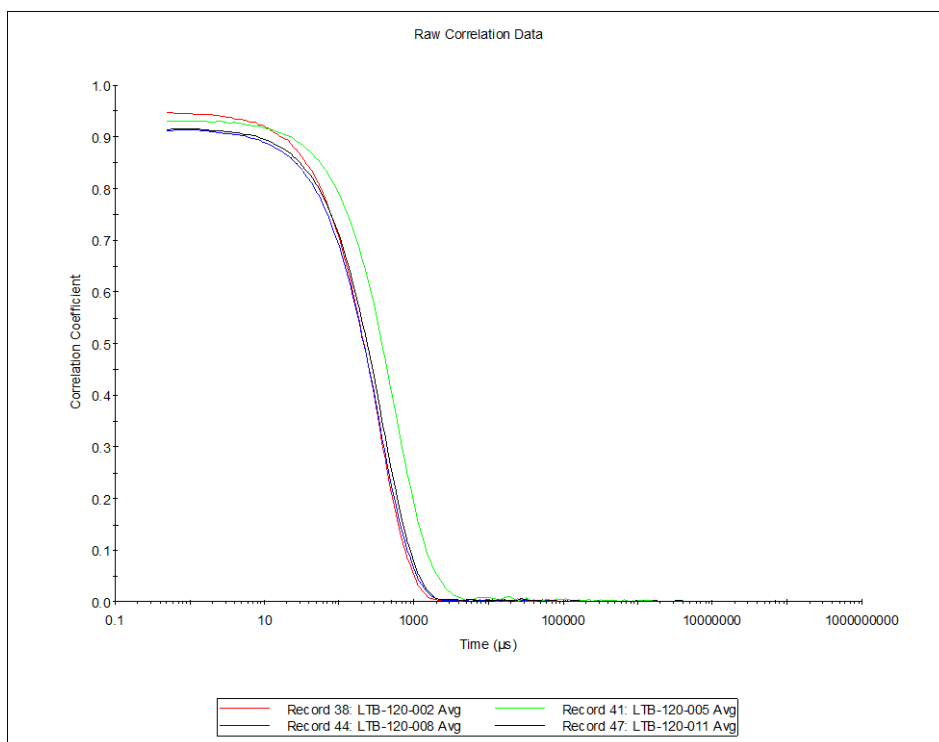


Figure 107 Graph showing the raw correlation data for DLS measurements in different solutions containing a mixture of the *exo amide RhB* polymer and DNA strands in TBE 1x buffer. Refer to Table 3 to determine which DNA strands were present, if any, in the samples.

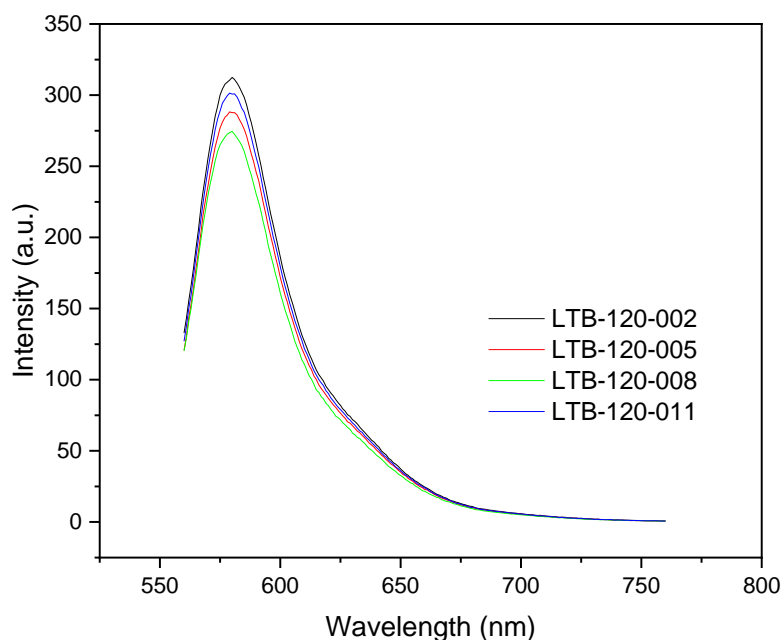


Figure 108 Graph showing the emission spectra recorded using fluorescence spectroscopy for different solutions containing a mixture of the *exo amide RhB* polymer and DNA strands in TBE 1x buffer. Refer to Table 3 to determine which DNA strands were present, if any, in the samples.

Unlike in the water, the TBE 1x buffer showed more promising results. LTB-120-005, which was the sample that contained DNA 1 showed some differences in both the raw correlation data and the size distribution by intensity. The difference between the peak size distribution by intensity in LTB-120-002 (approx. 250 nm) and LTB-120-005 (approx. 500 nm) is roughly 250 nm which is a significant difference. However, the fluorescence wasn't significantly quenched for sample LTB-120-005. In fact, the sample LTB-120-008, which showed no real change in the DLS results was quenched more than sample LTB-120-005. In conclusion, the results in the TBE 1x buffer solution were more promising than results in water but not sufficiently convincing to consider pursuing further analysis.

TAMg 1x buffer results:

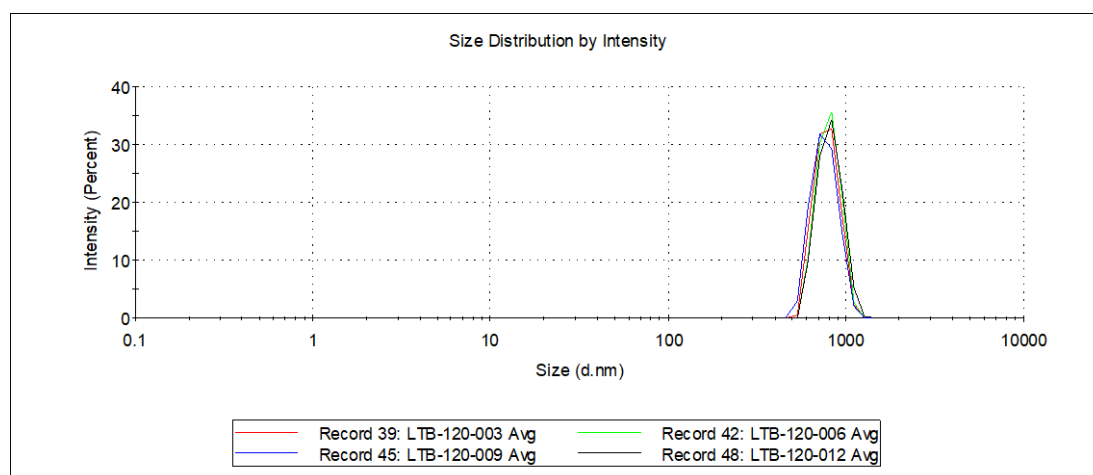


Figure 109 Graph showing the size distribution of particles by intensity in different solutions containing a mixture of the exo amide RhB polymer and DNA strands in TAMg 1x buffer. Refer to Table 3 to determine which DNA strands were present, if any, in the samples.

The results in the TAMg 1x buffer solutions for the DLS measurements showed very little change at all when DNA strands were added. However, the overall size of the structures was almost 1000 nm in size which is significantly larger than in the other two buffer solutions. Albeit, it is not clear why this is the case and lack of time meant that this could not be investigated further. Moreover, the fluorescence measurements showed no significant quenching. Therefore, no further experiments were pursued with the TAMg 1x buffer solutions.

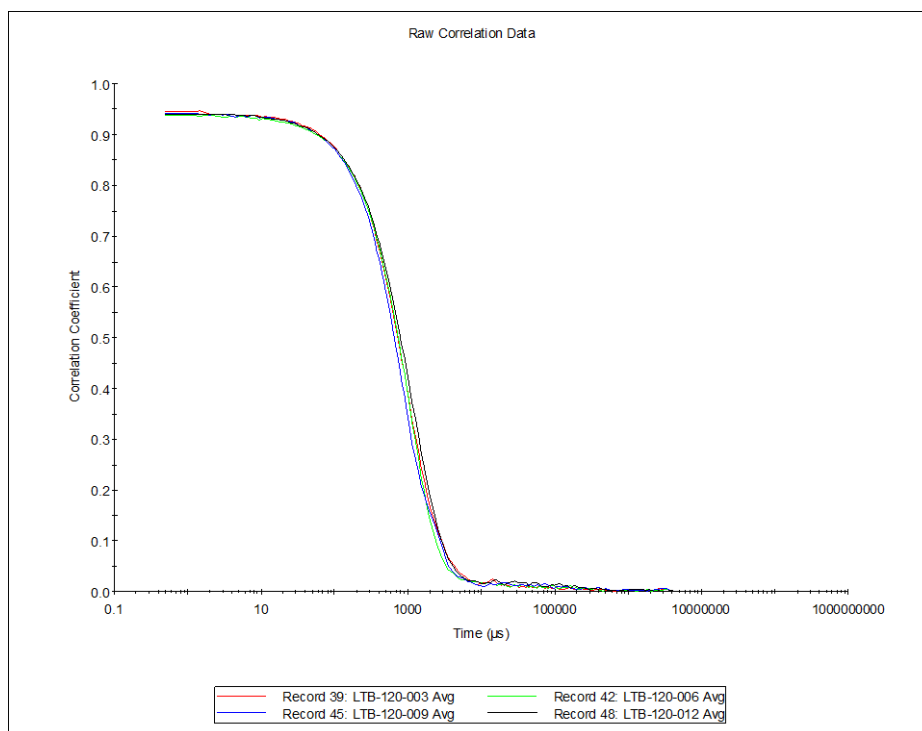


Figure 110 Graph showing the raw correlation data for DLS measurements in different solutions containing a mixture of the exo amide RhB polymer and DNA strands in TAMg 1x buffer. Refer to Table 3 to determine which DNA strands were present, if any, in the samples.

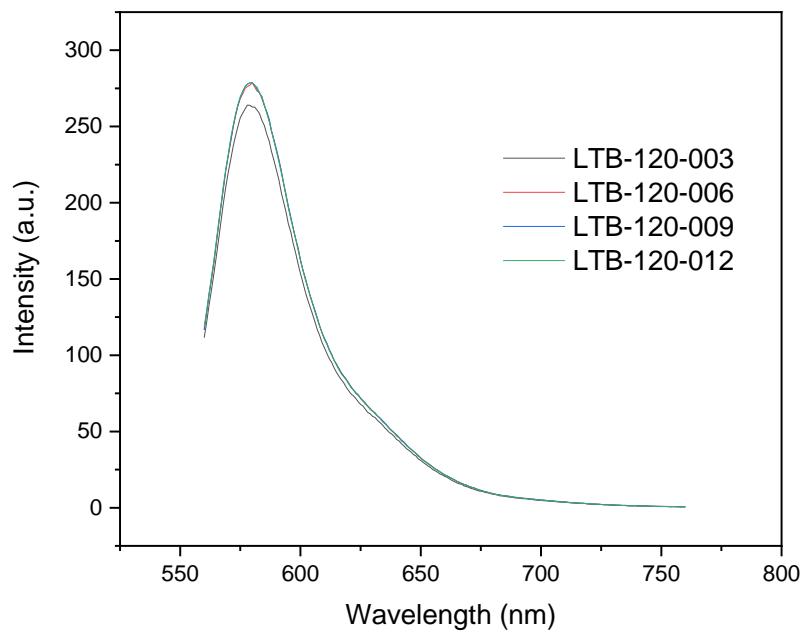


Figure 111 Graph showing the emission spectra recorded using fluorescence spectroscopy for different solutions containing a mixture of the exo amide RhB polymer and DNA strands in TAMg 1x buffer. Refer to Table 3 to determine which DNA strands were present, if any, in the samples.

Overall, the results from the intercalation studies were not as promising as expected. However, the polymer used was not as clean as it could have been. This is because such a small amount of the monomer had polymerised using the old catalyst, which was very poor. Due to time constraints, further studies using the much cleaner polymer synthesised using the new catalyst were not completed. Although, it is expected that using the cleaner polymer would yield better results.

Furthermore, from these studies it can be seen that the TBE 1x buffer gave the most promising results when compared to the other buffer systems used and therefore future work could focus more on that specific buffer system.

Since completion of the project, a funded period of 2 months was allocated for further work on the exo amide RhB polymer. During this time, copolymerisation was achieved with a mPEG-based monomer and self-assembly in acetone/water afforded well defined micelles that were very evenly distributed, as determined by both DLS and TEM measurements.

Conclusion:

The successful optimization of the isomerisation of carbic anhydride from the *endo* to *exo* isomer was achieved. Both bulk (neat heating) and small scale (microwave synthesis) procedures were developed by adjusting literature procedures through experimentation with different conditions. These previous procedures either used toxic solvents, required many recrystallisations or were not easily repeatable. The reaction is seemingly a simple transformation, however, the similarity between the *endo* and *exo* isomers proved challenging both in terms of the conversion and isolation of the product. Therefore, the yield of the isomerisation was always low and typically around 15-20 %. The method proved repeatable when it was successfully used by a group of undergraduate students in their final year of study.

Amino acid, amino alcohol and diamine linkers were all successfully attached to carbic anhydride during the project. The glycine and 5-amino-1-pentanol linkers which were attached were previously detailed well and the literature procedures were followed very closely. The *exo* himoyl glycine crystals grown were very pure and single crystal XRD was utilized to determine its crystal structure, which was previously unsolved and had only been solved for the *endo* isomer⁶⁹.

The synthesis of the diamine linker was not as straight forward due to the array of differing methodologies for its synthesis and purification in the literature. Therefore, a new simple procedure for the reaction between carbic anhydride and ethylenediamine was developed. Unlike other reported procedures, it did not require protection/deprotection or the use of column chromatography to isolate the product. Whilst it may not be the highest yielding method, it provided a very accessible route to complex monomers such as those synthesized during this project. Therefore, it could be utilized along with the optimized isomerisation of carbic anhydride in undergraduate labs and research groups to introduce them to ROMP and provide them with the means to experiment with the addition of functional units via amide formation.

The successful synthesis of complex novel fluorescent monomers for ROMP has been achieved via a relatively simple synthetic pathway and structures of the monomers, *endo/exo* amide RhB, were confirmed by single crystal XRD. Whilst the *endo/exo* ester RhB monomers were synthesized and characterized by NMR techniques, their purity was not determined, and their structure could not be confirmed by single crystal XRD as crystals could not be grown. Similar monomers have been reported in the literature where they were linked to

rhodamine b through ester formation using linkers of similar length^{35,39,40}. However, RhB-based ROMP monomers where rhodamine b is attached to the linker via an amide bond have not been reported in the literature.

Successful polymerization of the complex monomer, *exo* amide RhB, was achieved using ROMP, firstly with a partially degraded Grubbs 3rd generation catalyst and later with a fresh fully functional Grubbs 3rd generation catalyst.

Initial attempts to intercalate the *exo* amide RhB homopolymer with DNA strands appeared to be unsuccessful. However, these attempts were made with the low-quality polymer synthesized using the partially degraded catalyst. Rhodamine b is a well-known intercalator of DNA and more dedicated research towards the intercalation of this polymer could likely yield positive results.

The scope of the *exo* amide RhB monomer is not limited to DNA intercalation. It could be used, like previous RhB-based monomers as part of a copolymer for the purpose of multimodal imaging or theranostics. Furthermore, the monomer is particularly interesting due to the fact it can be present in either its open or spiro lactam form, where the latter was present in the crystal structure. This opens a vast realm of possibilities as rhodamine spiro lactams (RSLs) have been investigated for their use in detecting changes in pH⁷⁰ as well as the detection of metal ions⁷¹. Therefore, the novel monomer, *exo* amide RhB, synthesized during this project could prove to be extremely useful, bringing ROMP and RSL research together.

Experimental:

General information:

Experiments were carried out under normal atmosphere within a fume hood unless stated otherwise. The Grubbs 3rd generation catalyst was stored under a nitrogen atmosphere in a Schlenk tube in the absence of light. Thin layer chromatography was run on ALUGRAM SIL G/UV₂₅₄ plates and column chromatography was run using silica gel 0.060 – 0.200 mm, 60 Å. Microwave experiments were carried out in a sealed 10 ml vessel in a CEM Discover SP microwave system.

NMR data was collected on a Bruker AV II MHz spectrometer, at room temperature, and spectra were referenced to the residual solvent signal of the NMR solvent used. Spectra were processed using ACDLABS software. ¹H NMR data presented in format: ¹H NMR (Frequency, Solvent): δ = shift in ppm (coupling pattern, *J* = coupling constant, number of protons, structure assignment). ¹³C NMR data presented in format: ¹³C NMR (Frequency, Solvent): δ = shift in ppm (structure assignment).

Single crystal XRD data was collected on a Rigaku Oxford Diffraction SuperNova A S2 single crystal diffractometer using a Cu radiation source.

IR spectra were obtained on an IR-Affinity-1S Shimadzu spectrometer and samples were recorded in their standard state. Data from IR spectra are presented in format: IR: $\nu_{\text{max}}/\text{cm}^{-1}$ peak (functional group assignment).

GC-MS data was collected on an Agilent 6890 series GC with MS detector. Exo percentage was calculated from the integration of the area under each peak as determined by the software. Mass spectra data reported in format: *m/z*: molecular ion.

DLS measurements were recorded using a Zetasizer Nano ZS instrument from Malvern Panalytical Ltd. The measurements were recorded at 25 °C using a sample refractive index value of 1.450 and an absorption value of 0.001. The dispersant used was water with a refractive index of 1.330 and a viscosity of 0.8872 cP. Automatic attenuation was used. Samples were run in a quartz cell and measurements were taken after an equilibration time of 2 minutes.

Fluorescence measurements were made using a Cary Eclipse Fluorescence Spectrophotometer by Agilent Technologies. Emission spectra were recorded within the range of 560 – 760 nm and excitation was set at 550 nm. Excitation and emission slit sizes were set at 5 nm. The scan rate was set at 600 nm / min with a data interval of 1.000 and an averaging time of 0.1 second. The excitation filter was set to auto, the emission filter set to open and the PMT detector voltage set to 600 V. The multicell holder accessory was used and the samples were measured in a quartz cell.

Materials

Endo Carbic Anhydride used in all experiments was Carbic anhydride, 99% from Acros Organics. *Exo* carbic anhydride was prepared by isomerisation of the *endo* isomer. 5-amino-1-pentanol 97% and Rhodamine B 98% were commercially available from Acros Organics and used without further purification. Ethylenediamine 99% was commercially available from Avocado Research Chemicals and used without further purification. Glycine was commercially available from Sigma Aldrich and used without further purification. All solvents used were bought commercially and were used without additional purification. For the DNA intercalation studies, DNA1 was 5'-CTGTATGGTCAACTG-3' and DNA2 was 5'-CAGTTGACCATACAG-3' and were commercially available from Integrated DNA Technologies. The buffer solution TBE 1x was prepared by diluting a TBE 10x solution made up of Tris base (108 g), boric acid (55 g) and EDTA (7.45 g) in water (1 L). TAMg 1x buffer solution was prepared by diluting a TAMg 10x solution. TAMg 10x was prepared in a 1 L volumetric flask using Tris base (54.51 g) and Mg(OAc)₂·4H₂O (26.8 g) which were taken up in water (900 mL), the pH was adjusted to 8 by the addition of acetic acid and the total volume was made up to 1 L by the addition of water.

Thermal isomerization of carbic anhydride:

Neat Heating method:

Endo carbic anhydride (100 g, 0.609 mol) was added to a round bottomed flask with condenser attached. The solid was heated (180 °C, 2 h) gently to avoid charring. Note: A yellow-orange colour is okay but if the liquid

turns orange-brown then the temperature should be lowered slightly. After heating, the orange liquid was left to cool slightly and then toluene (190 ml) was added. Some solidification occurred due to the cold toluene and so the solution was heated under reflux until all solid had dissolved. The solution was left to cool slowly to RT and the top of the flask was covered before leaving the flask overnight for crystallisation to occur. Once crystallisation had occurred, the solvent was carefully decanted off and the product, LTB-47-001, was collected by vacuum filtration, washed with toluene (3 ml) and dried. The crystals did not dry fully but were weighed (57.070 g, 0.348 mol) and the product, LTB-47-001 was analysed by ^1H NMR.

Recrystallisation of LTB-47-001:

Toluene (140 ml) was added to the crude product, LTB-47-001 (57.070 g, 0.348 mol) and the solution was heated until all solid had dissolved. The solution was filtered whilst still hot to remove some fine insoluble impurities and the clear, pale-yellow filtrate was heated again to ensure all solid had dissolved. The solution was left to cool to RT and was covered to avoid loss of solvent during crystallisation. The solution was left overnight and once crystallised; the solvent was decanted off. The crystals were collected by vacuum filtration, washed with toluene (3 ml) and left to dry. The product, LTB-47-002, was weighed (25.020 g, 0.152 mol) and analysed by ^1H NMR.

Recrystallisation of LTB-47-002:

Toluene (60 ml) was added to LTB-47-002 (25.020 g, 0.152 mol) and the solution was heated until all solid had dissolved. The solution was left to cool to RT, covered and left to crystallise overnight. Once crystals had formed, the remaining solvent was decanted off and crystals were collected by vacuum filtration. The product, LTB-47-003 (19.568 g, 0.119 mol) was analysed by ^1H NMR.

Recrystallisation of LTB-47-003:

Toluene (50 ml) was added to LTB-47-003 (19.568 g, 0.119 mol) and the solution was heated until all solid had dissolved. The solution was left to cool to RT, covered and left to recrystallize. After crystallisation, the remaining solvent was decanted off, the crystals were collected by vacuum filtration and were dried. The product LTB-47-004 (16.909 g, 0.103 mol) was analysed by ^1H NMR.

Recrystallisation of LTB-47-004:

LTB-47-004 (16.909 g, 0.103 mol) was dissolved in minimum amount of hot toluene (43 ml – Note: This was added slowly over 30 min so some solvent may have escaped, therefore 43 ml may not be the exact minimum amount of hot solvent needed.) and the solution was stirred until all solid had dissolved. The flask was left to cool to RT, covered and allowed to crystallise overnight. The crystals were collected by vacuum filtration, dried, and the product, LTB-47-005 (15.084 g, 0.092 mol) was analysed by ¹H NMR where hardly a trace of the *endo* isomer could be observed.

Note: The remaining solvent that is decanted off during each of the steps above can be added together, concentrated *in vacuo* and the isomerisation procedure repeated to improve overall yield if desired. However, if this is to be done then every effort must be made to remove residual toluene before heating as residual toluene greatly hinders the isomerisation.

$$\text{Percentage yield} = \frac{15.084 \text{ g}}{100.000 \text{ g}} \times 100 = 15\%$$

M.P. 141-144 °C (lit.^{51,52}, 140-142 °C)

IR: $\nu_{\text{max}}/\text{cm}^{-1}$ 2997 (C-H alkane stretching), 2885 (C-H alkane stretching), 1853 (C=O stretching), 1828 (C=O stretching), 1770 (C=O stretch).

¹H NMR (400 MHz, CDCl₃): δ_{ppm} 1.47 (*d*, *J* = 10.23 Hz, 1H, C-H bridge), 1.70 (*dt*, *J* = 10.29, 1.55 Hz, 1H, C-H bridge), 3.03 (*d*, *J* = 1.34 Hz, 2H, CHCO), 3.49 (*m*, 2H, =CHCH), 6.36 (*t*, *J* = 1.70 Hz, 2H, =CH).

¹³C NMR (100 MHz, CDCl₃): δ_{ppm} 171.60 (CO), 137.98 (=CH), 48.78 (CHCO), 46.90 (=CHCH), 44.14 (CH₂ bridge).

m/z: 164.0.

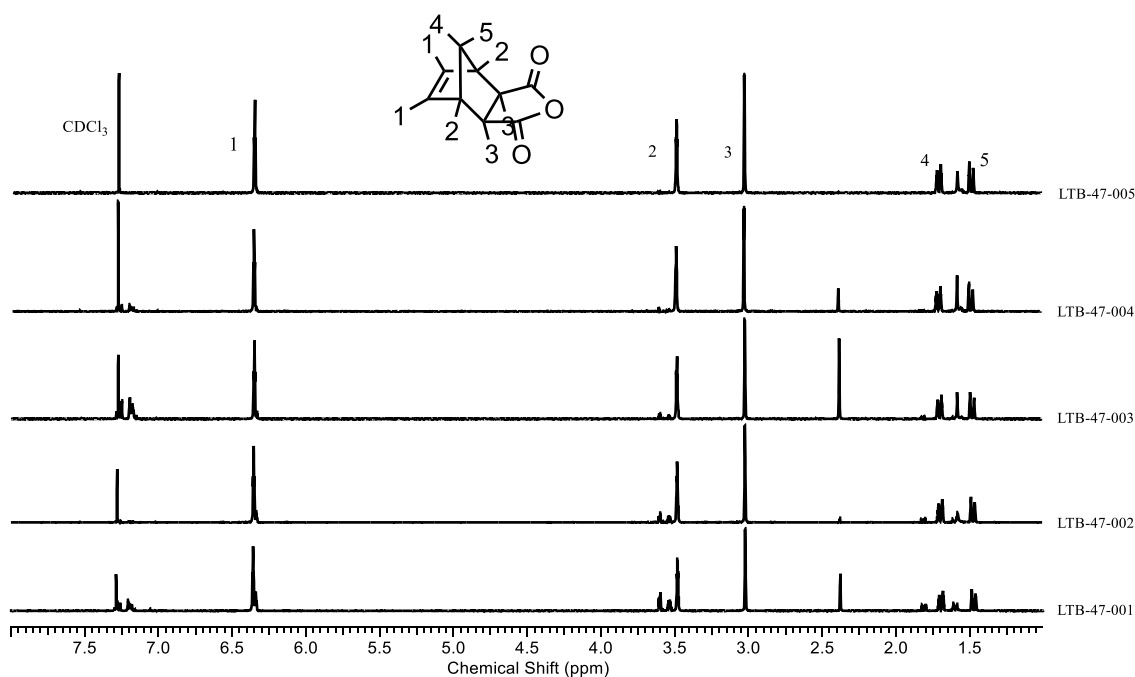


Figure 112 ^1H NMR spectra of *exo* carbic anhydride after successive crystallisations.

Microwave method:

Endo Carbic Anhydride (2.00 g, 12.2 mmol) and Toluene (4 cm³) were added to a microwave vial along with a magnetic stirrer. The vial was heated (200 °C, 10 min) by microwave irradiation. After completion, the microwave vial was cooled to 60 °C, the stirrer was carefully removed, and the vial was left upright with the top covered to cool to room temperature. After 3 days, crystallisation had occurred, and the solvent was decanted off (Note: Further *exo* can be recovered from solvent by removing solvent *in vacuo*, re-dissolving solid in toluene (1:2 ratio in g:ml) and following same microwave procedure as above.). The crude product is collected by vacuum filtration, washed with toluene and dried. The crude product, LTB-24-001, was weighed (0.692 g, 4.2 mmol) and analysed by ^1H NMR and found to still contain a small amount of *endo*.

Recrystallisation:

The crude product, LTB-24-001 (0.69 g, 4.2 mmol) was added to a conical flask and dissolved in toluene (2 ml) with heating. Once all solid had dissolved, the flask was left to cool at an angle with the top of the flask covered (to avoid loss of solvent). Once crystals had formed, the solvent was decanted off and the crystals were collected

by vacuum filtration. The crystals were washed with toluene (1ml), dried, and the product, LTB-24-002 (0.405 g, 2.46 mmol, 20% yield) was analysed by ^1H NMR and GC-MS (97% *exo*).

Note: The microwave reactor has a possible 10 min ramping period to reach the specified temperature (200 °C). These ramping periods are not included as part of the reaction time.

Synthesis of ROMP monomers – adding linkers:

Exo-himoyl glycine:

Glycine (2.286 g, 30.5 mmol), *exo* carbic anhydride (5.008 g, 30.5 mmol) and sodium sulfate (2.081 g) were added to DMF (110 cm³) and the mixture was heated under reflux (70°C, 4 days) in an oil bath.

$$\textit{Theoretical yield} = 0.0305 \text{ mol} \times 221.209 \text{ g mol}^{-1} = 6.747 \text{ g}$$

The solution was left to cool and then filtered to remove a small amount of solid that did not go into solution. DMF was removed on rotary evaporator (approx. 70°C) and the remaining residue was dissolved in ethyl acetate (100 cm³). The solution was washed with saturated ammonium chloride solution (9 x 50 cm³). The aqueous washings were divided into 2 aliquots and each aliquot was washed once with ethyl acetate (30 cm³). The washings from the organic layers were combined and then dried over magnesium sulfate. The mixture was filtered, and ethyl acetate removed *in vacuo* giving a white crystalline solid as the crude product, LTB-38-001 (4.819 g).

Recrystallisation of LTB-38-001:

The crude product, LTB-38-001 (4.617 g (Recoverable yield with spatula)), was dissolved in the minimum amount of hot ethyl acetate (21 cm³). The solution was left to cool to RT at an angle with the top of the flask covered to avoid loss of solvent. Note: The flask was left completely untouched straight after being taken off the heat to avoid premature crystallisation. After being left to crystallise overnight, large colourless crystals had formed. The remaining solvent was decanted carefully into a round-bottomed flask (LTB-38-F01) and the crystals were collected by vacuum filtration. The product, LTB-38-002, was weighed (2.228 g) and found to be pure by ^1H NMR and ^{13}C NMR. COSY and HSQC NMR of the product were also collected for characterisation.

Recovery from LTB-38-F01:

The solvent was removed *in vacuo*, leaving a white solid (2.274 g). The solid was dissolved in ethyl acetate (9 cm³) and heated until all solid had dissolved. Note: Avoid getting too hot to minimise loss of solvent. The solution was left to cool to RT at an angle with the top of the flask covered to avoid loss of solvent. After crystallisation had occurred, the remaining solvent was decanted off and the product, LTB-38-F02, was collected by vacuum filtration and weighed (1.030 g).

The overall yield and percentage yield for the reaction is calculated below:

$$\text{Overall yield} = 2.228 \text{ g} + 1.030 \text{ g} = 3.258 \text{ g}$$

$$\text{Percentage yield} = \frac{3.258}{6.747} \times 100 = 48 \%$$

M.P. 160 – 162 °C. (lit., ⁵⁶120 – 122 °C, ⁵⁷129.5 – 130.5 °C, ⁶149 – 150 °C.).

IR: $\nu_{\text{max}}/\text{cm}^{-1}$ 3071 (C-H alkene stretching), 2994 (C-H alkane stretching), 2947 (C-H alkane stretching), 1748 (C=O carboxylic acid stretching), 1674 (C=O dicarboximide stretching).

¹H NMR (400 MHz, CDCl₃): δ_{ppm} 1.54 (*dt*, *J* = 1.58, 9.98 Hz, 1H, CH₂ bridge), 1.64 (*d*, *J* = 9.98 Hz, 1H, CH₂ bridge), 2.79 (*d*, *J* = 1.22 Hz, 2H, CHCO), 3.34 (*t*, *J* = 1.70 Hz, 2H, =CHCH), 4.30 (*s*, 2H, NCH₂), 6.33 (*t*, *J* = 1.83 Hz, 2H, =CH).

¹³C NMR (100 MHz, CDCl₃): δ_{ppm} 39.03 (NCH₂), 42.87 (CH₂), 45.43 (=CHCH), 48.05 (CHCO), 138.01 (C=C), 171.29 (COOH), 177.12 (CON).

m/z: 221.0

Crystal data: (C₁₁H₁₁NO₄), *M_r* = 221.21, monoclinic, *a* = 6.29482(14) Å, *b* = 13.8975(3) Å, *c* = 11.1692(2) Å, α = 90°, β = 90.663(2)°, γ = 90°, *V* = 977.04(4) Å³, *Z* = 4, *P*2 (1)/*c*, *D_c* = 1.504 g/cm³, μ = 0.976 mm⁻¹, *T* = 100(2) K.

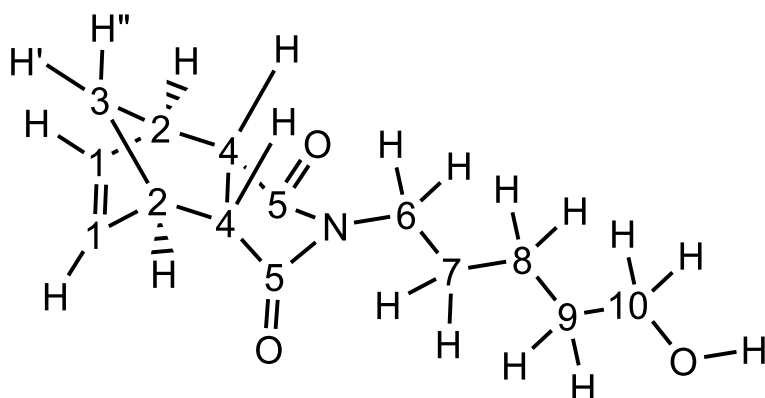
N-(hydroxypentanyl)-*cis*-5-norbornene-*endo*-2,3-dicarboximide:

To a round-bottomed flask, *endo* carbic anhydride (3.92 g, 23.8 mmol), Toluene (70 cm³) and Triethylamine (385 μ l) were added. The solution was stirred at RT until all solid had dissolved. 5-amino-1-pentanol (2.45* g, 23.8 mmol) was added to the stirring solution. A dean-stark trap was then attached, and the solution was heated

under reflux (155 °C, 3 h). Once cooled, the solution was concentrated *in vacuo* to yield the crude product as a yellow oil. The crude product was dissolved in DCM (120 cm³) and washed with HCl (2 x 20 cm³, 0.1 M) and brine (2 x 20 cm³). The organic phase was dried over magnesium sulfate, filtered by gravity and the solvent (DCM) was removed on a rotary evaporator. The product, LTB-42-001 (4.819g, 81%) was left as a yellow oil and analysed by ¹H NMR.

* 2.45 g was the amount weighed out but the melting point of 5-amino-1-pentanol is ~ 33 °C so after weighing, and during transfer, some of it had melted and was unable to be transferred to the reaction vessel (approx. 0.2 g). Therefore, expect slightly lower yield.

IR: $\nu_{\max}/\text{cm}^{-1}$ 3447 (O-H alcohol stretching), 2940 (C-H alkane stretching), 2866 (C-H alkane stretching), 1763 (C=O stretching), 1736 (C=O stretching), 1682 (C=O dicarboximide stretching).



¹H NMR (400 MHz, CDCl₃): δ_{ppm} 1.32 (m, 2H, 8), 1.47 (m, 2H, 7), 1.56 (m, 3H, 3'' & 9), 1.74 (dt, $J = 8.8, 1.6$ Hz, 1H, 3'), 3.26 (dd, $J = 2.9, 1.6$ Hz, 2H, 4), 3.35 (t, $J = 7.3$ Hz, 2H, 6), 3.39 (m, 2H, 2), 3.63 (t, $J = 6.5$ Hz, 2H, 10), 6.11 (t, $J = 1.8$ Hz, 2H, 1).

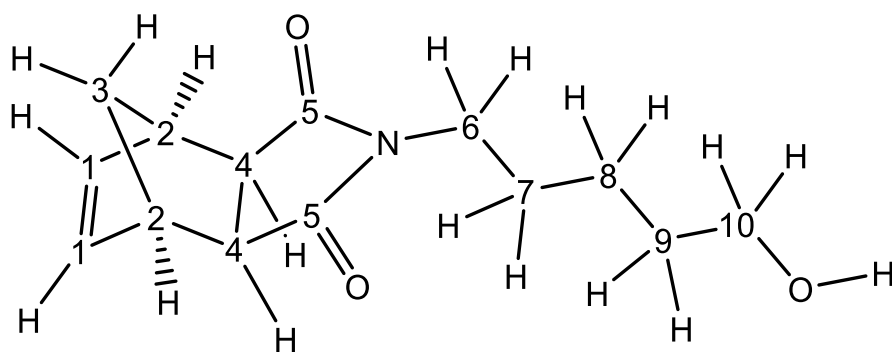
¹³C NMR (100 MHz, CDCl₃): δ_{ppm} 22.99 (8), 27.53 (7), 32.09 (9), 38.22 (6), 44.91 (2), 45.74 (4), 52.26 (3), 62.59 (10), 134.44 (1), 177.92 (5).

m/z : 249.1

N-(hydroxypentanyl)-*cis*-5-norbornene-*exo*-2,3-dicarboximide:

Exo carbic anhydride (3.92 g, 23.8 mmol), triethylamine (385 μ l, 2.38 mmol) and anti-bumping granules were added to toluene (70 ml) and the mixture was stirred with gentle heating until most of the carbic anhydride had dissolved. 5-amino-1-pentanol (2.45 g, 23.8 mmol) was crushed up, added to the stirring solution and a dean-stark trap was attached. The solution was heated (145 – 150 $^{\circ}$ C, 3 h). The solution was left to cool, filtered by gravity and concentrated *in vacuo*, leaving a dark yellow / orange oil. This crude product was dissolved in dichloromethane (100 ml), washed with HCl (2 x 25 ml, 0.1 M) and brine (2 x 25 ml) and the organic layer was dried over MgSO₄. The solvent was removed *in vacuo*, yielding the product, LTB-52-001 (5.474 g, 92%), which was analysed by ¹H, ¹³C, COSY and HSQC NMR. The product was also analysed by GC-MS and found to be >95 % pure.

IR: $\nu_{\max}/\text{cm}^{-1}$ 3447 (O-H alcohol stretching), 3065 (C-H alkene stretching), 2940 (C-H alkane stretching), 2876 (C-H alkane stretching), 2864 (C-H alkane stretching), 1767 (C=O stretching), 1734 (C=O stretching), 1684 (C=O dicarboximide stretching).



¹H NMR (400 MHz, CDCl₃): δ_{ppm} 1.25 (d, $J = 9.9$ Hz, 1H, 3'), 1.40 (m, 2H, 8), 1.54 (dt, $J = 9.8, 1.6$ Hz, 1H, 3'), 1.62 (m, 4H, 7 & 9), 2.70 (d, $J = 1.3$ Hz, 2H, 4), 3.30 (t, $J = 1.70$ Hz, 2H, 2), 3.50 (t, $J = 7.43$ Hz, 2H, 6), 3.66 (t, $J = 6.5$ Hz, 2H, 10), 6.31 (t, $J = 1.8$ Hz, 2H, 1).

¹³C NMR (100 MHz, CDCl₃): δ_{ppm} 23.10 (8), 27.53 (7/9), 32.11 (7/9), 38.52 (6), 42.74 (3), 45.18 (2), 47.83 (4), 62.59 (10), 137.84 (1), 178.16 (5).

m/z : 249.1

Endo-N-(2-Aminoethyl)-5-norbornene-2,3-dicarboximide:

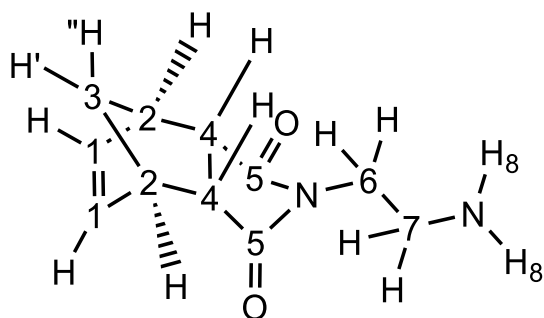
To a stirring solution of *endo* carbic anhydride (5.00 g, 30.5 mmol) in toluene (80 ml), was added ethylenediamine (8.15 ml, 121.9 mmol) and a white precipitate formed. The solution was heated to reflux (110 °C, 18 h) and the precipitate re-dissolved. The solution was left to cool to room temperature and the solvent was removed *in vacuo*. The residue was taken up in toluene (150 ml) and washed with water (2 x 50 ml). Note: The water was first added to the flask to take up as much undissolved residue as possible. The organic toluene layer was disposed of as the product stays in the aqueous layer. The aqueous layer was washed with DCM (3 x 50 ml) and the combined organic washings were combined, dried over MgSO₄ and filtered by gravity. The solvent was removed *in vacuo*, yielding the product, LTB-86-001 (1.818 g) which was analysed by ¹H NMR.

To obtain more product, the remaining aqueous layer was washed with DCM (2 x 50 ml). The combined organic washings were dried over MgSO₄, filtered by gravity and the solvent removed *in vacuo*, yielding more product, LTB-86-002 (0.238 g) and was analysed by ¹H NMR.

The overall yield was therefore 1.818 g + 0.238 g = 2.056 g (33%).

M.P. 76 – 78 °C (lit., ²⁷60 – 62 °C).

IR: $\nu_{\max}/\text{cm}^{-1}$ 3381 (N-H amine stretching), 2997 (C-H alkane stretching), 2965 (C-H alkane stretching), 2940 (C-H alkane stretching), 2860 (C-H alkane stretching), 1759 (C=O stretching), 1684 (C=O dicarboximide stretching), 1655 (C=C alkene stretching).



¹H NMR (400 MHz, CDCl₃): δ_{ppm} 1.10 (*br s*, 2H, 8), 1.55 (*d*, $J = 8.8$ Hz, 1H, 3''), 1.74 (*dt*, $J = 8.8, 1.7$ Hz, 1H, 3'), 2.74 (*t*, $J = 6.4$ Hz, 2H, 7), 3.77 (*dd*, $J = 2.9, 1.6$ Hz, 2H, 4), 3.39 (*m*, 2H, 2), 3.40 (*t*, $J = 6.3$ Hz, 2H, 6), 6.12 (*t*, $J = 1.9$ Hz, 2H, 1).

^{13}C NMR (100 MHz, CDCl_3): δ_{ppm} 40.14 (7), 47.71 (6), 44.92 (2), 45.80 (4), 52.32 (3), 134.58 (1), 177.96 (5).

m/z : 207.0

Exo-N-(2-Aminoethyl)-5-norbornene-2,3-dicarboximide:

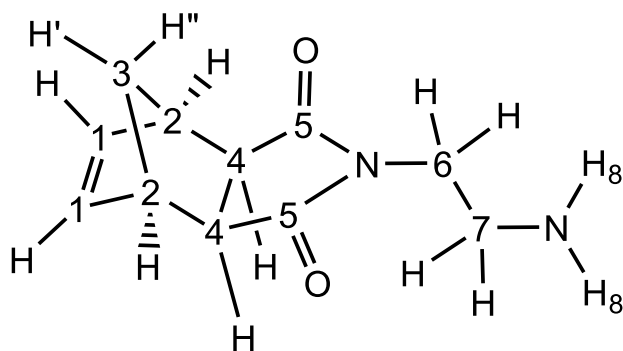
Exo carbic anhydride (5.00 g, 30.5 mmol) and toluene (80 ml) were added to a round-bottomed flask and stirred at room temperature until all solid had dissolved. Ethylenediamine (8.15 ml, 121.9 mmol) was slowly added to the stirring solution which caused a white precipitate to form. Additional toluene (50 ml) was added and the solution was stirred and heated under reflux overnight. The solution was left to cool, and the solvent was removed *in vacuo*, affording the crude product, LTB-94-001 (5.682 g), which was analysed by ^1H NMR.

Work-up:

The crude product, LTB-94-001 (5.682 g) was taken up in toluene (100 ml) and added to a separating funnel. Any additional residue was taken up in water (70 ml) and added to the separating funnel. The aqueous layer was extracted, and the organic layer was washed with additional water (30 ml). The product is expected in the aqueous layer and so the organic toluene layer was disposed of. The aqueous layer was then washed with DCM (50 ml) and brine (25 ml). The organic layer was extracted, and the aqueous layer was again washed with DCM (50 ml) and brine (25 ml). The organic layer was extracted, and the aqueous layer was washed with DCM (50 ml) and brine (25 ml). The organic layer was extracted, and the aqueous layer was washed with DCM (50 ml) for the final time. The combined organic DCM washings were dried over MgSO_4 , filtered by gravity and the solvent removed *in vacuo*, yielding a yellow oil which slowly crystallised as product, LTB-94-002 (2.373 g, 38%). The product was analysed by ^1H NMR.

M.P. 70 – 72 °C

IR: $\nu_{\text{max}}/\text{cm}^{-1}$ 3385 (N-H amine stretching), 3329 (N-H amine stretching), 2984 (C-H alkane stretching), 2951 (C-H alkane stretching), 2882 (C-H alkane stretching), 2851 (C-H alkane stretching), 1763 (C=O stretching), 1682 (C=O dicarboximide stretching).



^1H NMR (400 MHz, CDCl_3): δ_{ppm} 1.16 (*br s*, 2H, 8), 1.33 (*dt*, $J = 9.8, 1.4$ Hz, 1H, 3''), 1.49 (*dt*, $J = 9.9, 1.6$ Hz, 1H, 3'), 2.68 (*d*, $J = 1.3$ Hz, 2H, 4), 2.87 (*t*, $J = 6.4$ Hz, 2H, 7), 3.25 (*t*, $J = 1.7$ Hz, 2H, 2), 3.52 (*t*, $J = 6.5$ Hz, 2H, 6), 6.26 (*t*, $J = 1.8$ Hz, 2H, 1).

^{13}C NMR (100 MHz, CDCl_3): δ_{ppm} 39.95 (7), 41.45 (6), 42.84 (3), 45.19 (2), 47.86 (4), 137.82 (1), 178.39 (5).

m/z : 207.0

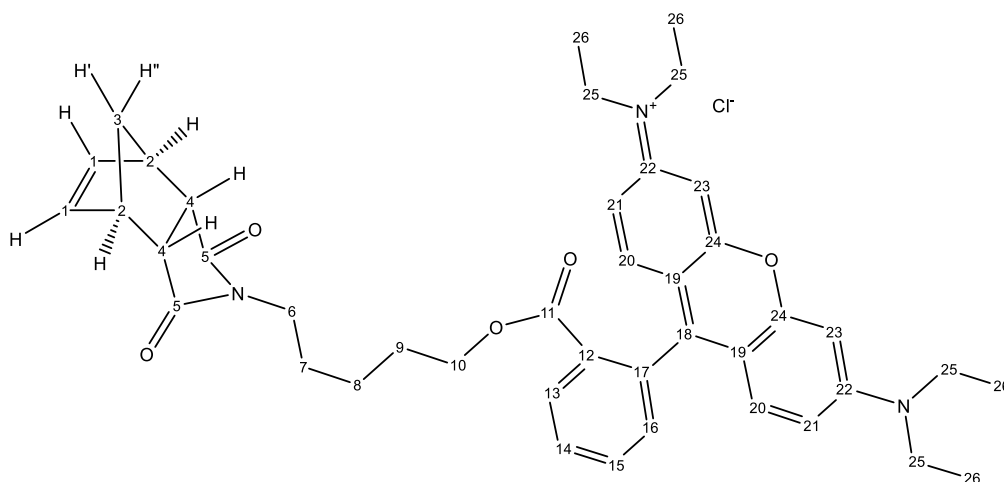
Synthesis of ROMP monomers – Adding functionality:

Endo-ester-RhB:

N-(hydroxypentanyl)-*cis*-5-norbornene-*endo*-2,3-dicarboximide (802 mg, 3.2 mmol), rhodamine-B (1.80 g, 3.8 mmol), DCC (1.13 g, 5.5 mmol) and DMAP (431 mg, 3.53 mmol) were added to DCM (60 ml) and the solution was left to stir (3 days, RT) in a stoppered flask. After stirring, the stirrer was removed and the solvent removed *in vacuo*, yielding the crude product, LTB-56-001, which was analysed by ^1H NMR.

A sample of the crude product, LTB-56-001 (300 mg), was weighed out and purified by column chromatography ($R_f = 0.26$, DCM:MeOH 15:1). The fractions containing only one spot by TLC were combined and the solvent was removed *in vacuo*, yielding the purified product, LTB-56-002 (136 mg, 6%), as a shiny brown solid. Note: This is just an isolated yield as only 300 mg of the crude was purified by column. The product was analysed by ^1H , ^{13}C , COSY, DEPT and HSQC NMR.

IR: $\nu_{\text{max}}/\text{cm}^{-1}$ 3356 (O-H stretching (starting material)), 3063 (C-H aromatic stretching), 2972 (C-H alkane stretching), 2932 (C-H alkane stretching), 2868 (C-H alkane stretching), 1763 (C=O stretching), 1715 (C=O ester stretching), 1690 (C=O dicarboximide stretching), 1647 (C=C alkene stretching), 1584 (C=C aromatic stretching).



^1H NMR (400 MHz, CDCl_3): δ_{ppm} 1.16 (*m*, 2H, 8), 1.35 (*t*, $J = 7.1$ Hz, 12H, 26), 1.39 (*m*, 2H, 7), 1.49 (*m*, 2H, 9), 1.57 (*d*, $J = 8.8$ Hz, 1H, 3''), 1.75 (*dt*, $J = 8.8$ Hz, 1.5 Hz, 1H, 3'), 3.27 (*m*, 4H, 4 & 6), 3.39 (*d*, $J = 1.2$ Hz, 2H, 2), 3.67 (*m*, 8H, 25), 4.01 (*t*, $J = 6.5$ Hz, 2H, 10), 6.06 (*t*, $J = 1.8$ Hz, 2H, 1), 6.87 (*d*, $J = 2.4$ Hz, 2H, 23), 6.93 (*dd*, $J = 9.5, 2.4$ Hz, 2H, 21), 7.09 (*d*, $J = 9.5$ Hz, 2H, 20), 7.34 (*dd*, $J = 7.5, 1.0$ Hz, 1H, 16), 7.76 (*td*, $J = 7.7, 1.2$ Hz, 1H, 14), 7.84 (*td*, $J = 7.6, 1.3$ Hz, 1H, 15), 8.30 (*dd*, $J = 7.9, 1.0$ Hz, 1H, 13).

^{13}C NMR (100 MHz, CDCl_3): δ_{ppm} 12.68 (26), 23.26 (8), 27.35 (7), 27.87 (9), 37.94 (6), 44.90 (2), 45.75 (4), 46.16 (25), 52.28 (3), 65.44 (10), 96.45 (23), 113.57 (21), 114.26 (*quaternary*), 129.99 (*quaternary*), 130.31 (16), 130.39 (14), 131.30 (20), 133.12 (15 & 13), 134.41 (1), 155.59 (*quaternary*), 157.77 (*quaternary*), 158.88 (*quaternary*), 165.04 (11), 177.72 (5).

Exo-ester-RhB:

N-(hydroxypentanyl)-*cis*-5-norbornene-*exo*-2,3-dicarboximide (808 mg, 3.2 mmol), DCC (1.13 g, 5.5 mmol), DMAP (431 mg, 3.5 mmol), rhodamine-B (1.80 g, 3.8 mmol) and DCM (60 ml) were added to a round-bottomed flask and the solution was stirred (23 h, RT). Once complete, the solvent was removed *in vacuo*, yielding the crude product, LTB-60-001 (4.396 g), as a shiny brown solid which was analysed by ^1H NMR. Column chromatography ($R_f = 0.28$, DCM:MeOH 15:1) was used to purify the crude product.

Columns:

Due to a large amount of crude product (4.396 g), it was purified by two separate columns. The products of these two columns were combined and a third column was done to further purify the product.

Column 1:

The crude product (1.866 g) was loaded onto the column. Mostly pure product, LTB-60-002 (0.541 g), was obtained by combining the fractions containing one spot and removing the solvent *in vacuo*. An analytical sample was also obtained by selecting one fraction, removing the solvent *in vacuo*, and analysing it by NMR.

Column 2:

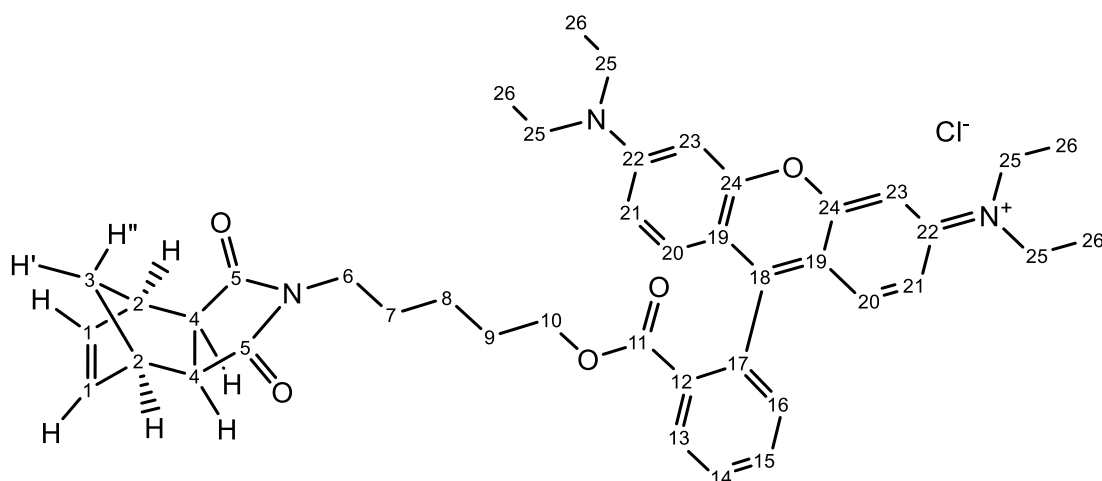
The crude product (2.135 g) was loaded onto the column. The fractions that contained one spot were combined and the solvent removed *in vacuo*, yielding mostly pure product, LTB-60-003 (0.811 g).

Column 3:

LTB-60-002 (0.541 g) and LTB-60-003 (0.811 g) were combined as LTB-60-004 (1.352 g), which was purified by column chromatography. The fractions containing only one spot were combined, the solvent was removed *in vacuo*, and the purified product, LTB-60-005 (0.736 g, 32 %) was collected and analysed by NMR. An analytical sample was also obtained by selecting one fraction, removing the solvent *in vacuo*, and analysing it by NMR.

M.P. 120 – 130 °C

IR: $\nu_{\max}/\text{cm}^{-1}$ 3360 (O-H stretching (starting material)), 3057 (C-H aromatic stretching), 2972 (C-H alkane stretching), 2932 (C-H alkane stretching), 2868 (C-H alkane stretching), 1769 (C=O stretching), 1717 (C=O ester stretching), 1692 (C=O dicarboximide stretching), 1647 (C=C alkene stretching), 1582 (C=C aromatic stretching).



^1H NMR (400 MHz, CDCl_3): δ_{ppm} 1.19 (m, 2H, 8), 1.24 (m, 1H, 3''), 1.34 (t, $J = 7.1$ Hz, 12H, 26), 1.50 (m, 5H, 3', 7 & 9), 2.68 (d, $J = 0.9$ Hz, 2H, 4), 3.26 (s, 2H, 2), 3.40 (t, $J = 7.6$ Hz, 2H, 6), 3.66 (m, 8H, 25), 4.02 (t, $J = 6.5$ Hz, 2H, 10), 6.30 (t, $J = 1.7$ Hz, 2H, 1), 6.85 (d, $J = 2.4$ Hz, 2H, 23), 6.93 (dd, $J = 9.5, 2.4$ Hz, 2H, 21), 7.08 (d, $J = 9.5$ Hz, 2H, 20), 7.32 (dd, $J = 7.5, 0.9$ Hz, 1H, 16), 7.75 (m, 1H, 14), 7.83 (m, 1H, 15), 8.29 (dd, $J = 7.9, 1.0$ Hz, 1H, 13).

^{13}C NMR (100 MHz, CDCl_3): δ_{ppm} 12.68 (26), 23.37 (8), 27.35 (7/9), 27.88 (7/9), 38.27 (6), 42.71 (3), 45.15 (2), 46.17 (25), 47.81 (4), 65.37 (10), 96.40 (23), 113.54 (quaternary), 114.28 (21), 129.97 (quaternary), 130.30 (16), 130.39 (14), 131.30 (20 & 13), 133.12 (15), 133.57 (quaternary), 137.80 (1), 155.58 (quaternary), 157.75 (quaternary), 158.86 (quaternary), 165.03 (11), 178.02 (5).

Endo-amide-RhB:

A flask was charged with *Endo*-N-(2-aminoethyl)-5-norbornene-2,3-dicarboximide (334 mg, 1.62 mmol), Rhodamine B (900 mg, 1.88 mmol), EDC hydrochloride (525 mg, 2.74 mmol), DMAP (216 mg, 1.77 mmol) and DCM (60 cm^3). The solution was stirred (48 h, RT). After stirring was complete, the solvent was removed *in vacuo* leaving a purple residue.

Work-up:

As much of the residue as possible was taken up in ethyl acetate (2 x 50 cm^3). Water (50 cm^3) was also added to the residue and as much of the residue was taken up in water as possible. The organic and aqueous phases were added to a separating funnel and the organic layer was extracted. The solvent was removed *in vacuo*, yielding the product, LTB-82-001, which was analysed by ^1H NMR. The ^1H NMR showed that the product contained some residual ethyl acetate that could affect the integration of important peaks on the NMR. LTB-82-001 was then taken up in DCM (approx. 30 cm^3) and the solvent was then removed *in vacuo*. This was repeated 3 times and the product, LTB-82-002 (0.640 g, 59 %), was analysed by ^1H NMR showing that an almost pure product had been obtained (apart from what appears to be a small amount of residual rhodamine B).

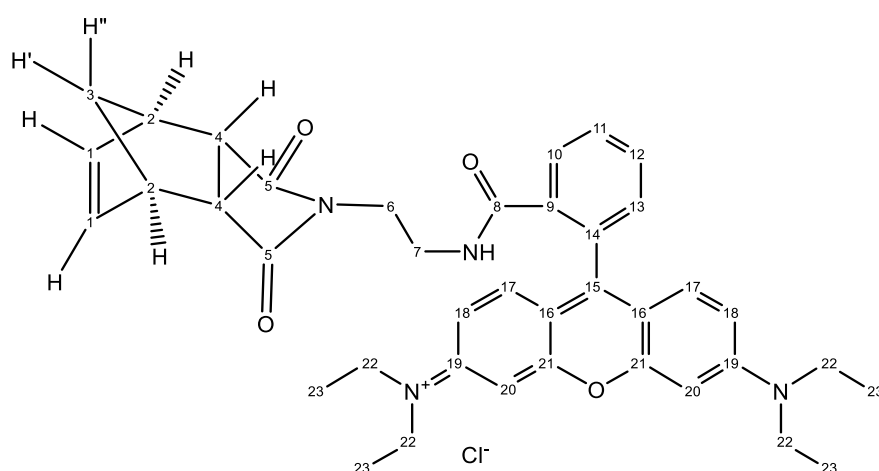
Crystallisation:

A small amount of product, LTB-82-002, was taken up in the minimum amount of ethyl acetate and the flask was covered slightly to allow the solvent to come off slowly. The slow evaporation led to the growth of crystals which appeared pink/red but under the microscope were colourless with some pink on the surface. The crystals being

colourless was confusing at first until a single crystal XRD experiment was run which found that the rhodamine moiety had ring closed, thereby removing the extended aromatic system which gives rise to the fluorescence. The pink on the surface could have been some residual rhodamine b or some of the ring opened version of the rhodamine moiety.

M.P. 174 – 176 °C

IR: $\nu_{\max}/\text{cm}^{-1}$ 2974 (C-H alkane stretching), 2932 (C-H alkane stretching), 2891 (C-H alkane stretching), 2874 (C-H alkane stretching), 1771 (C=O stretching), 1734 (C=O stretching), 1695 (C=O amide stretching), 1684 (C=O dicarboximide stretching), 1616 (C=C alkene stretching), 1516 (C=C aromatic stretching).



^1H NMR (400 MHz, CDCl_3): δ_{ppm} 1.07 (t, $J = 7.1$ Hz, 12H, 23), 1.36 (d, $J = 8.6$ Hz, 1H, 3''), 1.55 (d, $J = 8.6$ Hz, 1H, 3'), 2.92 (s, 1H, NH amide), 3.05 (dd, $J = 2.9, 1.5$ Hz, 2H, 4), 3.14 (s, 4H, 6 & 7), 3.17 (m, 2H, 2), 3.24 (m, 8H, 22), 5.88 (t, $J = 1.7$ Hz, 2H, 1), 6.20 (dd, $J = 8.9, 2.6$ Hz, 2H, 18), 6.31 (d, $J = 2.6$ Hz, 2H, 20), 6.39 (d, $J = 8.9$ Hz, 2H, 17), 6.93 (m, 1H, 13), 7.29 (m, 1H, 11), 7.32 (m, 1H, 12), 7.76 (m, 1H, 10).

^{13}C NMR (100 MHz, CDCl_3): δ_{ppm} 12.64 (23), 37.39 (6/7), 38.29 (6/7), 44.50 (22), 45.95 (4), 52.09 (3), 65.23 (quaternary), 97.79 (20), 105.43 (quaternary), 108.07 (18), 122.72 (10), 123.78 (13), 127.95 (11/12), 129.09 (17), 130.90 (quaternary), 132.40 (11/12), 134.34 (1), 148.73 (quaternary), 153.40 (quaternary), 153.59 (quaternary), 168.72 (8), 177.58 (5).

Crystal data: ($\text{C}_{39}\text{H}_{42}\text{N}_4\text{O}_4$), $M_r = 630.76$, triclinic, $a = 10.4936(3)$ Å, $b = 12.3484(3)$ Å, $c = 16.1383(4)$ Å, $\alpha = 99.335(2)^\circ$, $\beta = 102.497(2)^\circ$, $\gamma = 112.561(2)^\circ$, $V = 1814.32(9)$ Å³, $Z = 2$, $P-1$, $D_c = 1.175$ g / cm³, $\mu = 0.624$ mm⁻¹, $T = 293(2)$ K.

Exo-amide-RhB:

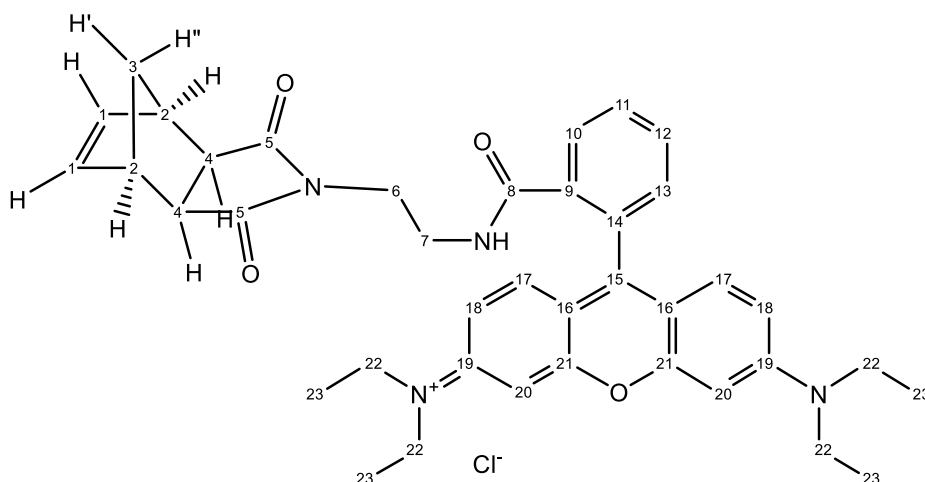
Exo-N-(2-aminoethyl)-5-norbornene-2,3-dicarboximide (334 mg, 1.6 mmol), EDC-hydrochloride (525 mg, 2.7 mmol) and DMAP (216 mg, 1.8 mmol) were added to DCM (60 ml) in a round-bottomed flask and stirred until all solid had dissolved. Rhodamine-B (900 mg, 1.9 mmol) was added to the stirring solution which was stoppered and left to stir (3 days, RT). Once complete, the solvent was removed *in vacuo*, leaving the crude product, LTB-98-001 (2.399 g), as a purple solid.

Work-up:

Ethyl acetate (2 x 60 ml) was added to the crude residue and was swirled vigorously to dissolve as much as possible before being transferred to a separating funnel. Water (2 x 50 ml) was also added to the crude residue and swirled vigorously to dissolve as much as possible before transfer to the separating funnel. The organic layer was extracted, and the aqueous layer was washed with ethyl acetate (2 x 25 ml). The combined organic extracts were back extracted with water (25 ml). The organic extracts were dried over MgSO₄, filtered by gravity and the solvent was removed *in vacuo*. The resulting residue was taken up in DCM (approx. 25 ml) and the solvent was removed *in vacuo*. The residue was again taken up in DCM (approx. 25 ml) and the solvent removed *in vacuo*. For the final time, the residue was taken up in DCM (approx. 25 ml) and the solvent was removed *in vacuo*, yielding the product, LTB-98-002 (0.492 g, 46%), as a pink/purple solid.

M.P. 132 – 135 °C

IR: $\nu_{\max}/\text{cm}^{-1}$ 2968 (C-H alkane stretching), 2918 (C-H alkane stretching), 2872 (C-H alkane stretching), 2849 (C-H alkane stretching), 1773 (C=O stretching), 1749 (C=O stretching), 1697 (C=O amide stretching), 1636 (C=C alkene stretching), 1541 (C=C aromatic stretching), 1508 (C=C aromatic stretching).



^1H NMR (400 MHz, CDCl_3): δ_{ppm} 1.10 (t, $J = 6.6$ Hz, 13 H, 23 & 3''), 1.34 (d, $J = 9.5$ Hz, 1H, 3'), 2.49 (s, 2H, 4), 2.92 (s, 1H, NH amide), 3.09 (s, 2H, 2), 3.27 (m, 10H, 22 & 7), 3.37 (t, $J = 5.7$ Hz, 2H, 6), 6.14 (s, 2H, 1), 6.22 (dd, $J = 8.9$, 2.6 Hz, 2H, 18), 6.34 (d, $J = 2.4$ Hz, 2H, 20), 6.43 (d, $J = 8.8$ Hz, 2H, 17), 6.95 (m, 1H, 13), 7.32 (m, 1H, 11), 7.34 (m, 1H, 12), 7.80 (m, 1H, 10).

^{13}C NMR (100 MHz, CDCl_3): δ_{ppm} 12.65 (23), 37.81 (6), 38.41 (7), 43.06 (3), 44.27 (22), 44.83 (2), 47.92 (4), 65.28 (quaternary), 97.74 (20), 105.38 (quaternary), 108.03 (18), 122.69 (10), 123.79 (13), 127.98 (11/12), 129.05 (17), 130.89 (quaternary), 132.44 (11/12), 137.63 (1), 148.72 (quaternary), 153.42 (quaternary), 153.58 (quaternary), 168.82 (8), 177.91 (5).

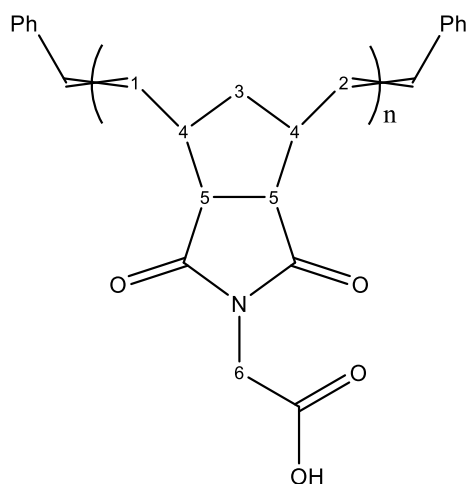
Crystal data: ($\text{C}_{39}\text{H}_{42}\text{N}_4\text{O}_4$), $M_r = 630.76$, orthorhombic, $a = 15.72214(17)$ Å, $b = 19.9433(2)$ Å, $c = 20.9335(3)$ Å, $\alpha = 90^\circ$, $\beta = 90^\circ$, $\gamma = 90^\circ$, $V = 6563.71(13)$ Å 3 , $Z = 8$, Pbca , $D_c = 1.277$ g / cm^3 , $\mu = 0.663$ mm^{-1} , $T = 150.0(3)$ K.

Polymerisation:

Poly *exo* himoyl glycine:

Exo himoyl glycine (12.70 mg, 0.0565 mmol) was dissolved in dry DCM (approximately 3 mL) and stirred (10 min). Grubbs 3rd generation catalyst (1.70 mg, 0.0019 mmol) was weighed and transferred to the reaction vial which was flushed with nitrogen before being sealed and allowed to stir (3 h, RT). The mixture was quenched with a few drops of a dilute solution of benzaldehyde in THF and the solution was stirred (10 min). The solvent was removed *in vacuo*, yielding a white-grey residue which was washed with diethyl ether (2 mL). The residue was

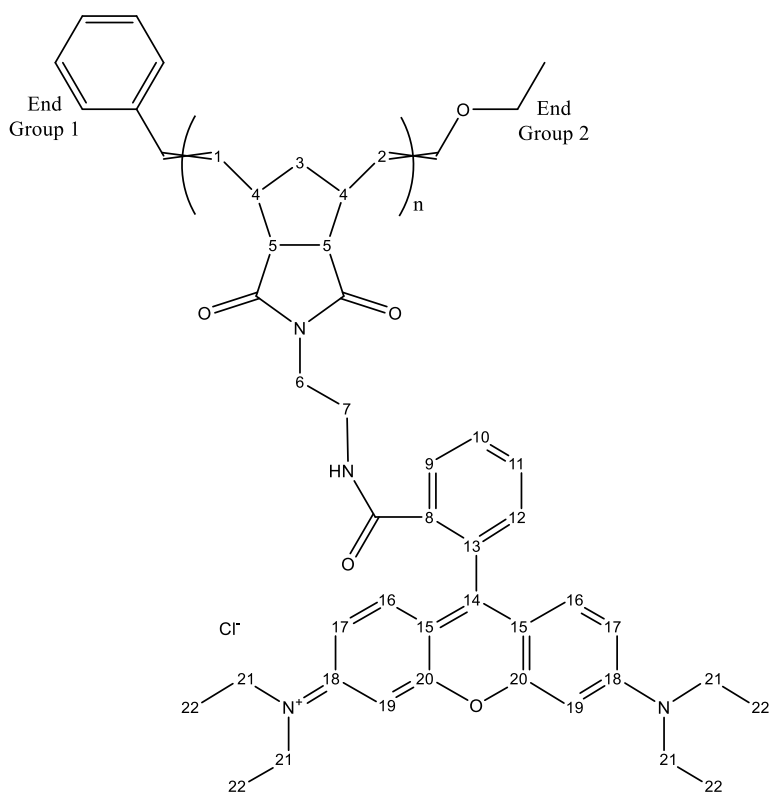
washed again with diethyl ether (2 mL) and the residue was dried. This resulting residue, LTB-104-001, was taken up in DMSO-d6 and analysed by ^1H NMR.



^1H NMR (400 MHz, DMSO-d6): δ_{ppm} 1.48 (3), 2.01 (5), 3.14 (4), 4.01 (6), 5.47 (1/2 *cis*), 5.67 (1/2 *trans*), 7.10 (*end groups*).

Poly *exo* amide RhB:

Grubbs 3rd generation catalyst (1.00 mg, 0.00113 mmol) was taken up in dry DCM (0.5 mL) and stirred until all solid had dissolved. The solution was added to *exo* amide RhB (15.09 mg, 0.0226 mmol) and allowed to stir (1.5 h, RT). The reaction was quenched by the addition of ethyl vinyl ether (1 drop) and the solution was left to stir (10 min). The solution was transferred to a PCR tube, where the solvent was removed by blowing with compressed air until a small amount of solvent remained. Diethyl ether (2 mL) was added to the PCR tube, causing a precipitate to form. The PCR tube was placed on a centrifuge to collect the precipitate, after which the remaining solvent was decanted off. The residue was washed again with diethyl ether (2 mL) and the product (11 mg, 73%) was dried under high vacuum. The product was analysed by ^1H NMR.



^1H NMR (400 MHz, CDCl_3): δ_{ppm} 1.13 (22), 1.46 (3), 1.71 (5), 2.08 (*amide NH*), 2.84 (6 & 7), 3.11 (4), 3.30 (21), 5.42 (1/2 *cis*), 5.73 (1/2 *trans*), 6.35 (17), 6.45 (19), 6.59 (16), 6.98 (12), 7.34 (10 & 11), 7.81 (9).

DNA Intercalation:

Poly *exo* amide RhB (1 mmol wrt. monomer) in THF (20 μL) and either No DNA, DNA1 (1mmol wrt. bases), DNA2 (1mmol wrt. bases) or a mix of both DNA1 & DNA2 in the specific buffer solution (water, TBE 1x or TAMg 1x,) (200 μL) were combined to give a final volume of 220 μL . These solutions were analysed by DLS and fluorescence spectroscopy where each measurement was repeated three times and averaged.

References:

- 1 T. L. Choi and R. H. Grubbs, *Angew. Chemie - Int. Ed.*, 2003, **42**, 1743–1746.
- 2 A. E. Madkour, A. H. R. Koch, K. Lienkamp and G. N. Tew, *Macromolecules*, 2010, **43**, 4557–4561.
- 3 D. A. Robson, M. R. Giles, M. North, S. C. G. Biagini, R. Gareth Davies, V. C. Gibson and E. L. Marshall, *Chem. Commun.*, 2002, 235–236.
- 4 Y. C. Teo and Y. Xia, *Macromolecules*, 2015, **48**, 5656–5662.
- 5 M. Hollauf, G. Trimmel and A. C. Knall, *Monatshefte fur Chemie*, 2015, **146**, 1063–1080.
- 6 S. C. . Biagini, S. M. Bush, V. C. Gibson, L. Mazzariol, M. North, W. G. Teasdale, C. M. Williams, G. Zago and D. Zamuner, *Tetrahedron*, 1995, **51**, 7247–7262.
- 7 P. Jean-Louis Hérisson and Y. Chauvin, *Die Makromol. Chemie*, 1971, **141**, 161–176.
- 8 M. Schaefer, N. Hanik and A. F. M. Kilbinger, *Macromolecules*, 2012, **45**, 6807–6818.
- 9 M. A. Sowers, J. R. McCombs, Y. Wang, J. T. Paletta, S. W. Morton, E. C. Dreaden, M. D. Boska, M. Francesca Ottaviani, P. T. Hammond, A. Rajca and J. A. Johnson, *Nat. Commun.*, 2014, **5**, 1–9.
- 10 S. Hilf, R. H. Grubbs and A. F. M. Kilbinger, *J. Am. Chem. Soc.*, 2008, **130**, 11040–11048.
- 11 G. C. Bazan, J. H. Oskam, H.-N. Cho, L. Y. Park and R. R. Schrock, *J. Am. Chem. Soc.*, 1991, **113**, 6899–6907.
- 12 R. R. Schrock, J. S. Murdzek, G. C. Bazan, J. Robbins, M. Dimare and M. O'Regan, *J. Am. Chem. Soc.*, 1990, **112**, 3875–3886.
- 13 P. Schwab, R. H. Grubbs and J. W. Ziller, *J. Am. Chem. Soc.*, 2002, **118**, 100–110.
- 14 P. Schwab, M. B. France, J. W. Ziller and R. H. Grubbs, *Angew. Chemie Int. Ed. English*, 1995, **34**, 2039–2041.
- 15 M. Scholl, S. Ding, C. Woo Lee, R. H. Grubbs and R. H. Angew, *Angew. Chem., Int. Ed. Engl.*, 1998, **133**, 953–956.
- 16 C. W. Bielawski and R. H. Grubbs, *Angew. Chemie - Int. Ed.*, 2000, **39**, 2903–2906.
- 17 E. Khosravi, W. J. Feast, A. A. Al-Hajaji and T. Leejarkpai, *J. Mol. Catal. A Chem.*, 2000, **160**, 1–11.
- 18 G. C. Bazan, R. R. Schrock, H.-N. Cho and V. C. Gibson¹, *Macromolecules*, 1991, **24**, 4495–4502.
- 19 T.-L. Choi and R. H. Grubbs, *Angew. Chemie Int. Ed.*, 2003, **42**, 1743–1746.
- 20 J. Das Sarma, L. Shashank, H. Dinda, I. Chakraborty, S. Mukherjee, R. Shunmugam and R. Bhattacharyya, *Macromolecules*, 2015, **48**, 6791–6800.
- 21 D. Craig, *J. Am. Chem. Soc.*, 1951, **73**, 4889–4892.
- 22 M. Bolte, A. Degen and E. Egert, *Acta Crystallogr. Sect. C Cryst. Struct. Commun.*, 2000, **56**, 1338–1342.

- 23 F. E. Rogers and S. W. Quan, *J. Phys. Chem.*, 1973, **77**, 828–831.
- 24 L. Rulíšek, P. Šebek, Z. Havlas, R. Hrabal, P. Čapek and A. Svatoš, *J. Org. Chem.*, 2005, **70**, 6295–6302.
- 25 S. C. G. Biagini, M. P. Coles, V. C. Gibson, M. R. Giles, E. L. Marshall and M. North, *Polymer (Guildf.)*, 2002, **39**, 1007–1014.
- 26 R. B. Woodward and H. Baer, *J. Am. Chem. Soc.*, 1948, **70**, 1161–1166.
- 27 R. G. Davies, V. C. Gibson, M. B. Hursthouse, M. E. Light, E. L. Marshall, M. North, D. A. Robson, I. Thompson, A. J. P. White, J. Williams and P. J. Williams, *J. Chem. Soc. Perkin Trans. 1*, 2002, 3365–3381.
- 28 X. Li, S. L. Prukop, S. L. Biswal and R. Verduzco, *Macromolecules*, 2012, **45**, 7118–7127.
- 29 Y. Xia and R. H. Grubbs, *Macromolecules*, 2009, **42**, 3761–3766.
- 30 M. Zhang, P. Vedantham, D. L. Flynn and P. R. Hanson, *J. Org. Chem.*, 2004, **69**, 8340–8344.
- 31 M. Alizadeh and A. F. M. Kilbinger, *Macromolecules*, 2018, **51**, 4363–4369.
- 32 F. Liu, S. Mu, Q. Zhao, Y. Long, Y. Liu, H. Gu, X. Liu, L. Zhang and G. Qiu, *Macromol. Chem. Phys.*, 2018, **219**, 1800273.
- 33 F. M. Pfeffer, T. Gunnlaugsson, P. Jensen and P. E. Kruger, *Org. Lett.*, 2005, **7**, 5357–5360.
- 34 R. Baumgartner, H. Fu, Z. Song, Y. Lin and J. Cheng, *Nat. Chem.*, 2017, **9**, 614–622.
- 35 N. Xie, K. Feng, B. Chen, M. Zhao, L. P. Zhang, C. H. Tung, L. Z. Wu and S. Peng, *Chem. Commun.*, 2014, **50**, 9539–9542.
- 36 M. Rogosnitzky and S. Branch, *BioMetals*, 2016, **29**, 365–376.
- 37 T. Kanda, T. Fukusato, M. Matsuda, K. Toyoda, H. Oba, J. Kotoku, T. Haruyama, K. Kitajima and S. Furui, *Radiology*, 2015, **276**, 228–232.
- 38 P. S. Yao, Q. Y. Cao, R. P. Peng and J. H. Liu, *J. Photochem. Photobiol. A Chem.*, 2015, **305**, 11–18.
- 39 K. Feng, N. Xie, B. Chen, C. H. Tung and L. Z. Wu, *Biomacromolecules*, 2016, **17**, 538–545.
- 40 J. Shao, L.-Z. Wu, C.-H. Tung, N. Xie, K. Feng and B. Chen, *Polym. Chem.*, 2017, **9**, 77–86.
- 41 H. Maeda, L. W. Seymour and Y. Miyamoto, *Bioconjug. Chem.*, 1992, **3**, 351–362.
- 42 W. D. Sasikala and A. Mukherjee, *Phys. Chem. Chem. Phys.*, 2016, **18**, 10383–10391.
- 43 D. Sabolova, P. Kristian and M. Kozurkova, *J. Appl. Toxicol.*, 2020, **40**, 64–71.
- 44 S. Mukhopadhyay, M. M. Islam, M. Chakraborty, N. Gupta, P. Pandya and A. Al Masum, *Dye. Pigment.*, 2013, **99**, 412–422.
- 45 M. Karimi Goftar and N. M. Kor, *Acta Biol. Indica*, 2015, **4**, 197–204.
- 46 J. B. Matson and R. H. Grubbs, *J. Am. Chem. Soc.*, 2008, **130**, 6731–6733.
- 47 J. P. Cole, J. J. Lessard, C. K. Lyon, B. T. Tuten and E. B. Berda, *Polym. Chem.*, 2015, **6**, 22.
- 48 B. G. Shin, M. S. Jang, D. Y. Yoon and W. Heitz, *Macromol. Rapid Commun.*, 2004, **25**, 728–732.

- 49 M. Karplus, *J. Chem. Phys.*, 1959, **30**, 11–15.
- 50 C. G. Gianopoulos, B. Zarychta, S. Cenedese, V. V. Zhurov and A. A. Pinkerton, *J. Phys. Chem. A*, 2016, **120**, 4059–4070.
- 51 M. Hara, Y. Odaira and S. Tsutsumi, *Tetrahedron*, 1966, **22**, 95–100.
- 52 K. K. W. To, X. Wang, C. W. Yu, Y. P. Ho and S. C. F. Au-Yeung, *Bioorganic Med. Chem.*, 2004, **12**, 4565–4573.
- 53 CN104130228 (A), *Pat. CN104130228 Espac. - Bibliogr. data*, 2016.
- 54 K. Alder and G. Stein, *Justus Liebig's Ann. der Chemie*, 1932, **496**, 204–251.
- 55 K. Alder and G. Stein, *Justus Liebig's Ann. der Chemie*, 1933, **504**, 216–257.
- 56 I. N. Tarabara, Y. S. Bondarenko, A. A. Zhurakovskii and L. I. Kas'yan, *Russ. J. Org. Chem.*, 2007, **43**, 1297–1304.
- 57 M. Shang, R. N. Warrenner, D. N. Butler, Y. Murata and D. Margetić, *Mol. Divers.*, 2011, **15**, 541–560.
- 58 S. C. G. Biagini and A. L. Parry, *J. Polym. Sci. Part A Polym. Chem.*, 2007, **45**, 3178–3190.
- 59 M. A. Tlenkopatchev, S. Fomine, L. Fomina, R. Gaviño and T. Ogawa, *Polym. J.*, 1997, **29**, 622–625.
- 60 M. Tlenkopatchev, S. Fomine, E. Miranda, L. Fomina and T. Ogawa, *Polym. J.*, 1995, **27**, 1173–1179.
- 61 N. Xie, K. Feng, B. Chen, C. H. Tung and L. Z. Wu, *New J. Chem.*, 2016, **40**, 3252–3260.
- 62 K. P. Patel, E. M. Gayakwad, V. V. Patil and G. S. Shankarling, *Adv. Synth. Catal.*, 2019, **361**, 2107–2116.
- 63 J. Liu, Y. Zhong, P. Lu, Y. Hong, J. W. Y. Lam, M. Faisal, Y. Yu, K. S. Wong and B. Z. Tang, *Polym. Chem.*, 2010, **1**, 426.
- 64 T. Förster, *Ann. Phys.*, 1948, **437**, 55–75.
- 65 I. L. Arbeloa and K. K. Rohatgi-Mukherjee, *Chem. Phys. Lett.*, 1986, **128**, 474–479.
- 66 S. Mordon, V. Maunoury, J. M. Devoisselle, Y. Abbas and D. Coustaud, *J. Photochem. Photobiol. B Biol.*, 1992, **13**, 307–314.
- 67 A. Rhoden Smith and B. L. Iverson, *J. Am. Chem. Soc.*, 2013, **135**, 12783–12789.
- 68 N. T. Chen, C. Y. Wu, C. Y. Chung, Y. Hwu, S. H. Cheng, C. Y. Mou and L. W. Lo, *PLoS One*, 2012, **7**, e44947.
- 69 M. Akkurt, A. Jarrahpour, P. Shirvani and M. N. Tahir, *Acta Crystallogr. Sect. E Struct. Reports Online*, 2013, **69**, o1404.
- 70 W. L. Czaplowski, G. E. Purnell, C. A. Roberts, R. M. Allred and E. J. Harbron, *Org. Biomol. Chem.*, 2014, **12**, 526–533.
- 71 X. Chen, T. Pradhan, F. Wang, J. S. Kim and J. Yoon, *Chem. Rev.*, 2012, **112**, 1910–1956.